



HAL
open science

Crosstalk between FGF and Notch signaling pathways during the collective migration of parapineal cells in the left right asymmetric zebrafish brain

Lu Wei

► **To cite this version:**

Lu Wei. Crosstalk between FGF and Notch signaling pathways during the collective migration of parapineal cells in the left right asymmetric zebrafish brain. *Development Biology*. Université Paul Sabatier - Toulouse III, 2018. English. NNT : 2018TOU30197 . tel-02282171

HAL Id: tel-02282171

<https://theses.hal.science/tel-02282171>

Submitted on 9 Sep 2019

HAL is a multi-disciplinary open access archive for the deposit and dissemination of scientific research documents, whether they are published or not. The documents may come from teaching and research institutions in France or abroad, or from public or private research centers.

L'archive ouverte pluridisciplinaire **HAL**, est destinée au dépôt et à la diffusion de documents scientifiques de niveau recherche, publiés ou non, émanant des établissements d'enseignement et de recherche français ou étrangers, des laboratoires publics ou privés.



THÈSE

En vue de l'obtention du DOCTORAT DE L'UNIVERSITÉ DE TOULOUSE

Délivré par l'Université Toulouse 3 - Paul Sabatier

Présentée et soutenue par

LU WEI

Le 26 novembre 2018

Interaction entre les voies de signalisation FGF et Notch lors de la migration de la parapineale dans le cerveau asymétrique du poisson zèbre

Ecole doctorale : **BSB - Biologie, Santé, Biotechnologies**

Spécialité : **BIOLOGIE DU DEVELOPPEMENT**

Unité de recherche :

CBD - Centre de Biologie du Développement

Thèse dirigée par

Patrick BLADER et Myriam ROUSSIGNE

Jury

Mme Virginie LECAUDEY, Rapporteur

M. Maximilian FURTHAUER, Rapporteur

M. Julien FALK, Examineur

Mme Cathy SOULA, Examineur

M. Patrick BLADER, Directeur de thèse

Mme Myriam ROUSSIGNE, Co-directeur de thèse



Thèse

De l'Université Toulouse 3 Paul Sabatier (UT3 Paul Sabatier)

Crosstalk between FGF and Notch signaling pathways during the collective migration of parapineal cells in the asymmetric zebrafish brain

Présentée et soutenue par

Lu WEI

26 November, 2018

Ecole doctore : **BSB – Biologie, Santé, Biotechnologies**

Specialité : **BIOLOGIE DU DEVELOPPEMENT**

Unité de recherche : **Centre de Biologie Intégrative (CBI),**

Centre de Biologie de Développement (CBD)

Toulouse France

Thèse dirigée par

Myriam Roussigné and Patrick Blader

Jury

Prof. Cathy Soula: President of Jury

Dr. Virginie Lecaudey: Rapportrice

Dr. Maximilian Furthauer: Rapporteur

Dr. Julien Falk: Examiner

Dr. Patrick Blader: Co-director of Thesis

Dr. Myriam Roussigne: Co-director of Thesis

Acknowledgements

I would like to thank many people for helping me during my Ph.D. First, I would like to thank my supervisors Dr. Myriam Roussigne and Dr. Patrick Blader, for their knowledge, patience and example. I consider myself particularly lucky for having had the opportunity to meet them, which allowed me to grow both as scientist and as a human. A big thanks to Myr for all your scientific guidance, encouragement and believing in me. I will never forget our everyday brainstorm on FGF and Notch signaling pathway.

Besides my supervisors, I would like to thank the rest of my thesis jury: Prof. Virginie Lecaudey, Dr. Maximilian. Furthauer, Dr. Falk Julien, Prof. Cathy Soula and Dr. Richard Poole, for accepting to read and evaluate my thesis work. I would also like to thank Dr. Matthias Carl and Dr. Xiaobo Wang, for their helpful feedback during the committee meeting.

Next, I would like to thank all the past and present members of Blader team. Especially Julie, Elise and Pascale for helping me critically analyze my data and interpret their biological significance. Thanks a lot Aurelie, Aurore and Clair, for all day to day help, scientific discussions and of course teaching me French, also for the time spent both on the bench and outside from the lab. I will still remember “DJ Lu” and “LuLuSong” singing in the lab next many years. Thanks Pascale, Aurore and Myr for your cakes. Thanks Aurore for taking care of fish facility. Thanks Julie and Aurelie for lab management and taking care of reagents and anything I needed. Thanks Amir, Raph, Vero and Pauline and other past members of the lab to share funny moments.

I would like to thank all the people in CBD building for their kindness, especially Chiung-Yueh, for being so kind with me and being there whenever I needed. I would specially thank Caroline, Michele and Fabienne for their encouragement.

My stay in Toulouse would be boring without my dear friends outside the lab. Thanks Tong Xiaohui, Chen Qian, Tang Mingxing, Kevin, Ola and Suharv for all the fun, joy and laughter we shared. My deep gratitude goes to my best friend Chuxian for always being there whenever I needed.

I cannot thank enough to my family for their unconditional love, support and motivation. Thanks for believing in me. Lastly, I offer my heartily thankful to a special person, my boyfriend Sun Zhong, who inspired me and encouraged me, always being there whenever I needed; I feel close even we are in such long distance relationship, I am grateful to build solid and valuable relationships with this very special person. Finally, I offer my best wishes to all of those who supported me in any respect during the last three years as they made my stay in France unforgettable.

Résumé

Lors du développement de l'asymétrie gauche droite dans le cerveau du poisson zèbre, un petit groupe de cellules, le parapinéale, migre collectivement depuis la ligne médiane vers la partie gauche de l'épithalamus. Cette migration est déficiente dans des mutants pour le gène *fgf8*, indiquant que le facteur Fgf8 (Fibroblast Growth Factor 8), sécrété de part et d'autre de la ligne médiane, est requis pour la migration. Cependant, l'orientation gauche de la migration dépend de l'activation, plus précocement dans l'épithalamus gauche, de la voie de signalisation Nodal/TGF β (Transforming Growth Factor). Par conséquent, la parapinéale est un modèle de choix pour comprendre comment les cellules migrent collectivement en réponse aux Fgf et pour étudier comment d'autres voies de signalisation modulent ce processus.

L'imagerie en temps réel d'un transgène rapporteur de la signalisation FGF a révélé que la voie FGF est activée préférentiellement dans quelques cellules de tête, c'est à dire localisées au front de migration. L'expression globale d'un récepteur aux Fgf activé de façon constitutive (CA-FgfR1) interfère avec la migration de la parapinéale en contexte sauvage mais est capable de restaurer à la fois la migration de la parapinéale et l'activation focale de la voie FGF au front de migration dans les mutants *fgf8*^{-/-}. De plus, l'activation focale de la voie FGF dans seulement quelques cellules de parapinéale est suffisante pour restaurer la migration de tout le collectif dans les mutants *fgf8*^{-/-}. Finalement, nos données montrent que la signalisation Nodal contribue à restreindre et à biaiser l'activation de la voie FGF afin d'orienter la migration de la parapinéale vers le côté gauche (Manuscript n°1).

Par la suite, mes travaux de thèse ont visé à comprendre comment l'activation de la voie FGF est restreinte à quelques cellules, bien que toutes les cellules de parapinéale semblent compétentes pour activer la voie. Nos résultats montrent que la signalisation Notch est capable de restreindre l'activation de la voie FGF. La perte ou le gain de fonction de la voie Notch entraînent respectivement une augmentation ou une diminution de l'activité FGF, associés à des défauts de migration de la parapinéale dans les deux contextes. De plus, la diminution ou l'augmentation artificielle du niveau d'activation de la voie FGF peut respectivement restaurer la migration de la parapinéale ou aggraver les défauts de migration en absence d'activité Notch. Nos données indiquent que la signalisation Notch restreint l'activation de la voie FGF au sein des cellules de parapinéale pour permettre la migration du collectif (Manuscript n°2). La voie Notch est également requise pour la spécification d'un nombre correct de cellules de parapinéale, indépendamment de la voie FGF. En parallèle, nous avons analysé la fonction de MMP2 (Matrix Metalloprotease 2), une protéine exprimée mosaïquement dans la parapinéale et candidate pour moduler la signalisation FGF. Cependant, nous n'avons observé aucun défaut de spécification ou de migration de la parapinéale dans les embryons mutants pour le gène *mmp2*^{-/-} (Manuscript n°3).

Mon travail de thèse révèle un rôle de la voie Notch pour restreindre l'activation de la signalisation FGF dans quelques cellules de parapinéale, un processus qui est biaisé par la voie Nodal afin d'orienter la migration du collectif vers la gauche. Ces données pourraient permettre de mieux comprendre les interactions entre les voies de signalisation FGF, Notch et Nodal dans d'autres modèles de migration cellulaire collective comme, par exemple, la migration des cellules cancéreuses.

Mots clés: Signalisation FGF, signalisation Notch, migration collective, asymétrie, la parapinéale, poisson zèbre

Summary

During the establishment of left-right asymmetry in the zebrafish brain, a small group of cells, the parapineal, collectively migrates from the dorsal midline of the epithalamus to the left in most wild-type embryos. Parapineal migration requires Fibroblastic Growth Factor 8 (Fgf8), a secreted signal expressed bilaterally in epithalamic tissues surrounding the parapineal. The left bias in the orientation of parapineal migration depends on the activity of Cyclops, a secreted factor of the Nodal/TGF β family that is transiently expressed in the left epithalamus prior to parapineal migration. Therefore, the parapineal provides a powerful new model to understand FGF dependent collective cell migration and to study how other signaling pathways modulate this process.

Live imaging of an FGF reporter transgene revealed that the FGF pathway is activated in only few parapineal cells that are usually located at the leading edge of migration. Global expression of a constitutively activated Fgf receptor (CA-FGFR) delays migration in wild-type, while it partially restores both parapineal migration and focal activation of the FGF reporter transgene in *fgf8*^{-/-} mutant embryos. Importantly, focal activation of FGF signaling in few parapineal cells is sufficient to restore collective migration in *fgf8*^{-/-} mutants. Finally, Nodal asymmetry contributes to restrict and left-bias the activation of the FGF pathway (Manuscript n°1).

Following this work, my thesis project aimed at understanding how the activation of the FGF pathway is restricted to few cells, despite all parapineal cells apparently being competent to activate the pathway. We showed that Notch signaling is able to restrict FGF activity. Loss or gain of function of the Notch pathway respectively triggers an increase or decrease in FGF activity, which correlate with PP migration defects. Moreover, decreasing or increasing FGF activity levels respectively rescues or aggravates parapineal migration defects in Notch loss-of-function context. Our data indicate that Notch signaling restricts the activation of the FGF pathway within parapineal cells to promote their collective migration (Manuscript n°2). We also found that Notch pathway is required for the specification of a correct number of parapineal cells, independently of FGF pathway. In parallel, we analysed the function of MMP2 (Matrix Metalloprotease 2), a protein mosaically expressed in the parapineal and a candidate to modulate FGF signaling. However, we found no significant defects in the specification or migration of parapineal cells in *mmp2*^{-/-} mutant embryos (Manuscript n°3).

My PhD work reveals a role for Notch signaling in restricting the activation of FGF signaling within few parapineal cells, a process that is biased by Nodal pathway to the left and required for the migration of the entire parapineal. These data provide insights into the interaction of FGF, Notch and Nodal/TGF β signaling pathways that may be applicable to other models of collective cell migration, such as cancer cells migration for instance.

Key words: FGF signaling, Notch signaling, collective migration, asymmetry, parapineal, zebrafish

INTRODUCTION	6
I. Left-Right (LR) asymmetry in the animal kingdom and models.....	8
1.1 Left/Right asymmetry is widespread from invertebrates to humans.....	8
1.2 Brain asymmetries across evolution	10
1.2.1 Brain asymmetry in human.....	10
1.2.2 Brain lateralization is widespread in animals	12
1.2.3 The need of models to study brain lateralization	14
1.2.4 Brain asymmetry model: Epithalamus.....	14
II. The zebrafish epithalamus: a model to study the development of left-right (LR) brain asymmetry .	17
2.1 Zebrafish, a genetic model organism to understand vertebrate development	17
2.2 General presentation of the zebrafish epithalamus	19
2.2.1 Anatomical asymmetries in the zebrafish epithalamus.....	19
2.2.2 Function of the zebrafish epithalamus	21
2.2.3 Epithalamic asymmetries develop stepwise in zebrafish	23
2.2.4 Multiple signaling pathways involved in establishing epithalamic asymmetry.....	23
2.3 Mechanisms involved in symmetry breaking and epithalamus laterality.	27
2.3.1 Symmetry breaking at the Kupffer’s vesicle.....	27
2.3.2 Notch signaling is required for initial left-right symmetry breaking.....	29
2.3.3 Signal transfer from Kupffer’s vesicle to the epithalamus.....	29
2.3.4 Asymmetric Nodal signaling determines epithalamus laterality	31
2.4 Mechanisms underlying the development of habenular asymmetry.....	33
2.4.1 Role of asymmetric habenular neurogenesis	33
2.4.2 Role of the parapineal.....	37
2.4.2.1 Wnt inhibition promotes ‘left habenula character’ downstream of the parapineal.....	37
2.4.2.2 Parapineal size matters.....	39
2.5 Specification and migration of the parapineal.....	41
2.5.1 Role of Tbx2b transcription factor	41
2.5.2 Role of Fgf8 signal	41
2.6 Conclusion.....	44
III. Signaling mechanisms underlying collective cell migration	46

3.1 Collective cell migration is a widespread process	46
3.2 Function of FGF signaling pathway in collective cell migration	50
3.2.1 FGF signaling is implicated in various models of cell migration	50
3.2.2 Multiples roles of FGF signaling during the migration of the lateral line primordium in zebrafish.....	54
3.3 Interaction between FGF and Notch signaling in cell migration.....	57
3.3.1 Crosstalk between FGF and Notch signaling in lateral line primordium.....	57
3.3.2 Crosstalk between FGF and Notch signaling in <i>Drosophila</i> trachea	58
RESULTS	61
I. Focal activation of FGF pathway promotes parapineal migration	62
I.1 Context, Aim and Summary of Manuscript n°1	62
I.2 Manuscript n°1 (PNAS, online).....	63
II. Notch signalling promotes parapineal migration through restricting FGF activity but controls the specification of PP cells independently of FGF pathway.....	64
II.1 Context, Aim and Summary of Manuscript n°2	64
II.2 Manuscript n°2 (in preparation)	65
II.3 Additional data on the role of Notch signaling in the specification and migration of parapineal cells.....	104
II.4 Materials and Methods.....	123
III. Expression and function of the Matrix Metalloprotease 2 (MMP2) gene in the zebrafish epithalamus.....	125
III.1 Context, Aim and Summary of manuscript n°3	125
III.2 Manuscript n°3 (in preparation)	126
IV. Toward a better characterization of mature parapineal function: preliminary study of the expression of Opsins in parapineal	149
IV.1 Context and aim.....	149
IV.2 Preliminary results on Opsin expression in parapineal	151
IV.3 Discussion and Prospectives	152
DISCUSSION and PROSPECTIVES	153
I. How does the Notch pathway restrict FGF signaling to promote parapineal migration?	155

I.1 Time windows of Notch requirement..... 155

I.2 Molecular mechanisms of Notch mediated restriction of FGF pathway..... 157

II. Synergic or parallel role of the Nodal pathway in restricting FGF pathway? 159

III. How does Notch control the specification of parapineal cells?..... 161

REFERENCES 167

INTRODUCTION

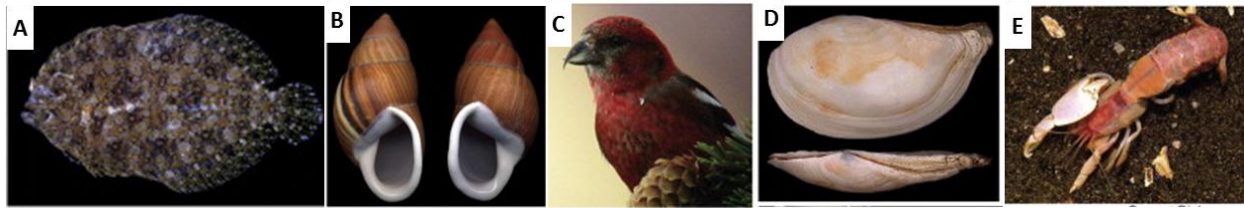


Fig. 1 Examples of morphological asymmetries in different animal groups.

(A) *Bothus lunatus*, a flatfish whose eyes lie on the left side of the head. (B) *Amphidromus heerianus*, a snail having both dextral (left image) and sinistral (right image) forms. (C) *Loxia leucoptera*, a crossbill finch where the upper mandible crosses randomly to the left or right of the lower one (to the left here). (D) *Pandora inaequalvis*, a bivalve that lies horizontally near the sediment-water interface on either the right or left valve. (E) *Neotrypaea californiensis*, a large male thalassinid mud shrimp with an enlarged right claw. Taken from (Palmer, 2009).

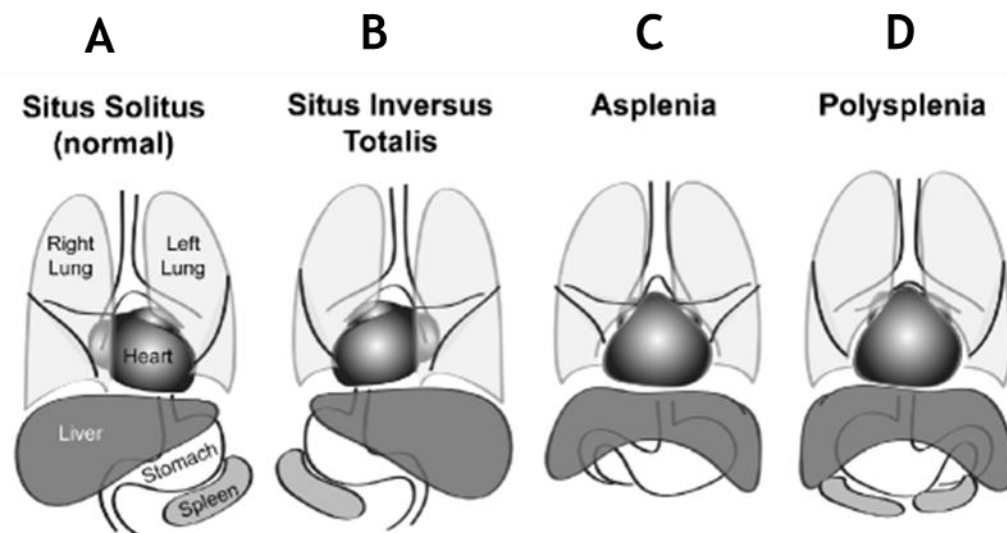


Fig. 2 Three types of variation in the position of the inner organs in human heterotaxy syndrome.

(A) *situs solitus* (normal). (B) *situs inversus totalis*; (C) Right-isomerism (Double right lung and Asplenia); (D) Left-isomerism (Double left lung and Polysplenia). Taken from (Degenhardt and Rychik, 2016).

I. Left-Right (LR) asymmetry in the animal kingdom and models

1.1 Left/Right asymmetry is widespread from invertebrates to humans

Left/Right (LR) asymmetry is found throughout the animal kingdom, from invertebrates to vertebrates and examples of LR asymmetry are shown in **Fig. 1** (Palmer, 2009). For instance, snails have both dextral (left image) and sinistral (right image) coiled shells; fiddler crabs have an enlarged claw (Davis, 1978); flatfishes have both eyes on the same side of the head (Bisazza et al., 1998; Palmer, 2009; Soukup, 2017). But LR asymmetry can be more subtle such as, for instance, the asymmetries in diaphragm muscle and in phrenic nerves innervation pattern described in mouse embryos (Charoy et al., 2017). Left/Right asymmetry is also found in humans, most notably in the location of unpaired organs, such as the heart, liver, spleen, stomach, and colon. Specific examples include the liver and gallbladder located on the right side, stomach and spleen located on the left, the cardiac apex that points to the left, the aortic arch that is found on the left and the large intestine that follows a right-to-left course (**Fig. 2A**) (Peeters and Devriendt, 2006). Asymmetry can also be found in paired organs, like kidneys and lungs. For instance, three lobes are found in the right lung while two lobes are found in the left lung (**Fig. 2A**) (Peeters and Devriendt, 2006). In its normal state, LR asymmetrical position of organs is called *situs solitus* (SS). The failure to generate normal LR asymmetry can be grouped in three categories. The first, called *situs inversus totalis*, is a symmetric reversal in global *situs* orientation that results in a complete mirror image of normal *situs solitus*, occurring in 1 of 6000-8000 live births (**Fig. 2B**) (Degenhardt and Rychik, 2016). The second, called *situs ambiguous* or heterotaxia, involves a defect in the asymmetry of unpaired organs that leads to at least one organ showing a reversed LR axis orientation, and is found in 1/10,000 births (**Fig. 2C**) (Lin et al., 2000). The third, called *isomerism*, is often associated *situs ambiguous* and refers to a defect in asymmetry of paired organs that usually have distinct right and left forms such as lungs. Right isomerism is often associated with asplenia (absence of normal spleen shown in **Fig.2C**) and left isomerism with polysplenia (duplicated spleens shown in (**Fig. 2D**) (Afzelius, 1995; Casey and Hackett, 2000; Ferencz, 1993; Shiraishi, 2016). LR asymmetry can also be found in the brain. I will describe in more details brain asymmetry in the subsequent section.

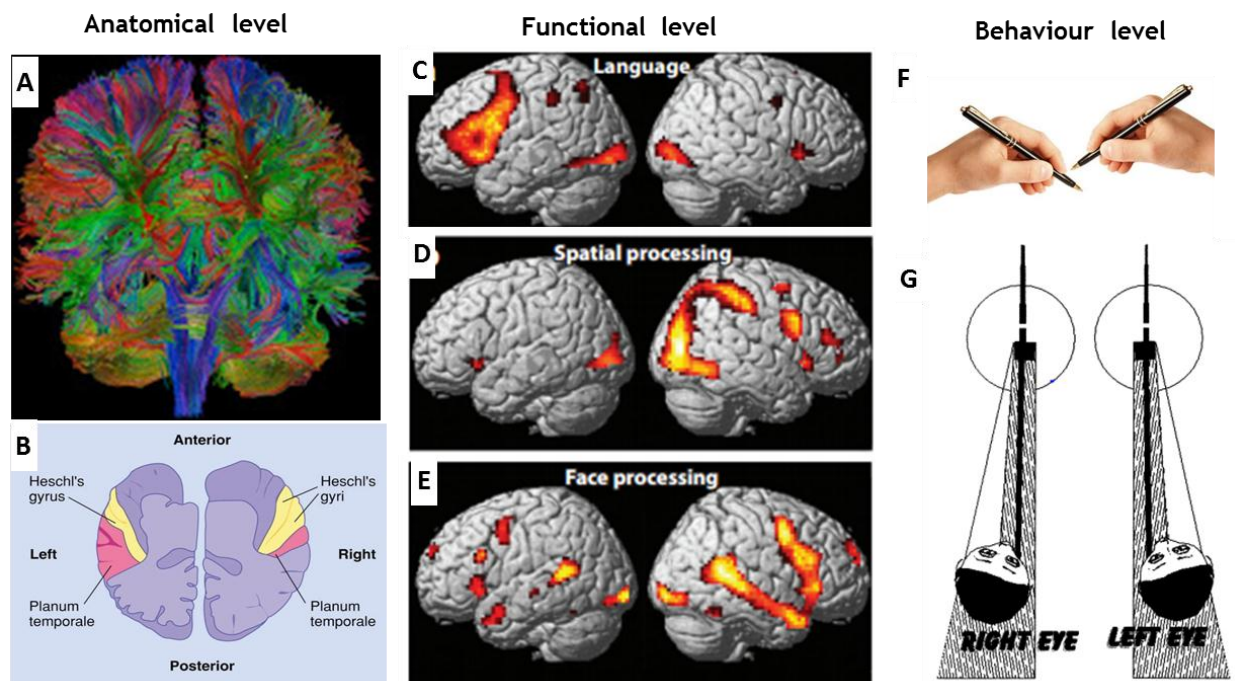


Fig. 3 Brain lateralization in human is found at anatomical level, functional level and behavior level.

(A) DTI (Dense Tensor Imaging) allows visualizing subtle LR asymmetries in brain axonal tracts (Taken from [Dennis and Thompson, 2013](#)); (B) schematic view of a brain section with the planum temporal (PT) displaying a larger area on the left side than the right side (Taken from [Aleman-Gomez, Y., et al., 2006](#)); (C-E) Functional MRI (Magnetic resonance Imaging) showing asymmetrical activation in human brain elicited by speech production, spatial processing and face processing, respectively ([Reproduced by Badzakova-Trajkov, et al., 2010](#)); (F) Handness in writing (Taken from [Cameron and Rogers, 1999](#)); (G) eye preference use in shooting ([Job et al., 1998](#)).

1.2 Brain asymmetries across evolution

1.2.1 Brain asymmetry in human

The human brain has two hemispheres that displaying asymmetry at the anatomical and functional level. Advanced imaging approaches, such as PET (positron emission tomography), MRI (magnetic resonance imaging), and DTI (diffusion tensor imaging), have allowed the visualization of subtle LR asymmetries in the brain, in gray matter, axonal tracts, and neuronal activities (**Fig. 3A**) (Dennis and Thompson, 2013; Hervé et al., 2013). Notably, anatomical asymmetry can be detected in the planum temporal (PT), a region within the temporal lobe of the human cerebral cortex involved in language, which occupies a greater area on the left side of the brain (Trilobed) than on the right (Bilobed) in 65% of adults (**Fig. 3B**) (Geschwind and Levitsky, 1968).

LR structural asymmetry is associated with functional asymmetry, or lateralization of certain cognitive tasks. For instance, language is processed predominantly in the left hemisphere, although the link between language lateralization and structural asymmetry in the planum temporal is not clear so far (**Fig. 3C**) (Tzourio-Mazoyer et al., 2018). On the other hand, the right hemisphere is dominant for others tasks, such as spatial attention (**Fig. 3D**) (De Renzi, 1982) and facial expression (a stronger emotion on the left side of their face) (**Fig. 3E**) (Sackeim et al., 1978). Other examples include problem solving, logical interpretations, and viewing details that are processed preferentially by the left hemisphere, and global viewing and visual spatial tasks such as solving puzzles and drawing geometrical figures that involve preferentially the right hemisphere (Gazzaniga, 2005).

Finally, hemispheric specialization in human is obvious at behavioral level, such as handedness, and foot and eye preference (Nachshon et al., 1983). The behavioral asymmetries of handedness is biased to one side within the population, as about 90% of the people preferentially use their right hand for various fine tasks (**Fig. 3F**) (Cameron and Rogers, 1999; Duboc et al., 2015). In shooting, eye preference rather than hand preference determines how one holds the gun (**Fig. 3G**) (Job et al., 1998).

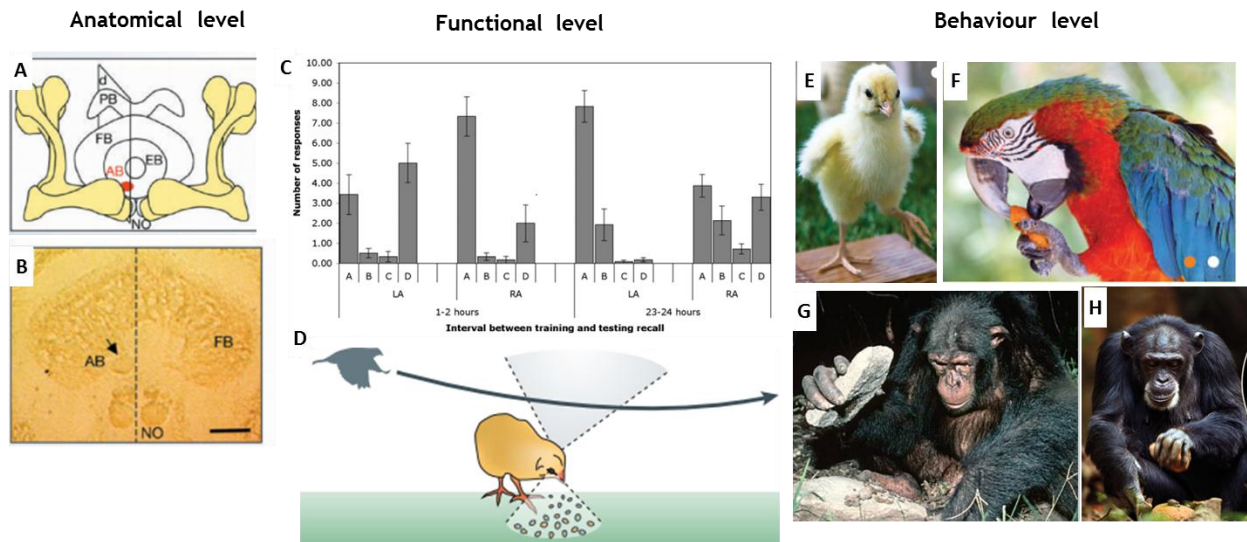


Fig. 4 Brain asymmetry in animals is found at anatomical, functional and behavior levels.

Schematic (A) or Frontal paraffin section (B) showing the asymmetric body (AB) on one side of the *Drosophila* brain (arrow) (Pascual et al., 2004). (C) Recall of memory at 1-2 hours and 23-24 hours after training. All bees were trained using both antennae and tested for recall using either the left (LA) or right antenna (RA), the other being covered with latex (Rogers and Vallortigara, 2008). (D) Visual lateralization in birds. The right eye is better at tasks such as discriminating grain and the left eye is better at tasks such as detecting moving predators (Concha et al., 2012). (E-F) Paw preference use in different animal; E) Newly hatched chicks predominantly used their right foot to step onto a platform (Taken from Casey and Martino 2000). F) Captive parrots tended to use their left feet to pick up and manipulate food items such as carrots (Taken from Friedmann and Davis, 1938). (G-H) Chimpanzees exhibit a 70% right-handed preference for many tasks. Picture of a right-handed chimp (G) and left-handed chimp (H) (Rogers, 2009).

1.2.2 Brain lateralization is widespread in animals

LR asymmetry is a general feature of animal brains, and many examples of anatomical asymmetries or lateralized behaviors have been reported in animal kingdom (reviewed in [Andrew, 1991](#); [Bradshaw and Rogers, 1993](#); [Ward and Hopkins, 1993](#)). Interestingly, in both vertebrates and invertebrates, structural brain asymmetries, such as the asymmetrical position of neural structures in the brain, or behavioral asymmetries have been correlated with cognitive skills. For instance, *Drosophila* in which the asymmetric body (AB) (**Fig. 4A**), a small nucleus in the brain, is only found on the right side display more efficient long-term memory than those with a bilateral AB (**Fig. 4B**) ([Pascual et al., 2004](#)). In honeybees, short-term memory of odors is better recovered if odors are presented to the right antenna, whereas it is the opposite for long-term memory (**Fig. 4C**) ([Rogers and Vallortigara, 2008](#)). In mice, spatial learning and working memory are reduced if hippocampal asymmetry is disrupted ([Goto et al., 2010](#)). The functional asymmetry also shown in chicks: the right eye (left hemisphere) is better at discriminating grains from background and the left eye (right hemisphere) is better at detecting moving predators (**Fig. 4D**) ([Concha et al., 2012](#)).

Hemispheric specialization is also evident at behavioral levels in many animals. For year's researchers have been uncovering hand, foot, fin, or paw preferences across the animal kingdom ([Rogers, 2009](#)). For instance, newly hatched chicks predominantly use their right foot to step onto a platform (**Fig. 4E**) ([Casey and Martino, 2000](#)). Similarly, parrots tend to use their left foot to pick up and manipulate food items (**Fig. 4F**) ([Friedmann and Davis, 1938](#)). Chimpanzees also display some degree of handedness and exhibit a 70% right-handed preference for many tasks (**Fig. 4G-4H**) ([Rogers, 2009](#)). The brain of a right-handed chimp has a larger motor-hand area in the left cerebral hemisphere, while that feature is more prominent in the right hemisphere of a left-handed chimp ([Rogers, 2009](#)).

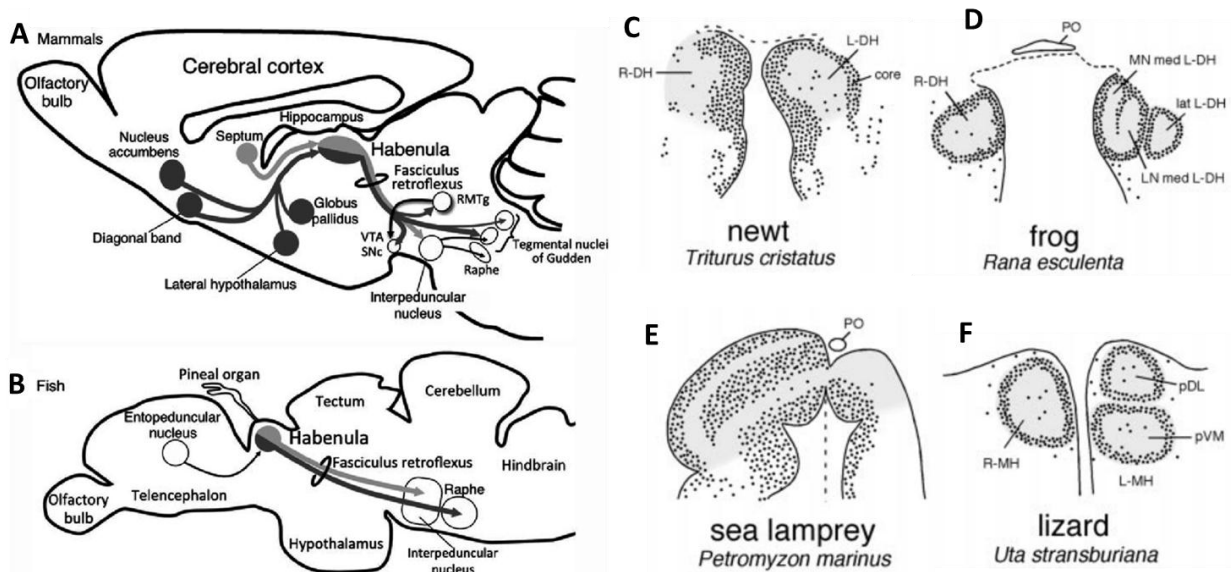


Fig. 5 The epithalamus of vertebrates and selected examples of habenular asymmetry.

Schematic of sagittal sections of the mammals brain (A. modified from [Nieuwenhuys, 1998e](#)) and of the fish brain (B. modified from [Kardong, 1995](#)) showing habenular nuclei and their connectivity. (C-F) Schematic showing asymmetry in habenular nuclei in different vertebrates. In the newt, neurons of the left dorsal habenula organize into a layer that extends far more laterally than in the right dorsal habenula (C). In Frog, the left dorsal habenula is divided into a lateral sub-nucleus similar to the right dorsal habenula and to a medial subnucleus showing unique features (D). In sea lamprey, the right habenula is hypertrophied compared to the left one (E). In lizard, the medial habenula nucleus is subdivided into two components in left side while not in the right side (F). (Taken from [Concha and Wilson, 2001](#)).

1.2.3 The need of models to study brain lateralization

Left right asymmetry seems very important for brain function in humans as neuronal pathologies such as autism (Herbert et al., 2004), stuttering (Sato et al., 2011b), dyslexia (Heim and Keil, 2004), and schizophrenia (Mitchell and Crow, 2005) are correlated with abnormal patterns of functional and structural asymmetries. The prevalence of left- or mixed-handedness is increased from 10% in the general population to between 20% (Dragovic and Hammond, 2005) and 40% (Webb et al., 2013) in schizophrenic patients, for instance. However, it is difficult to evaluate the function of genes in the development of LR asymmetry in human. As such, pertinent model systems allow us to investigate the development of brain asymmetry at the genetic and cellular levels and/or the impact of structural asymmetries on cognition and lateralized behaviors. Several species have emerged as useful models: chicks (Rajendra and Rogers, 1993; Rogers, 1982), pigeons (Rogers, 2002, 2014), the nematode *Caenorhabditis elegans* (Hobert, 2014; Taylor et al., 2010) and zebrafish (Ariyomo and Watt, 2013). Because they are genetic models system, the nematode and the zebrafish allow scientists to address brain asymmetry at different levels of complexity: from gene function to cell identity, from neuronal circuitry to cognitive ability and behavior.

1.2.4 Brain asymmetry model: Epithalamus

The epithalamus is one of the fundamental longitudinal subdivisions of the diencephalon in vertebrates brain, together with the dorsal thalamus (dTH), ventral thalamus (vTH) and hypothalamus (hTH); it takes its name from its location 'above' ('*epi*') the thalamus (Fig. 5) (Concha and Wilson, 2001). The epithalamus consists of two structures: the pineal complex and habenulae. Whereas the pineal complex corresponds to a median evagination situated along the diencephalic roof plate, the habenulae are bilateral structures surrounding the lateral walls of the third ventricle (Fig. 5A-5B). The pineal complex on the dorsal midline of the diencephalon is composed of the pineal organ, or epiphysis, and the parapineal or parietal eye. The habenulae are asymmetric in different vertebrates, such as newt, frog, sea lamprey or lizard

(Fig. 5C-5F) (Braitenberg and Kemali, 1970; Concha Miguel L, 2001; Meek and Nieuwenhuys, 1998). Asymmetric connectivity between the pineal complex and the left habenula has also been described in many phyla, including lampreys, teleosts and lizards (Engbretson et al., 1981; Korf and Wagner, 1981; Yañez and Anadon, 1994).

The epithalamus is one of the best described and most conserved asymmetric brain structure, as it has been described in many phyla including reptiles, frogs, and fish (Concha Miguel L, 2001; Snelson and Gamse, 2009). Over the past 30 years, the zebrafish has emerged as a model to address the development of LR asymmetry in the epithalamus and functional consequences. For my PhD project, I have focused on this model which I will describe in more detail in chapter II.

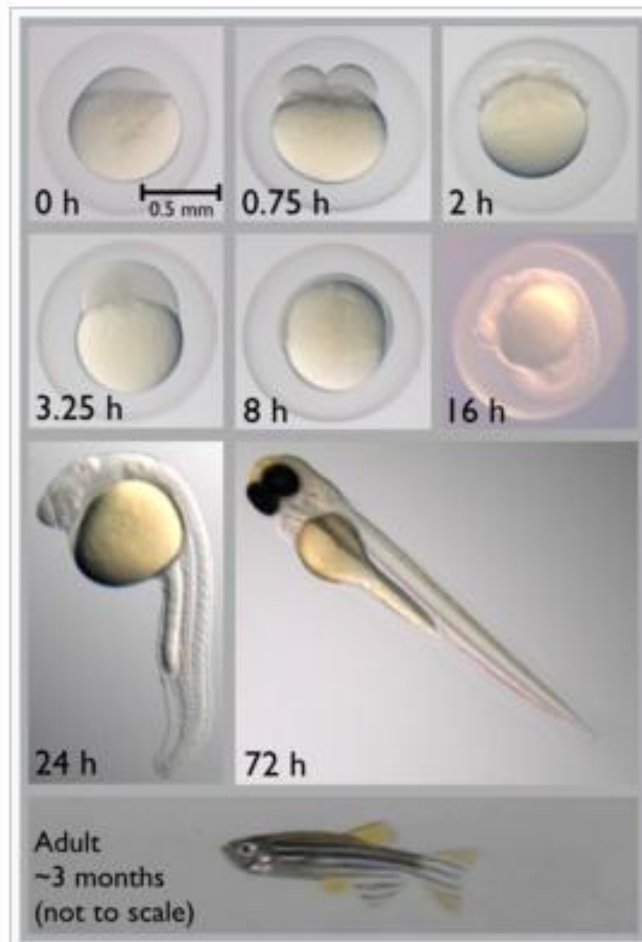


Fig. 6 Stages of zebrafish development. (Taken from [Kimmel et al., 1995](#))

II. The zebrafish epithalamus: a model to study the development of left-right (LR) brain asymmetry

2.1 Zebrafish, a genetic model organism to understand vertebrate development

zebrafish (*Danio rerio*) is a tropical freshwater fish originating from India that has become an important and widely used vertebrate model organism in development. Zebrafish can produce hundreds of eggs; the embryos are transparent, grow fast, develop externally and, thus, can be observed and manipulated easily at all stages (**Fig. 6**) (Kimmel et al., 1995). Comparison of the human and zebrafish reference genomes shows that approximately 70% of human genes have at least one obvious zebrafish orthologue (Howe et al., 2013). In contrast to *Drosophila* and *C.elegans*, the zebrafish is a vertebrate and its major organs and tissues display significant homology with human's one. The zebrafish first rose to prominence through a series of large-scale genetic screens to isolate mutations affecting embryonic development, thus allowing us to study genes regulating specific developmental processes. The zebrafish genome has been sequenced by the Sanger Center (<https://www.sanger.ac.uk/science/data/zebrafish-genome-project>) and this provides a powerful tool for the identification of genes mutated in the initial genetic screens. The genome sequence also proved useful for reverse genetic approaches such as antisense morpholino-modified oligonucleotides (MO). MO-injected embryos have been shown to phenocopy the mutation of genes (Nasevicius and Ekker, 2000). More recently, synthetic nucleases based on zinc-fingers (ZFNs) or transcription activator-like effectors (TALENs) have been employed to make targeted mutations at specific loci (Gaj et al., 2013). These two systems have now largely been replaced by the CRISPR/Cas9 system, which has been shown to work efficiently for the generation of insertions and deletions in growing number genes (Chang, 2013; Hwang et al., 2013; Jao et al., 2013). Moreover, techniques such as time-lapse imaging, lineage-tracing, cellular transplantation (Kimmel et al., 1989), construction of transgenic lines (Davidson et al., 2003; Kurita et al., 2004; Meng et al., 1998), laser based cell ablation (Concha et al., 2003) or opto-genetic control of neuron activity (Del Bene and Wyart, 2012; Wyart and Del Bene, 2011) have also been employed. All of tools have been successfully used to study gene

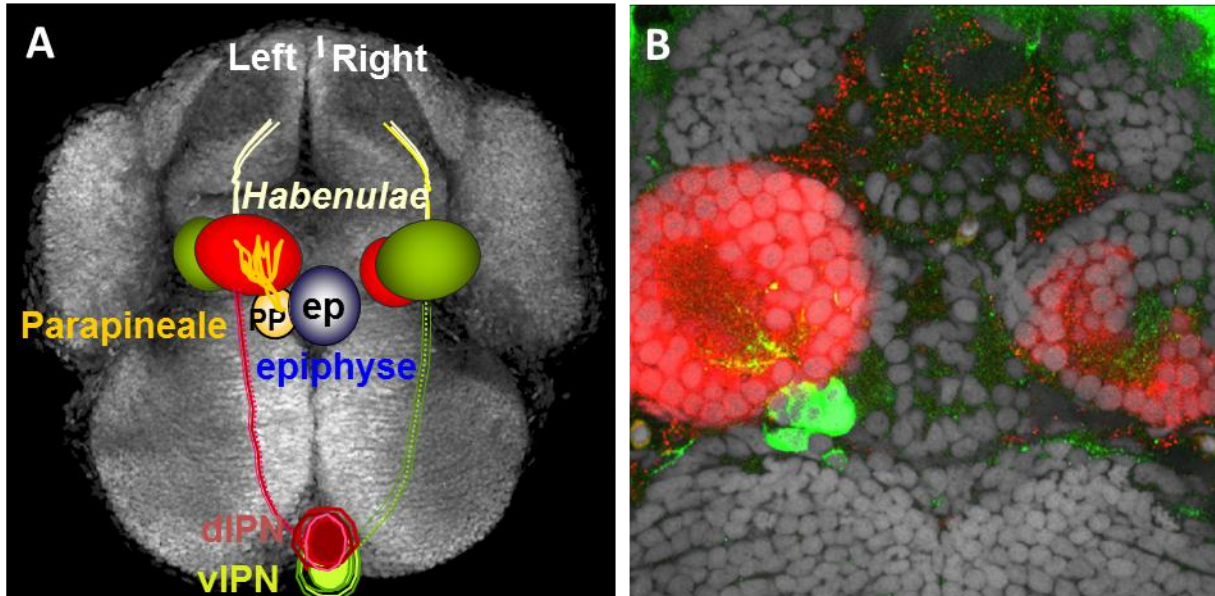


Fig. 7 Epithalamic asymmetry in zebrafish.

(A) Schematic of the main asymmetric features of the epithalamus superimposed on a dorsal confocal projection of a 3 days old zebrafish larval brain labelled with cell nuclei. The epithalamus is composed of habenulae (green and red), parapineal (PP, yellow) and epiphysis (ep, blue). (B) Confocal section showing the expression of *leftover* (red) predominantly in the left habenula, and the parapineal expressing the *Tg(ET11:GFP)* transgene (green) at 72 hpf.

function during organogenesis and also to model various human diseases. Thus, zebrafish has proven to be a very powerful genetic vertebrate model to study many biological processes.

2.2 General presentation of the zebrafish epithalamus

2.2.1 Anatomical asymmetries in the zebrafish epithalamus

As described more generally above, the zebrafish epithalamus is a dorsal sub-division of the diencephalon and consists of a pair of nuclei called the habenulae and of the pineal complex. The pineal complex is composed of the epiphysis or pineal gland and the parapineal nucleus. The epiphysis is a small light-sensitive structure located at the dorsal midline of the diencephalon (Cau et al., 2008). The parapineal arises from the segregation of 15-20 cells from the anterior part of the pineal complex, beginning at 24 hours post fertilization (hpf). Around 28-30 hpf, the parapineal starts migrating to the left side of the epiphysis in about 95% of individuals within a population. Subsequently, axons extend from parapineal neurons to contact the left medial habenular (Concha et al., 2000; Gamse et al., 2002).

The zebrafish habenulae consist of a dorsal left-right asymmetric domain and a ventral symmetric nucleus. Within the dorsal habenula (dHb), two main sub-nuclei have been historically defined that display LR differences in molecular markers: a lateral sub-division (ldHb; expressing the *kctd12.1* (potassium channel tetramerisation domain 12.1)/*leftover* gene) that is larger on the left side and a medial sub-division (mdHb) that expresses *dex/kctd8* and/or *ron/kctd12* and is bigger in the right habenula (Fig. 7B) (Gamse et al., 2005; Gamse et al., 2003). These asymmetries in the expression of various habenular markers correlate with asymmetric projection patterns from the habenulae. Indeed, habenular neurons extend long axons towards a midbrain structure called the interpeduncular nucleus (IPN) through the fasciculus retroflexi (FR) tract (Snelson and Gamse, 2009). The left habenula, through the left FR, mainly innervates the dorsal IPN, while the right habenula, through the right FR, preferentially innervates the ventral IPN, thus converting LR asymmetry in the habenulae into dorsal/ventral differences (Fig. 7A) (Aizawa et al., 2005; Gamse et al., 2005).

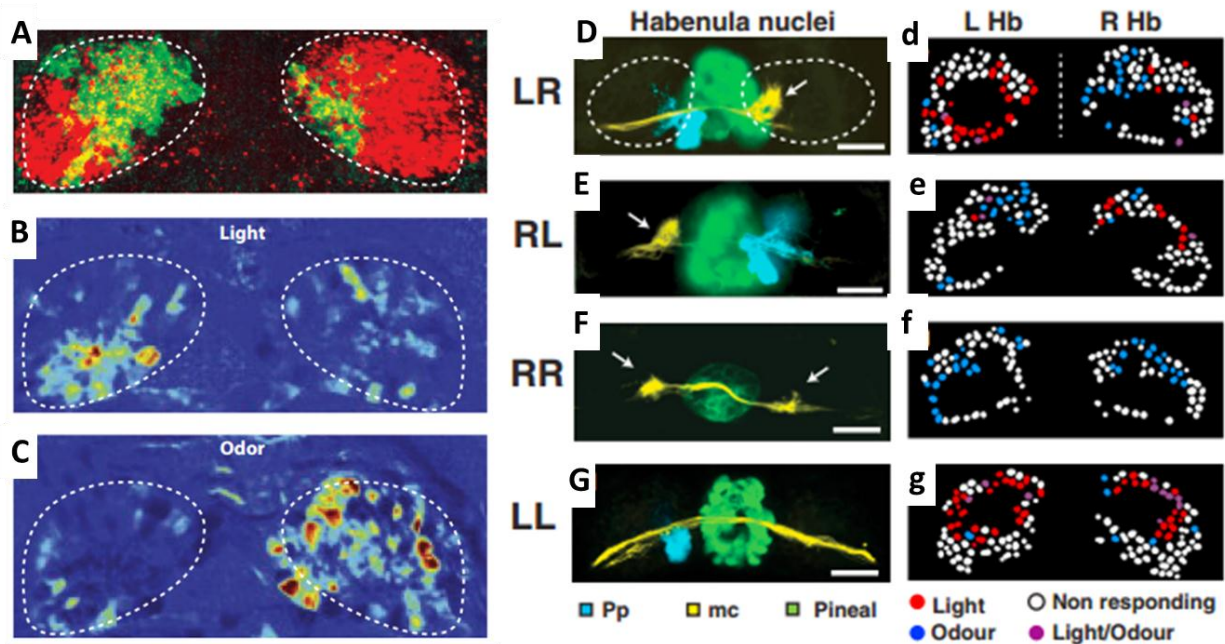


Fig. 8 Left right asymmetry in habenular responses to light or odor in zebrafish.

(A) Molecular asymmetry in zebrafish habenulae: expression of *kctd8* (red, broader in the right habenula) and *Tg(Et(gata2a:EGFP)^{pkus8})* (green, broader in the left habenula) (Taken from Husken et al., 2013). (B-C) Color-coded calcium signals showing the left-right lateralized response of dorsal habenular neurons to a non-lateralized presentation of light (B) and odor (C) stimuli (Taken from Dreosti et al., 2014). (D-G) Confocal images showing the epithalamus of embryos at 96 hpf with a normally lateralized brain (LR) (D) reversed brain asymmetries (RL) (E) double-right habenulae (RR) in parapineal ablated embryos (F) double left habenulae (LL) in IWR1-treated embryos (G). *Tg(foxD3:GFP)* transgene marks the epiphysis (green) and the parapineal (pseudo-colored in blue); *Tg(Ihx2a:Gap43-YFP)* (yellow) labels a neuropil region denser in the right habenula (arrow) (d-g) Images showing the lateralization of neuronal responses to light (red) and odor (blue) in the corresponding D-G embryos (Taken from Dreosti et al., 2014).

2.2.2 Function of the zebrafish epithalamus

The pineal gland in zebrafish contains projection neurons and photoreceptors and is involved in light detection and the regulation of circadian rhythms. In this regard, the pineal gland has two related functions: it collects light/dark information from the environment via dedicated photoreceptor neurons and secretes melatonin in response to day-night time conditions to control circadian cycles (Idda et al., 2012).

As part of a conserved conduction system connecting the forebrain to midbrain nuclei, the habenulae have been implicated in various behaviours such as fear responses in zebrafish (Agetsuma et al., 2010) and reward or nicotine driven behaviours in mammals (Lawson et al., 2014). In zebrafish, the asymmetry in the dorsal habenular that is observed at the molecular level (Fig. 7 and Fig. 8A) is associated with functional asymmetries. For instance, light stimuli are processed predominantly in left habenular neurons while right habenular neurons are specialized in odor processing (Fig. 8B-C) (Dreosti et al., 2014). The activity of habenular neurons relative to either odor or light are predictably changed when habenular asymmetry is lost, in the case of "double-left (LL)" or "double-right (RR)" habenulae (Fig. 8D-G) (Dreosti et al., 2014). Lateralization of habenular function has also been reported to be important for social behavior in zebrafish. For instance, Chou *et al.* characterized the function of the lateral and medial asymmetric nuclei in the dorsal habenulae (dHb) during fighting: they show that silencing the lateral nucleus of the dorsal habenula (LdHb) reduced the likelihood of winning a fight, whereas silencing the medial part (mdHb) increased the likelihood of winning (Chou et al., 2016).

As yet, no function for the mature parapineal nucleus has been reported in zebrafish. This said, the parapineal is known to be required for the subsequent development of habenular asymmetry: indeed, parapineal ablation at early stages (28-32 hpf) results in symmetric expression of genes such as *lov* in habenular neurons (Gamse et al., 2003; Snelson et al., 2008).

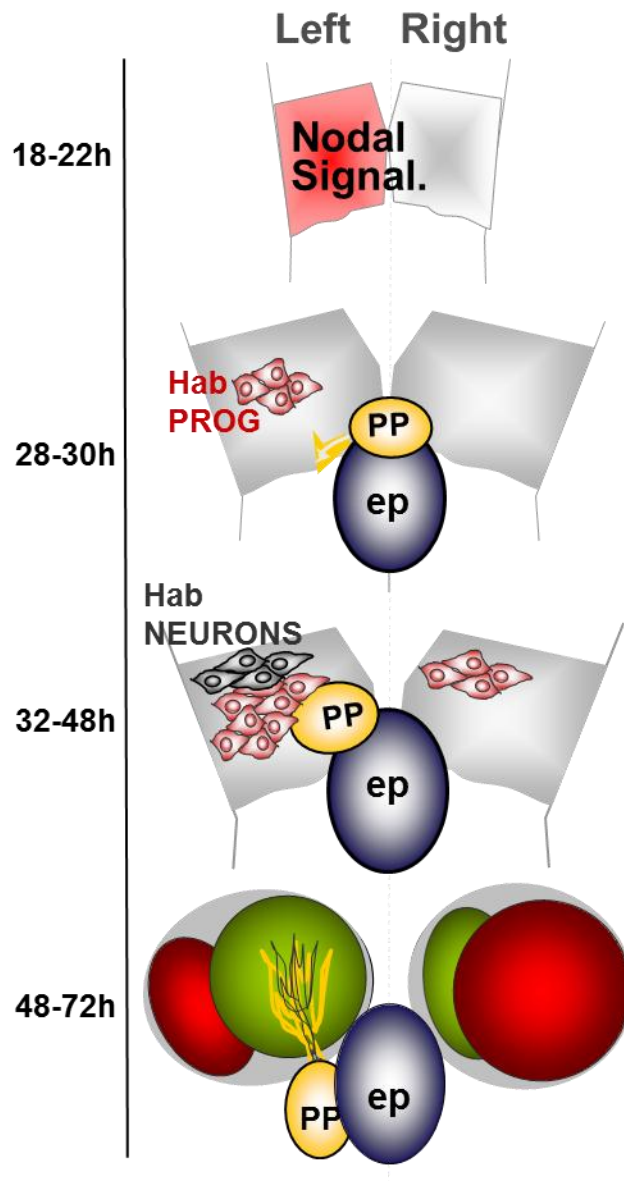


Fig. 9 Schematics describing the stepwise development of left-right asymmetry in the zebrafish epithalamus.

Nodal signaling is activated on the left epithalamus (light red) at 18-22 hpf; the parpineal (PP) starts to migrate leftward while habenuar progenitors (pink cells) first appear on the left side of the brain at 28-30 hpf; the PP is required for the establishment of habenuar asymmetry at 32-48 hpf, the habenuar display sub-types neurons at 48-72 hpf.

2.2.3 Epithalamic asymmetries develop stepwise in zebrafish

The earliest molecular evidence for epithalamic asymmetry in zebrafish embryos is the expression of the *nodal*-related gene *ndr2/Cyclops* on the left side of the epithalamus at 18 hpf. This is followed at 28 hpf by the first morphologically detectable asymmetry, when the parapineal (PP), specified from the anterior part of the pineal gland, starts to migrate to the left. Subsequently, asymmetry in the generation of the dorsal habenulae is detected, with progenitors and early-born neurons being found earlier in the left habenula than in the right habenula from about 30 hpf. By 72 hpf, asymmetries of the epithalamus are largely developed: dorsal habenular neurons display lateral or medial identity and have sent projection to the dorsal or ventral part of the interpeduncular nucleus, respectively. At the same time, the left habenula receives axonal afferents from the PP (**Fig. 9**) and the right habenula receives afferents from the olfactory bulb ([Hendricks and Jesuthasan, 2007](#); [Miyasaka et al., 2009](#)).

2.2.4 Multiple signaling pathways involved in establishing epithalamic asymmetry

Molecular and genetic studies have revealed that many signaling pathways are involved in the development of epithalamic asymmetry, including Nodal, Notch, FGF, Wnt pathways. Here, I will briefly describe the canonical versions of these pathways.

The Nodal signaling pathway is predominantly known for its role in mesoderm induction ([Boutet, 2017](#); [Halpern et al., 2003](#); [Signore et al., 2016](#); [Zinski et al., 2017](#)). Nodal-related proteins are a subclass of TGF- β -related ligands that bind as dimers to Nodal type I and type II receptor tetramers in the presence of co-factors such as One-eyed Pinhead/Crypto. Binding leads to activation of the serine/threonine kinase domain of the Nodal receptor, which in turn induces phosphorylation of Smad2. Phosphorylated Smad2 then binds to Smad4 and translocate into the nucleus to activate target genes in complexes with FoxH1. Target genes of the Nodal pathway include *lefty1* and *lefty2*,

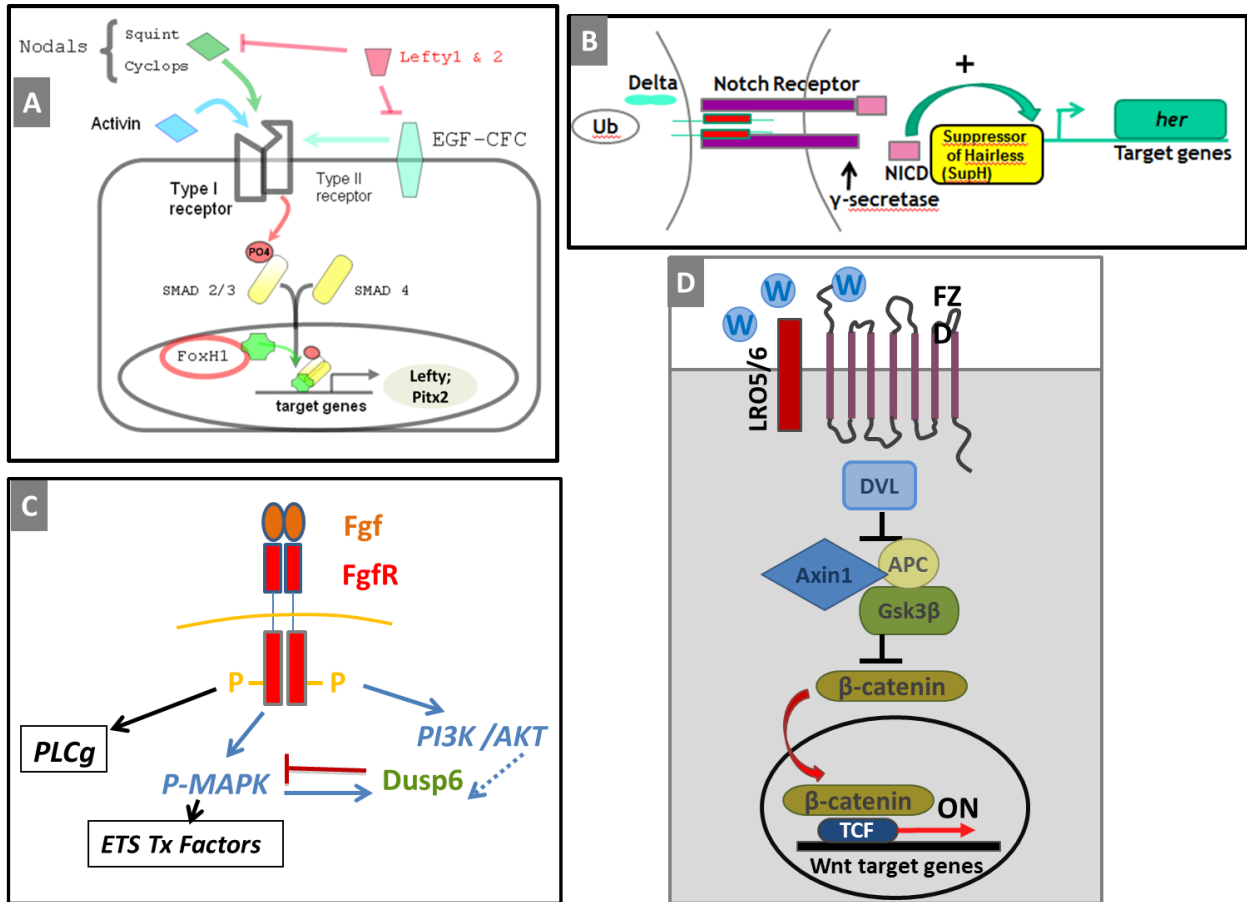


Fig. 10 Schematic representation of four signaling pathways, which are Nodal, Notch, FGF, Wnt.

- (A) Nodal Signaling pathway.
- (B) Notch signaling pathway.
- (C) FGF signaling pathway.
- (D) Wnt signaling pathway.

which act as feedback inhibitors of the Nodal pathway, and *pitx2*, a homeobox transcription factor (**Fig. 10A**).

Notch signaling plays a major role in the development of embryonic nervous system through a process known as lateral inhibition ([Beatus and Lendahl, 1998](#); [Krämer, 2001](#); [Lathia et al., 2008](#)). Notch proteins are transmembrane receptors that bind transmembrane ligands, including members of the Delta and Jagged families. Ubiquitin ligase activity, provided by members of the Mindbomb (Mib) family, in cells expressing Notch ligands promotes ligand endocytosis and pathway activation. Binding of ligand to the extracellular domain of Notch receptor in neighboring cells triggers proteolytic cleavage and release of the Notch intracellular domain (NICD) in a γ -secretase dependent manner. NICD then translocates into the nucleus where it interacts with Suppressor of Hairless (SuH) or Rbpj to regulate the transcription of Notch target genes, such as members of the Hairy/Enhancer of split family (*her* genes in zebrafish) (**Fig. 10B**).

Fibroblast growth factor (FGF) signaling is involved in the regulation of many development processes, such as morphogenesis, differentiation, proliferation and migration ([Böttcher and Niehrs, 2004](#); [Guillemot and Zimmer, 2011](#); [Thisse and Thisse, 2005](#)). Fgf ligands bind to tyrosine kinase Fgf receptors, leading to receptor dimerization and activation of intracellular cascades. The FGF signaling pathway can trigger the activation of at least three downstream cascades: the MAPK pathway, the PLC γ pathway and the PI3K/AKT pathway. Target genes of the FGF pathway include positive effector (ETS family transcription factors) and negative feedback inhibitors, such as *dusp6* (**Fig. 10C**).

Like the signaling pathways described above, Wnt signaling is involved in a wide variety of developmental processes ([Carl et al., 2007](#); [Fradkin et al., 2005](#); [Hüsken and Carl, 2013](#); [Inestrosa and Varela-Nallar, 2014](#)). Wnt ligands bind to Frizzled/LRP receptor complexes. Binding promotes Dishevelled (DVL) dependent recruitment of the β -catenin destruction complex to the membrane; this complex consists of cytosolic proteins like Axin-1, adenomatous polyposis coli (APC), protein phosphatase 2A (PP2A), glycogen synthase kinase 3 beta (GSK3 β)

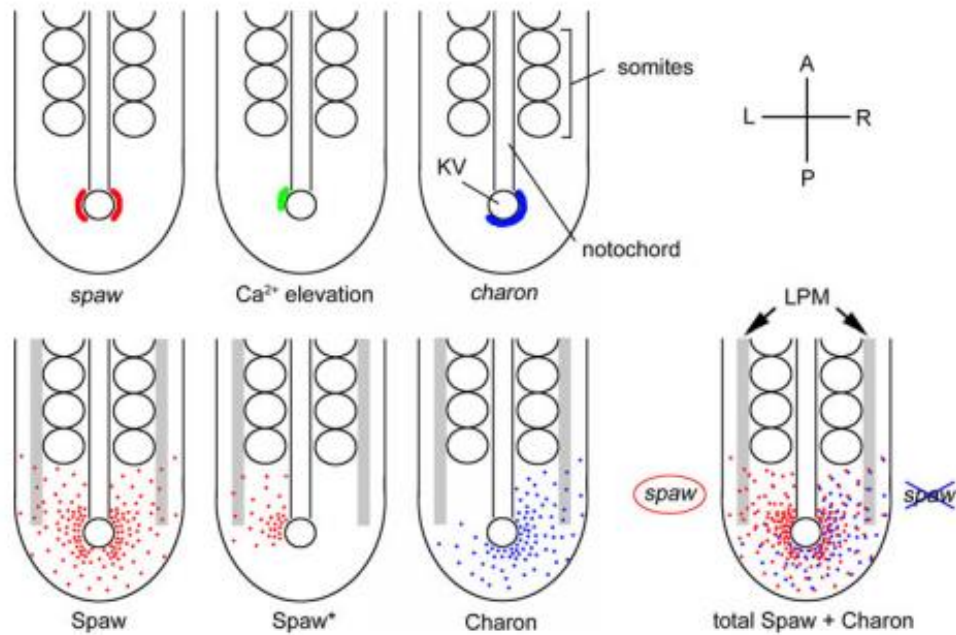


Fig. 11 Symmetry breaking at the Kupffer's vesicle and signal transfer to the lateral plate mesoderm.

First, *spaw* is expressed bilaterally (red) around the Kupffer's vesicle (KV) and it diffuses symmetrically in the tail-bud (red dots); there is Ca^{2+} elevation (green) only on the left side of KV and *Charon* expression becomes asymmetric (blue) in a fluid flow-dependent way, then diffusing toward the right side. *Charon* antagonizes *spaw* by binding to it and, this way, *spaw* cannot activate its own expression in the right lateral plate mesoderm (LPM); thus *spaw* expression is enriched in the left LPM. Upper panels show gene expression while lower panels represent the expected diffusion patterns of the corresponding proteins (Taken from (Matsui and Bessho, 2012)).

and casein kinase 1 α (Ck1 α). Activation of the pathway blocks β -catenin degradation. Therefore, β -catenin can translocate into the nucleus, where it binds to transcription factors of Tcf family and triggers activation of Wnt downstream target genes (**Fig. 10D**) (MacDonald et al., 2009).

2.3 Mechanisms involved in symmetry breaking and epithalamus laterality.

2.3.1 Symmetry breaking at the Kupffer's vesicle.

The mechanisms by which bilateral symmetry is initially broken during development seem highly variable between the various model organisms studied. In *Xenopus*, the initial bilateral symmetry is broken very early after the first cleavage stage and involves ions flows (Vandenberg et al., 2013). In zebrafish, as in mammals, the establishment of initial asymmetry depends a ciliated organ, called Kupffer's vesicle (KV) or Node in mammals, that forms during the second half of gastrulation and early somitogenesis stages (Hirokawa et al., 2006). In the KV, a leftward movement of fluid, called nodal flow, is generated by the rotation of cilia that are tilted toward the posterior of KV cells. Cilia orientation in the KV, which is essential for directional KV flow and subsequent asymmetric morphogenesis, is controlled by a functional interaction between Myosin1D and VanGogh-like2, a component of the PCP pathway (Juan et al., 2018).

Nodal, a transforming growth factor- β (TGF- β) family protein, is required for establishing LR asymmetry in all vertebrates. In zebrafish, the *nodal*-related gene *ndr3/southpaw (spaw)* is expressed bilaterally around the KV at 4-6 somite stage (**Fig. 11**) (Long et al., 2003). In response to counterclockwise fluid flow within Kupffer's vesicle (KV), intracellular Ca^{2+} levels increase in cells on the left side of the vesicle, which induces localized phosphorylation of Ca^{2+} /CaM-dependent protein kinase II (CaMK-II); this stimulates the further release of Ca^{2+} from the endoplasmic reticulum (ER) as well as extracellular Ca^{2+} influx (Francescato et al., 2010; Juryneć et al., 2008; Sarmah et al., 2005). This Ca^{2+} signaling is crucial for restricting activation of Spaw to the left side of KV (**Fig. 11**). *Charon*, a member of the Cerberus/Dan family, is also essential

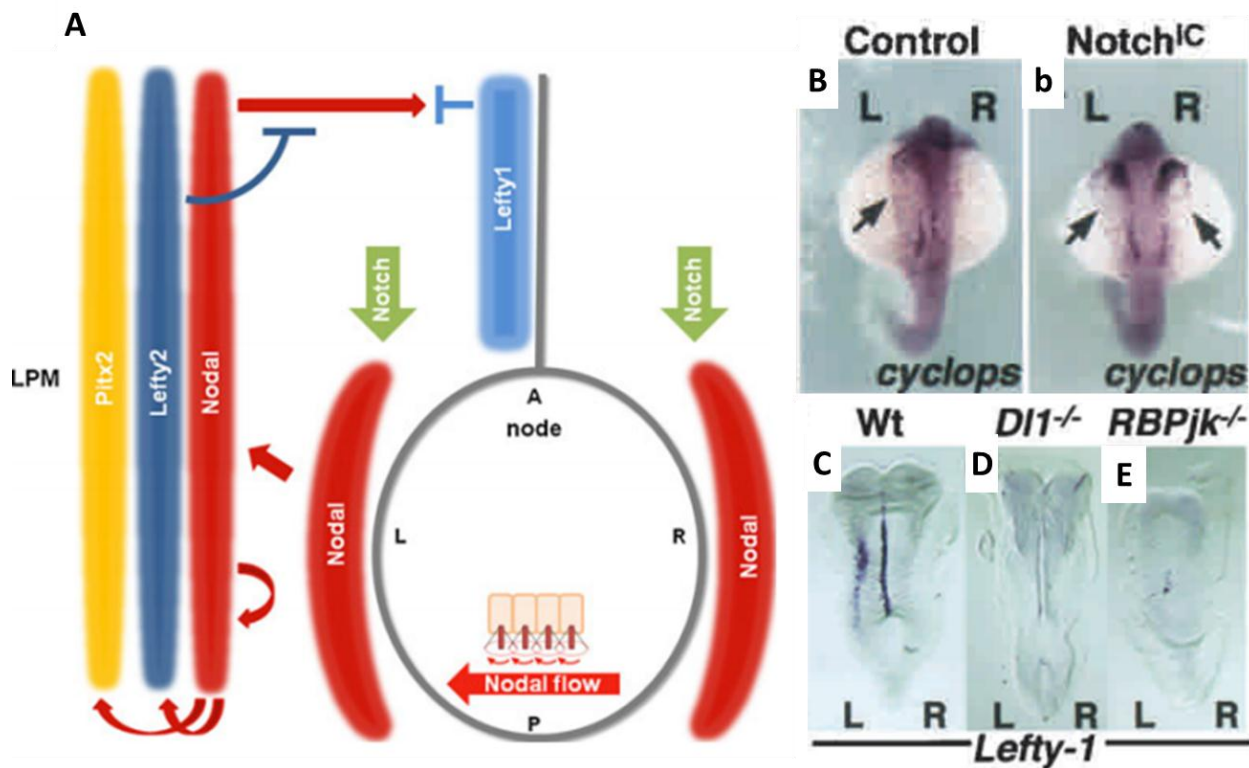


Fig. 12 Role of Notch pathway in the early establishment of left-right asymmetry.

(A) Schematic summarizing the role of Notch pathway in left-right (LR) asymmetry cascades in mouse embryos. Notch induces perinodal expression of Nodal, which is necessary for expression of Nodal in the left LPM; Nodal in turn drives the expression of its target genes, Lefty2 and Pitx2 in LPM (Taken from [Kato et al., 2011](#)). **(B,b)** Dorsal view of embryos showing the expression of Nodal-related gene *Cyclops* in zebrafish control embryos or in embryos injected with mRNA encoding Notch intracellular domain (Notch^{IC}) at 24 hpf (Gain of function for Notch pathway). **(C-E)** Expression of Lefty1 is absent in both *DII1*^{-/-} and *RBPjk*^{-/-} mice embryos (Loss of function for Notch pathway) ([Krebs et al., 2003](#); [Raya et al., 2003](#)).

for generating asymmetric Spaw activity around the KV (Hashimoto et al., 2004). *Charon* is expressed on both sides of KV cells at 6 somite stage, but its expression switches to a "right sided" pattern around at 8-10 somite stages in a KV fluid flow-dependent manner; this creates a gradient of

Charon on the right that inhibits Spaw activity (Lopes et al., 2010). Taken together, the positive feedback loop of leftward Ca^{2+} signals and the rightward inhibitor of *Charon* restrict the activity of Spaw. In turn, strong left-sided Spaw activity induces *spaw* expression in the left LPM by positive feedback (Fig. 11) (Matsui and Bessho, 2012).

2.3.2 Notch signaling is required for initial left-right symmetry breaking

While we know that Nodal signaling plays an essential role during the early symmetry breaking issue, others cellular signaling pathways including Notch, Hedgehog, FGF, Wnt, and BMP have been implicated in the establishment of early asymmetry. For instance, Notch activity is necessary and sufficient for the expression of Nodal around the node, through a direct binding of Rbpj/Su(H) to the promoter of *nodal* gene (Kato, 2011; Krebs et al., 2003; Raya et al., 2003). Nodal ligand Cyclops is expressed in both left and right LPM in gain of function (GOF) for Notch activity in zebrafish and the Nodal target Lefty1 is absent in loss of function (LOF) for Notch pathway in mouse (Fig. 12B-E) (Raya et al., 2003). As described above, *nodal/spaw* expression around the KV/Node is critical for its asymmetric expression later in the left LPM. Therefore, Notch pathway is required for expression of Nodal/Spaw in the area surrounding the KV and not directly for expression in the LPM (Krebs et al., 2003; Raya et al., 2003) (Fig. 12A).

2.3.3 Signal transfer from Kupffer's vesicle to the epithalamus

As mentioned above, left-sided Spaw activity in the KV induces its own expression in the left lateral plate mesoderm (LPM) (Fig. 11) (Matsui and Bessho, 2012). Therefore, the LR information generated in the KV is transmitted to the LPM during early somite stages. This

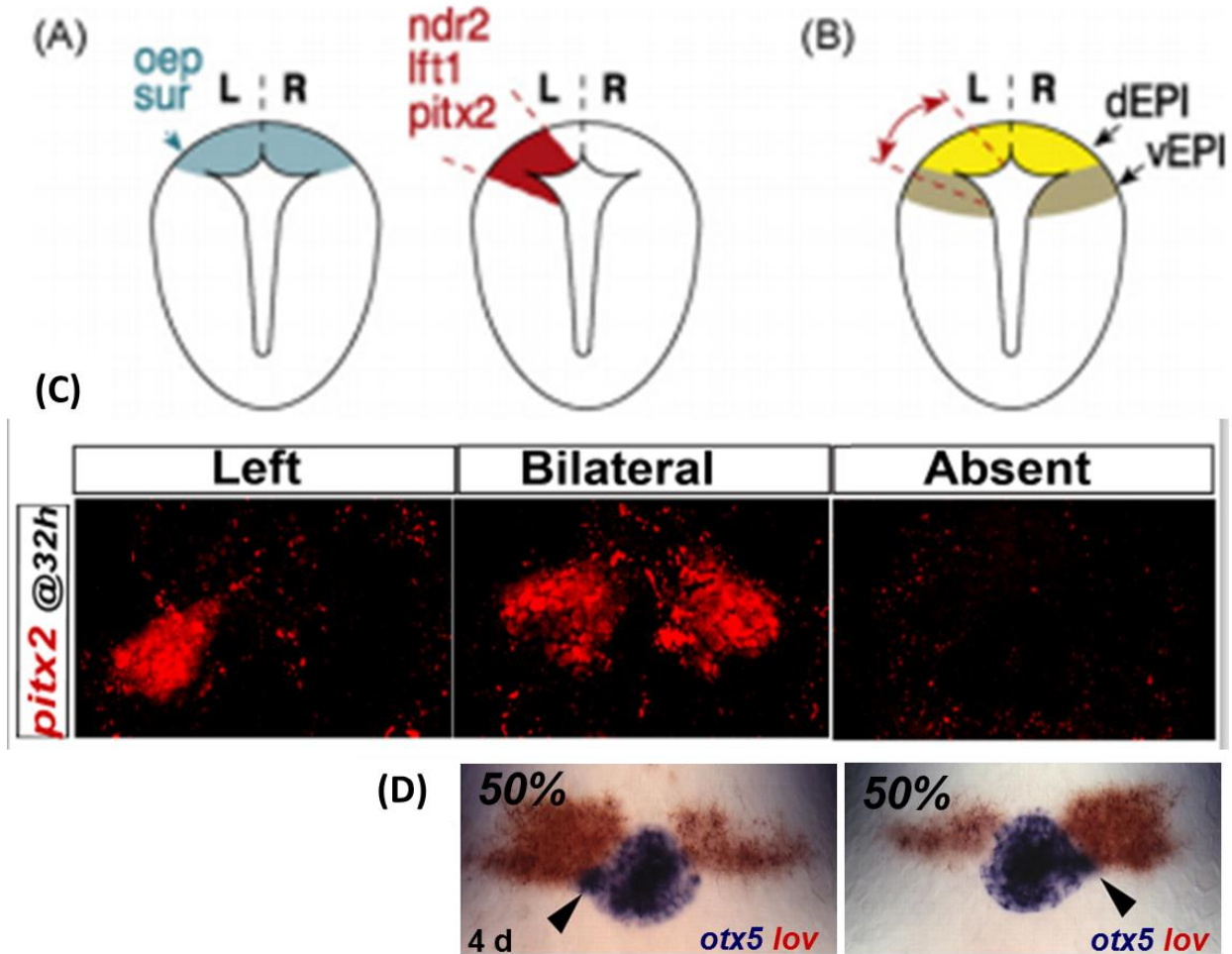


Fig. 13 The role of Nodal signaling in controlling the laterality of epithalamic asymmetry.

(A) Schematic coronal view of the diencephalon at 24 hpf showing bilateral expression of the Nodal cofactor EGF-CFC/*one-eyed pinhead* (*oep*) and of the transcription effector *FoxH1/sur* (blue) in the epithalamus. Nodal pathway is activated only on the left as revealed by the left-sided expression of *ndr2* and of its downstream target *lefty1* and *pitx2* (red). (B) Asymmetric Nodal expression (red dotted line) is contained in both dorsal (dEPI, yellow) and ventral (vEPI, brown) regions of the left epithalamus (red arrow) (Concha et al., 2003). (C) Confocal sections showing the expression of *pitx2* at 32 hpf in control embryos (Left) or in embryos where Nodal pathway is either bilateral or absent. (D) In context where Nodal is absent or bilateral, parapineal (PP) migration (blue, arrowhead) and the pattern of habenular asymmetry (red) are randomized while PP migration is left oriented in 95% of wild-type (Gamse et al., 2003).

asymmetric expression of Nodal in the LPM underlies the establishment of LR asymmetry in visceral organs.

Finally, LR asymmetry in the LPM is conveyed to the epithalamus as it will trigger asymmetric expression of another Nodal-related ligand 2 (Ndr2/Cyclops) in the left epithalamus. In contrast to our understanding of the developmental events that lead to Nodal asymmetric expression in

the LPM, how asymmetry is "transferred" from the LPM to the epithalamus is not understood yet. However, as for LR asymmetry in visceral organs, the establishment of brain asymmetry involves Nodal activity on the left side; this reveals the reiterative function of Nodal pathway in the establishment of LR asymmetries in embryo.

2.3.4 Asymmetric Nodal signaling determines epithalamus laterality

In the zebrafish epithalamus, components of the Nodal signaling pathway are expressed asymmetrically; they include the Nodal-related ligand 2 (Ndr2/Cyclops) (Liang et al., 2000; Rebagliati et al., 1998; Thisse and Thisse, 1999) and its target genes, the diffusible negative regulator Lefty1 (Bisgrove et al., 1999) and the transcription factor Pitx2c (Essner et al., 2000) (Fig. 13A) (Concha et al., 2009), which all appear on the left from 18 hpf, 20 hpf, or 22 hpf respectively. Other indispensable components of the pathway such as the EGF-CFC cofactor *one-eyed pinhead* (Oep) (Concha et al., 2000) and the downstream transcription factor Schmalspur (FoxH1/Sur) (Concha et al., 2000) are expressed bilaterally in the epithalamus, indicating that both sides are competent to activate Nodal signaling (Fig. 13A) (Concha et al., 2009). Asymmetric expression of Ndr2/Cyclops comprises both dorsal and ventral regions of the left epithalamus that is thought to correspond to the left half of the parapineal anlage and a part of the left habenula (Fig. 13B) (Concha et al., 2003).

The role of Nodal signaling during the establishment of LR asymmetry in zebrafish epithalamus has been addressed using mutants for components of the Nodal pathway, mutants that render the pathway active bilaterally, and pharmacological inhibitors of the

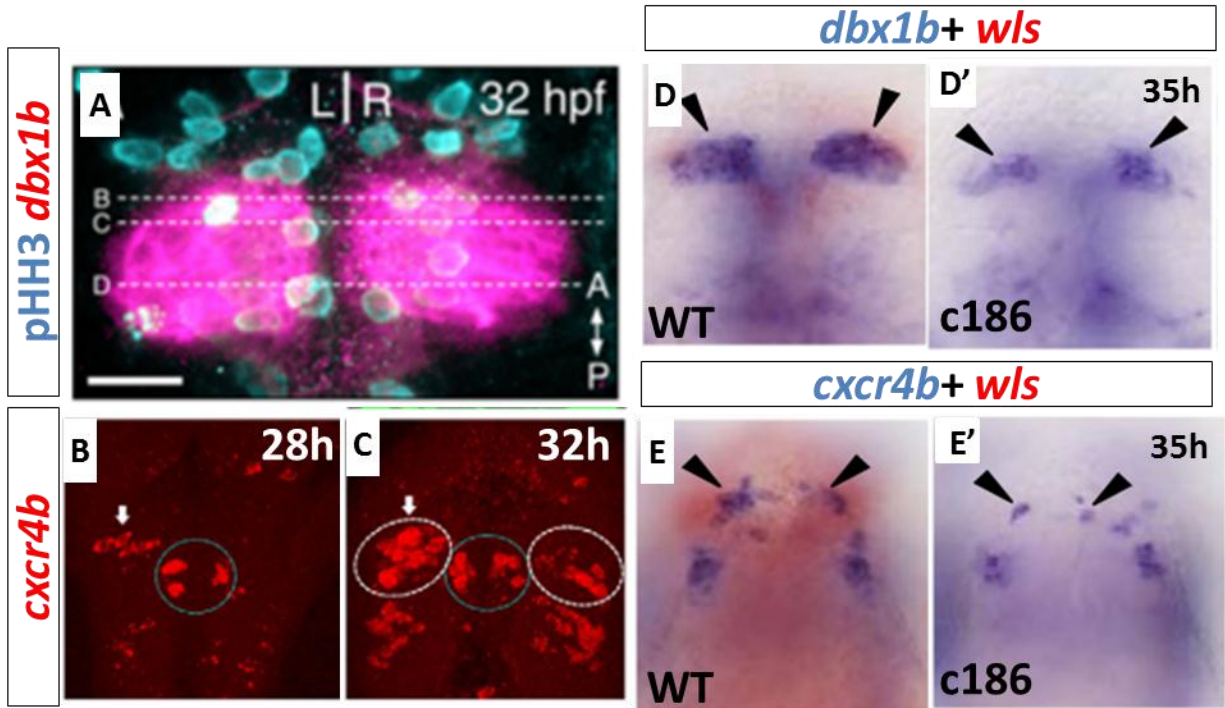


Fig. 14 Habenuar precursors first appear on the left epithalamus and are reduced in *wntless* mutants.

(A) Dorsal view of the epithalamus showing *dbx1b* expression in habenuar precursors (pink) and phosphohistone H3 (blue) (Taken from Dean et al., 2014). (B-C) Confocal sections showing the asymmetric expression of *cxcr4b* in newly born habenuar neurons/progenitors at 28 and 32 hpf (Taken from Roussgine et al., 2009). (D-E') Dorsal views of *dbx1b* and *cxcr4b* expression in wild-types and *wls* mutant embryos at 35 hpf (Taken from Kuan et al., 2015).

Nodal receptor (Roussigné et al., 2009). When Nodal expression is symmetric (either absent or bilateral), as shown by the expression of the pathway target *pitx2* at 32 hpf (Fig. 13C), epithalamic asymmetry still develops but the handedness/laterality of the asymmetry is reversed in 50% of embryos, with the parapineal randomly migrating to the right and the left and habenular asymmetry being mirror imaged in half of the embryos (Fig. 13D). Thus, the function of Nodal is to provide a bias to the laterality of epithalamic asymmetry but not to impose asymmetry *per se* (Concha et al., 2000; Gamse et al., 2003).

2.4 Mechanisms underlying the development of habenular asymmetry

2.4.1 Role of asymmetric habenular neurogenesis

In the zebrafish epithalamus, precursors of the dorsal habenula (dHb) can be identified by the expression of the homeodomain transcription factor *dbx1b* (Dean et al., 2014). *Dbx1b* expression is detected broadly from 20-24 hpf in presumptive dorsal habenula (Fig. 14A) (Dean et al., 2014). Later, around 28 hpf, the chemokine (C-X-C motif) receptor 4b (*cxcr4b*) is detected in few habenular progenitors or early born neurons (Roussigné et al., 2009) (Fig. 14B-C). Interestingly, *cxcr4b+* habenular cells and later HuC/D expressing habenular neurons are first detected on the left side, indicating that the timing of early habenular neurogenesis is LR asymmetric (Roussigné et al., 2009).

Generation of dorsal habenular domain relies on the activity of the Shh, Wnt and FGF signaling pathways. Shh signaling has been reported to promote early development of the dHb in between 16 and 24 hpf, as pharmacological inhibition of Shh pathway at later stages no longer affects habenular size (Halluin et al., 2016; Roberson and Halpern, 2017). In addition to Shh, Wnt signaling plays a role in the establishment of the dHb precursor pool: Wntless (*wls*) is a transmembrane protein required for Wnt ligands secretion; in *wls* mutants, the size of both the *dbx1b* and *cxcr4b* precursor pools is reduced (Fig. 14D-E') (Kuan et al., 2015). Finally, FGF signaling is also required for habenular development as the size of habenular nuclei is severely

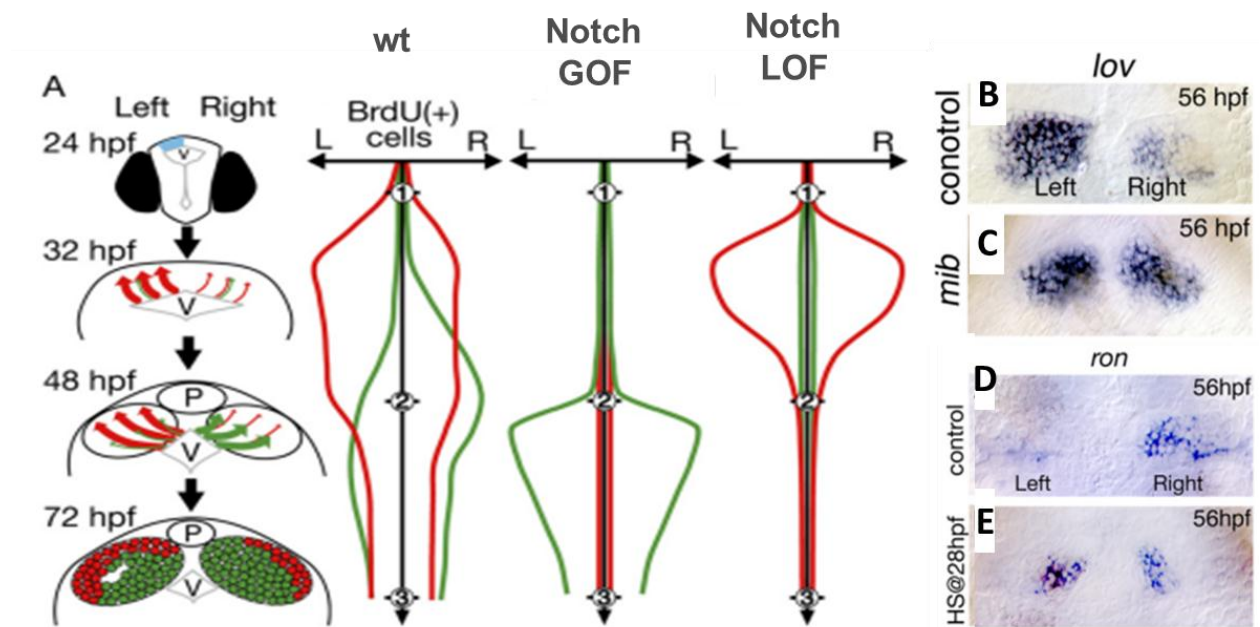


Fig 15. Asymmetric waves of neuronal differentiation contribute to control the fate of habenular neurons.

(A) Schematic showing two waves of habenular neurogenesis giving rise to habenular neurons of the dorsal lateral (Red) or medial (Green) sub-nuclei in wild-type (wt), in contexts where neurogenesis is repressed (gain of function (GOF) for Notch from 28 hpf) or in context of premature excessive neurogenesis (in loss of function (LOF) for Notch pathway). (B-C) Dorsal views showing *lov* expression in habenulae at 56 hpf in control and *mib*^{ta52b} mutant embryos (Taken from Aizawa et al., 2007). (D-E) Dorsal views showing *ron* mRNA expression in habenulae of controls and Tg(*hsp70:gal4*)^{kca4}; Tg(*UAS:myc-notch1a-intra*)^{kca3} embryos at 56 hpf after heat shock at 28 hpf (Taken from Aizawa et al., 2007).

reduced in *fgf8*^{-/-} mutants (Regan et al., 2009). Wnt signaling seems to act through FGF signaling in the generation of dHb neurons (Halluin et al., 2016; Roberson and Halpern, 2017); it is thought that the role of Wnt is to define the domain of FGF signaling in the dHb but not the level of *fgf8a* per se (Halluin et al., 2016; Roberson and Halpern, 2017).

Habenular precursors have an equal possibility to become neurons of the lateral dorsal habenula (ldHb) or of the medial dHb (mdHb) neurons (Fig. 15A), as determined at later stages by the expression of *leftover/kctd12.1* or *ron/kctd12* and *dex/kctd8* respectively (Aizawa et al., 2007). A study suggested that this LR asymmetry in cell fate is controlled by LR difference in the timing of habenular neurogenesis (Aizawa et al., 2007). Aizawa et al show that habenular neurons differentiate asymmetrically with habenular progenitors leaving the cell cycle on the left side (from around 24 to 36 hpf) before the right side (from 36 to 48 hpf) (Fig. 15A). Furthermore, they show that modulating the timing of neurogenesis, through gain or loss of function for Notch signaling, affect the identity of habenular neurons. Indeed, blocking Notch signaling results in premature habenular neurogenesis and in an increase in lateral markers, a "double left" phenotype (Fig. 15B-C). In contrast, when the Notch pathway is artificially activated globally at 28 hpf, neurogenesis is delayed and dHb neurons expressing medial markers are mainly formed on both side of the epithalamus at the expense of those expressing lateral markers, leading to a "double right" phenotype (Fig. 15D-E) (Aizawa et al., 2007). Therefore, the authors concluded that an asymmetric timing in habenular neurogenesis controls the identity of habenular neurons and that neurons that differentiate early have a higher potential to become lateral dHb neurons, while neurons born later predominately become medial dHb neurons (Fig. 15A) (Aizawa et al., 2007). However, in their study, the author did not analyze whether affecting Notch signaling impacts the specification and migration of the PP that might indirectly affect habenular asymmetry.

While LR asymmetric waves in habenular neurogenesis could impact on the fate of habenular neurons (Aizawa et al., 2007), the early LR asymmetry detected in first born habenular neurons does not seem to contribute to habenular asymmetry (Roussigné et al., 2009). Indeed, previous

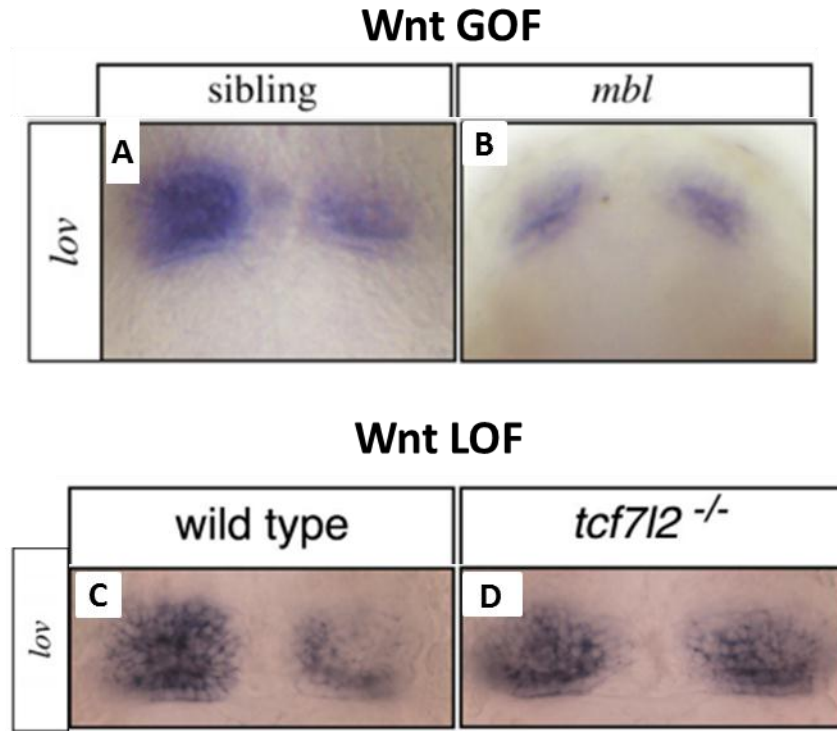


Fig.16 Gain or Loss of function for Wnt signaling result respectively in ‘double right’ or ‘double left’ symmetric habenulae.

(A-B) Dorsal views of the habenulae showing bilaterally symmetric *lov* expression (‘double right’) *mbl* mutant (Wnt GOF) (Taken from [Carl et al., 2007](#)). (C-D) Dorsal views of the habenulae showing symmetric *lov* expression (‘double left’) in *tcf712* mutant (Wnt GOF) (Taken from [Hüsken et al., 2014](#)).

data in the lab have shown that, at earlier stages, asymmetry in the appearance of the first habenular neurons is driven by Nodal signaling; when Nodal signaling is rendered symmetric, either absent or bilateral, this LR asymmetry in early born neurons is lost but habenular asymmetry still develop later although with a randomized pattern (Roussigné et al., 2009).

2.4.2 Role of the parapineal

The timing of appearance of the first *lov* expressing neurons in the left habenula coincides with parapineal differentiation and migration (Gamse et al., 2003). While the timing of habenular neurogenesis appears to play a role in the identity of the neurons that are generated, this appears to have limited importance relative to the requirement for the parapineal. Indeed, when the parapineal is ablated prior to its migration, no effect is detected in the asymmetry of early habenular neurogenesis but both left and right habenular neurons adopt a right identity (Concha et al., 2000; Gamse et al., 2002; Roussigné et al., 2009). Thus, the critical step in the establishment of epithalamic asymmetry appear to be the formation and oriented migration of the parapineal.

2.4.2.1 Wnt inhibition promotes ‘left habenula character’ downstream of the parapineal

While the important role for the parapineal in the establishment of epithalamic asymmetry has been known for nearly 15 years, our understanding of the signal provided by the parapineal that influences left habenular identity remains elusive. This said, several studies suggest that the acquisition of lateral and medial dHb fates requires modulation of Wnt signaling (Carl et al., 2007; Hüsken and Carl, 2013; Hüsken et al., 2014). Indeed, over-activation of Wnt/Axin1/ β -catenin signaling, as is the case in masterblind (*mb1*) mutant embryos, causes a “double right” habenular phenotype (Fig. 16A-B) (Carl et al., 2007; Hüsken and Carl, 2013; Hüsken et al., 2014). On the contrary, loss of function for Wnt signaling caused by mutation in *tcf7l2*, a gene

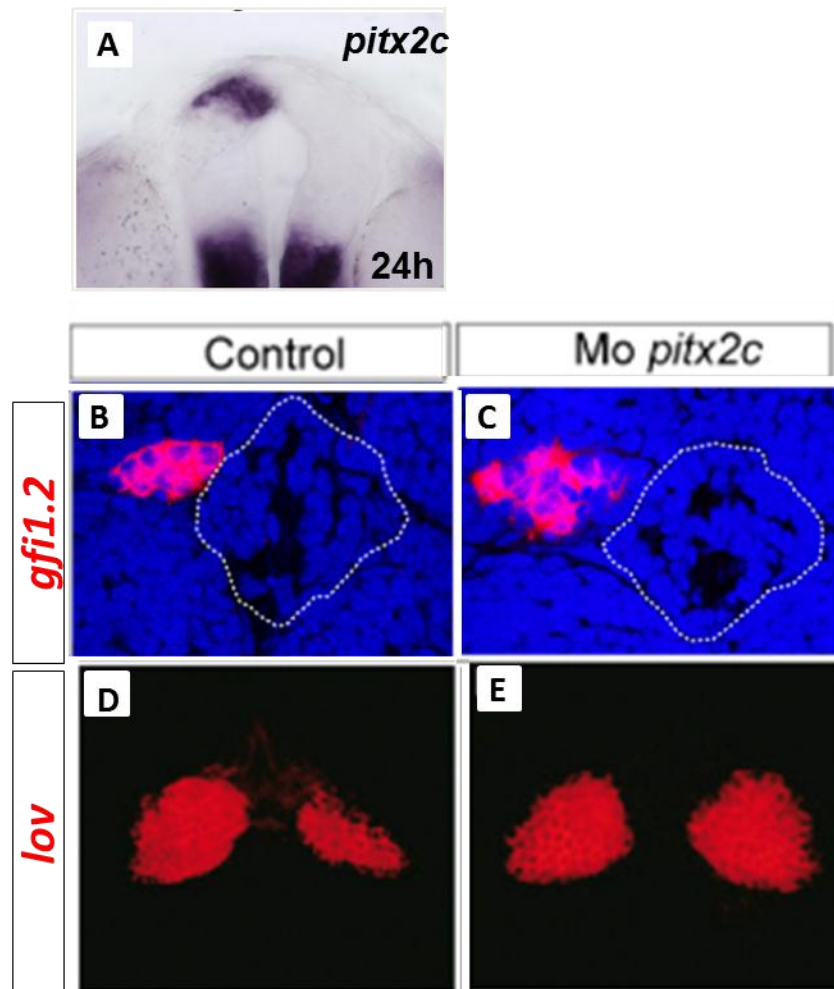


Fig.17 *pitx2c* morphants display bilaterally symmetric habenulae and larger parapineal.

(A) *pitx2c* mRNA expression in the left side of the brain at 24 hpf. (B-C) Confocal sections showing *gf11ab* expression in the parapineal of control and *pitx2c* morphant embryos at 72 hpf; parapineal is bigger in *pitx2* morphants. (D-E) Confocal sections showing "double left" expression of *lov* in *pitx2c* morphant embryos at 48 hpf. Taken from (Garric et al., 2014).

encoding a transcriptional regulator of Wnt signaling, results in “double left” phenotype (**Fig. 16C-D**) (Carl et al., 2007; Hüsken and Carl, 2013; Hüsken et al., 2014). Tcf712 is expressed bilaterally in habenular neurons. Importantly, ablating the parapineal in *tcf712* mutants also results in “double left” embryos (Carl et al., 2007; Hüsken and Carl, 2013; Hüsken et al., 2014). Together, this suggests that Tcf712 acts cell autonomously to prevent left character. The role of the parapineal, therefore, would be to suppress Wnt activity on the left, thus permitting the development of left habenular character.

2.4.2.2 Parapineal size matters

The parapineal signal that modulates Wnt signaling in the left habenula is still unknown. A recent study suggests, however, that it is highly potent. Indeed, loss of function for *pitx2c*, a Nodal target gene that is expressed in the left epithalamus (**Fig. 17A**), leads to a “double left” expression of *lov* in habenulae in a manner similar to the loss of *tcf712* function (**Fig. 17D-E**), but that is accompanied by an increase in parapineal cell number (**Fig. 17B-C**) (Garric et al., 2014). Unlike for *tcf712*, however, complete ablation of the parapineal in the absence of Pitx2c results in “double right” habenulae phenotypes embryos. On the other hand, partial parapineal ablation in the absence of Pitx2c rescues the habenular asymmetry to wild-type levels (Garric et al., 2014). These results indicate that restricting parapineal cell number is important for the development of habenular asymmetry; correct parapineal size might limit the extent that the parapineal can modulate the Wnt pathway so that it only affects the left habenula.

Therefore, both the specification of a correct number of parapineal cells and their leftward collective migration are critical for the subsequent development of anatomical and functional asymmetries in zebrafish brain. These steps are nevertheless poorly understood.

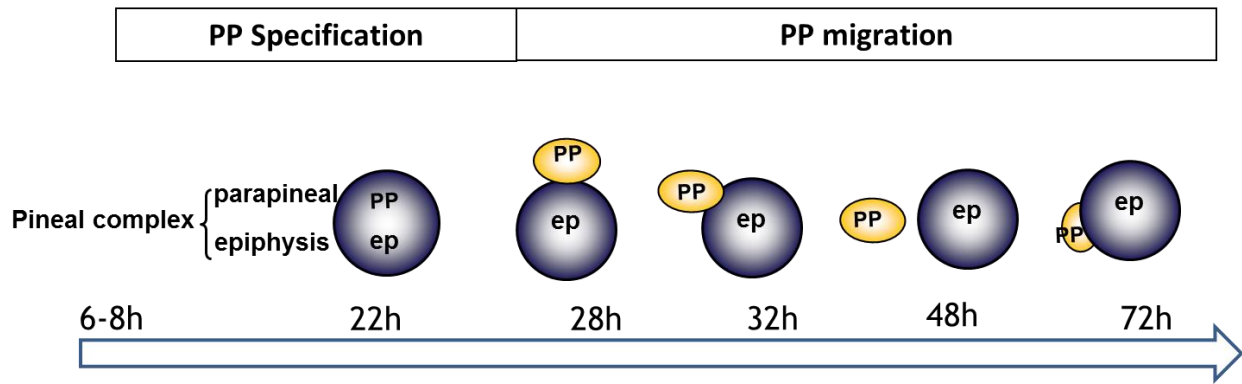


Fig.18 Timeline of parapineal specification and migration.

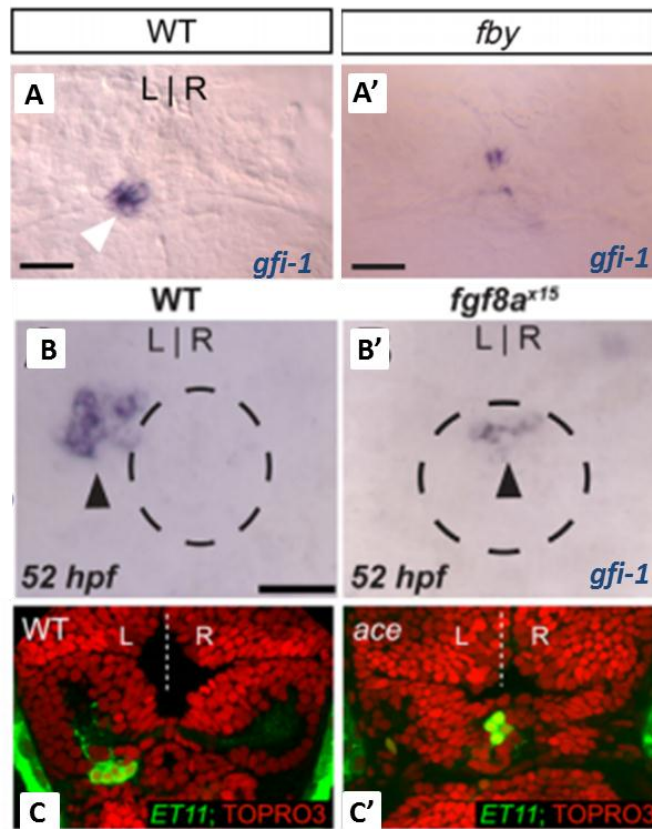


Fig.19. Parapineal specification and migration require *Tbx2b* and *Fgf8* signal.

(A-B') Dorsal views showing *gfi1ab* mRNA expression in WT (A, B) and *tbx2b*^{-/-} mutants (*fby*) (A') or *fgf8*^{-/-} null mutant embryos (*fgf8a*^{x15}) (B') (Taken from Snelson et al., 2008b; Clanton et al., 2013). (C-C') Confocal sections showing the PP (labelled by the expression of Tg(*ET11:GFP*)) in wild-type (WT) and in *fgf8*^{-/-} hypomorphic mutant embryos (*fgf8a*^{ti282}/*ace*); Topro3 label cell nuclei in red (Taken from Regan et al., 2009).

2.5 Specification and migration of the parapineal

2.5.1 Role of Tbx2b transcription factor

The parapineal (PP) is specified bilaterally from the anterior part of the epiphysis around 22 hpf. After the parapineal delaminates (26-28 hpf), it becomes organized in a rosette-like structure that first migrates to the left (28-36 hpf), then posteriorly (36-48 hpf), and finally back toward the midline (48-72 hpf) (**Fig. 18**).

The specification of the PP requires the transcription factor Tbx2b ([Snelson et al., 2008a](#); [Snelson et al., 2008b](#)). Mutation in *tbx2b/from beyond (fby)* gene, which lead to a truncation of Tbx2b upstream of its DNA-binding domain, results in the development of fewer PP cells that remain as a loosely associated group near the midline (**Fig. 19A-A'**); this leads to a "double right" habenulae. The failure of PP to migrate in *fby* appears to be due to the lack of formation of a true PP rosette rather than the reduced number of parapineal cells as partial PP ablations before migration in wild-type embryos can result in a number of parapineal cells comparable to that found in *fby* mutants but that are still able to migrate correctly ([Snelson et al., 2008b](#)). Despite its broad expression in the epithalamus, mutations in *tbx2b/fby* do not affect the epiphysis ([Snelson et al., 2008b](#)). On the other hand, mutations in the *floating head (flh)* gene, which encodes a homeodomain protein, result in the pineal organ being smaller, but does not affect parapineal specification and migration ([Snelson et al., 2008a](#)). While Flh activates *tbx2b* transcription in pineal complex precursors ([Cau and Wilson, 2003](#)), expression of *tbx2b* is unaffected in the parapineal in *flh* mutants; homozygous double *flh/fby* mutants show an additive phenotype, suggesting that *flh* and *tbx2b* function in parallel to regulate pineal and parapineal development, respectively.

2.5.2 Role of Fgf8 signal

Specification of the parapineal (PP) also requires Fgf8a. In *fgf8a^{x15}* mutants, a putative null allele, the number of PP cells is reduced and more cone photoreceptors cells (Arr3a+ cells) are

concomitantly detected in the anterior pineal anlage (Clanton et al., 2013). It appears, therefore, that precursors of the anterior pineal complex are bipotent and require Fgf8a to become PP cells. Indeed, *fgf8a*^{x15} leads to defect in parapineal specification (Fig. 19B-B') (Clanton et al., 2013). Fgf8a seems to act together with Tbx2b to promote parapineal specification as *fgf8a*^{x15} mutant embryos injected with morpholinos against *tbx2b* (*tbx2b*^{MO}) display significantly fewer parapineal cells than either *tbx2b*^{MO} or *fgf8a*^{x15} mutant alone.

Interestingly, in hypomorphic mutant allele of the *fgf8a* gene (*fgf8a*^{ti282/acerebelar/ace}) or in embryos treated with low dose of SU5402 (10 μM), the parapineal is specified and display a wild-type number of cells, but often fails to leave the dorsal midline (Fig. 19C-C') (Regan et al., 2009). Providing an exogenous source of Fgf8 (by implanting an Fgf8 coated bead) restores parapineal

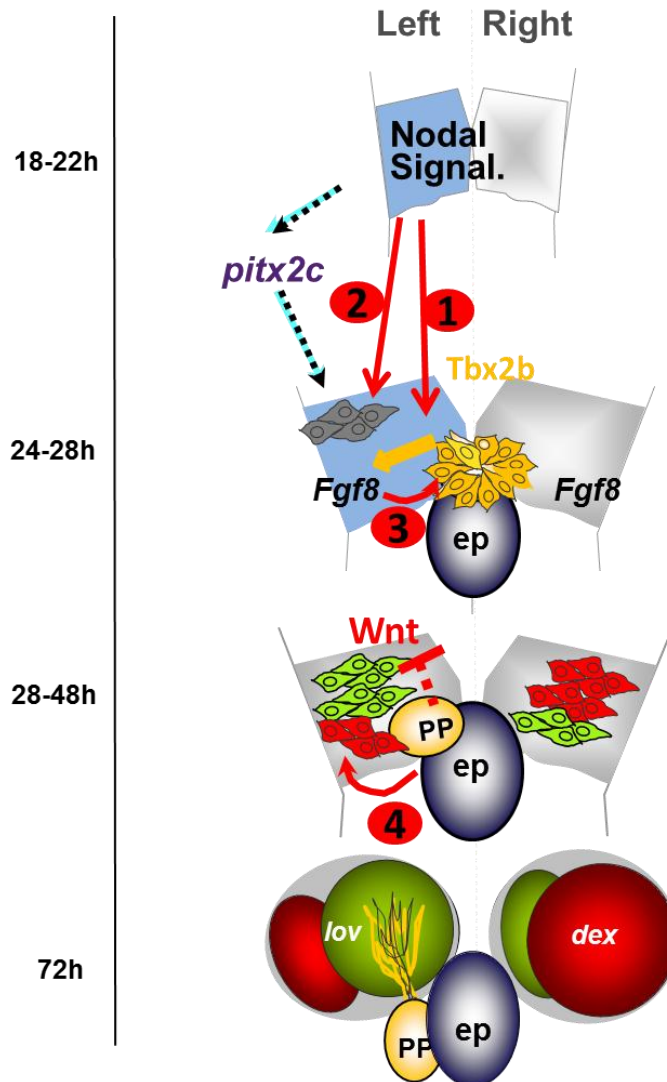


Fig. 20 Model summarizing the signaling mechanisms involved in epithalamus asymmetry.

Nodal signaling is activated in the left epithalamus from 18 hpf (18-22 hpf, blue) and orients parapineal (PP) migration leftward from 28 hpf (Concha et al., 2000)(Fig. 20-1); Nodal activity also drives an asymmetry in the pool of early born habenular progenitor/neurons (gray cells at 28 hpf) (Roussigné et al., 2009) (Fig. 20-2). Tbx2b transcription factor and Fgf8 signal, expressed bilaterally by the surrounding epithalamic cells, are required for the formation of the PP (Snelson et al., 2008b; Clanton et al., 2013). Fgf8 signal is also required for PP migration from 28 hpf (Regan et al., 2009) (Fig. 20-3). Once parapineal starts migrating, it promotes habenular asymmetry, *ie* the specification of lateral versus (green cells) medial habenular (red cells) neural sub-types (Gamse et al., 2003) (Fig. 20-4). This role of the PP in habenular asymmetry might involve an inhibition of Wnt/Tcf pathway in left habenular progenitors (Hüsken et al., 2014). From 24 to 48 hpf, habenular neurons are generated through two differentiation waves that might also impact the specification of lateral versus medial habenular neural subtypes (Aizawa et al., 2007).

migration in weak *fgf8*^{ti282} alleles (Regan et al., 2009). However, in the presence of Nodal activity, parapineal migration remains oriented to the left regardless of whether the Fgf8 coated bead was implanted on the left or right side of the epithalamus. On the other hand, a right source of exogenous Fgf8 can orient migration to the right in the absence of Nodal activity. Therefore, Fgf8 signal is required for PP migration in addition to PP specification. Moreover, oriented parapineal migration depends on the coordinated activities of the Nodal and FGF signaling pathways. Whether these both pathways interact and how they are integrated by epithalamic cells to promote collective migration of PP cells, however, remains unknown.

2.6 Conclusion

Over the past 20 years, the zebrafish epithalamus has emerged as a model to address the development of left right (LR) asymmetry in the brain and the impact of these asymmetries on brain function (Model in **Fig 20**). The first anatomical LR asymmetry detected in the epithalamus appears to be the formation and oriented migration of the parapineal (PP). This step is critical for the subsequent establishment of structural and functional asymmetries in habenular nuclei. The leftward migration of PP collective depends on both TGF β /Nodal and FGF signaling pathways: bilateral Fgf8 promotes the migration of PP cells while Nodal provides a left-bias to the migration. The crosstalk between FGF and Nodal pathways during collective cell migration is not well documented. Therefore, the PP provides a powerful new model to understand how these pathways can interact during collective cell migration. In the next section, I will describe in more details collective cell migration and how signaling pathways modulate this process.

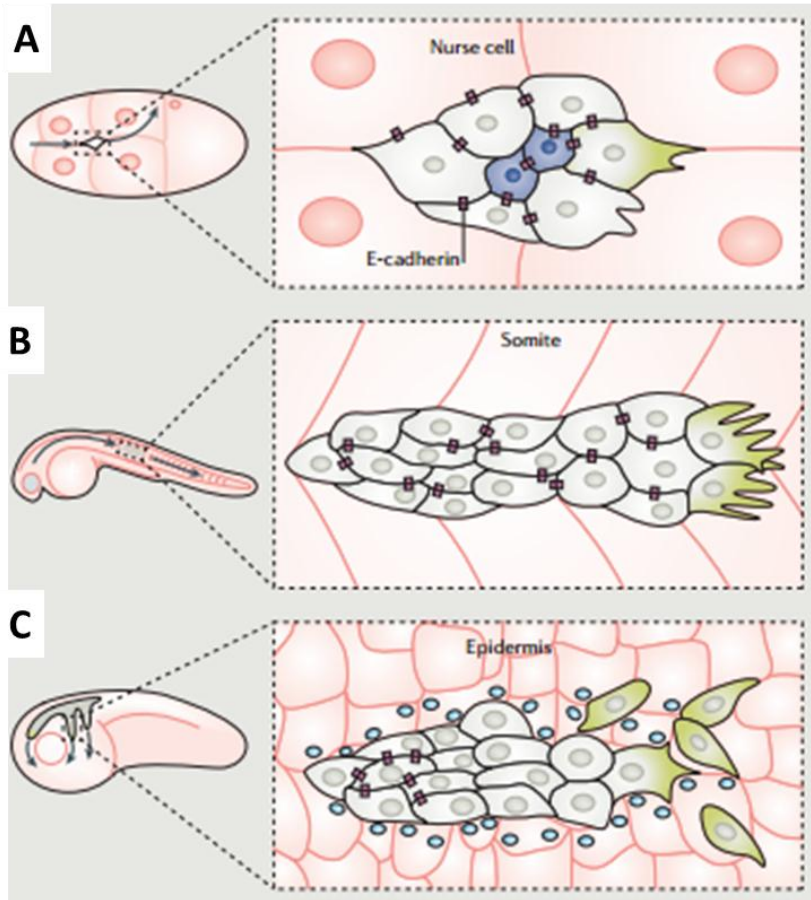


Fig 21. Examples of collective cell migration during embryonic development.

A) The border cells cluster is composed of non-motile polar cells and motile neighboring cells that migrate with the *Drosophila* egg chamber. **B)** The lateral line in *Zebrafish* is a cluster of more than 100 cells that migrates from the head to the tail of embryos to deposit neuromasts sensory organs. **C)** The neural crest cells in *Xenopus* migrate from dorsal neural tube ventrally to form many head structures. (Taken from [Mayor et al. 2016](#))

III. Signaling mechanisms underlying collective cell migration

3.1 Collective cell migration is a widespread process

During embryonic development, cells often migrate in groups to form tissues and organs (Weijer, 2009). This process, called collective cell migration, is commonly found for example during the morphogenesis of branching organs (kidney, lung, salivary) (Lu and Werb, 2008), heart regeneration (Wang et al., 2015) and angiogenesis (Gerhardt et al., 2003). Collective cell migration is also broadly found in adults later in life; for instance, upon skin injury, wound healing involves collective cell migration to trigger the formation and remodeling of new repaired tissue (Campbell and Casanova, 2016). Finally, collective cell migration is seen when tumor cells invade new tissues during metastasis (Bravo-Cordero et al., 2012; Iliina and Friedl, 2009).

Among well-studied *in vivo* models of collective migrations during development, we find:

1) Border cells in *Drosophila*. Border cells derive from cells in the anterior follicular epithelium of the egg chamber that delaminate, during oogenesis and migrate between nurse cell to reach the oocyte (Fig. 21A); the group is composed of 4-6 cells clustered around a pair of non-migrating polar cells (Campbell and Casanova, 2016; Mayor and Etienne-Manneville, 2016).

2) The lateral line primordium (LLP) in zebrafish. The LLP is formed by a group of more than 100 cells that migrates from the head to the tail of the embryos under the skin of the fish, depositing a series of rosette-like organs called neuromasts that are required for sensing water flow (Fig. 21B) (Ghysen et al., 2007).

3) Neural crest cells. Neural crest cells are a collective of cells that emerge from the dorsal part of the neural tube and migrate ventrally through the embryo, where they contribute to diverse cell lineages such as melanocytes, glia, peripheral and enteric neurons, and the craniofacial skeleton (Fig. 21C) (Graham, 2003).

Migrating collectively provides certain advantages over migrating as individual cells. During collective cell migration, cells interact with each other to coordinate their motion and to share

tasks. Collective movement relies on cell interplay not only between migrating neighbors but also with the surrounding environment. They interchange between lamellipodium-based and bleb-based motility depending on the stiffness and composition of their environment, which can include extracellular matrix components and surrounding cells (Ladoux and Mège, 2017). Cell-cell interactions strongly influence how cells move and what regulates their migration. When a cell meets another cell, for instance, it often stops moving for a short time (contact inhibition) prior to forming cell-cell adhesions or changing its direction of migration (van Helvert et al., 2018). Coordinated by soluble or matrix signals, cells may be guided to a particular place, or migrate randomly with frequent direction change by rotation (Ridley, 2015).

Cell collectives can be of different size, can adopt different multicellular arrangements such as sheets, chains or groups with variable cohesivity; they can migrate in different environments and over variable distances. Over the past decades, advances in genetic methods and imaging tools have given scientists the opportunity to observe and study collective cell migration *in vivo*. For instance, studies on the migration of border cells and tracheal cells in *Drosophila*, neural crest in *Xenopus* or the lateral line primordium (LLP) and vascular system in zebrafish, have revealed the behavior of individual cells within migrating collectives (Aman and Piotrowski, 2011; Friedl and Gilmour, 2009; Ochoa-Espinosa and Affolter, 2012; Pocha and Montell, 2014). These works have highlighted the importance of cell communication between leaders and followers but also revealed that there are many different ways of steering a cell collective (Theveneau and Linker, 2017). Here I will quickly describe what we have learnt from several model systems.

During sprouting of blood vessels, cells at the leading edge of migration, or tip cells, display a highly dynamic actin cytoskeleton and are mechanically coupled via cadherins and actomyosin to their direct followers. One tip cell responds to vascular-endothelium-derived growth factor (VEGF) and adopts a pseudomesenchymal phenotype with distinctive lamellipodia. Epithelial/endothelial collectives resemble a bicycle with multiple riders, with all riders being interconnected and contributing to migration. The tip cell (front rider) is responsible for sensing

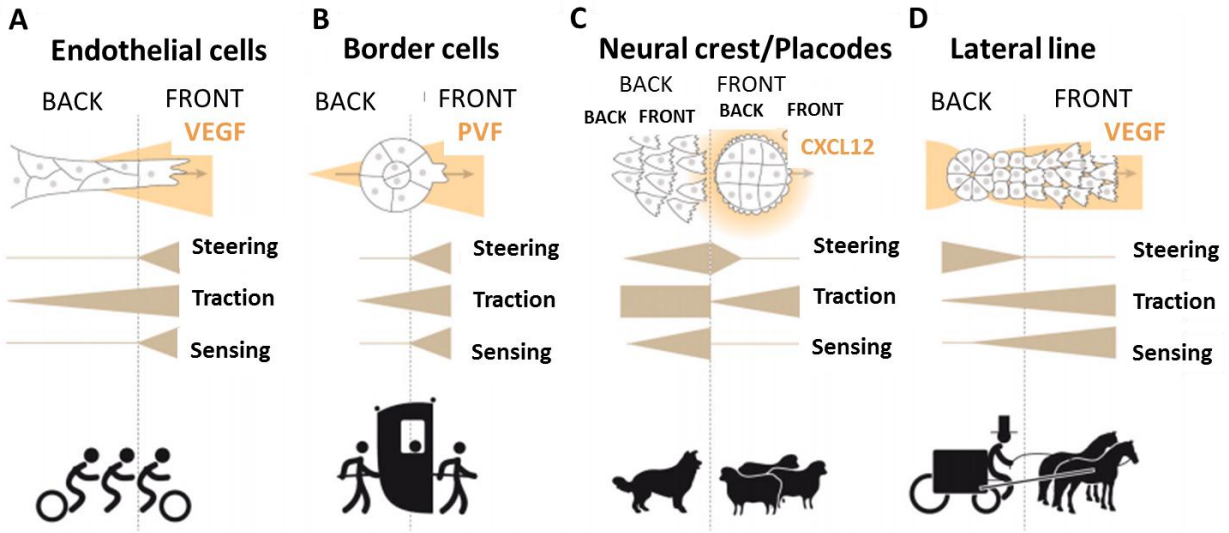


Fig 22. The many ways of steering a cell collective.

A) During endothelial cell migration, one tip cell responds to VEGF and displays a pseudomesenchymal phenotype but traction force is shared among cells. This works as a bicycle with multiple riders (tandem, triplets, quads or quints). **B)** The border cell cluster consists of 5-6 migrating cells organized around 2 immotile polar cells. This works as several persons carrying a sedan chair, the person at the front setting the direction. **C)** Epithelial placodes and mesenchymal neural crest cells have distinct motility (low for placodes and high for neural crest). This works as a sheepdog (neural crest cells) and livestock (placodes) interaction: the sheepdog (highly motile) is attracted by the livestock (gregarious) and the livestock only moves to go away from the sheepdog. **D)** The Lateral line primordium works as horse-drawn carriage. The driver in the carriage (back cells) is responsible for steering while horses (front cells) follow available instructions and pull the whole structure. Taken from (Theveneau and Linker, 2017).

the environment and giving the direction of cyclist, but traction force is shared among cyclists (**Fig. 22A**) (Theveneau and Linker, 2017; Ubezio et al., 2016; Yang et al., 2016).

Drosophila Border cells cluster consists of a small group of migrating cells (5-6 cells) organized around a core of two immobile cells named polar cells (Bianco et al., 2007). In border cells, during the linear migration phase, a leader emerges in response to a platelet-derived/vascular endothelium-derived growth factor homologue (PVF) chemoattractant, but all cells are mechanically coupled and traction is shared. Leader-follower roles are maintained by mechanical coupling preventing excessively protrusive activity in follower cells. However, a follower cell can occasionally take over the lead position, suggesting that leader cell identity is not fixed (Cliffe et al., 2017). Thus, the border cell cluster can work as a litter with several active carriers carrying passive passengers. Traction is shared among all cells, but the front cell sets the direction (**Fig. 22B**) (Cai et al., 2014; Cliffe et al., 2017; Malet-Engra et al., 2015).

Ganglia of the cranial nerves VII, IX and X are formed by neural crest and epibranchial placodal cells (Theveneau and Mayor, 2011). In *Xenopus* neural crest/placode system, cells have intrinsic motility with neural crest cells being more motile than placodal cells. Placodes migrate at the front and neural crest at the back, displaying chase-and-run (attraction-repulsion) behavior but no with directionality on their own. Neural crest cells sense placodes via Cxcl12. Placodes do not sense an external cue but are repelled through contact with the neural crest. The heterotypic neural crest/placode relationship works similarly to a dog (neural crest, highly motile) guiding livestock (placodes, gregarious). The livestock only moves to get away from the sheepdog; when they are separated, motility is conserved but directionality is lost (**Fig. 22C**) (Theveneau et al., 2013).

In zebrafish lateral line primordium (LLP). Cells at the leading edge of the migrating primordium are mesenchymal while follower cells display epithelial characters. Homogenous Cxcl12 distribution is transiently and locally converted into a gradient by the follower cells. Front cells sense this gradient and steer migration in the right direction relative to the gradient. As such, the LLP functions as a horse and carriage with the driver (back cells) setting the direction (by forming the gradient) while the horses (front cells) follow instructions provided by the driver

and pull the whole structure forward. When the two are separated, horses remain motile but lose directionality, while the carriage stops moving (**Fig 22D**) (Dambly-Chaudière et al., 2007; David et al., 2002).

While some underlying coherence can be found, these systems have also indicated that many features of collective cell migration vary between models. It is interesting, therefore, to study and compare various cell migration models in order to understand the many ways of controlling the movement of cell collectives. Furthermore, although recent advances in our understanding of cell migration have been achieved through the study of these systems, we are still far from fully understanding how cells can collectively sense and integrate molecular/chemical and physical/mechanical signals from the surrounding environment. This said, major chemical cues that are repetitively employed during cell migration are members of the FGF (Fibroblast Growth Factor) family. In the next part, I will describe in more details some of what we know about the roles of FGF signaling pathway in controlling cell migration.

3.2 Function of FGF signaling pathway in collective cell migration

3.2.1 FGF signaling is implicated in various models of cell migration

Collective movement of cells is essential during development but, the molecular mechanisms that this process is still not fully understood. One actor implicated in this process is the Fibroblast Growth Factor (FGF) signaling pathway, which can promote cell migration in ways that vary from one model to another.

During vertebrate gastrulation, both the specification and migration of the mesoderm require FGF signaling. In *Xenopus*, four Fgf ligants (Fgf2, Fgf3, Fgf4 and Fgf9) are expressed maternally or in the newly formed mesoderm, and required during gastrulation: if the activity of FGF pathway is inhibited by over-expression of a dominant-negative Fgf receptor, there is a reduction in mesoderm formation accompanied by defective gastrulation movements, involving

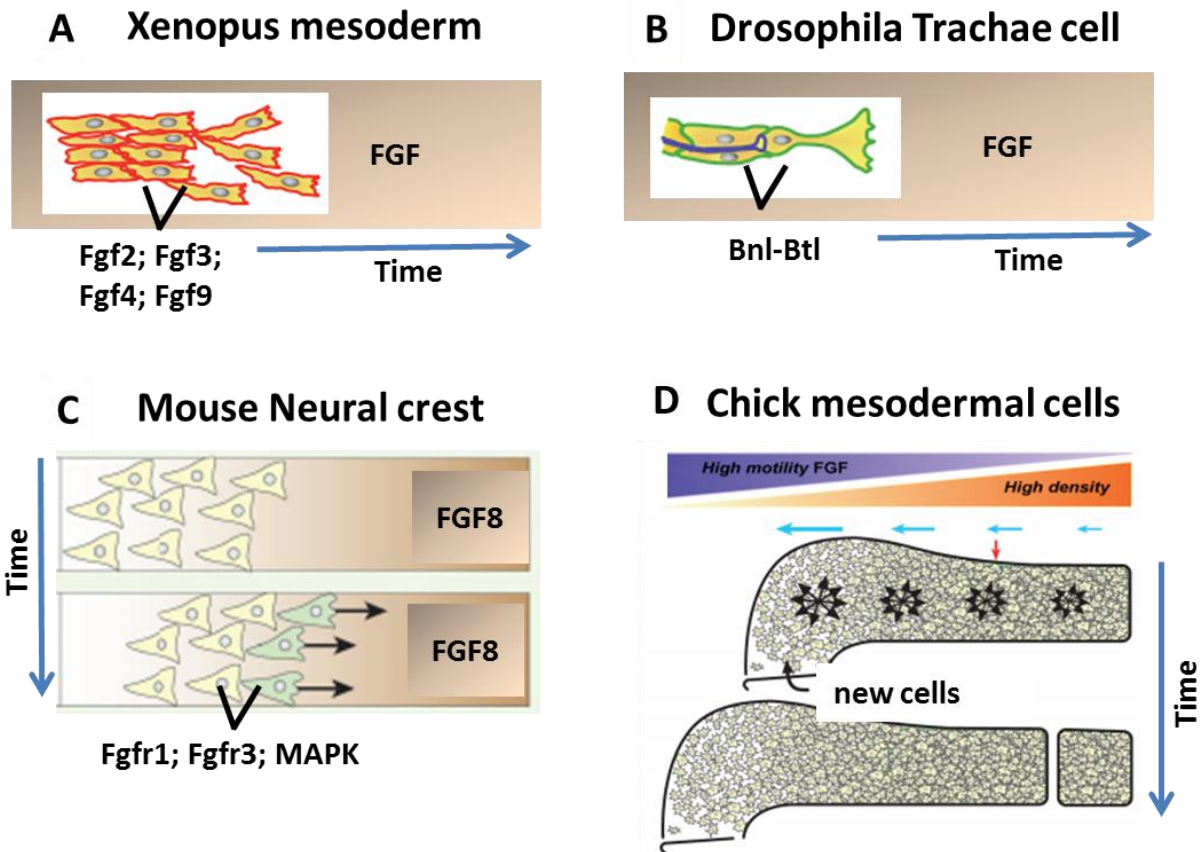


Fig 23. FGF signaling is involved in many models of cell migration.

A) During gastrulation in *Xenopus* embryos, the formation and movement of mesoderm cells are controlled by four types of Fgf (Fgf2, Fgf3, Fgf4, Fgf9) that are expressed in mesoderm cells (Modified by [Campbell and Casanova 2016](#)). **B)** In *drosophila* trachea system, tracheal cells migration and branching morphogenesis are controlled by FGF signaling and Bnl-Btl Fgf ligand-receptor (Modified by [Campbell and Casanova 2016](#)). **C)** Neural crest cells in mouse are attracted toward an FGF8 source. **D)** Chick embryo elongation. Upper panel: Schema showing the gradient of FGF mediated random motility (lavender gradient) opposed to the gradient of cellular density (orange gradient) in the presomitic mesoderm (PSM). Lower panel: Schematic of the left presomitic mesoderm (PSM) at two consecutive stages of embryo elongation. While new cells are entering the PSM, cell density increases in the anterior side of the PSM (right side of the panel); this cell density gradient together with FGF mediated random cell motility (black arrow clusters) create a directional bias for migrating cells and promote elongation toward the posterior side (horizontal blue arrows). Modified by ([Bénazéraf et al., 2010](#)).

problems with the collective involution of mesoderm at the blastopore (**Fig. 23A**) (Slack et al., 1996). Sivak *et al* could dissect both role of FGF pathway in mesoderm specification and migration: they have shown that two feedback inhibitors of FGF pathway, Sprouty and Spred, can modulate different signaling pathways downstream of the Fgf receptor to coordinate and switch between mesoderm specification and migration: Sprouty proteins inhibit Ca²⁺ signaling and morphogenesis leaving MAPK activation and mesoderm specification intact while Spreds inhibit specifically MAPK activation and mesoderm specification (Sivak et al., 2005).

During the formation of trachea in *Drosophila*, the FGF pathway controls tracheal cell migration and the pattern of tracheal branching. The *Drosophila* gene *branchless (bnl)*, which encodes a homolog of vertebrate Fgfs, is required for this process. Mis-expression of *bnl* induces the formation of branches as well as misroutes the position of these new branches, resulting in massive networks of ectopic branches; this suggests that Fgf acts as a chemotactic signal in this model (**Fig. 23B**) (Sutherland et al., 1996).

In mouse, FGF8 is also described to act as a chemoattractant for cardiac neural crest cells. Neural crest cells express FGF receptors (FGFR) 1 and 3 and migrate toward an FGF8 source in a manner requiring MAPK/ERK signaling. Blocking FGF signaling slows down neural crest migration, while ectopic sites of FGF8 enhance neural crest migration (**Fig. 23C**) (Sato et al., 2011a).

However, in other models, FGF pathway has been shown to promote cell motility rather than chemotaxis (Bénazéraf et al., 2010). During anterior-posterior extension of Chick embryos, a gradient of cell motion along the caudal presomitic mesoderm (PSM) parallels an FGF/MAPK activity gradient that is important for embryo axis elongation; both gain- and loss-of-function of FGF signalling lead to disruption of cell motility gradient and block axis elongation (**Fig. 23D**). Unexpectedly, Benazeraf *et al* showed that FGF signalling do not promote oriented individual cell movements in the PSM but is rather required for random cell motility. Therefore, Fgf8 promotes random cell motility while a gradient in cell density gives the orientation to migrating cells to control posterior elongation in the embryos (Bénazéraf et al., 2010).

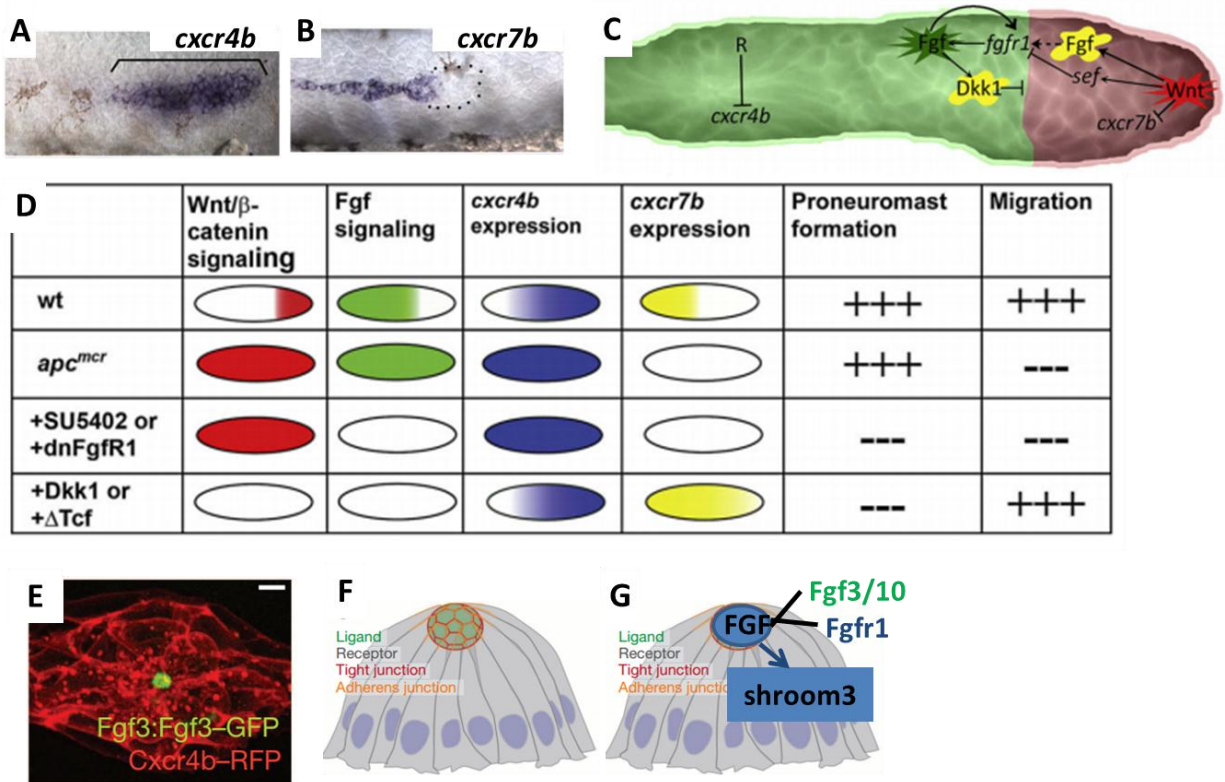


Fig 24. Signaling mechanisms and genetic interactions in the Lateral Line Primordium (LLP).

A-B) *In situ* hybridization showing the expression of *cxcr4b* (A) and *cxcr7b* (B) in the LLP (Taken from Aman and Piotrowski, 2008). **C)** Schematic models of Wnt and FGF pathway interaction in the LLP. In wild-type, Wnt signaling activated in the leading zone leads to the activation of FGF signaling in trailing zone. FGF signaling induces *dkk1* to block Wnt pathway activation in the trailing zone, and Wnt signaling induces *sef* to block FGF pathway activation in the leading zone. *Cxcr7b* expression is inhibited by Wnt signaling in leading zone (Taken from (Aman and Piotrowski, 2008)). **D)** Summary of gene expression patterns and related phenotypes in different contexts where Wnt pathway is ectopically activated (*apc^{mcr}*), inhibited (+*Dkk1* or + Δ Tcf) or in context of FGF inhibition (+SU5402 or +dnFgfR1) (Taken from (Aman and Piotrowski, 2008)). **E)** Microluminal localization of Fgf3-GFP fusion protein in Tg(*Fgf3:Fgf3-GFP*) embryos; membranes are labeled with Tg(*cxcr4b:Cxcr4b-RFP*) (Taken from (Durdu et al., 2014)). **F)** Schematic representation of the forming neuromast organ with central lumen on apical side of the rosette (Taken from (Durdu et al., 2014)). **G)** *shroom3* is expressed downstream of FGF signaling and contributes to rosette formation in LLP. Taken from (Ernst et al., 2012)).

Finally, the lateral line primordium (LLP) is one of the cell migration models where the function of FGF has been best described. In this model, the FGF pathway plays multiple roles, highlighting the complexity of FGF signaling functions in cell migration. I will present this model in more details below.

3.2.2 Multiples roles of FGF signaling during the migration of the lateral line primordium in zebrafish.

The fish lateral line consists of rosette-shaped sensory organs, called neuromasts, which are arrayed along the flank and are involved in sensing water flow. Neuromasts are cell clusters made of central sensory hair cells that are surrounded by support cells (Dambly-Chaudière et al., 2003). During embryonic stages, neuromasts are deposited at regular intervals along the flank of the fish by the migrating lateral line primordium (LLP); the primordium consists of a group of about 100 cells that migrate from the head to the tip of the tail. The LLP migrates along a trail of the chemokine Cxcl12a (also known as Sdf1a (stromal cell-derived factor 1) found at the level of the horizontal myoseptum (David et al., 2002; Li et al., 2004). The direction of LLP migration is not triggered by graded expression of Cxcl12a along this path. Instead, a local gradient is created *de novo* by the LLP through the differential expression of two chemokine receptors, Cxcr4b and Cxcr7b (Fig. 24A-C) (Dambly-Chaudière et al., 2007; Valentin et al., 2007). Indeed, while the front half of the primordium expresses the Cxcr4b receptor, which ensures the response of leader cells to Cxcl12a, the rear half of primordium expresses Cxcr7 receptor, which does not signal in response to Cxcl12a binding, but induces the rapid internalization of Cxcl12a. The action of this receptor, therefore, creates a local depletion of the chemokine at the back of the LLP (Fig. 24A-B). Thus, a front to rear gradient in the expression of Cxcr4b and Cxcr7 and their differential response to Cxcl12a creates a local gradient of Cxcl12a chemokine which then orients LLP migration (Donà et al., 2013; Venkiteswaran et al., 2013).

The polarized expression of *cxcr4b* and *cxcr7b* requires the FGF and Wnt signaling pathways (Fig. 24C) (Aman and Piotrowski, 2008). Wnt/ β -catenin signaling in the leading cells activates the

expression of Fgf ligands Fgf3 and Fgf10. Indeed, their expression is lost in the absence of Wnt/ β -catenin signaling. But the Wnt/ β -catenin pathway also induces the expression of Sef, a feedback inhibitor of the FGF pathway, which restricts the activation of FGF pathway in the trailing zone; Sef expression is expanded in ectopically activated Wnt/ β -catenin pathway (*apc^{mcr}*) and abolished in loss of Wnt activity (Dkk1) (**Fig. 24C, 24D**). In turn, FGF pathway activation in trailing cells induces the expression of *dkk1*, an inhibitor of the Wnt pathway, which contributes to restrict the activation of Wnt pathway to the leading zone. Evidence for this includes: *dkk1* is upregulated in *apc^{mcr}* mutants, which show global Wnt/ β -catenin pathway activation; SU5402 treatment blocks the FGF pathway and leads to ectopic expansion of Wnt/ β -catenin signalling in the trailing region; *dkk1* knockdown with morpholinos also causes expansion of Wnt/ β -catenin signalling targets (**Fig 24C, 24D**). Localized Wnt/ β -catenin signalling is necessary for asymmetric expression of the Cxcr4b and Cxcr7b chemokine receptors (**Fig. 24C, 24D**). Indeed, whereas ectopically activating the Wnt/ β -catenin pathway, as in *apc^{mcr}* mutants or in context of FGF inhibition (SU5402 or dnFgfR1), leads to expansion of *cxcr4b* and loss of *cxcr7b*, loss of Wnt/ β -catenin signaling (Dkk1 or Δ Tcf) leads to an expansion of *cxcr7b* into the leading zone of the primordium (**Fig. 24D**) (Aman and Piotrowski, 2008; Dalle Nogare et al., 2014).

FGF signaling not only sets up asymmetry in chemokine receptor expression in the LLP but also couples epithelial morphogenesis in pro-neuromast to the migration of LLP (Donà et al., 2013; Durdu et al., 2014; Lecaudey et al., 2008). Indeed, the assembly of pro-neuromast at the rear of the LLP requires FGF signaling (Lecaudey et al., 2008; Nechiporuk and Raible, 2008). Two Fgf ligands, Fgf3 and Fgf10, are expressed by a central pro-neuromast cell and activate the FGF pathway in neighboring cells via the Fgf receptor 1 (Fgfr1) (**Fig. 24F-G**). Performing time-lapse imaging on embryos in which FGF signaling is inhibited or hyper-activated showed that apical constriction in pro-neuromast is affected (**Fig. 24G**) (Lecaudey et al., 2008; Nechiporuk and Raible, 2008). Ernst et al subsequently showed that Shroom3, a regulator of non-muscle myosin (NMII) activity, acts downstream of activated Fgfr1 and mediates apical constriction during pro-neuromast formation (**Fig. 24F, 24G**) (Ernst et al., 2012). More recently, using a *Tg(Fgf3:Fgf3-GFP)* transgenic line, Durdu et al observed that high levels of Fgf ligand protein accumulate in

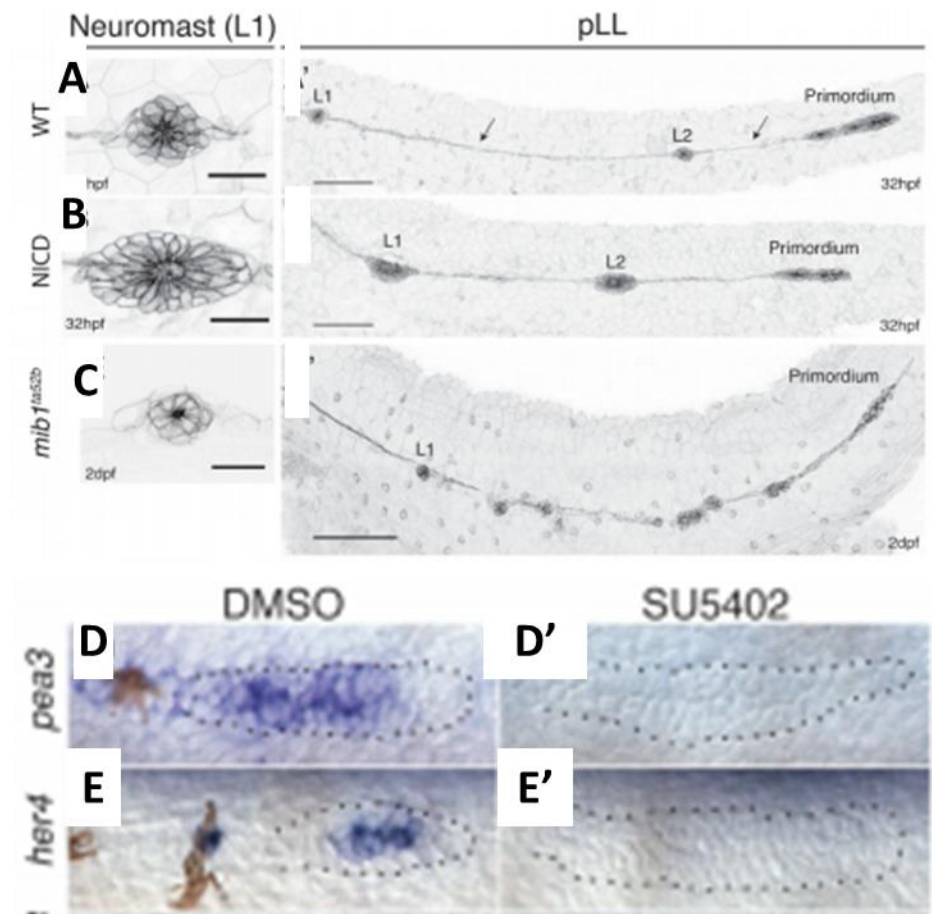


Fig 25. Notch signaling is required for neuromasts formation and primordium migration downstream of FGF signaling.

A-C) Compared to wild-type (WT) (A), neuromasts are larger in NICD expressing embryos (Notch gain of function, B) and smaller in *mib1^{ta52b}* embryos (Notch loss of function, C). Space between deposited neuromasts is affected in NICD expressing embryos (B) and in *mib1^{ta52b}* mutants (C). **D-E')** The expression of FGF target gene, *pea3*, and Notch target gene, *her4*, are reduced/absent upon treatment with FgfR1 inhibitor SU5402 compared with DMSO treated controls. Taken from (Kozlovskaja-Gumbriene et al. 2017).

the lumen of the forming pro-neuromasts (**Fig. 24E, 24F**) ([Durdu et al., 2014](#)). Genetic inhibition and laser micropuncture experiments showed that these local luminal accumulations create a signaling center that can coordinate rosette morphogenesis at the rear of the LLP, thus allowing LLP migration.

LLP migration not only requires FGF signaling and its interaction with Wnt signaling pathway, but also interaction with others pathway, such as Notch. In next section, I will describe more details about interaction between FGF signaling and Notch signaling during cell migration.

3.3 Interaction between FGF and Notch signaling in cell migration

3.3.1 Crosstalk between FGF and Notch signaling in lateral line primordium

A recent study has shown that the Notch pathway controls the size of neuromasts in the zebrafish lateral line. Indeed, up-regulating Notch pathway by over-expressing the intracellular domain of the Notch1a receptor (NICD) leads to a larger neuromasts (**Fig. 25A-B**) ([Kozlovskaja-Gumbrienė et al., 2017](#)); down-regulation of Notch pathway results in smaller neuromasts compared with wild-types (**Fig. 25A, 26C**). Both Notch gain-of-function and loss-of-function affect the spacing of neuromast deposition in addition of neuromast size (**Fig. 25A-25C**). Interestingly, Kozlovskaja-Gumbrienė *et al* have shown that Notch pathway acts downstream of FGF pathway to induce and maintain pro-neuromasts in LLP. Indeed, Notch pathway activity is highly reduced upon treatment with the FGF pathway inhibitor SU5402 (**Fig. 25D-E'**). Moreover, in contexts where FGF pathway or MAPK activity are inhibited, ectopic expression of NICD can rescue neuromasts formation, suggesting that Notch acts downstream and independently of FGF-MAPK-Shroom3 signaling ([Kozlovskaja-Gumbrienė et al., 2017](#)).

Interestingly, a recent study describes that Mindbomb1 (Mib1) ubiquitin ligase contributes to persistent directional cell migration in both cell culture and in the LLP through a Notch independent process ([Mizoguchi et al., 2017](#)). Mizoguchi *et al* showed that Mib1 ubiquitinates a novel substrate Ctnnd1, a positive regulator of the small GTPase Rac1. Rac1 is one of the small

GTPases that acts as a regulatory switch between persistent directional and random cell migration by cycling between a GDP-bound inactive form and a GTP-bound active form (Pankov et al., 2005). Through triggering hyperactivation of Rac1, *mib* mutation leads to an increased random cell migration (Mizoguchi et al., 2017).

Therefore, in addition to its function in promoting Notch pathway mediated rosette formation downstream of FGF pathway (Kozlovskaja-Gumbriené et al., 2017), Midbomb can also controls persistent directional cell migration during LLP migration by regulating the Ctnnd1-Rac1 pathway, independently of Notch signaling (Kozlovskaja-Gumbriené et al., 2017; Mizoguchi et al., 2017).

3.3.2 Crosstalk between FGF and Notch signaling in *Drosophila* trachea

The tracheal system of *Drosophila* is composed of a branched network of epithelial tubes that transports oxygen throughout the developing larvae. It is formed through a series of sequential branching events in each embryonic hemisegment (Sutherland et al., 1996). Tracheal system development requires an Fgf signal (known as Branchless, Bnl) (Sutherland et al., 1996) and its receptor (known as Breathless, Btl) (Lee et al., 1996). During tracheal branching morphogenesis, there are three steps (Ikeya and Hayashi, 1999). During the first induction stage (Fig. 26A), Btl/FgfR is expressed in all tracheal cells and is activated by Bnl/Fgf expressed by cells in the adjacent mesenchyme (Klämbt et al., 1992). At this point, Notch signaling is inactive in all tracheal cells but the interaction between Bnl/Fgf and Btl/FgfR drives Delta (DI) expression in all tracheal cells via the MAPK pathway. In the second lateral inhibition stage (Fig. 26B), Notch signaling is activated by all cells with the exception of the future tip cell, which expresses the highest level of DI as well as the tip-cell marker Esg (Fuse et al., 1994); activated Notch signaling represses tip cell fate by inhibiting Esg in trailing cells. Indeed, Ghabrial *et al* showed that in Notch LOF (N^{ts}) mutants embryos, there is a large clusters of cells aggregated at the lead position, while Notch GOF in N^{ACT} embryos had the opposite effect, arresting outgrowth and stalling cells near the base of the branch (Fig. 26D-F) (Ghabrial and Krasnow, 2006). In the third

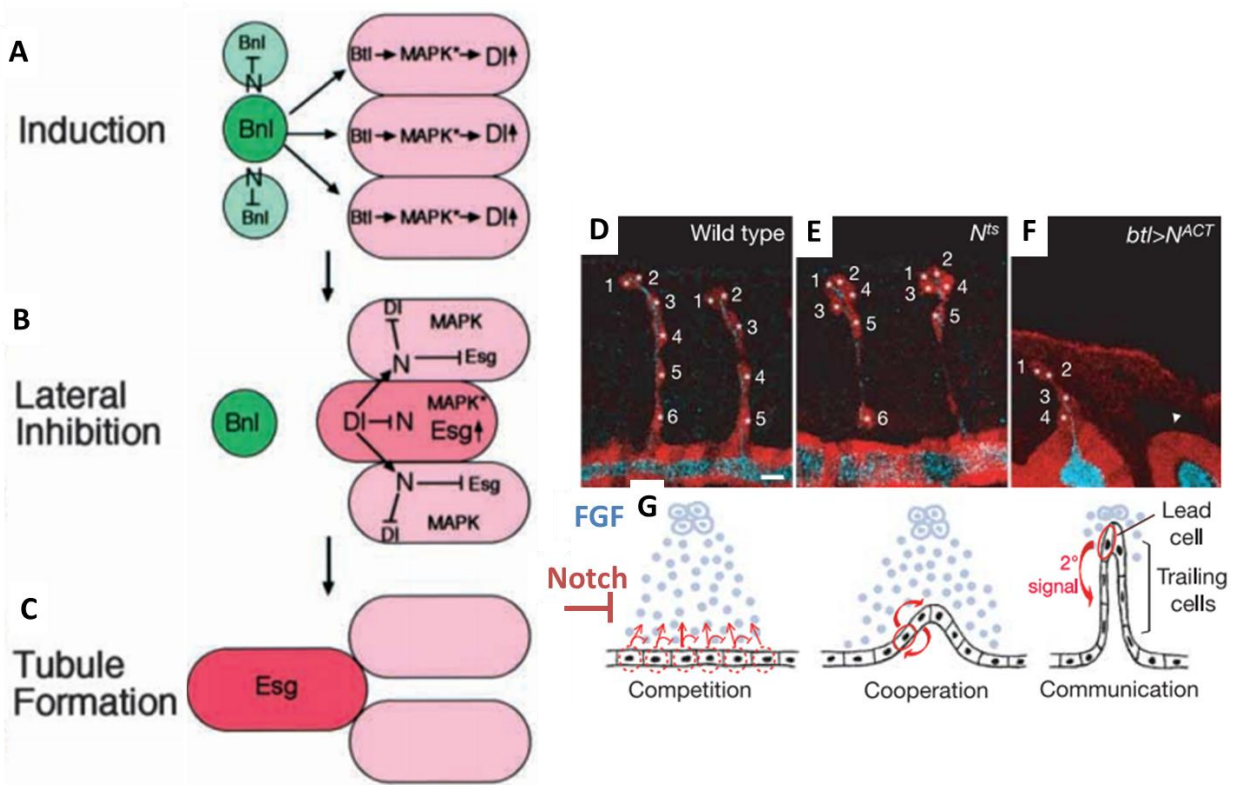


Fig 26. Role of Notch and FGF pathway activity during tubule formation in tracheal branches.

(A-C) **A**) Induction stage. Bnl/Fgf activates its receptor Btl/FgfR in tracheal cells. Btl/FgfR induces MAPK activation that then activates Delta (DI) expression. Bnl/Fgf expression is restricted by Notch pathway (N) in tracheal environment. **B**) Lateral inhibition stage. Induced DI activates Notch signaling in its neighbor trailing cells; DI and Notch signaling results in the activation of *esg* gene and higher MAPK signaling in the future tip cell. **C**) Tube formation. A single cell with high level of DI and *esg* expression is selected to be tip cell. Other tracheal cells become stalk cells. Taken from (Ikeya and Hayashi, 1999).

(D-G) Cell in wild-type tracheal dorsal branch (DB) are evenly distributed (D). Notch inactivation (N^{ts}) caused the migration of extra cells to the trachea tip (E). Constitutive Notch activity (N^{ACT}) inhibited branch outgrowth, particularly in posterior part in which some tracheal cells completely failed to bud (F). (G) Social interactions between tracheal cells during budding. Three panels show budding tracheal cells expressing the FGFR moving to FGF signaling center (Blue dot). The first panel illustrates cell competition via Notch-mediated pathway (inhibition red arrow) as tracheal cells compete for the lead position; the second panel illustrates cell cooperation; the third panel illustrates cell communication: leading cell might send a secondary signal to trailing cells, inducing them to become stalk cells. Taken from (Ghabrial and Krasnow, 2006)

tubule formation stage (**Fig. 26C**), high MAPK and Esg expression in the tip cell drive cell shape changes and/or cell motility leading to primary branch outgrowth. When the cell is selected to be tip cell in the lead position, it might send a secondary signal to the trailing cells, inducing them to follow tip cell and become stalk cells (**Fig. 26G**) ([Ghabrial and Krasnow, 2006](#)).

Therefore, tracheal cells within the migrating group compete for the leading position and the leadership is taken by the cell with the highest FgfR activity. This difference in levels of FGF activity between the future tip cell and the rest of the cells in the cluster requires Notch signaling. However, the mechanism by which Notch signaling pathway controls this FGF dependent tip cell selection is not clear yet.

RESULTS

I. Focal activation of FGF pathway promotes parapineal migration

I.1 Context, Aim and Summary of Manuscript n°1

During the establishment of left-right brain asymmetry, a small group of cells, the parapineal (PP), collectively migrates from the midline to the left. Local Fgf8 signaling is required for PP cells to migrate away from the midline (Regan et al., 2009). Although Fgf8 is expressed bilaterally in the epithalamus, the PP migrates to the left in most wild-type embryos. This bias in the orientation/laterality of PP migration depends on the activity of Cyclops (Concha et al., 2003; Regan et al., 2009), a secreted signal of the Nodal/TGF β family that is transiently expressed in the left epithalamus prior to PP migration (Concha et al., 2003; Regan et al., 2009). In embryos lacking Cyclops/Nodal, asymmetry develops but the PP migrates to the left or to the right with equal probability (Concha et al., 2000). Thus, one signaling pathway promotes PP cell migration (FGF) while another (Nodal/TGF β) imparts directionality to the migration (Regan et al., 2009).

When I arrived in the team, Myriam Roussigné was addressing how Fgf8 promotes PP migration and how the Nodal pathway biases migration orientation. By imaging an FGF reporter transgenic line, *Tg(dusp6:d2EGFP)*, Myriam had shown that the FGF pathway is activated in only a few cells of the PP that are usually located at the leading edge of the migrating PP. Her data also suggested that this focal activation of FGF signaling was required for PP migration. I contributed to show that global constitutive activation of FGF signaling delays PP migration in wild-type embryos, while it partially restores both PP migration and mosaic expression of *Tg(dusp6:d2EGFP)* in *fgf8*^{-/-} mutant embryos. Importantly, focal activation of FGF signaling in few PP cells is sufficient to promote PP migration in *fgf8*^{-/-} mutants. Finally, we have shown that Nodal signaling contributes to the restriction and leftwards bias of FGF activation. Therefore, our results show that the distinct cell state in the level of FGF pathway activity defines cells at the front and rear of the PP and is required to promote its migration in a FGF-dependent manner (Manuscript n°1)

I.2 Manuscript n°1:

Left/right asymmetric collective migration of paraneal cells is mediated by focal FGF signaling activity in leading cells.

Myriam Roussigné^{1#†*}, Lu Wei^{1#}, Erika Tsingos³, Franz Kuchling³, Mansour Alkobtawi⁴, Matina Tsalavouta², Joachim Wittbrodt³, Matthias Carl^{5,6}, Patrick Blader^{1†}, Stephen W. Wilson^{2†}.

¹ Centre de Biologie du Développement (CBD, UMR5547), Centre de Biologie Intégrative (CBI, FR 3743), Université de Toulouse (UPS), CNRS, 31062, France.

² Department of Cell and Developmental Biology, UCL, Gower Street, London WC1E 6BT, UK.

³ Centre for Organismal Studies (COS) Heidelberg, Germany.

⁴ Université Paris Sud (UMR3347), Institut Curie/CNRS/U1201 INSERM, 91405 ORSAY, France

⁵ Heidelberg University, Medical Faculty Mannheim, Department of Cell and Molecular Biology, D-68167 Mannheim, Germany.

⁶ Center for Integrative Biology (CIBIO), University of Trento, Italy

These authors contributed equally to experimental work

† Joint senior authors.

* Author for correspondence: myriam.roussigne@univ-tlse3.fr

PNAS, On line, the 3rd October 2018



Left/right asymmetric collective migration of parapineal cells is mediated by focal FGF signaling activity in leading cells

Myriam Roussigne^{a,1,2,3}, Lu Wei^{a,1}, Erika Tsingos^b, Franz Kuchling^b, Mansour Alkobtawi^c, Matina Tsalavouta^d, Joachim Wittbrodt^b, Matthias Carl^{e,f}, Patrick Blader^{a,2}, and Stephen W. Wilson^{d,2}

^aCentre de Biologie Intégrative (FR 3743), Centre de Biologie du Développement (UMR5547), Université de Toulouse, CNRS, F-31062 Toulouse, France; ^bCentre for Organismal Studies, Heidelberg University, 69120 Heidelberg, Germany; ^cInstitut Curie/CNRS/U1021 INSERM, Université Paris Sud (UMR3347), 91405 Orsay, France; ^dDepartment of Cell and Developmental Biology, University College London, WC1E 6BT London, United Kingdom; ^eDepartment of Cell and Molecular Biology, Heidelberg University, D-68167 Mannheim, Germany; and ^fCenter for Integrative Biology, University of Trento, 38123 Trento, Italy

Edited by Igor B. Dawid, The Eunice Kennedy Shriver National Institute of Child Health and Human Development, National Institutes of Health, Bethesda, MD, and approved August 29, 2018 (received for review July 18, 2018)

The ability of cells to collectively interpret surrounding environmental signals underpins their capacity to coordinate their migration in various contexts, including embryonic development and cancer metastasis. One tractable model for studying collective migration is the parapineal, a left-sided group of neurons that arises from bilaterally positioned precursors that undergo a collective migration to the left side of the brain. In zebrafish, the migration of these cells requires *Fgf8* and, in this study, we resolve how FGF signaling correlates with—and impacts the migratory dynamics of—the parapineal cell collective. The temporal and spatial dynamics of an FGF reporter transgene reveal that FGF signaling is activated in only few parapineal cells usually located at the leading edge of the parapineal during its migration. Overexpressing a constitutively active Fgf receptor compromises parapineal migration in wild-type embryos, while it partially restores both parapineal migration and mosaic expression of the FGF reporter transgene in *fgf8*^{-/-} mutant embryos. Focal activation of FGF signaling in few parapineal cells is sufficient to promote the migration of the whole parapineal collective. Finally, we show that asymmetric Nodal signaling contributes to the restriction and leftwards bias of FGF pathway activation. Our data indicate that the first overt morphological asymmetry in the zebrafish brain is promoted by FGF pathway activation in cells that lead the collective migration of the parapineal to the left. This study shows that cell-state differences in FGF signaling in front versus rear cells is required to promote migration in a model of FGF-dependent collective migration.

collective cell migration | FGF signaling pathway | left/right brain asymmetry | Nodal signaling pathway | zebrafish brain development

The formation of tissue and organs during embryonic development relies on the ability of cells to coordinate their behavior through physical and chemical communication between each other and with their environment. Striking examples of collective cell behavior are directed cell migrations, which occur widely during development, tissue repair, regeneration, angiogenesis, and metastasis. In these different contexts, coherent actions of cells improve the robustness and efficiency of their collective migration (1–4). Collective migration also facilitates cell differentiation and morphogenesis through maintenance of cell–cell interactions and signaling during migration (5–7). Collective migration is thus the predominant mode of migration adopted by epithelial and mesenchymal cells (8, 9).

Cells can migrate in different size groups, over variable distances, and in mechanically different environments, and can adopt different multicellular arrangements, such as sheets, chains, or groups with variable cohesivity. Over the last decade, advances in genetic methods and imaging tools have considerably improved our ability to observe and study collective cell migration in vivo. For example, studies imaging the migration of border cells and tracheal cells in *Drosophila*, and the lateral line

primordium (LLP) and vascular system in zebrafish, have revealed the behavior of individual cells within the migrating group and have highlighted some common features of collective cell migration, such as the importance of cell communication between leaders and followers (1, 3, 5, 6). These studies also indicate that many features of cell migration vary between models. For example, although FGF signaling is implicated in many cell migration events, its function varies from a role in promoting chemotaxis (10–13), cell motility (14), and cell adhesion (15) or in coupling migration to epithelial morphogenesis (16–20). Despite progress in our understanding of cell migration, we are still far from fully understanding how cells collectively interpret signals from the surrounding environment and, consequently, there remains a need for studies that correlate, in vivo, dynamic signaling events with individual cell behaviors.

In the present study, we analyze the unusual left-sided migration of the parapineal in the zebrafish brain as an optically and genetically tractable model for studying collective cell migration. The parapineal is a small group of 15–20 cells located in the epithalamic region of the forebrain. In zebrafish, the epithalamus has been intensively studied as a powerful model to understand how

Significance

The ability of cells to migrate collectively underlies many biological processes. The parapineal is a small group of cells that requires *Fgf8* to migrate from the midline to the left side of the zebrafish forebrain. Studying the dynamics of FGF pathway activation reveals that FGF activity is restricted to a few left-sided parapineal cells. Global activation of the FGF pathway interferes with parapineal migration in wild-type embryos, while focal activation in few parapineal cells can restore migration in *fgf8*^{-/-} mutants, indicating that FGF pathway activation in leading cells is required for collective migration. We show that focal FGF activity is influenced by left-sided Nodal signaling. Our findings may apply to other contexts of FGF-dependent cell migration during development or metastasis.

Author contributions: M.R. and S.W.W. designed research; M.R., L.W., E.T., F.K., M.A., M.T., and M.C. performed research; E.T., F.K., J.W., and M.C. contributed new reagents/analytic tools; M.R., P.B., and S.W.W. analyzed data; and M.R. and S.W.W. wrote the paper.

The authors declare no conflict of interest.

This article is a PNAS Direct Submission.

This open access article is distributed under Creative Commons Attribution-NonCommercial-NoDerivatives License 4.0 (CC BY-NC-ND).

¹M.R. and L.W. contributed equally to this work.

²M.R., P.B., and S.W.W. contributed equally to this work.

³To whom correspondence should be addressed. Email: myriam.roussigne@univ-tlse3.fr.

This article contains supporting information online at www.pnas.org/lookup/suppl/doi:10.1073/pnas.1812016115/-DCSupplemental.

left-right (LR) asymmetry develops in the brain (21–24). It is composed of a pair of asymmetric nuclei called the habenulae and of the photoreceptive pineal complex, which itself consists of the medially located epiphysis and, to its left, the parapineal. Although it almost always resides on the left, the parapineal derives from a group of cells that span the midline, delaminate from the anterior epiphysis, and collectively migrate leftward to lie adjacent to the left habenula (25). The function of the mature parapineal is not clear but during development it has an instructive role in the development of LR differences between the habenulae (25–29).

We have previously shown that local Fgf8 signaling is required for parapineal cells to migrate away from the midline (30). Although Fgf8 is expressed bilaterally in the epithalamus, the parapineal migrates to the left in most wild-type embryos. This bias in the orientation/laterality of parapineal migration depends on the activity of Cyclops (25, 30), a secreted signal of the Nodal/TGF- β family that is transiently expressed in the left epithalamus before parapineal migration (31–33). In embryos lacking Cyclops/Nodal, asymmetry develops but the parapineal migrates to the left or to the right with equal probability (32). Thus, one signaling pathway promotes parapineal cell migration (FGF), while another (Nodal/TGF- β) imparts directionality to the migration (30).

In this study, we elucidate the mechanisms by which Fgf8 promotes parapineal migration. Using a well-established genetically encoded dynamic reporter of FGF signaling activity (34), we observe that just a few parapineal cells, most often located on the left posterior side, show FGF pathway reporter transgene activation. This mosaic and asymmetric expression of *Tg(dusp6:d2EGFP)* FGF reporter in the parapineal recapitulates the pattern of endogenous *dusp6* gene expression and is dependent on Fgf8. Time-lapse confocal imaging in live embryos shows that the dynamics of FGF reporter activity correlates with the behavior of migrating parapineal cells and that transgene expression is enriched in leading parapineal cells throughout migration. Global expression of a constitutively active Fgf receptor (CA-FgfR1) is able to partially rescue parapineal migration in *fgf8*^{-/-} mutants. However, despite the global expression of the activated receptor, FGF reporter transgene activity resolves to leading cells as in wild-type embryos. This suggests that focal activation of the FGF pathway promotes parapineal migration. Supporting this finding, the focal expression of CA-FgfR1 in few parapineal cells is sufficient to partially restore parapineal migration in *fgf8*^{-/-} mutants. Finally, we show that left-sided Nodal activity is required for the lateralization and restriction of FGF pathway activation and that absent or bilateral Nodal signaling contexts differ in their impact on the pattern of FGF pathway activation. Altogether, our data indicate that Fgf8 triggers a focal activation of the FGF pathway in leading parapineal cells that is influenced by left-sided Nodal activity, and this in turn promotes the migration of the whole parapineal cell collective.

Results

Focal and Lateralized Activation of *Tg(dusp6:d2EGFP)* FGF Signaling Reporter Transgene in the Parapineal. Although *fgf8* is expressed bilaterally in the epithalamus before and during parapineal migration (30), whether Fgf8-dependent parapineal migration requires pathway activation in the parapineal or in surrounding cells is not known. To resolve the spatial and temporal dynamics of FGF signaling in the epithalamus, we used an FGF pathway reporter transgenic line, *Tg(dusp6:d2EGFP)^{pt6}*, in which a destabilized version of green fluorescent protein (d2EGFP) is expressed under the control of the *dusp6/mkp3* gene promoter (34). *dusp6/mkp3* is a well-characterized direct and immediate FGF target gene involved in negative feedback inhibition of FGF signaling (35–37).

Confocal imaging of the epithalamus in *Tg(dusp6:d2EGFP)* embryos revealed robust transgene expression in a few parapineal cells that are usually found at the border between the parapineal and the epiphysis on the left side of the parapineal at the onset of migration (Fig. 1 A–B'). Because the pattern of d2EGFP expression was variable from one embryo to another, we quantified the number and position of expressing cells in the parapineals of 32-h postfertilization (hpf) embryos; at this stage,

parapineal cells are organized in a rosette-like structure that is distinct from the epiphysis and can easily be delineated by staining nuclei. At 32 hpf, an average of 5.8 (± 2.7) cells expressed *Tg(dusp6:d2EGFP)* with variable intensity of a total average of 16.8 (± 5.6) parapineal cells per embryo. The d2EGFP⁺ cells were frequently found on the left posterior quadrants of the parapineal (Fig. 1 F and G) (an average of 1.2 d2EGFP⁺ cells per embryo in semiquadrant 5 and 1.4 in semiquadrant 6) as well as in the posterior semiquadrant 4 (Fig. 1 F and G) (0.9 cells d2EGFP⁺ cells per embryo). Thus, while total parapineal cells distribute equally along a clockface 2pm to 8pm axis (Fig. 1G), the distribution of d2EGFP⁺ cells is enriched in the posterior and left side of the parapineal. This localized expression of the FGF reporter transgene recapitulated the expression of the endogenous *dusp6* gene in the epithalamus; although *dusp6* mRNA was weakly detected by in situ hybridization, when visible, it overlapped with d2EGFP staining in the parapineal and elsewhere (SI Appendix, Fig. S1 A–C'). The spatial localization of *Tg(dusp6:d2EGFP)^{pt6}* expression was also confirmed with a second allele of the reporter transgene [*Tg(dusp6:d2EGFP)^{pt8}*] (SI Appendix, Fig. S1 D–E').

Expression of the *Tg(dusp6:d2EGFP)* Transgene Depends on Fgf8. Although *Tg(dusp6:d2EGFP)* transgene expression generally recapitulates *dusp6* expression and depends on FGF pathway activity (34), in some contexts it has been shown to depend on Lef1, a transcriptional activator of the Wnt pathway (38). To determine whether *Tg(dusp6:d2EGFP)* expression in the parapineal reflects FGF pathway activation, we treated *Tg(dusp6:d2EGFP)* embryos with the SU5402 inhibitor of FGF signaling (39) between 25 and 35 hpf. Although d2EGFP was still detected in some tissues, it was abolished in the parapineal, suggesting that expression of the *Tg(dusp6:d2EGFP)* transgene reflects activation of the FGF pathway in parapineal cells (Fig. 1 C–D'). Consequently, the loss of *Tg(dusp6:d2EGFP)* expression in the parapineal correlates with compromised parapineal migration in comparably SU5402-treated embryos (30).

Several Fgf ligands are expressed in the epithalamus (40) but only Fgf8 has been shown to influence parapineal migration (30). To determine whether FGF pathway activation in parapineal cells depends on Fgf8, we analyzed the expression of *Tg(dusp6:d2EGFP)* in *fgf8^{ti282a}/acerebellar (ace)* mutant embryos. Because the parapineal is not always easy to detect in *fgf8*^{-/-} mutants, we used *sox1a* expression to delineate parapineal cells (40).

In most *fgf8*^{-/-} embryos, *Tg(dusp6:d2EGFP)* expression was either absent or markedly reduced in the parapineal (Fig. 1 I–J''), indicating that Fgf8 is required to activate the FGF pathway reporter in the parapineal. The loss of d2EGFP expression was not completely penetrant as, in some mutant embryos (Fig. 1 K–K''), the expression of *Tg(dusp6:d2EGFP)* was similar to control embryos (Fig. 1 H–H''); this lack of penetrance has also been noted for the parapineal migration phenotype (30) and may be due to the hypomorphic nature of the *fgf8^{ti282a}* mutation (41) or compensatory activity of other Fgf ligands. However, overall, the average number of *Tg(dusp6:d2EGFP)*⁺ cells was significantly decreased in *fgf8*^{-/-} mutants (SI Appendix, Fig. S2 A and C), while the total number of *sox1a*-expressing parapineal cells was not affected [average of 10.2 (± 4.2) *sox1a*⁺ cells in controls and of 10.2 (± 4.7) in mutants] (Fig. 1 H'–K'' and SI Appendix, Fig. S2 B and D).

Altogether, our results show Fgf8-dependent FGF pathway activation in a few cells on the posterior and left side of the parapineal at the time of onset of migration.

Localized *Tg(dusp6:d2EGFP)* Expression Correlates with Time and Direction of Parapineal Migration. To assess how activation of the FGF pathway correlates with the temporal dynamics of parapineal migration, we performed time-lapse analysis of the distribution of *Tg(dusp6:d2EGFP)*-expressing cells before and during migration (Fig. 2 A–H, SI Appendix, Fig. S3, and Movies S1–S4). For 37 embryos, movies were for 10- to 14-h periods from the onset of migration (from 26–28 hpf to 36–40 hpf). In

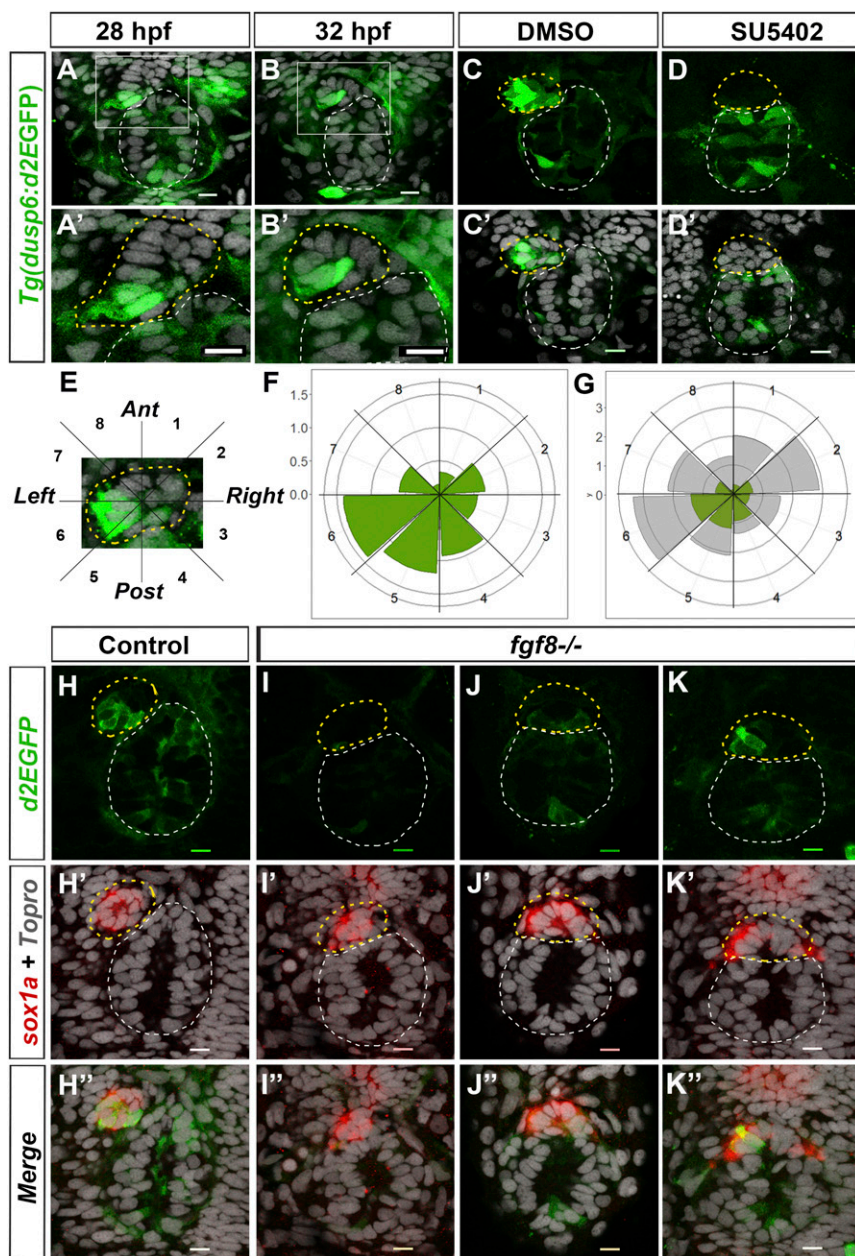


Fig. 1. The *Tg(dusp6:d2EGFP)* FGF pathway reporter is focally activated in the parapineal by Fgf8. (A–B') Confocal sections showing expression of *Tg(dusp6:d2EGFP)* (green) in the epithalami of 28-hpf (A) or 32-hpf (B) embryos with cell nuclei labeled (Topro-3, gray) and parapineal (yellow circle). White boxes in A and B are magnified in A' and B'. (C–D') Confocal maximum projections (C and D) or sections (C' and D') of the epithalami of 35-hpf *Tg(dusp6:d2EGFP)* embryos treated with DMSO (C and C') or SU5402 (D and D') immunostained for GFP (green) and additionally for nuclei (C' and D'; gray). In the control embryos (C and C'; $n = 10$), *Tg(dusp6:d2EGFP)* is expressed in both the epiphysis and the parapineal; in the SU5402 treated embryos (D and D'; $n = 11$), *Tg(dusp6:d2EGFP)* is absent in the parapineal. (E) Image of a 32-hpf parapineal defining eight 45° semi-quadrants (1–8) along the antero-posterior and LR axes relative to the mean position of the parapineal (center). (F and G) Polar graphs showing the distribution and mean number of total (G, gray) or *Tg(dusp6:d2EGFP)*⁺ (F and G, green) parapineal cells in each 45° semi-quadrant relative to the parapineal mean position (center) at 32 hpf; the distribution of total (gray) and *Tg(dusp6:d2EGFP)*⁺ cells (green) are shown at the same scale in G. The radial axis (vertical scale on the left side of polar graphs) represents the mean number of cells per semi-quadrant ($n = 27$ embryos). (H–K'') Confocal sections showing the expression of *Tg(dusp6:d2EGFP)* (green) and *sox1a* (red) at 32 hpf in control embryos (H–H''; $n = 34$) and in three illustrative *fgf8*^{-/-} mutant embryos (I–K'') displaying no expression (I and I') weakly and barely lateralized expression (J–J'') or relatively normally patterned (K and K''). The distribution and mean number of *Tg(dusp6:d2EGFP)*⁻ and *sox1a*-expressing cells are quantified in *SI Appendix, Fig. S2*. In all panels (A–D' and H–K''), embryo view is dorsal, anterior is up. (Scale bars, 10 μ m.)

four cases, we analyzed a 22-h period from 26 to 48 hpf and averaged the number and position of *Tg(dusp6:d2EGFP)*-expressing cells for each time point (Fig. 2 I–N).

Before migration, localized expression of *Tg(dusp6:d2EGFP)* usually predicted the direction of subsequent parapineal migration. At 26–28 hpf, presumptive parapineal cells are detected at the midline in the most anterior part of the pineal complex and subsequently organize into a rosette-like structure. At this stage, in the majority of embryos, a few cells express weakly *Tg(dusp6:d2EGFP)* on the left, usually at the border between epiphysis and parapineal ($n = 26$ of 41) (Fig. 2A and *SI Appendix, Fig. S4A–A''*). In other embryos, d2EGFP⁺ cells were also detected at the epiphysis–parapineal border but on both the left and right sides ($n = 10$ of 41) or on the right side only ($n = 5$ of 41) (*SI Appendix, Figs. S3A and S4B–C''*); subsequently, right-sided *Tg(dusp6:d2EGFP)*⁺ cells either relocated to the left side ($n = 5$ of 10 and $n = 3$ of 5, respectively) (*Movie S2*) or stopped expressing the transgene. From 28 to 32 hpf (Fig. 2 B–D, J, and K and *SI Appendix, Fig. S3I*), expression of *Tg(dusp6:d2EGFP)* became more robust in the left-posterior

quadrant at the border between the epiphysis and the parapineal. This robust lateralized d2EGFP expression correlated with an active phase of leftward and caudally directed migration; the distance of parapineal migration was usually highest between 32 and 36 hpf [about 14 μ m (± 5 μ m) over the 4-h period, $n = 4$] (Fig. 2K).

Tg(dusp6:d2EGFP) expression continued to delineate cells at the leading edge of the parapineal throughout the period of migration. At 36 hpf, the expression of *Tg(dusp6:d2EGFP)* usually remained very strong on the left and posterior sides of the parapineal (Fig. 2 E and L). However, from 36 to 40 hpf, transgene expression progressively decreased in cells at the front while concomitantly arising in medially positioned parapineal cells. This change prefigured a caudal reorientation of parapineal migration from 40 to 44 hpf and medial/caudal reorientation from 44 to 48 hpf (Fig. 2 F, G, M, and N and *SI Appendix, Fig. S3 F, G, I, and J*). By 48 hpf, *Tg(dusp6:d2EGFP)* expression was only retained weakly in cells at the interface with the epiphysis (Fig. 2H, *SI Appendix, Fig. S3H*, and *Movies S1 and S2*).

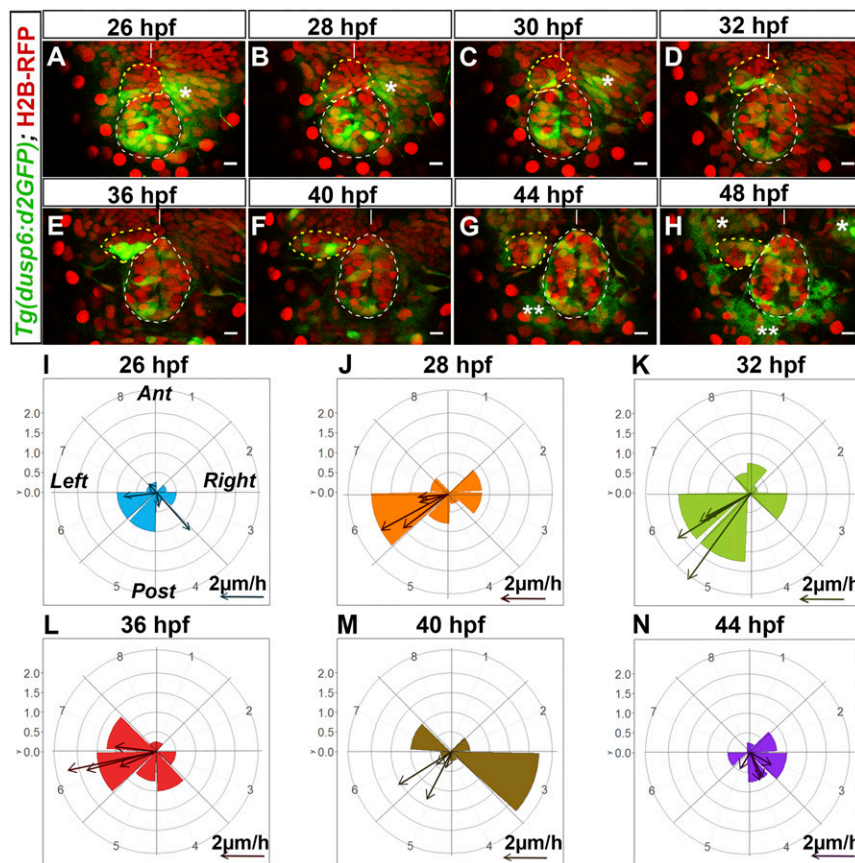


Fig. 2. *Tg(dusp6:d2EGFP)* expression is enriched in cells at the leading edge of the migrating parapineal. (A–H) Time series of thin confocal maximum projection (3 μ m) of the brain of a live *Tg(dusp6:d2EGFP)^{pt6}* (green) embryo (embryo no. 1 shown in [Movie S1](#)) expressing H2B-RFP protein (red) in cell nuclei at different stages of development (26, 28, 30, 32, 36, 40, 44, 48 hpf). The epiphysis and the parapineal are shown as white or yellow dotted circles. *Tg(dusp6:d2EGFP)* is also expressed in the presumptive habenulae, shown by an asterisk (*); two asterisks (**) indicate autofluorescence that appears from 44 hpf. Embryo view is dorsal, anterior is up. (Scale bars, 10 μ m.) Position of *Tg(dusp6:d2EGFP)⁺* cells relative to the mean position of all parapineal cells at different stages of parapineal migration are shown in [SI Appendix, Fig. S3I](#). (I–N) Polar graph showing the distribution of *Tg(dusp6:d2EGFP)* cells per 45 °C semiquadrant (1–8) relative to the parapineal mean position (center) and the antero-posterior line at a given time point: 26 hpf (I), 28 hpf (J), 32 hpf (K), 36 hpf (L), 40 hpf (M), and 44 hpf (N). The radial axis (0–2, vertical scale, upper left) represents the mean number of *Tg(dusp6:d2EGFP)⁺* parapineal cells per semiquadrant and per embryo ($n = 4$). At each specific time point, arrows show the orientation of migration for each of the four embryos [defined by the extrapolated line passing through the parapineal mean positions at T and at T + 2 h (for 26 hpf) or T + 4 h (28, 32, 36, 40, 44 hpf)]. The length of the arrow is proportional to the extrapolated distance migrated per hour. Anterior (Ant), posterior (Post), left and right orientations are shown in the I graph.

At all stages of parapineal migration but most often during the active phase of migration between 30 and 36 hpf, protrusions characteristic of active migratory behavior were visible on *Tg(dusp6:d2EGFP)*-expressing parapineal cells ([Movies S1, S2, and S4](#)) (42). Our approach of visualizing protrusions using photoverted cytoplasmic Kaede in *Tg(flhBAC:Kaede)^{vu376}* embryos did not enable unequivocal allocation of protrusions to individual cells (and may miss fine processes) but we were nevertheless able to quantify processes on *Tg(dusp6:d2EGFP)*-expressing and *Tg(dusp6:d2EGFP)*-negative parapineal cells. Although *Tg(dusp6:d2EGFP)*-negative parapineal cells did display protrusions ([SI Appendix, Fig. S5 A–B'](#) and [Movie S5](#)), they were about half as frequent as on *Tg(dusp6:d2EGFP)*-expressing cells ([SI Appendix, Fig. S5C](#)). Because there were about half as many *Tg(dusp6:d2EGFP)*-expressing cells as *Tg(dusp6:d2EGFP)*-negative cells (Fig. 1), visible protrusions were consequently about four times more frequent in parapineal cells that express *Tg(dusp6:d2EGFP)* FGF reporter transgenes than those that do not. Moreover, we found that long protrusions were predominantly observed on *Tg(dusp6:d2EGFP)⁺* cells ([SI Appendix, Fig. S5D](#)).

Taken together, these data suggest that FGF signaling pathway activity is robustly enriched at the leading edge of the parapineal during its migration and raises the question of whether localized pathway activation is required for effective migration.

Global Ectopic Expression of CA-FgfR1 Compromises Parapineal Migration.

In 3 of 41 imaged embryos, we noticed that an increase in the number of *Tg(dusp6:d2EGFP)*-expressing cells correlated with delayed migration ([Movie S3](#)). To assess if restriction of pathway activation to a few parapineal cells is required for migration, we activated the FGF pathway broadly before and during the initiation of migration using a transgenic line in which CA-FgfR1 is under the control of a heat-shock inducible promoter (43). Heat shocking *Tg(hsp70:ca-fgfr1)* transgenic embryos resulted in strong ectopic expression of the endogenous *dusp6* gene but only for up to 2 to

3 h after heat shock ([SI Appendix, Fig. S6 A–E](#)). Therefore, to ensure that the CA-FgfR1 transgene is expressed throughout the period of initiation of parapineal migration, we performed a first heat shock at 26 hpf, a second at 29 hpf and, in some cases, a third at 32 hpf.

Constitutive FgfR1 activation during the early stage of parapineal migration often led to reduced or occasionally absent migration ([SI Appendix, Fig. S6 F–I](#)). The parapineal migrated at least 25 μ m away from the midline to the left in about 90% of heat-shocked control embryos ($n = 32$ of 35) ([SI Appendix, Fig. S6H](#), light blue), whereas in embryos expressing CA-FgfR1, this frequency decreased to 60% ($n = 21$ of 35) ([SI Appendix, Fig. S6H](#), dark blue) ($P = 0.023$); in the remaining CA-FgfR1-expressing embryos, the parapineal either migrated partially (between -15 and -25 μ m in $n = 9$ of 35) or did not migrate (within -15 μ m and $+15$ μ m of the midline in $n = 4$ of 35) ([SI Appendix, Fig. S6H](#), dark blue). Although receptor activation compromised the extent of migration, when migration did occur, its direction to the left was not affected ([SI Appendix, Figs. S3I and S6G](#)).

These results suggest that widespread activation of FgfR signaling compromises parapineal migration, although less severely than when FGF signaling is absent (30).

Global Ectopic Expression of Fgf8 or CA-FgfR1 Rescues Parapineal Migration in *fgf8^{-/-}* Mutants.

In the experiments above, exogenous FgfR1 activation occurs in the context of normal Fgf8-mediated signaling in the epithalamus and consequently it is not possible to disentangle the contribution of endogenous and exogenous pathway activation to migration. To more cleanly resolve the requirement of FGF pathway activation on parapineal migration, we expressed CA-FgfR1 or Fgf8 ligand itself in *fgf8^{-/-}* mutant embryos and assessed effects upon migration.

Widespread expression of CA-FgfR1 during the period when the parapineal initiates its migration reduced the penetrance and

expressivity of the parapineal migration deficit in *fgf8*^{-/-} embryos. In most control embryos (90%, *n* = 15 of 17), the mean position of parapineal cells is between -25 and -55 μm to the left of the midline (Fig. 3 *A* and *E*, light blue) and, as above, this frequency decreased upon expression of CA-FgfR1 (56%, *n* = 9 of 16) (Fig. 3 *A* and *E*, dark blue). Also as expected, in the absence of the *Tg(hsp70:ca-fgfr1)* transgene, the parapineal failed to migrate in about half of the *fgf8*^{-/-} embryos (*n* = 17 of 32) while, in the other half, it migrated normally (*n* = 7 of 32) or at least partially toward the left (between -15 and -25 μm in *n* = 7 of 32); rarely, the parapineal was found to migrate on the right side (*n* = 1 of 32) (Fig. 3 *C* and *E*, light red). In contrast, in *fgf8*^{-/-} mutant embryos with activated CA-FgfR1, only 3 of 32 embryos failed to show any migration, while the parapineal migrated normally or partially leftward in respectively 56% (*n* = 18 of 32) and 25% (*n* = 8 of 32) of the embryos or migrated rightward (*n* = 3 of 32) (Fig. 3 *C* and *E*, dark red). This leftward shift in the mean position of the parapineal in *fgf8*^{-/-}; *Tg(hsp70:ca-fgfr1)*⁺ embryos after heat shock (Fig. 3 *E* and *F*) (*P* = 0.039, *SI Appendix, Table S1*) indicates that global activation of FgfR1 can partially rescue parapineal migration without a major effect on leftward orientation. There was no rescue of migration in mutant embryos that were not heat-shocked before parapineal migration (Fig. 3 *E* and *F*).

Because Fgf8 can influence the specification of the parapineal (40), one possibility is that pathway activation might improve migration in *fgf8* mutants indirectly by increasing the number of parapineal cells. However, the number of *gfi1ab*-expressing parapineal cells did not vary significantly between control and *fgf8*^{-/-} mutant embryos not carrying the *Tg(hsp70:ca-fgfr1)* transgene [12.4 (±3.8) for controls vs. 11.5 (±3.6) cells for *fgf8*^{-/-} mutants; adjusted *P* = 1 in pairwise Wilcoxon test] nor between heat-shocked embryos that do or do not carry the *Tg(hsp70:ca-fgfr1)* transgene [11.5 (±3.6) cells for *fgf8*^{-/-}; compared with 12.4 (±3.3) cells for *fgf8*^{-/-}; *Tg(hsp70:ca-fgfr1)*^{+/+}; adjusted *P* = 1]. Therefore, the activation of FgfR signaling does not affect parapineal cell number but promotes its migration.

Supporting the conclusions above, global activation of Fgf8 ligand by heat shocking *Tg(hsp70:fgf8)* embryos at 26 and 29 hpf similarly partially restored parapineal migration without influencing parapineal size or its leftward orientation (*SI Appendix, Fig. S7*).

Rescue of Parapineal Migration by Ectopic Expression of CA-FgfR1 Correlates with Restoration of Localized Expression of *Tg(dusp6:d2EGFP)*. Because *fgf8* is expressed broadly in the epithalamus and parapineal migration still usually occurs after widespread FgfR activation, one possibility is that if spatially localized activation of signaling is important for migration, then this may occur downstream of ligand and receptor. To ascertain if this may be the case, we assessed expression of *Tg(dusp6:d2EGFP)* reporter transgene in *fgf8*^{-/-} mutants following widespread activation of the *Tg(hsp70:ca-fgfr1)* transgene.

Global activation of FgfR1 restored *Tg(dusp6:d2EGFP)* expression within the parapineal and despite the nonlocalized expression of CA-FgfR1, within a few hours, the FGF pathway reporter was only activated mosaically as in the wild-type condition. As mentioned above (Fig. 1), the expression of *Tg(dusp6:d2EGFP)* was either absent or strongly decreased in the parapineal of *fgf8*^{-/-} mutants (Fig. 4 *C–C'*) and, when it was detectable in parapineal cells, expression was most often not lateralized (Fig. 4*G*). However, following expression of CA-FgfR1, within 3–6 h, *Tg(dusp6:d2EGFP)* expression was robustly detected in the parapineal of *fgf8*^{-/-} mutants (Fig. 4 *D–D'* and *H*) with a pattern that is very similar to that of control embryos (Fig. 4 *A–A'* and *E*).

These results show that in *fgf8*^{-/-} mutants that express CA-FgfR1, FGF signaling is reactivated mosaically despite the constitutively activated receptor being expressed ubiquitously. This suggests that the intracellular pathways downstream of the receptor are tightly and rapidly regulated to spatially localize pathway activation. This is also consistent with the observation that although *Tg(dusp6:d2EGFP)* expression was globally increased upon ectopic activation of FgfR1 in control wild-type

embryos, reporter transgene expression also rapidly resolved to being mosaic and enriched at the front of the migrating parapineal (Fig. 4 *A–A'* and *E* and *E'* vs. Fig. 4 *B–B'* and *F* and *F'*).

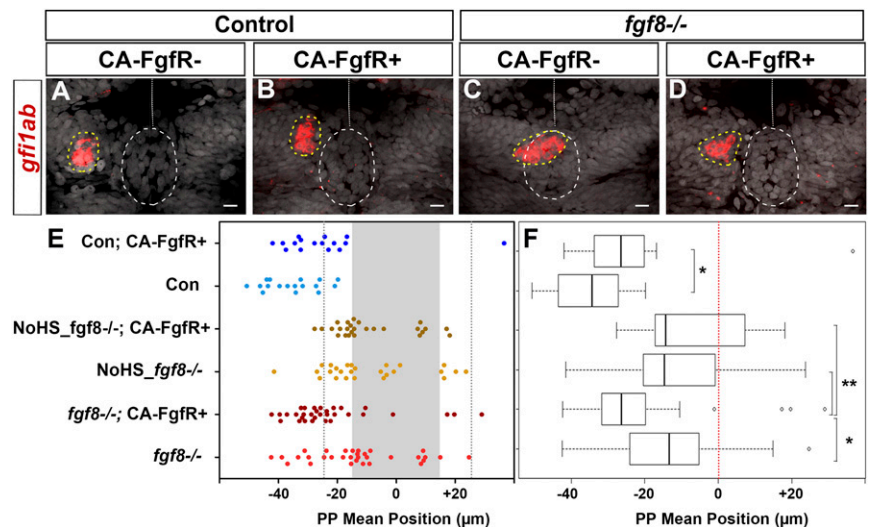
Targeted Focal Activation of CA-FgfR1 Expression in Few Parapineal Cells Improves Parapineal Migration in *fgf8*^{-/-} Mutants. The results above are consistent with localized FGF pathway activation mediating parapineal migration. However, they do not exclude the possibility that it is the activation of FGF signaling in neighboring habenular cells that indirectly promotes parapineal cell migration. Additionally, although *Tg(dusp6:d2EGFP)* is only expressed in some parapineal cells, it is still possible that other intracellular branches of the FGF pathway need to be activated in all parapineal cells. To address whether the observed focal activation of the FGF pathway in parapineal cells is indeed sufficient for parapineal migration, we tested whether we could restore parapineal migration in *fgf8*^{-/-} mutants by activating the FGF pathway in only few parapineal cells. To do so, we performed highly localized heat shock using an adapted infrared laser-evoked gene operator (IR-LEGO) optical system (44).

By irradiating two or three cells in the anterior part of the pineal complex where the future parapineal rosette forms, we could trigger the subsequent expression of CA-FgfR1 in ~six cells (*n* = 10) (Fig. 5 *A–D*). In irradiated *fgf8*^{-/-} embryos carrying the *Tg(hsp70:ca-fgfr1)* transgene (*n* = 30), the parapineal migrated leftward further than -15 μm in 60% of embryos (Fig. 5*E*, dark red) compared with only 33% of similarly treated *fgf8*^{-/-} mutant embryos lacking the transgene (Fig. 5*E'*, light red, and Fig. 5*F*) (*P* = 0.02 in Wilcoxon test). In these experiments, we never detected cells expressing CA-FgfR1 in the habenulae or other areas outside of the pineal complex, suggesting that activation of the FGF pathway is indeed required in parapineal cells. Therefore, we conclude that focal activation of CA-FgfR1 in a few parapineal cells is able to improve parapineal migration in *fgf8*^{-/-} mutants.

Nodal Signaling Restricts FGF Pathway Activation to the Left Posterior Side of the Parapineal. The orientation of parapineal migration depends on activation of Nodal signaling in the left epithalamus (32). Previous results described that absent or bilateral Nodal signaling in the brain lead to comparable outcomes on parapineal migration: that is, a randomization of directionality (25, 30, 32). To address whether the lateralization of FGF pathway activation is influenced by left-sided Nodal activity, we analyzed *Tg(dusp6:d2EGFP)* expression at the onset of parapineal migration in contexts where Nodal is either absent or bilateral following the injection of validated morpholino oligonucleotides against *southpaw* (*spaw* morphants; epithalamic Nodal signaling absent) (45) or *no tail* (*ntl* morphants; epithalamic Nodal signaling bilateral) (25), respectively (*SI Appendix, Table S2*).

As described in Figs. 1, 2, and 5, at 29–30 hpf, most parapineals showed a higher number of *Tg(dusp6:d2EGFP)*⁺ cells in the left than in the right posterior quadrant: for example, an asymmetry index (AI) in the number of *Tg(dusp6:d2EGFP)*-expressing cells was smaller than or equal to -0.2 in about 80% of control fish (Fig. 6 *A, B, G*, and *J* and *SI Appendix, Table S3*). In both contexts of absent or bilateral Nodal signaling, we observed a randomization of lateralized *Tg(dusp6:d2EGFP)* expression with one-third of embryos displaying a left bias (AI ≤ -0.2 in 38% of *ntl* morphants and in 34% of *spaw* morphants) (Fig. 6 *C* and *H–J* and *SI Appendix, Table S3*) and one-third displaying a right bias (AI ≥ +0.2 in 32% of both *ntl* and *spaw* morphants) (Fig. 6 *D, H', I'*, and *J* and *SI Appendix, Table S3*); in the remaining third of embryos, *Tg(dusp6:d2EGFP)* expression either was not (AI = 0) or was weakly lateralized (AI comprised between -0.2 and +0.2) (Fig. 6 *E, F, H', I'*, and *J* and *SI Appendix, Table S3*). While the distribution of AIs looks similar in *ntl* and *spaw* morphants, the variance of these AI was significantly higher in *ntl* morphants (AI more spread along the -1 +1 axis) than in *spaw* morphants (AI closer to the median 0) (variance ratio = 1.9, *P* = 0.045 in *F* test) (Fig. 6*J*). This reflects *Tg(dusp6:d2EGFP)* expression showing overall less lateralization in *spaw* morphants than in *ntl* morphants (Fig. 6*J*).

Fig. 3. FgfR1 receptor activation partially restores parapineal migration in *fgf8*^{-/-} mutants. (A–D) Confocal maximum projection (10 μm) showing *gfi1ab* expression (red) and cell nuclei (gray) in representative control embryos (A and B) and *fgf8*^{-/-} mutants (C and D) that express CA-FgfR1 (B and D) or not (A and C); embryo view is dorsal, anterior is up. (Scale bars, 10 μm.) Control embryos are siblings of *fgf8*^{-/-} mutants and thus correspond to both wild-type or *fgf8*^{+/-} heterozygotes. *gfi1ab* expression marks the parapineal (yellow circle) while cell nuclei staining allows us to define the epiphysis (white circle) and the brain midline (straight dotted white line). (E) Dot plot showing, for each embryo, the mean parapineal position in micrometers distant to the brain midline ($x = 0$), at 52 hpf, in control embryos (Con, blue dots) and in *fgf8*^{-/-} mutant embryos (*fgf8*^{-/-}, red dots) that expressed (CA-FgfR⁺, dark color) or not (light color) CA-FgfR1 after a heat shock at 26 and 29 hpf; “NoHS_ *fgf8*^{-/-}; CA-FgfR⁺” and “NoHS_ *fgf8*^{-/-}” correspond to *fgf8*^{-/-} mutants that do or do not carry the *Tg(hsp70:ca-fgfr1)* transgene but were not heat-shocked (dark and light yellow dots, respectively). Gray-shaded zone (–15 μm and +15 μm) define the “no migration” domain as corresponding to the average width of the epiphysis; gray dotted lines show –25 μm and +25 μm. (F) Boxplot showing the distribution of parapineal mean position relative to the brain midline (reference 0, red dotted line) in the same embryos. Parapineal mean position is shifted toward the midline in wild-type embryos expressing CA-FgfR1 (dark blue in E; $n = 16$) compared with control embryos that do not express CA-FgfR1 (light blue in E; $n = 17$); $P = 0.023$ (Wilcoxon test). The expression of CA-FgfR1 partially restores parapineal migration in *fgf8*^{-/-} mutants (dark vs. light red in E; $n = 32$); $P = 0.039$. Parapineal mean position did not differ significantly between *fgf8*^{-/-} mutants that do or do not carry the *Tg(hsp70:ca-fgfr1)* transgene but were not heat-shocked (dark versus light yellow in E; $n = 26$); $P = 1$ (see pairwise Wilcoxon test in *SI Appendix, Table S1*). Statistical significance is indicated in F, * $P < 0.05$, ** $P < 0.01$.



The difference observed in the pattern of *Tg(dusp6:d2EGFP)* expression in contexts of absent or bilateral Nodal signaling correlated with a difference in the timing of initiation of parapineal migration. At 29–30 hpf, the parapineal rosette is formed and has usually initiated its migration toward the left side in control embryos: for example, in over 90% of control embryos, the parapineal mean position was displaced more than 5 μm to the left of the midline (Fig. 6L and *SI Appendix, Table S4*). At this stage, the parapineal in *ntl* morphants had usually started to migrate toward the left (30%, $n = 37$) or the right side (35%, $n = 37$) or was observed at/near the midline (35% of embryos with a parapineal mean position between –5 μm and +5 μm, $n = 37$) (Fig. 6L and *SI Appendix, Table S4*). In contrast, the parapineal was found at the midline in most *spaw* morphants at this stage (76%, $n = 38$), while it had initiated its migration toward the left or the right side in only 11% and 13% of the embryos, respectively (Fig. 6L and *SI Appendix, Table S4*). This delay in parapineal migration in *spaw* morphants was not due to a global delay of development as, at that time point, the parapineal rosette was clearly visible in the anterior epiphysis (Fig. 6E and F). Moreover, as late as 36–38 hpf, the parapineal was still observed at the midline in about one-quarter of *spaw* morphants (25%, $n = 32$) (*SI Appendix, Fig. S8 C and C'* and *Table S5*) while, at this stage, the parapineal had initiated migration in all controls ($n = 17$) (*SI Appendix, Fig. S8 A and A'*) and in all *ntl* morphants (54% with a left and 46% with a right parapineal, $n = 26$) (*SI Appendix, Fig. S8 B and B'*).

Finally, the total number of *Tg(dusp6:d2EGFP)*⁺ parapineal cells was increased in *spaw* morphants at 30 hpf (mean = 9.7; median = 9.5) compared with control embryos (mean = 7.6; median = 7.0) (Fig. 6K) ($P = 0.026$, Welch *t* test). The number of *Tg(dusp6:d2EGFP)*⁺ cells was also slightly increased in *ntl* morphants (mean = 8.3; median = 9.0), although this difference is not significant ($P = 0.41$, Welch *t* test).

In summary, we show that left-sided *Tg(dusp6:d2EGFP)* activation is Nodal signaling-dependent. In the presence of bilateral Nodal signaling, *Tg(dusp6:d2EGFP)* expression is no longer consistently lateralized to the left, although expression is usually spatially restricted within the parapineal as in wild-type; this correlates with the parapineal initiating its migration toward the left or the right in most embryos from 29 to 30 hpf. Consistent lateralization of *Tg(dusp6:d2EGFP)* expression is also compromised in the absence of Nodal signaling but, in this condi-

tion, expression is generally less restricted and less lateralized within the parapineal and this correlates with delayed parapineal migration.

Discussion

In this study we show that during their leftward migration, parapineal cells respond to Fgf8 and that, despite it being likely that all parapineal cells are exposed to Fgf ligands, FGF signaling is activated focally in only few cells usually located at the leading edge. Activation of FGF reporter transgene expression in parapineal leading cells is lost in *fgf8*^{-/-} mutant embryos in which parapineal migration is compromised. Widespread activation of the FGF pathway in *fgf8*^{-/-} mutant embryos rescues migration, while concomitantly restoring the localized expression of *Tg(dusp6:d2EGFP)* at the leading edge of the parapineal and targeted activation of the FGF pathway in a small number of parapineal cells is sufficient to promote parapineal migration in *fgf8*^{-/-} mutants. Finally we show that lateralized Nodal signaling influences the spatial localization and restriction of *Tg(dusp6:d2EGFP)* expression and subsequent timing and direction of parapineal migration. Our results show that parapineal cells respond as a collective rather than as individuals to environmental signals and that the capacity of parapineal cells to coordinate cellular responses to such signals impacts the ability of the parapineal to undergo efficient directed collective migration.

During border cell migration and tracheal sprouting in *Drosophila* or during endothelial cell migration in vertebrate angiogenesis, selection and guidance of cells at the migration front, so-called leading cells or tip cells, are dependent on receptor tyrosine kinase (RTK) signaling (3). Here, we establish the parapineal as an example of a freely migrating group of cells that depends on RTK signaling for the selection of leading cells and promotion of migration. Although *Tg(dusp6:d2EGFP)* expression is always detected in cells located at the migration front during the active phase of migration, in some embryos it can also be detected at the rear or on the lateral side of the parapineal rosette and the intensity of transgene activation can also vary among expressing cells. This variability in the number, position, and fluorescence intensity of *Tg(dusp6:d2EGFP)*⁺ cells might reflect the dynamic nature of the cell-to-cell communication events within the parapineal that define leading cells and that may mediate competition

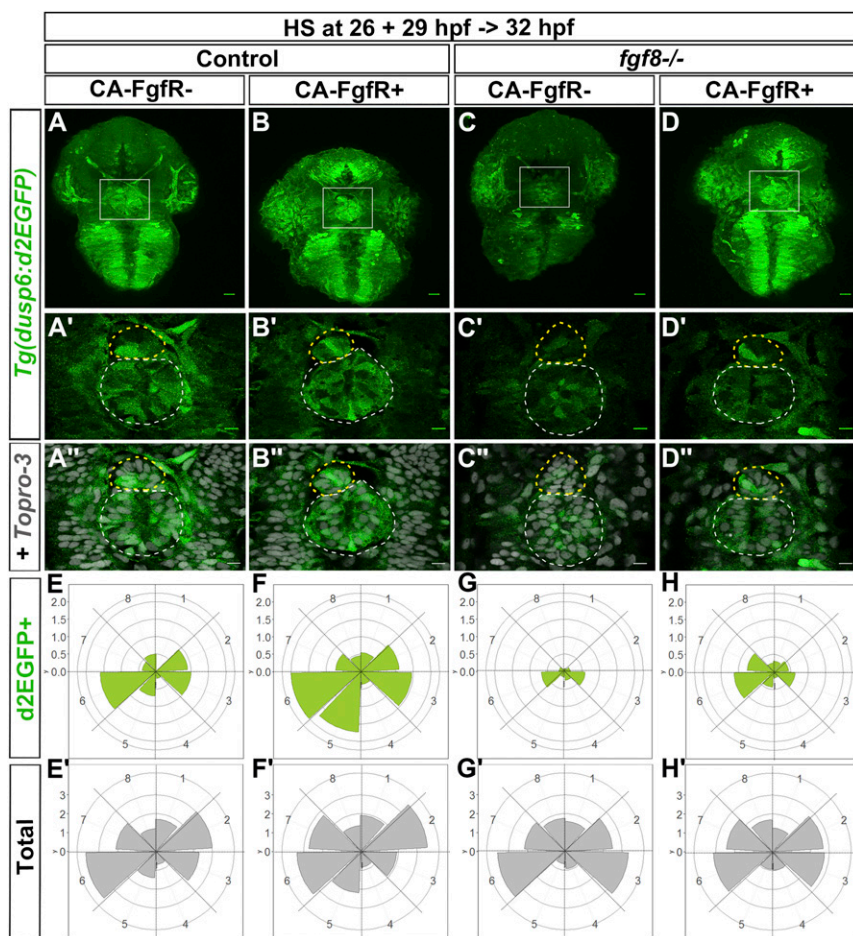


Fig. 4. Global overexpression of CA-FgfR1 in *fgf8*^{-/-} mutants rescues focal left-sided expression of *Tg(dusp6:d2EGFP)*. (A–D') Confocal maximum projection (55 μ m) showing the whole head (A–D) or confocal sections (A'–D') showing the epithalamus of 32-hpf *Tg(dusp6:d2EGFP)* control embryos (A–B') or *Tg(dusp6:d2EGFP)* *fgf8*^{-/-} mutants (C–D') that express (B–B' and D–D') or not (A–A' and C–C') *Tg(hsp70:ca-fgfr1)* transgene after heat shock at 26 and 29 hpf. (Scale bars, 25 μ m in A–D and 10 μ m in A'–D'.) The image in A'–D' corresponds to the image in A'–D' (green) superimposed on nuclear staining (gray) allowing visualization of the epiphysis (white circle) and paripineal (yellow circle); embryo view is dorsal, anterior is up. (E–H') Polar graphs showing the distribution and mean number of total (E'–H') or *Tg(dusp6:d2EGFP)*⁺ (E–H) paripineal cells in each 45° semiquadrant (1–8) relative to the paripineal mean position (center) at 32 hpf. Cell distribution and mean number are shown for control embryos that express (F and F'; *n* = 11) or not (E and E'; *n* = 10) CA-FgfR1 transgene and for *fgf8*^{-/-} mutants that express (H and H'; *n* = 16) or not (G and G'; *n* = 12) CA-FgfR1. Radial axis (vertical scale on the left side) represent the mean number of *Tg(dusp6:d2EGFP)*⁺ paripineal cells (green area in E–H, scale 0–2) or all paripineal cells (gray area in E'–H', scale 0–3) per semiquadrant and per embryo. The expression of *Tg(dusp6:d2EGFP)* is increased in the paripineal of embryos expressing CA-FgfR1 although it is still mosaic and enriched on the left/posterior side (B–B' and F; *n* = 11) as in controls (A–A' and E; *n* = 10). In *fgf8*^{-/-} embryos, *Tg(dusp6:d2EGFP)* is either not expressed in the paripineal or weakly detected (C–C' and G; *n* = 12) while its expression is rescued in the paripineal of *fgf8*^{-/-} embryos expressing CA-FgfR1 transgene (D–D' and H; *n* = 16).

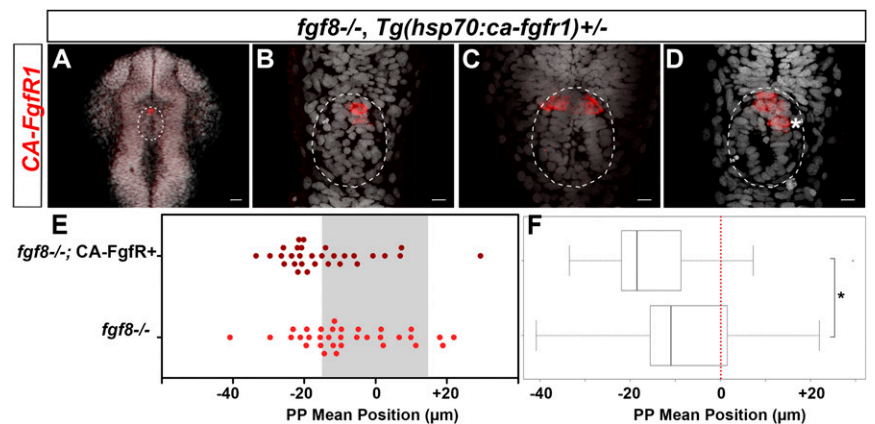
among paripineal cells for the leading position; indeed, during the active phase of migration, paripineal cells can exchange the leading position as cyclists do in the peleton (Movie S4). A similar dynamic in leader-exchange has also been described during *Drosophila* border cell migration (46) and vessel sprouting in zebrafish (47), and may provide a way for the migrating cluster to better adapt to the environment. Such variability in the number and in the position of *Tg(dusp6:d2EGFP)*-expressing cells could underlie the variability that exists in the timing of paripineal migration in wild-type embryos. Indeed, we noticed that paripineal migration is more frequently delayed in the rare embryos in which *Tg(dusp6:d2EGFP)*-expressing cells are initially found on both sides or on the right side only than when they locate to the left side at the onset of migration.

One interesting aspect of our study is the relative robustness of paripineal migration in response to global activation of FGF signaling. Various observations suggest that all paripineal cells are competent to activate the FGF pathway; for example, ablating the left or the right side of the presumptive paripineal results in the remaining half migrating normally, indicating that both left and right paripineal cells are competent to migrate toward the left (25). Moreover, we show that all paripineal cells can activate expression of the *dusp6* gene rapidly after ectopic expression of Fgf8 (SI Appendix, Fig. S9). Although all paripineal cells seem able to respond to Fgf8, activation of FGF signaling is nonetheless restricted to few cells. This suggests the existence of a mechanism downstream of the activated receptor that permits pathway activation in a few cells while silencing it in others. The processes involved in restricting FGF pathway activation are likely functional in *fgf8*^{-/-} mutants, as we can rescue the mosaic pattern of *Tg(dusp6:d2EGFP)* expression after global misexpression of CA-FgfR1. The mechanisms restricting FGF

pathway activation are likely to depend on paripineal cells being able to communicate their state of FGF pathway activation. In both the *Drosophila* tracheal system and vertebrate vessel sprouting, Notch-Delta signaling contributes to tip cell selection by restricting the ability of follower cells to activate RTK signaling (48–50), and this pathway is an obvious candidate for a comparable role in the paripineal.

The mechanisms underlying the roles of the FGF signaling pathway in collective migration vary depending on the context in which they have been addressed and even within the same model of cell migration (51). In the zebrafish LLP for example, FGF signaling is required upstream of Notch signaling for the epithelialization and apical constriction that underlies neuromast rosette formation at the back of the primordium, thereby coupling morphogenesis with LLP migration (16–20, 52). Besides this Notch-mediated role in rosette self-organization (52), FGF signaling is also required in this system to trigger the coalescence of the LLP at the onset of migration (12), to maintain LLP polarity via restriction of Wnt/ β -catenin signaling to the leading zone (53), and to maintain cohesion among cells of the cluster during migration, as trailing cells are attracted toward Fgf signals produced by leading cells (54). However, despite progress in understanding the various specific functions of the FGF pathway in promoting cell migration, it is not clear yet how Fgf signals are interpreted by cell collectives. In *Drosophila*, expression of an active version of the PDGF and VEGF related receptor (PVR) receptor in a single border cell can rescue migration of the entire cluster in the absence of ligand (55). This study suggested that it is the difference in RTK signaling levels between cells in the cluster rather than, or in addition to, an asymmetry in RTK signaling at the level of the individual cells (along the leading to trailing axis of the migrating cell) that triggers migration. In contrast, expression of a constitutively

Fig. 5. Focal activation of FGF signaling in few parapineal cells partially restores parapineal migration in *fgf8*^{-/-} mutants. (A–D) Confocal 40- μ m maximum projection and confocal thin 2- μ m projections (B–D) showing the expression of the *ca-fgfr1* transgene by in situ hybridization (red) in four different representative *fgf8*^{-/-}; *Tg(hsp70:ca-fgfr1)*^{+/-} embryos, 1–2 h after two cells were irradiated in the anterior epiphysis. (Scale bars, 25 μ m in A and 10 μ m in B–D.) Superimposed nuclear staining (Topro-3, gray) visualizes the pineal complex (white circle) consisting of both the pineal and the parapineal at this stage (26–28 hpf). *ca-fgfr1* mRNA is only detected in the anterior pineal complex, in three cells (A and B) or six cells (C and D), the average number being 6 CA-FgfR1-expressing cells ($n = 10$ embryos). Given their location in the anterior pineal complex, most of these CA-FgfR1-expressing cells are expected to become parapineal cells; some more posterior cells (*) might become epiphyseal cells; embryo view is dorsal, anterior is up. (E) Dot plot showing, for each embryo, the mean parapineal position in micrometers distant to the brain midline ($x = 0$), at 52 hpf, in *fgf8*^{-/-} mutants that were locally heat-shocked (two to three irradiated cells) between 25 and 29 hpf; gray-shaded zone ($-15 \mu\text{m}$ and $+15 \mu\text{m}$) defines the average width of the epiphysis. Parapineal mean position in *fgf8*^{-/-} mutant embryos carrying the *Tg(hsp70:ca-fgfr1)* transgene is slightly shifted toward the left (dark red dots, $n = 30$) compared with *fgf8*^{-/-} mutants that do not express CA-FgfR1 (light red dots, $n = 33$). (F) Boxplot showing the distribution of parapineal mean position relative to the brain midline (reference 0) in same embryos. Local expression of CA-FgfR1 in few parapineal cells partially rescues parapineal migration ($P = 0.02$; Wilcoxon test; * indicates statistical significance in F).



active Breathless Fgf receptor in a single cell is not sufficient to rescue the migration of *Drosophila* tracheal cells (56), despite expression of a wild-type FGF doing so (57). Therefore, in tracheal cells, the activation of FGF signaling needs to be asymmetrically distributed, not only between cells in the cluster as in border cells, but within the cell itself for it to become a leading cell and to drive the migration of the whole cluster.

Here, we show that parapineal migration can be restored by expressing constitutively activated CA-FgfR1 focally in few cells in a context of reduced ligand level. Therefore, our results differ from those described for *Drosophila* tracheal cells and suggest that, similar to border cells, differences in the levels of FGF pathway activation between parapineal cells can define leading cells and promote migration. The fact that global activation of FgfR1 delays migration in wild-type embryos further supports this idea. However, in contrast to what has been suggested by studies in border cells (58), we show that parapineal migration can also be restored in *fgf8*^{-/-} mutants by expressing constitutively activated CA-FgfR1 in all cells as, in this context, the global activation of FGF signaling resolves to become spatially restricted downstream of the activated receptor. Therefore, our data highlight common features and point out important differences in the mechanisms underlying the interpretation of Fgf signals in different models of Fgf-dependent collective cell migration.

One unusual feature of parapineal migration is that it almost always is directed to the left side of the brain. This is a consequence of bilaterally expressed Fgf8 promoting cell migration while left-sided expression of Cyclops, a Nodal/TGF- β signal, determines directionality (25, 30). Our results show that consistent left-sided lateralization of *Tg(dusp6:d2EGFP)* expression is lost when unilateral Nodal pathway activation is abrogated, and this correlates with randomized parapineal cell migration. Our results also reveal Nodal-dependent influence upon restriction of *Tg(dusp6:d2EGFP)* expression to a few parapineal cells, which in turn influences the timing of onset of parapineal migration. Indeed, although absent or bilateral Nodal signaling both result in randomized parapineal migration (29, 30, 32), we find that these two contexts differ in their impact on the pattern of FGF activation. Bilateral Nodal signaling leads to a randomization of *Tg(dusp6:d2EGFP)* lateralization and a randomization of parapineal migration without significant delay. In contrast, in absence of Nodal pathway activation, lateralization and restriction of *Tg(dusp6:d2EGFP)* expression is reduced and this correlates with delayed parapineal cell migration. Therefore, our data suggest that Nodal signaling direc-

tionally biases and times parapineal migration by contributing to the restriction and lateralization of Fgf signaling.

This work sets the stage for studies aimed at understanding how the Nodal pathway could contribute to restrict the activation of the FGF pathway to a few leading cells and how it provides a leftwards bias to the focal FGF pathway activation.

Materials and Methods

Fish Lines. Adults heterozygous for the *fgf8* mutation (*fgf8*^{ti282a}/*lacerebellar/ace*) (59) were identified by PCR genotyping (60). Heterozygous embryos carrying the *Tg(hsp70:fgf8a)*^{x17} transgenic insertion were identified by PCR genotyping (61). Embryos heterozygous for *Tg(hsp70:ca-fgfr1;cryaa:DsRed)*^{pd3} (43) were identified by the presence of DsRed expression in the lens from 48 hpf or at 32 hpf by PCR, as described previously (62). *Tg(dusp6:d2EGFP)*^{pt6} and *Tg(dusp6:d2EGFP)*^{pt8} (34) lines were used as reporters for FGF pathway activity; *Tg(flhBAC:Kaede)*^{vu376} was used as marker of the pineal complex (40).

Quantification of the Number and Position of *Tg(dusp6:d2EGFP)*⁺ and *gfi1ab*⁺ Parapineal Cells. The position and number of parapineal cells negative or positive for the *Tg(dusp6:d2EGFP)* transgene were analyzed using the ImageJ software (ROI Manager tool), the position of each cell being defined by the center of the cell nucleus detected with the Topro-3 staining. For each parapineal cell, we calculate its x and y position relative to the center of the parapineal to create the polar graph (R Studio). Parapineal cells positive for the *gfi1ab* marker were counted using the Multipoint tool on ImageJ software and the position of each parapineal cell was measured relative to the brain midline (reference origin = 0) to define parapineal mean position.

Calculation of the AI of *Tg(dusp6:d2EGFP)* Expression. The AI of *Tg(dusp6:d2EGFP)* expression was calculated using the following equation: $n(Rp) - n(Lp)/n(Rp) + n(Lp)$, where $n(Rp)$ is the number of *Tg(dusp6:d2EGFP)*⁺ cells in the right posterior quadrant of the parapineal rosette and $n(Lp)$, the number in the left posterior quadrant.

Ethics Statement. All experiments were performed in accordance with both the guidelines from the European directive on the protection of animals used for scientific purposes (2010/63/UE) and national guidelines. In France, all animals were maintained in a facility certified by the French Ministry of Agriculture (approval no. A3155510). The work received the project no. APAFIS#3653-2016011512005922 on the 01/12/2016. M.R. received authorization to experiment on vertebrates models (311255556) from the Direction Départementale de la Protection des Populations de la Haute-Garonne. In Germany, all experimental procedures were performed according to the guidelines of the German animal welfare law and approved by the local government (Tierschutzgesetz §11, Abs. 1, Nr. 1, husbandry permit no. AZ

ACKNOWLEDGMENTS. We thank members of the P.B. and S.W.W. laboratories for insightful discussions; Michael Tsang for kindly providing *Tg(dusp6:d2EGFP)¹⁶* and *Tg(dusp6:d2EGFP)¹⁸* transgenic lines, as well as reagents and plasmids; Bruce Riley for the *Tg(hsp70:fgf8a)^{x17}* line; Qiling Xu for providing the *Tg(hsp70:ca-fgfr1)^{pd3}* line generated in Ken Poss's group; Pauline Rataud for technical assistance; Brice Ronsin from the Toulouse RIO Imaging platform; Stéphane Relexans, Richard Brimicombe, and Aurore Laire and the

University College London Fish Facility team for fish care; and Bertrand Benazerf, Damien Ramel, and Alain Vincent for critical reading of the manuscript. This work was supported by the Centre National de la Recherche Scientifique, the Institut National de la Santé et de la Recherche Médicale, Université de Toulouse III, Fondation pour la Recherche Médicale (DEQ20131029166), Fédération pour la Recherche sur le Cerveau, Association pour la Recherche sur le Cancer (PJA 20131200173), the European Community (254195), and the Wellcome Trust.

- Friedl P, Gilmour D (2009) Collective cell migration in morphogenesis, regeneration and cancer. *Nat Rev Mol Cell Biol* 10:445–457.
- Rørth P (2012) Fellow travellers: Emergent properties of collective cell migration. *EMBO Rep* 13:984–991.
- Pocha SM, Montell DJ (2014) Cellular and molecular mechanisms of single and collective cell migrations in *Drosophila*: Themes and variations. *Annu Rev Genet* 48:295–318.
- Scarpa E, Mayor R (2016) Collective cell migration in development. *J Cell Biol* 212:143–155.
- Aman A, Piotrowski T (2011) Cell-cell signaling interactions coordinate multiple cell behaviors that drive morphogenesis of the lateral line. *Cell Adhes Migr* 5:499–508.
- Ochoa-Espinosa A, Affolter M (2012) Branching morphogenesis: From cells to organs and back. *Cold Spring Harb Perspect Biol* 4:a008243.
- Gilmour D, Rembold M, Leptin M (2017) From morphogen to morphogenesis and back. *Nature* 541:311–320.
- Theveneau E, Mayor R (2013) Collective cell migration of epithelial and mesenchymal cells. *Cell Mol Life Sci* 70:3481–3492.
- Campbell K, Casanova J (2016) A common framework for EMT and collective cell migration. *Development* 143:4291–4300.
- Sutherland D, Samakovlis C, Krasnow MA (1996) Branchless encodes a *Drosophila* FGF homolog that controls tracheal cell migration and the pattern of branching. *Cell* 87:1091–1101.
- Sato A, et al. (2011) FGF8 signaling is chemotactic for cardiac neural crest cells. *Dev Biol* 354:18–30, and erratum (2012) 370:164.
- Breau MA, Wilson D, Wilkinson DG, Xu Q (2012) Chemokine and Fgf signalling act as opposing guidance cues in formation of the lateral line primordium. *Development* 139:2246–2253.
- Kadam S, Ghosh S, Stathopoulos A (2012) Synchronous and symmetric migration of *Drosophila* caudal visceral mesoderm cells requires dual input by two FGF ligands. *Development* 139:699–708.
- Bénazéraf B, et al. (2010) A random cell motility gradient downstream of FGF controls elongation of an amniote embryo. *Nature* 466:248–252.
- McMahon A, Reeves GT, Supatto W, Stathopoulos A (2010) Mesoderm migration in *Drosophila* is a multi-step process requiring FGF signaling and integrin activity. *Development* 137:2167–2175.
- Lecaudey V, Cakan-Akdogan G, Norton WHJ, Gilmour D (2008) Dynamic Fgf signaling couples morphogenesis and migration in the zebrafish lateral line primordium. *Development* 135:2695–2705.
- Nechiporuk A, Raible DW (2008) FGF-dependent mechanosensory organ patterning in zebrafish. *Science* 320:1774–1777.
- Ernst S, et al. (2012) Shroom3 is required downstream of FGF signalling to mediate proneuroblast assembly in zebrafish. *Development* 139:4571–4581.
- Harding MJ, Nechiporuk AV (2012) Fgfr-Ras-MAPK signaling is required for apical constriction via apical positioning of Rho-associated kinase during mechanosensory organ formation. *Development* 139:3130–3135.
- Durdu S, et al. (2014) Luminal signalling links cell communication to tissue architecture during organogenesis. *Nature* 515:120–124.
- Beretta CA, Dross N, Guitierrez-Triana JA, Ryu S, Carl M (2012) Habenula circuit development: Past, present, and future. *Front Neurosci* 6:51.
- Concha ML, Bianco IH, Wilson SW (2012) Encoding asymmetry within neural circuits. *Nat Rev Neurosci* 13:832–843.
- Duboc V, Dufourcq P, Blader P, Roussigné M (2015) Asymmetry of the brain: Development and implications. *Annu Rev Genet* 49:647–672.
- Roussigné M, Blader P, Wilson SW (2012) Breaking symmetry: The zebrafish as a model for understanding left-right asymmetry in the developing brain. *Dev Neurobiol* 72:269–281.
- Concha ML, et al. (2003) Local tissue interactions across the dorsal midline of the forebrain establish CNS laterality. *Neuron* 39:423–438.
- Aizawa H, et al. (2005) Laterotopic representation of left-right information onto the dorso-ventral axis of a zebrafish midbrain target nucleus. *Curr Biol* 15:238–243.
- Bianco IH, Carl M, Russell C, Clarke JD, Wilson SW (2008) Brain asymmetry is encoded at the level of axon terminal morphology. *Neural Dev* 3:9.
- Gamse JT, Thisse C, Thisse B, Halpern ME (2003) The parapineal mediates left-right asymmetry in the zebrafish diencephalon. *Development* 130:1059–1068.
- Gamse JT, et al. (2005) Directional asymmetry of the zebrafish epithalamus guides dorsoventral innervation of the midbrain target. *Development* 132:4869–4881.
- Regan JC, Concha ML, Roussigné M, Russell C, Wilson SW (2009) An Fgf8-dependent bistable cell migratory event establishes CNS asymmetry. *Neuron* 61:27–34.
- Bisgrove BW, Essner JJ, Yost HJ (2000) Multiple pathways in the midline regulate concordant brain, heart and gut left-right asymmetry. *Development* 127:3567–3579.
- Concha ML, Burdine RD, Russell C, Schier AF, Wilson SW (2000) A nodal signaling pathway regulates the laterality of neuroanatomical asymmetries in the zebrafish forebrain. *Neuron* 28:399–409.
- Liang JO, et al. (2000) Asymmetric nodal signaling in the zebrafish diencephalon positions the pineal organ. *Development* 127:5101–5112.
- Molina GA, Watkins SC, Tsang M (2007) Generation of FGF reporter transgenic zebrafish and their utility in chemical screens. *BMC Dev Biol* 7:62.
- Eblaghie MC, et al. (2003) Negative feedback regulation of FGF signaling levels by Pyst1/MKP3 in chick embryos. *Curr Biol* 13:1009–1018.
- Kawakami Y, et al. (2003) MKP3 mediates the cellular response to FGF8 signalling in the vertebrate limb. *Nat Cell Biol* 5:513–519.
- Tsang M, et al. (2004) A role for MKP3 in axial patterning of the zebrafish embryo. *Development* 131:2769–2779.
- Matsuda M, et al. (2013) Lef1 regulates Dusp6 to influence neuromast formation and spacing in the zebrafish posterior lateral line primordium. *Development* 140:2387–2397.
- Mohammadi M, et al. (1997) Structures of the tyrosine kinase domain of fibroblast growth factor receptor in complex with inhibitors. *Science* 276:955–960.
- Clanton JA, Hope KD, Gamse JT (2013) Fgf signaling governs cell fate in the zebrafish pineal complex. *Development* 140:323–332.
- Draper BW, Morcos PA, Kimmel CB (2001) Inhibition of zebrafish fgf8 pre-mRNA splicing with morpholino oligos: A quantifiable method for gene knockdown. *Genesis* 30:154–156.
- Ridley AJ (2015) Rho GTPase signalling in cell migration. *Curr Opin Cell Biol* 36:103–112.
- Marques SR, Lee Y, Poss KD, Yelon D (2008) Reiterative roles for FGF signaling in the establishment of size and proportion of the zebrafish heart. *Dev Biol* 321:397–406.
- Kamei Y, et al. (2009) Infrared laser-mediated gene induction in targeted single cells in vivo. *Nat Methods* 6:79–81.
- Long S, Ahmad N, Rebagliati M (2003) The zebrafish nodal-related gene southpaw is required for visceral and diencephalic left-right asymmetry. *Development* 130:2303–2316.
- Prasad M, Montell DJ (2007) Cellular and molecular mechanisms of border cell migration analyzed using time-lapse live-cell imaging. *Dev Cell* 12:997–1005.
- Jakobsson L, et al. (2010) Endothelial cells dynamically compete for the tip cell position during angiogenic sprouting. *Nat Cell Biol* 12:943–953.
- Ghabrial AS, Krasnow MA (2006) Social interactions among epithelial cells during tracheal branching morphogenesis. *Nature* 441:746–749.
- Ikeya T, Hayashi S (1999) Interplay of Notch and FGF signaling restricts cell fate and MAPK activation in the *Drosophila* trachea. *Development* 126:4455–4463.
- Siekmann AF, Lawson ND (2007) Notch signalling and the regulation of angiogenesis. *Cell Adhes Migr* 1:104–106.
- Bae Y-K, Trisnadi N, Kadam S, Stathopoulos A (2012) The role of FGF signaling in guiding coordinate movement of cell groups: Guidance cue and cell adhesion regulator? *Cell Adhes Migr* 6:397–403.
- Kozlovskaja-Gumbrienė A, et al. (2017) Proliferation-independent regulation of organ size by Fgf/Notch signaling. *eLife* 6:e21049.
- Aman A, Piotrowski T (2008) Wnt/beta-catenin and Fgf signaling control collective cell migration by restricting chemokine receptor expression. *Dev Cell* 15:749–761.
- Dalle Nogare D, et al. (2014) Leading and trailing cells cooperate in collective migration of the zebrafish posterior lateral line primordium. *Development* 141:3188–3196.
- Inaki M, Vishnu S, Cliffe A, Rørth P (2012) Effective guidance of collective migration based on differences in cell states. *Proc Natl Acad Sci USA* 109:2027–2032.
- Lebreton G, Casanova J (2016) Ligand-binding and constitutive FGF receptors in single *Drosophila* tracheal cells: Implications for the role of FGF in collective migration. *Dev Dyn* 245:372–378.
- Lebreton G, Casanova J (2014) Specification of leading and trailing cell features during collective migration in the *Drosophila* trachea. *J Cell Sci* 127:465–474.
- Poukkula M, Cliffe A, Chngede R, Rørth P (2011) Cell behaviors regulated by guidance cues in collective migration of border cells. *J Cell Biol* 192:513–524.
- Reifers F, et al. (1998) Fgf8 is mutated in zebrafish acerebellar (ace) mutants and is required for maintenance of midbrain-hindbrain boundary development and somitogenesis. *Development* 125:2381–2395.
- Albertson RC, Yelick PC (2007) Fgf8 haploinsufficiency results in distinct craniofacial defects in adult zebrafish. *Dev Biol* 306:505–515.
- Kwon H-J, Bhat N, Sweet EM, Cornell RA, Riley BB (2010) Identification of early requirements for preplacodal ectoderm and sensory organ development. *PLoS Genet* 6:e1001133.
- Gonzalez-Quevedo R, Lee Y, Poss KD, Wilkinson DG (2010) Neuronal regulation of the spatial patterning of neurogenesis. *Dev Cell* 18:136–147.

Supporting Information for

Left/right asymmetric collective migration of parapineal cells is mediated by focal FGF signalling activity in leading cells.

Myriam Roussigné^{a,1,2,#}, Lu Wei^{a,1}, Erika Tsingos^b, Franz Kuchling^b, Mansour Alkobtawi^c, Matina Tsalavouta^d, Joachim Wittbrodt^b, Matthias Carl^{e,f}, Patrick Blader^{a,2}, Stephen W. Wilson^{d,2}.

¹ These authors contributed equally to experimental work

² Joint senior authors.

[#] Author for correspondence: myriam.roussigne@univ-tlse3.fr

This PDF file includes:

SI Materials and Methods
Figs. S1 to S9
Tables S1 to S5
Captions for movies S1 to S5
References for SI reference citations

Other supplementary materials for this manuscript include the following:

Movies S1 to S5

SI. Materials and Methods

Embryos were raised and staged according to standard protocols (1).

Drug treatment

Embryos collected from *Tg(dusp6:d2EGFP)^{pt6}* outcrosses were dechorionated and treated from 25 hpf to 35 hpf with 10 μ M SU5402 (Calbiochem) diluted from a 10 mM DMSO based stock solution in E3 medium or with an equal volume of DMSO diluted in E3 medium (controls).

Ectopic expression of CA-FgfR1 and Fgf8

Global misexpression of CA-FgfR1 or Fgf8 was induced in *Tg(hsp70:ca-FgfR1; cryaa:DsRed)^{pd3}* or *Tg(hsp70:Fgf8a)^{x17}* heterozygote embryos respectively, by performing heat shock before parapineal migration (25-26 hpf) (39°C, 45 minutes); a second short heat shock (15 min, 39°C) was carried out 3h later (28-29 hpf). For Fig. 3, in some cases, we performed an additional short heat shock at 32 hpf (39°C, 15 min).

Morpholino injection

Morpholino oligonucleotides (MO) targeting *no tail (ntl)* (2) or *southpaw (spaw)* (3) were solubilized at 1 mM in water and diluted to 0.5 mM working concentration; about 8 ng for *ntl* MO and 12 ng for *spaw* were injected into *Tg(dusp6:d2EGFP)* eggs at one cell stage. Embryos were subsequently fixed at 29-30 hpf and/or at 36-38 hpf and analyzed by confocal imaging after Topro-3 nuclear staining. For some 29-30 hpf embryos, we performed *pitx2 in situ* hybridization as a read-out of Nodal activity in the epithalamus to confirm that injection of *ntl* MO and *spaw* MO resulted, as previously described, in a majority of embryos with bilateral (4) or absent Nodal pathway (3) activation in the brain, respectively (**Table S2**).

In situ hybridization and immunohistochemical stainings

Embryos were fixed overnight at 4°C in BT-FIX (61), after which they were dehydrated through ethanol series and stored at -20°C until use. *In situ* hybridizations were performed using

antisense DIG labeled probes for *gfi1ab* (5), *sox1a* (6), *dusp6* (7) and *ca-fgfr1* (8). Hybridization step was performed at 65°C for *dusp6* and *ca-fgfr1* probes or at 60°C for *gfi1ab* and *sox1a* probes, in hybridization mix (formamide 50%, 4X SSC, yeast tRNA 1 mg/mL, heparin 0.05 mg/mL, Roche blocking reagent 2%, CHAPS 0.1%, EDTA 5mM, Tween 0.08%); details of the *in situ* hybridization protocol are available upon request. *In situ* hybridizations were completed using Fast Red (from Roche or Sigma Aldrich) as an alkaline phosphatase substrate. Immunohistochemical stainings were performed in PBS containing 0.5% triton using anti-GFP (1/1000, Torrey Pines Biolabs) and Alexa 488 or Alexa 555-conjugated goat anti-rabbit IgG (1/1000, Molecular Probes). For nuclear staining, embryos were incubated in Topro-3 (1/1000, Molecular Probes) as previously described (9).

Image acquisition

Bright field pictures were taken on a Nikon eclipse 80i microscope. Confocal images of fixed embryos were acquired on upright Leica SP5 or SP8 microscopes, using the resonant fast mode and oil x63 (aperture 1.4) or x20 (aperture 1.4) objectives. Live imaging was performed on an upright Leica SP8 microscope using a water x25 objective or an inverted Zeiss 710 with a 63x oil objective. Confocal stacks were analyzed using ImageJ software.

Quantification of the number and position of *Tg(dusp6:d2EGFP)* positive parapineal cells

The position and number of parapineal cells negative or positive for expression of the *Tg(dusp6:d2EGFP)* transgene were analyzed using ImageJ software (ROI Manager tool), the position of each cell being defined by the center of the cell nucleus detected with Topro-3 staining. The total number of parapineal cells was estimated by counting cell nuclei in the parapineal rosette using Topro-3 staining (as described in Fig. 1F, Fig. 4, Fig. 6 and Fig. S2) or by using *sox1a* expression as a specific marker of parapineal cell identity (Fig. S2). For each parapineal cell, we calculate its x and y position relative to the center of the parapineal (calculated as the mean of x and y positions of all parapineal cells).

To avoid possible bias in the counting procedure, when different genetic contexts were analyzed and compared (Fig. S2, Fig. 4 and Fig. 6), we quantified the mean intensity of the d2EGFP staining in an area corresponding to the cell nucleus by using the ROI Manager Tool (ImageJ). We then defined an intensity threshold above which the cell was considered to be *Tg(dusp6:d2EGFP)+* and used the same intensity threshold to analyze the number of *Tg(dusp6:d2EGFP)+* cells in each different context.

To create polar graphs, we plotted and quantified the numbers of total and *Tg(dusp6:d2EGFP)* positive parapineal cells in each semi-quadrant (1 to 8) of the parapineal. Semi-quadrants were defined relative to a line passing from anterior to posterior through the parapineal mean position (reference 0; centre of the polar graph) and progressing clockwise from the most anterior position: 0-45°C (1), 45-90°C (2) and so on. The number of cells per semi-quadrant was divided by the total number of embryos analyzed to obtain the mean number of total or *Tg(dusp6:d2EGFP)* positive parapineal cells per semi-quadrant and per embryo (left vertical scale). The polar graphs were created on R Studio.

Calculation of the Asymmetry Index (AI) of *Tg(dusp6:d2EGFP)* expression

Compared to control embryos, expression of *Tg(dusp6:d2EGFP)* and laterality of parapineal migration in *ntl* and *spaw* morphants was variable. Consequently, for each embryo, we calculated the parapineal mean position relative to the midline (using Topro-3 as a nuclear marker as described above) and an asymmetry index of *Tg(dusp6:d2EGFP)* expression using the following equation: $[n(Rp) - n(Lp)] / [n(Rp) + n(Lp)]$, where $n(Rp)$ is the number of *Tg(dusp6:d2EGFP)* positive cells in the right posterior quadrant and $n(Lp)$, the number in the left posterior quadrant. This asymmetry index (AI) was used to define three groups of embryos, those with: expression of *Tg(dusp6:d2EGFP)* enriched on the left posterior side of the parapineal ($AI \leq -0.2$); expression enriched on the right posterior side of the parapineal ($AI \geq +0.2$); expression weakly or not lateralized ($-0.2 \leq AI \leq +0.2$, grey zone in Fig. 7J). Within each of these three groups and for each context (control, *ntl* MO, *spaw* MO), we averaged the

distribution and mean number of total or *Tg(dusp6:d2EGFP)* positive parapineal cells to create polar graphs in Fig. 6G-I”.

Live imaging and time-lapse analysis

One cell stage eggs carrying the *Tg(dusp6:d2EGFP)* transgene were injected with 50-100 pg of mRNA encoding the nuclear red fluorescent protein H2B-RFP. Embryos were anesthetized with MS-222 at 24-25 hpf and mounted in drops of low melting agarose (0.6% in fish water) on a plastic petri dish (50 mm diameter; 4-8 embryos per plate) for imaging on an upright microscope or on a plastic petri dish (35 mm diameter) with a coverslip at the bottom (14 mm glass diameter) for imaging on an inverted microscope. Petri dishes were filled with fish water containing 0.5x MS-222 (0.08 mg/ml) and 0.5x PTU (0.0015%) to impede pigment formation. The embryos were imaged at 22-24°C. For four long duration (22h) movies, we quantified the number and position of all parapineal cells at each time points (26, 28, 30, 32, 36, 40, 44, 48 hpf) on a dorsal and a ventral section (+4.5 μm ventral relative to the dorsal section) containing parapineal cells. This allowed us to approximate all parapineal cells as most were included in these two sections. Parapineal cells could be identified without ambiguity from 30 hpf as their nuclei organize in a rosette-like structure and were backtracked to confirm their parapineal identity at 26 hpf or 28 hpf. The position of each parapineal cell was defined as the center of the cell nucleus detected by the H2B-RFP expression using ImageJ software (ROI Manager tool). For each cell counted, the mean intensity of d2EGFP staining was measured in a circular area positioned on the center of the cell nucleus (ROI Manager tool); this allowed us to define in an objective way the most intense d2EGFP-expressing cell in Fig. S3I and S3J. The x mean and y mean of all parapineal cells as well as the x,y position of each *Tg(dusp6:d2EGFP)*+ cells were normalized for each time point using the anterior epiphysis ($y=0$) and the midline of the epiphysis lumen ($x=0$) as references. The anterior limit and midline of the epiphysis was consistently defined for each time point on a similar z-section (8 μm ventral to the most dorsal section containing the epiphysis). From these data, polar graphs were created as described for fixed embryos. The orientation and distance of migration at each specific time point was

defined by an extrapolated line passing through the parapineal mean positions at T and at T+2h (for time point 26 hpf) or T+4h (for time points 28, 32, 36, 40, 44 hpf).

Quantification of size and number of cytoplasmic protrusions in migrating parapineal cells.

To visualize cytoplasmic protrusions from parapineal cells, we performed time lapse imaging of *Tg(dusp6:d2EGFP)^{pt6}*, *Tg(flhBAC:Kaede)^{vu376}* double transgenic embryos that express Kaede in all the pineal complex including the parapineal (6). Kaede was photoconverted from green to red fluorescence using UV light (on a Zeiss 710 confocal), so that we could visualize the cytoplasm of all or most parapineal cells in red. The size and number of cytoplasmic protrusions were quantified on z-sections from 5 embryos live imaged between 29 and 36 hpf, using the ROI manager tool (ImageJ). To avoid bias, quantification was performed using the Kaede red channel, blind for the d2EGFP channel, and we analyzed subsequently whether the counted cytoplasmic protrusions were positive or negative for *Tg(dusp6:d2EGFP)* expression.

Quantification of the number and position of *gfi1ab* positive parapineal cells

Parapineal migration was assessed by detecting the expression of the marker gene *gfi1ab* at 52 hpf (5). The position and number of *gfi1ab* positive parapineal cells were analyzed using the Multipoint tool on ImageJ software and determined as the center of the cell nucleus detected with Topro-3 staining. The position of each parapineal cell was measured relative to the brain midline (reference origin =0) as determined by a line passing through the center of the lumen of the epiphysis. For each embryo, we calculated the mean position of parapineal cells. The rare embryos for which we detected less than 4 *gfi1ab* positive parapineal cells (n=6/69 for Fig. 3) were excluded from the datasets.

IR-LEGO local heat shock experiment

Eggs collected from crosses between *fgf8^{+/-}*, *Tg(hsp70:ca-fgfr1)^{+/-}* and *fgf8^{+/-}* fish were injected with mRNA encoding the H2B-RFP red fluorescent protein. At 24 hpf, *fgf8^{-/-}* embryos were

sorted based on their phenotype, anesthetized with MS-222 and embedded in a drop of Methylcellulose 2.5% on a petri dish (35 mm diameter) with a coverslip at the bottom (14 mm glass diameter). Embryos were imaged on a Nikon inverted spinning disk confocal microscope. H2B-RFP labeling of nuclei enabled visualization of the pineal complex given the stereotypical organization of cell nuclei around the lumen of the epiphysis and in the forming parapineal rosette. To irradiate target cells, we developed an optical system adapted from the IR-LEGO microscope described previously (10–12). An infrared laser (BrixX series narrow-bandwidth diode, Omicron) with nominal power output of 430 mW and a wavelength of 1480 nm was inserted into the beam path of the spinning disk microscope. We used a 60x (NA 1.3 immersion) objective in combination with a Zeiss immersion oil with an index of refraction $n=1.3339$, as it has a refractive index close to that of water while not exhibiting the strong absorption peak of water near 1480 nm. The laser was controlled with Omicron Laser Controller software, whereas for irradiation, the shutter was opened in a predetermined time-sequence that was triggered via an externally mounted Arduino Uno board controlled trigger. We tested different parameters of time and intensity and obtained the best activation of the *Tg(hsp70:ca-fgfr1)* transgene using time-sequences of 0.5 seconds and 80 mW intensity. On each embryo from 25 hpf to 29 hpf, we irradiated 2 to 3 cells located in the anterior part of the pineal complex. After focal heat shock, embryos recovered in fish water containing PTU 0.003% at 28°C. Some *fgf8^{-/-}* embryos (n=25 in total) were fixed 1h to 3h after the heat shock to check the induction of the CA-Fgfr1 transgene expression by *in situ* hybridisation; these embryos were genotyped for the presence of *Tg(hsp70:ca-fgfr1)* transgene (n=10/25). The remaining *fgf8^{-/-}* embryos (n= 65 in total) were fixed at 50 hpf after *Tg(hsp70:ca-fgfr1)* positive embryos were sorted by expression of dsRED in the lens. In both groups of irradiated *fgf8^{-/-}* mutants embryos (with or without CA-Fgfr1 transgene), we analyzed the mean position of the *gfi1ab* expressing parapineal cells relative to the midline as described in the previous section.

Statistical analysis

The mean position and number of parapineal cells were compared between datasets using R Studio software. For each dataset, we tested the assumption of normality with the Shapiro-Wilks test and variances homogeneity with the Bartlett test for multiple comparison or F test for two-sample comparison. When datasets were normal, we compared them with a two-sample T test or a Welsh T test when variances differed. When datasets did not distribute normally, we compared them using the Wilcoxon rank sum non-parametric test. For Fig. 3, we compared the four *fgf8*^{-/-} datasets (*fgf8*^{-/-} mutants carrying or not *Tg(hsp70:ca-fgfr1)* transgene and heat-shocked or not) two by two in a pairwise Wilcoxon test (p-value adjusted with Holm method) (Table S1). Unless otherwise mentioned in Figure legends, data are representative of at least three independent experiments. Numbers of parapineal cells are reported as mean ± standard deviation. Statistical significance is indicated on boxplots with one star (p-value<0.05) or two stars (p-value<0.01).

Data availability

The data that support the findings of this study are available from the corresponding author upon request.

Supplementary Figures S1 to S9

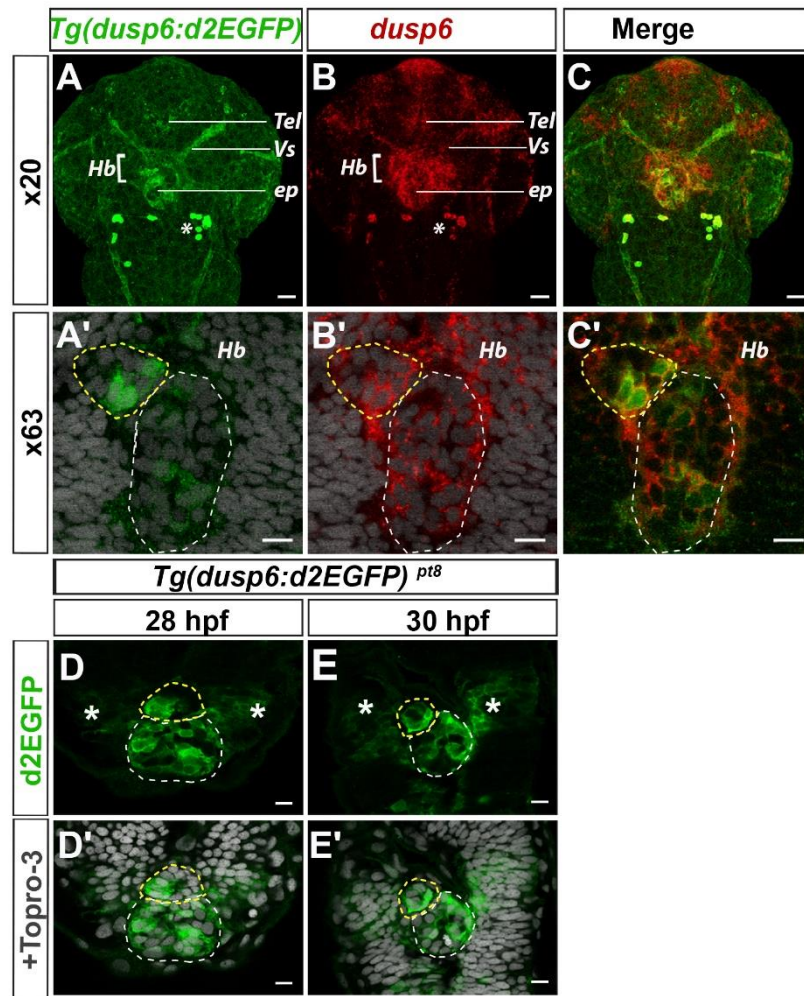


Figure S1. Endogenous *dusp6* and *Tg(dusp6:d2EGFP)^{pt8}* transgene are focally expressed in few parapineal cells as observed for the *Tg(dusp6:d2EGFP)^{pt6}* allele.

(A-C') *Tg(dusp6:d2EGFP)^{pt6}* expression recapitulates endogenous *dusp6* expression in the epithalamus. Confocal maximum projection (100 μ m, stepsize 2.5 μ m; scale bar: 25 μ m) (A-C) or high magnification confocal sections (A'-C'; scale bar: 10 μ m) showing the expression of *Tg(dusp6:d2EGFP)^{pt6}* after immunostaining against GFP (green; A, A') and *dusp6* gene (red; B, B') detected by *in situ* hybridization at 32 hpf; merges are shown in C and C'; pictures in A' and B' are merged with cell nuclear staining (Topro-3, grey). As for the *Tg(dusp6:d2EGFP)* transgene, the endogenous *dusp6* gene is expressed in both the epiphysis (ep, white circle) and the parapineal (yellow circle), in the head vessels (Vs), in the telencephalon (Tel), in the presumptive habenular domain (Hb) and in a group of neurons in the Tectum (*).

(D-E') d2EGFP shows localised parapineal expression in the pt8 *Tg(dusp6:d2EGFP)* allele as in the pt6 allele. Confocal sections showing the expression of *Tg(dusp6:d2EGFP)^{pt8}* transgene

(Green) at 28 hpf (D, D') and 30 hpf (E, E'), alone (D, E) or merged with nuclear staining (Topro-3, grey) (D', E'); scale bar: 10 μ m. *Tg(dusp6 :d2EGFP)^{pt6}* transgene is expressed in both in pineal (white circle) and in the parapineal (yellow circle); weak staining is also detected in the presumptive habenular domain (*). *Tg(dusp6 :d2EGFP)^{pt8}* expression in the parapineal is mosaic both at 28 hpf (n=10) and 30 hpf (n=7) and usually enriched at the leading edge as observed for *Tg(dusp6:d2EGFP)^{pt6}* allele (Figure 1). Embryos are viewed dorsally with anterior up. *In situ* hybridizations are representative of two independent experiments.

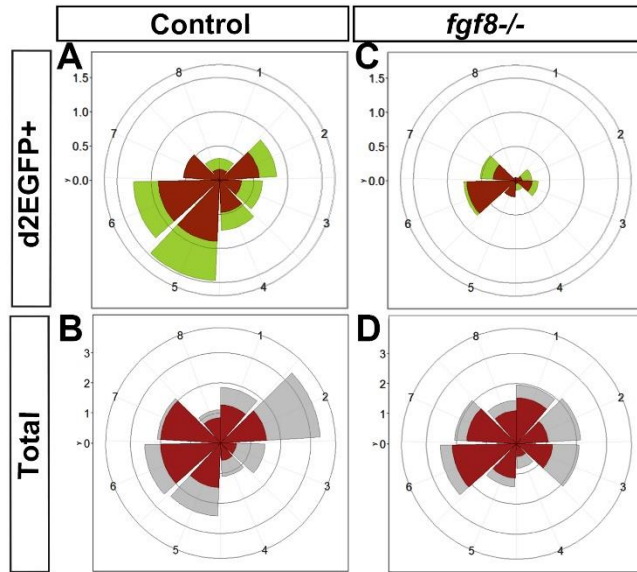


Figure S2. Focal expression of *Tg(dusp6:d2EGFP)* FGF pathway reporter in the parapineal depends on *Fgf8*.

Polar graph showing the distribution and mean number of total (B,D) and *Tg(dusp6:d2EGFP)* positive parapineal cells (A,C) in each of the eight 45°C semi-quadrants (1 to 8) relative to the parapineal mean position for control embryos (A,B; n=19) or *fgf8*^{-/-} mutants (C,D; n=21) at 32 hpf. The radial axis (vertical scale on the left side) represents the mean number of cells per semi-quadrant per embryo. The total number of parapineal cells was estimated by counting cell nuclei (grey area in B,D) or by using *sox1a* marker (red area in B,D); as some cells can be part of the parapineal rosette but do not express *sox1a*, the total number of *sox1a* positive parapineal cells (about 10 cells) is lower than the number that we estimated by counting cell nuclei in the parapineal rosette (about 16 cells) (B,D; red versus grey polar bars). Graph A and C show the distribution and mean number of *Tg(dusp6:d2EGFP)* expressing parapineal cells among the *sox1a* positive cells (red area in A,C) or among the total counted cell nuclei (green area in A,C); the distribution of *Tg(dusp6:d2EGFP)* positive cells, enriched in the left posterior quadrants 5 and 6, was similar in both cases (A, red versus green polar bars), validating the use of nuclear staining to define parapineal cells. The mean number of *Tg(dusp6:d2EGFP)* positive cells is strongly reduced in *fgf8*^{-/-} parapineals (C) while the total number of parapineal cells is not significantly reduced (D).

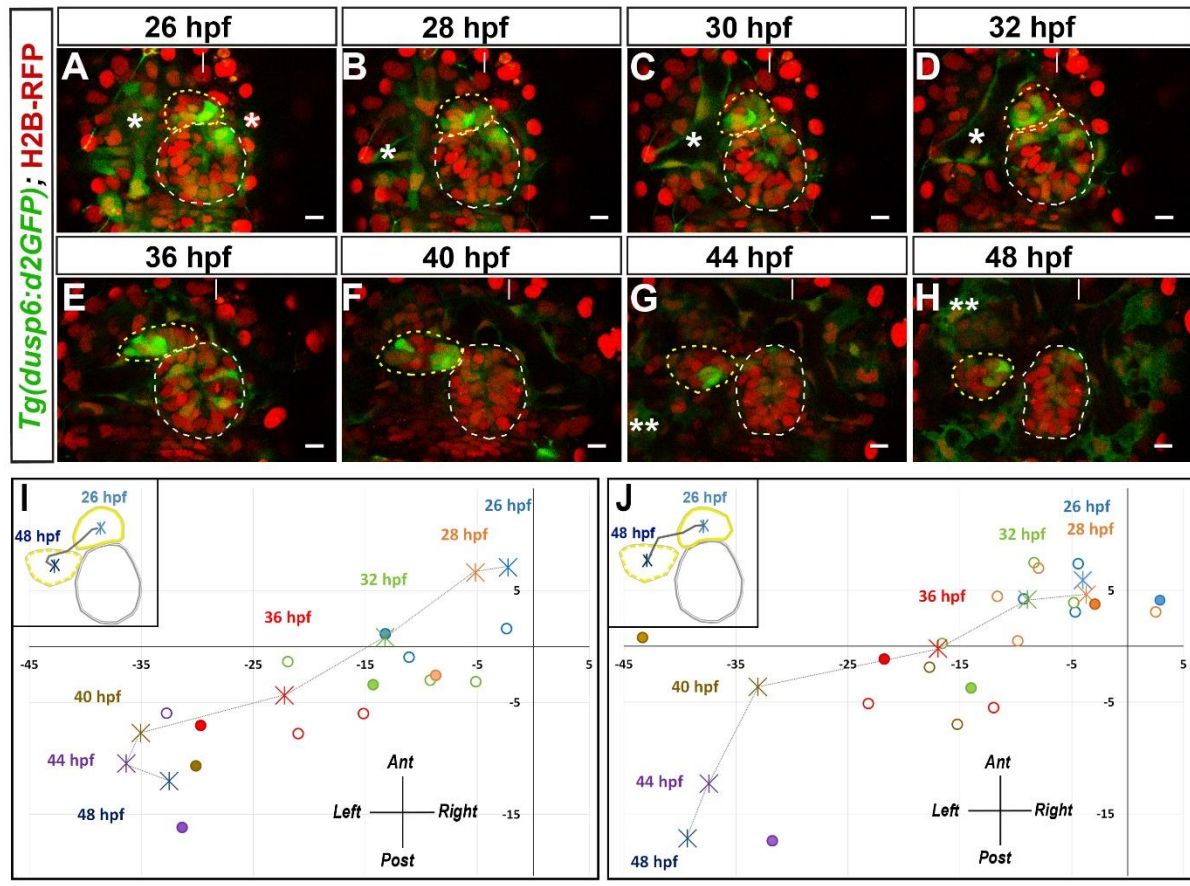


Figure S3. Focal activation of *Tg(dusp6:d2EGFP)* FGF reporter is enriched at the leading edge of the migrating parapineal.

(A-H) Comparable analysis to Figures 2A-2H for a second embryo: embryo n°2 shown in Movie S2.

(I) Position of *Tg(dusp6:d2EGFP)* positive cells (circle) relative to the mean position of all parapineal cells (star) analyzed on a representative confocal section of embryo n°1 (shown in Figures 2A-2H and Movie S1), at different stages of parapineal migration: 26 hpf (light blue), 28 hpf (orange), 30 hpf (yellow), 32 hpf (green), 36 hpf (red), 40 hpf (brown), 44 hpf (purple), 48 hpf (dark blue). The y line ($x=0$) represents the brain midline and the x line ($y=0$) represents the anterior limit of the epiphysis. For each time points, the brightest d2EGFP expressing cell is shown as a color filled mark (filled circle). Black dotted line represents the extrapolated displacement of the parapineal mean position from T to T+2h or T+4h. Left corner: schematic showing how the parapineal (yellow circle) migrates relative to epiphysis (grey circle) between 26 and 48 hpf.

(J) Comparable analysis to (I) for embryo n°2, shown in Figures S3A-S3H and in Movie S2.

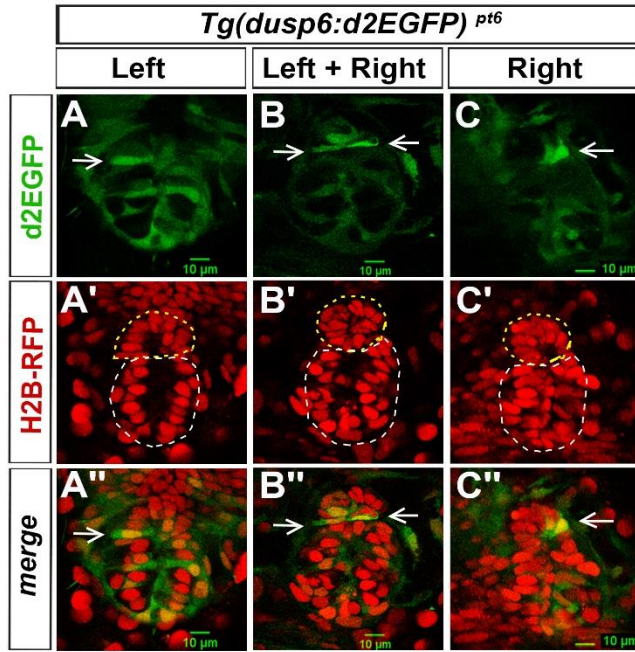


Figure S4. *Tg(dusp6:d2EGFP)* expression is initiated at the interface between the epiphysis and nascent parapineal.

Confocal section of live imaged *Tg(dusp6:d2EGFP)^{pt6}* embryos (green) expressing H2B-RFP protein (red) in cell nuclei between 26 and 28 hpf (A-C''); scale bar: 10 μ m. The epiphysis and the parapineal are shown as a white or yellow dotted circle in (A'-C'). When first detected in the parapineal, d2EGFP expression is usually found in one or two parapineal cells on the left posterior side (A-A''; n=26/41). In some cases, *Tg(dusp6:d2EGFP)* can be expressed on both left and right sided parapineal cells (B-B'' ; n=10/41) or rarely on right sided cells (C-C'' ; n=5/41). Embryo view is dorsal, anterior is up; white arrows show *Tg(dusp6:d2EGFP)* expressing cells in the parapineal.

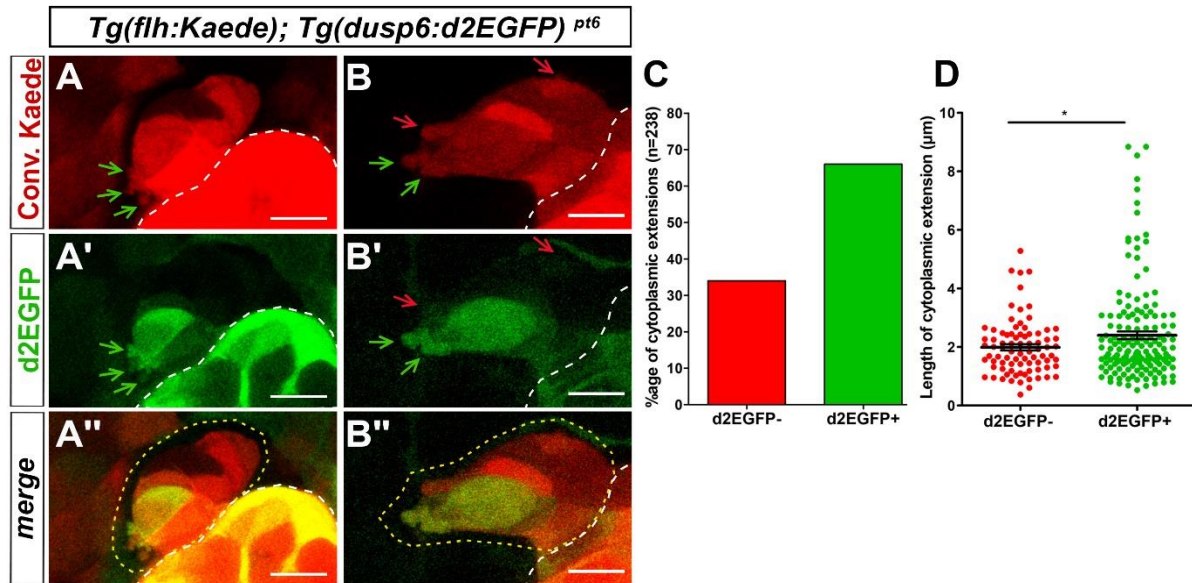


Figure S5. Cytoplasmic protrusions from parapineal cells are enriched in *Tg(dusp6:d2EGFP)* expressing cells and are longer.

(A-B'') Zoom-in illustrative confocal sections of 2 live imaged embryos showing the expression of *Tg(flh:Kaede)* transgene after photoconversion of Kaede (Red; A, B) and of *Tg(dusp6:d2EGFP)* FGF reporter (Green; A', B') at 32 hpf (A-A'') or 35 hpf (B-B''); merge are shown in A'' and B''; scale bar: 10 µm. The epiphysis and the parapineal are outlined with white or yellow dots (A-B''). Green arrows show cytoplasmic protrusions from parapineal cells expressing both d2EGFP and photoconverted Kaede while red arrows show cytoplasmic protrusions from parapineal cells expressing Kaede only.

(C) Graph showing the percentage of Kaede positive cytoplasmic protrusions observed from parapineal cells that were negative (red, d2EGFP-, 34%) or positive (green, d2EGFP+, 66%) for d2EGFP expression in *Tg(flh:Kaede); Tg(dusp6:d2EGFP)* transgenic embryos; a total of 238 protrusions were counted on 5 live imaged embryos.

(D) Dot plot showing the length of cytoplasmic protrusions that express photoconverted Kaede only (red, d2EGFP-, n=82) or Kaede plus *Tg(dusp6:d2EGFP)* (green, d2EGFP+, n=156). The average length of cytoplasmic protrusions is significantly higher in parapineal cells that express d2EGFP (Mean± SEM = 2.39 ± 0.13 µm) than in those that are d2EGFP negative (Mean± SEM=1.99 ± 0.10 µm); p=0.015 in a Welch's T Test (* indicates statistical significance).

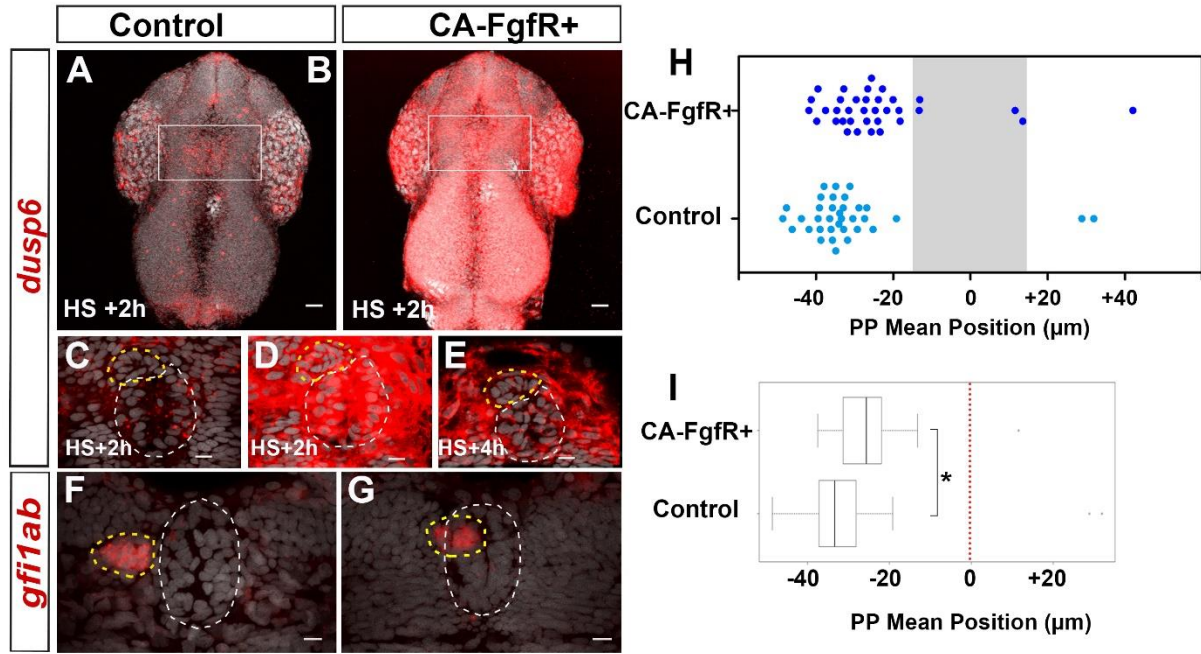


Fig. S6: Ectopic expression of a constitutively activated version of the FgfR1 receptor compromises parapineal migration in wild-type embryos.

(A-E) Confocal maximum projection (A, B) (100 μm projection with a 5 μm step size; scale bar: 25 μm) or confocal sections (C-E; scale bar: 10 μm) showing the expression of the endogenous *dusp6* gene (red) and cell nuclei (grey) in embryos that carry the *Tg(hsp70:ca-fgfr1)* transgene (B, D, E) or not (A, C). Zoom out embryos were heat-shocked at 26 and 29 hpf and fixed at 31 hpf, 2h after the last heat shock (A, n=16; B, n=9). Zoom in embryos were heat-shocked at 28 hpf (C, n=33; D, n=21) or 26 hpf (E, n=12) and fixed at 30 hpf respectively, 2h or 4h after heat shock.

(F, G) Confocal maximum projections (5 μm) showing *gf1ab* expression (red) and cell nuclei (grey) in the forebrain of 52 hpf embryos that carry the *Tg(hsp70:ca-fgfr1)* transgene (F) or not (G) after being heat-shocked at 26 hpf and 29 hpf. *gf1ab* expression labels the parapineal nucleus (yellow outline); epiphysis (white outline). In A-G, embryo view is dorsal, anterior is up.

(H) Dot plot showing, for each embryo, the mean parapineal position in μm distant to the brain midline (x=0) in embryos expressing (dark blue) or not (light blue) CA-FgfR1 after two heat-shocks at 26 hpf and 29 hpf or three heat-shock at 26, 29 and 32 hpf. Grey shaded zone between -15 μm and +15 μm defines the 'no migration' domain as corresponding to the average width of the epiphysis; grey dotted lines show -25 μm and +25 μm .

(I) Boxplot showing the distribution of parapineal mean position relative to the brain midline (reference 0, red dotted line) in embryos expressing CA-FgfR1 or in controls. Parapineal

migration is compromised in the embryos that overexpress CA-FgfR1 relative to control embryos; p-value=0.023 in a Wilcoxon test (* indicates statistical significance).

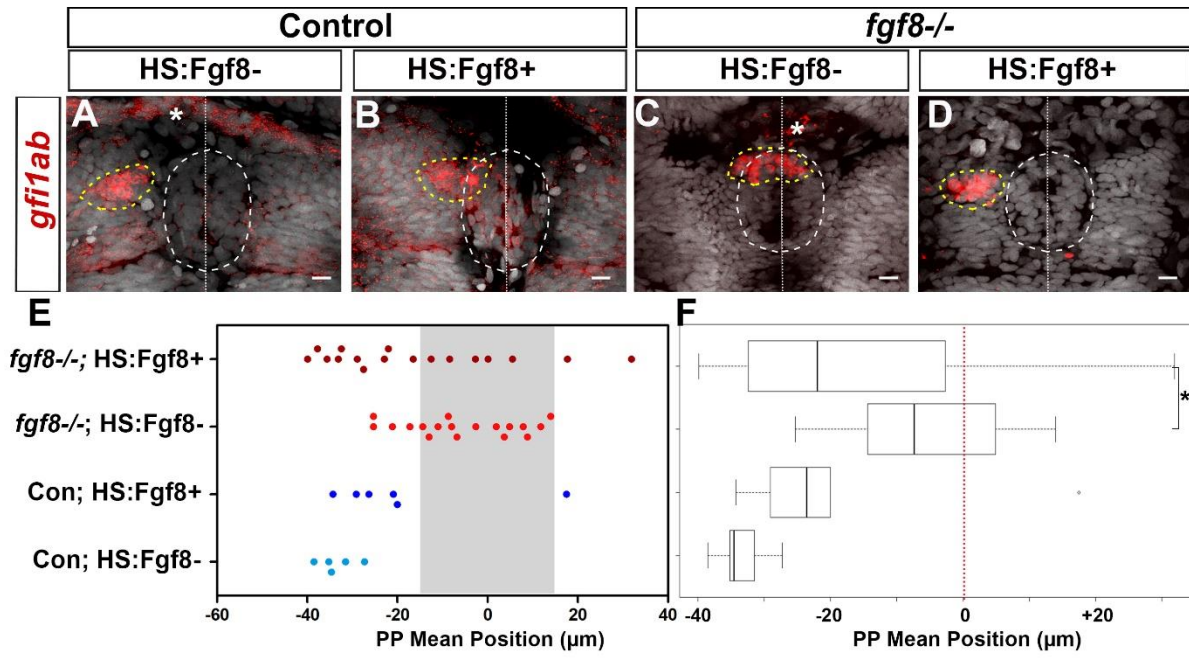


Figure S7: Ectopic and global expression of Fgf8 partially restores parapineal migration in *fgf8*^{-/-} mutants.

(A-D) Confocal (8 µm) maximum projection showing expression of *gf11ab* (red) with cell nuclei (Topro-3, grey) in the heads of representative control embryos (A-B) and *fgf8*^{-/-} mutants (C-D) that carry (B,D) or don't carry (A,C) the *Tg(hsp70:fgf8a)* transgene; scale bar: 10 µm. Control embryos are siblings of *fgf8*^{-/-} mutants thus corresponding to both wild-type and *fgf8*^{+/-} heterozygotes. All embryos were heat-shocked at 26 hpf and 29 hpf. The expression of *gf11ab* labels the parapineal nucleus (yellow outline) while global nuclear staining was used to visualize the epiphysis (white outline) and to define the brain midline (reference 0; dotted white line in the center of the epiphysis lumen). Non-specific fluorescent staining is shown as (*).

(E) Dot plot showing, for each embryo, the mean parapineal position in µm distant to the brain midline (x=0), at 52 hpf, in *fgf8*^{-/-} mutant embryos that express or not the *Tg(hsp70:fgf8a)* transgene after heat-shock at 25 hpf and 29 hpf. Grey shaded zone (-15 µm and +15 µm) define the 'no migration' domain as corresponding to the average width of the epiphysis. Parapineal migration is compromised in control embryos that express *Tg(hsp70:fgf8a)* transgene (B and E, light blue dots; n=5) compared to controls that do not (A and E, dark blue; n=6); p-value=0,03 in a Wilcoxon test. In *fgf8*^{-/-} mutants that do not express the *Tg(hsp70:fgf8a)* transgene, the parapineal either stays at the midline or migrates partially (C and E, light red; n=18) while the migration is partially rescued in mutants that over-express Fgf8 (D and E, dark red; n=17); p-value=0,049 in a Wilcoxon test.

(F) Boxplot showing the distribution of parapineal mean position relative to the brain midline (reference 0) in the same set of embryos; p-value=0,049 (* indicates statistical significance).

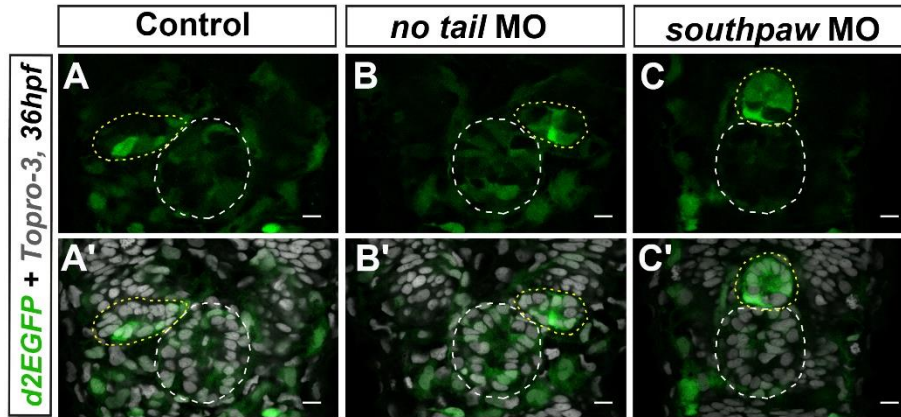


Figure S8: Parapineal migration is delayed in absence of Nodal signaling.

(A-C') Confocal sections showing the expression of *Tg(dusp6:d2EGFP)* (green) at 36 hpf in parapineals (yellow circles) of a control embryo (A, A'; n=17) and in illustrative *ntl* (B, B'; n=26) and *spaw* morphants (C, C'; n=32); images A'-C' show images A-C superimposed on nuclear staining (grey) allowing visualization of the epiphysis (white outline) and parapineal (yellow outline). At 36 hpf, the parapineal has migrated in all controls and *ntl* morphants but is still found at the midline in 25% of *spaw* morphants (numbers of embryo with a left, right or no migrated parapineal are shown in Table S5). Embryo view is dorsal, anterior is up; scale bars: 10 μ m.

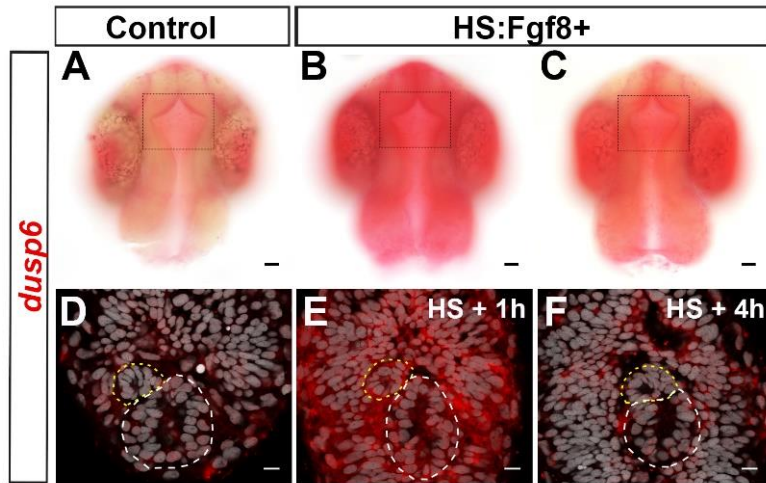


Figure S9. Global ectopic expression of Fgf8 induces *dusp6* expression.

(A-C) Bright field pictures (scale bar: 25 μm) showing the expression of the endogenous *dusp6* gene (red) and confocal sections (D-F; scale bar: 10 μm) showing the expression of the endogenous *dusp6* gene (red) and cell nuclei (grey) in representative embryos that carry the *Tg(hsp70:fgf8)* transgene (B-C, E-F) or not (A, D). Embryos were heat-shocked at 29 hpf (A-B, D-E; n=20 and n=27) or 26 hpf (C, F; n=19) and fixed at 30 hpf respectively 1h or 4h after heat shock. *In situ* hybridizations are representative of two independent experiments.

Supplementary Tables S1 to S5

Table S1. Pairwise comparisons of parapineal mean position between the four *fgf8*^{-/-} mutant embryo contexts presented Figure 4.

	<i>fgf8</i> ^{-/-}	<i>fgf8</i> ^{-/-} _CAFgfR ^{+/-}	No HS_ <i>fgf8</i> ^{-/-}
<i>fgf8</i> ^{-/-} _CAFgfR ^{+/-}	<u>0.03974</u>	-	-
No HS_ <i>fgf8</i> ^{-/-}	1.00000	<u>0.00252</u>	-
No HS_ <i>fgf8</i> ^{-/-} _CAFgfR ^{+/-}	1.00000	<u>0.00021</u>	1.00000

The datasets were compared on R Studio using the function 'pairwise.wilcox.test' with the p-value adjustment method 'holm'; 'No HS_': non heat shocked embryos.

Table S2. Proportions of embryos showing laterality of *pitx2* expression at 29 hpf.

<i>pitx2</i> expression	Control (n=28)	<i>ntl</i> MO (n=31)	<i>spaw</i> MO (n=25)
Left	75 %	0 %	4 %
Absent	0 %	3 %	84 %
Bilateral	** 25 %	97 %	8 %
Right	0 %	0 %	4 %

** Among the embryos annotated with a bilateral expression of *pitx2* (n=7/28, 25%), 5 embryos (18% of total embryos) clearly showed a stronger expression on the left side while only 2 embryos (7%) displayed a non-biased bilateral expression. Summary of 3 experiments.

Table S3. Distribution of embryos according to their asymmetry index (AI) in the number of *Tg(dusp6:d2EGFP)* positive cells in the left versus right posterior quadrant of the parapineal at 30 hpf.

AI in <i>Tg(dusp6:d2EGFP)</i>	Control (n=36)	<i>ntl</i> MO (n=37)	<i>spaw</i> MO (n=38)
Left (AI < or = -0,2)	78 %	38 %	34 %
Non Lateralized (-0,2 < AI < 0,2)	11 %	30 %	34 %
Right (AI > or = +0,2)	11 %	32 %	32 %

Table S4. Distribution of embryos according to their parapineal mean position (μm) relative to the brain midline ($x=0$) at 30 hpf.

Parapineal mean position (μm) at 30 hpf	Control (n=36)	<i>ntl</i> MO (n=37)	<i>spaw</i> MO (n=38)
Left ($< -5 \mu\text{m}$)	94 %	30 %	11 %
Midline ($-5 \mu\text{m} < > +5 \mu\text{m}$)	6 %	35 %	76 %
Right ($> +5 \mu\text{m}$)	0 %	35 %	13 %

Table S5. Distribution of embryos showing parapineal lateralization at 36-38hpf *.

Parapineal laterality at 36-38 hpf	Control (n=17)	<i>ntl</i> MO (n=26)	<i>spaw</i> MO (n=32)
Left	100 %	54 %	38 %
Midline	0 %	0 %	25 %
Right	0 %	46 %	38 %

* Summary of two experiments where embryos were fixed at 36 hpf or 38 hpf.

Captions for Movies S1 to S5

Movie S1. Dynamic expression of the *Tg(dusp6:d2EGFP)* FGF reporter transgene in the parapineal during its migration (embryo n°1).

Time series from 26 hpf to 48 hpf (1 frame /15 min) of thin confocal maximum projection (4.5 µm) of the dorsal brain of a live *Tg(dusp6 :d2EGFP)^{pt6}* embryo (green) expressing H2B-RFP protein (red) in cell nuclei. Embryo view is dorsal, anterior is up; the epiphysis and the parapineal are shown as a white or yellow circle respectively every 4h and the brain midline as the antero-posterior white line. *Tg(dusp6:d2EGFP)* expression is enriched in parapineal cells at the leading edge of the migration.

Movie S2. Dynamic expression of the *Tg(dusp6:d2EGFP)* FGF reporter in the parapineal during its migration (embryo n°2).

Time series from 26 hpf to 48 hpf (1 frame /15 min) of thin confocal maximum projections (4.5 µm) of the dorsal brain of a live *Tg(dusp6 :d2EGFP)^{pt6}* embryo (green) expressing H2B-RFP protein (red) in cell nuclei. Embryo view is dorsal, anterior is up; the epiphysis and the parapineal are shown as a white or yellow circle respectively every 4h and the brain midline as the anterior to posterior white line. The initial expression of *Tg(dusp6:d2EGFP)* on the right side correlates with a delay in the migration that only initiates at 30-32 hpf when d2EGFP expressing cells are eventually relocated to the left side.

Movie S3. Ectopic expression of the *Tg(dusp6:d2EGFP)* FGF reporter in the parapineal correlates with a delay in parapineal migration (embryo n°3).

Time series from 26 hpf to 48 hpf (1 frame /15 min) of thin confocal maximum projections (4.5 µm) of the dorsal brain of a live *Tg(dusp6:d2EGFP)^{pt6}* embryo (green) expressing H2B-RFP protein (red) in cell nuclei. Embryo view is dorsal, anterior is up; the epiphysis and the

parapineal are shown as white and yellow circles respectively every 4h and the brain midline as an anterior to posterior white line. Expression of the *Tg(dusp6:d2EGFP)* FGF reporter fails to be restricted to leading cells in the early migration phases; this correlates with a strong delay in parapineal migration that only starts around 38 hpf.

Movie S4. *Tg(dusp6:d2EGFP)* positive cells can exchange leading position (embryo n°4)

Time series from 30 hpf to 42 hpf (1 frame /15 min) of thin confocal maximum projection (4,5 μ m) of the dorsal brain of a live *Tg(dusp6:d2EGFP)^{pt6}* (green) embryo expressing H2B-RFP protein (red) in cell nuclei. Embryo view is dorsal, anterior is up; the epiphysis and the parapineal are shown as white and yellow circles respectively every 2h and brain midline as a white anterior to posterior line. *Tg(dusp6:d2EGFP)* positive cells are identified as n°1 to 3. Cell n°1, initially located at the border between the parapineal and the epiphysis, strongly expresses *Tg(dusp6:d2EGFP)* and remains at the leading front from 30 hpf to 36 hpf. As d2EGFP expression decreases in cell n°1, other parapineal cells (cell n°2 at 34-36 hpf and n°3 at 38 hpf) start expressing *Tg(dusp6:d2EGFP)* and behave as new leading cells.

Movie S5. Cytoplasmic protrusions from parapineal cells are enriched in *Tg(dusp6:d2EGFP)* expressing cells.

Time series from 29 hpf to 34 hpf (1 frame /15 min) of confocal sections of the head of a live embryo expressing *Tg(dusp6:d2EGFP)^{pt6}* (green) and *Tg(flh:Kaede)* transgene after photoconversion of Kaede H2B-RFP protein (red); scale bar: 10 μ m. The parapineal is shown as a yellow dotted circle on the first frame. Green arrows show cytoplasmic protrusions from parapineal cells expressing both d2EGFP and photoconverted Kaede while red arrows show cytoplasmic protrusions from parapineal cells expressing Kaede only.

References for SI reference citations

1. Westerfield M (2000) *The Zebrafish Book. A Guide for The Laboratory Use of Zebrafish (Danio rerio)*, 4th Edition; Eugene, University of Oregon Press. Available at: https://zfin.org/zf_info/zfbook/cont.html#cont4 [Accessed July 24, 2017].
2. Nasevicius A, Ekker SC (2000) Effective targeted gene “knockdown” in zebrafish. *Nat Genet* 26:216–20.
3. Long S, Ahmad N, Rebagliati M (2003) The zebrafish nodal-related gene southpaw is required for visceral and diencephalic left-right asymmetry. *Development* 130:2303–16.
4. Concha ML, et al. (2003) Local tissue interactions across the dorsal midline of the forebrain establish CNS laterality. *Neuron* 39:423–38.
5. Dufourcq P, Rastegar S, Strahle U, Blader P (2004) Parapineal specific expression of *gf11* in the zebrafish epithalamus. *Gene Expr Patterns* 4:53–7.
6. Clanton JA, Hope KD, Gamse JT (2013) Fgf signaling governs cell fate in the zebrafish pineal complex. *Development* 140(2):323–332.
7. Topp S, et al. (2008) Fgf signaling in the zebrafish adult brain: association of Fgf activity with ventricular zones but not cell proliferation. *J Comp Neurol* 510:422–39.
8. Neilson KM, Friesel R (1996) Ligand-independent activation of fibroblast growth factor receptors by point mutations in the extracellular, transmembrane, and kinase domains. *J Biol Chem* 271(40):25049–25057.
9. Roussigne M, Bianco IH, Wilson SW, Blader P (2009) Nodal signalling imposes left-right asymmetry upon neurogenesis in the habenular nuclei. *Development* 136:1549–57.
10. Kamei Y, et al. (2009) Infrared laser-mediated gene induction in targeted single cells in vivo. *Nat Methods* 6(1):79–81.
11. Deguchi T, et al. (2009) Infrared laser-mediated local gene induction in medaka, zebrafish and *Arabidopsis thaliana*. *Dev Growth Differ* 51(9):769–775.
12. Venero Galanternik M, Nikaido M, Yu Z, McKinney SA, Piotrowski T (2016) Localized Gene Induction by Infrared-Mediated Heat Shock. *Zebrafish* 13(6):537–540.

II. Notch signalling promotes parapineal migration through restricting FGF activity but controls the specification of PP cells independently of FGF pathway.

II.1 Context, Aim and Summary of Manuscript n°2 (in preparation)

One striking observation made in our study described in Manuscript n°1 is that broad induction of a constitutively active Fgf receptor partially restores migration in *fgf8*^{-/-} mutants. Furthermore, this correlates with left sided induction of the FGF reporter expression, despite broad expression of the activated receptor. These observations suggest the existence of a mechanism that restricts activation of FGF signaling downstream of the Fgf receptor. The focus of the second half of my PhD has been to understand how activation of the FGF pathway is restricted to a few PP cells despite all PP cells appearing competent to activate the pathway.

Myriam Roussigné had preliminary data showing an increase in the activation of the FGF pathway in *mindbomb* mutants (*mib*^{-/-}), a well-described context of loss of function for Notch pathway. To follow up these preliminary data, I have analyzed whether the Notch pathway could be a candidate to restrict FGF activity within PP cells. I first confirmed that Notch signaling restricts FGF activity: while Notch loss-of-function (LOF) up-regulated FGF signaling, Notch gain-of-function (GOF) reduces it; both contexts correlate with defects in PP migration. Furthermore, decreasing or increasing FGF signaling rescued or aggravated defects in PP migration in a Notch LOF context confirming a functional link between FGF and Notch signaling during PP migration. Therefore, our data indicate that Notch pathway is required for PP migration by restricting FGF activation within PP cells (Manuscript n°2).

In absence of Notch signaling, we also observed an increase in the number of *gfi1ab*⁺ and *sox1a*⁺ PP cells. Notch GOF gives the opposite phenotype regarding the specification of PP cells, *i.e.* a decreased number of *gfi1ab*⁺ and *sox1a*⁺ PP cells. Using drug treatment at different time windows, I could show that the roles of Notch signaling in the specification and migration of PP cells are independent and can be uncoupled.

To conclude, our data show that Notch pathway is required for both specification and migration of PP cells. Notch pathway restricts FGF activation within PP cells to promote their migration while the role of Notch in controlling the specification of PP cells seems independent of FGF pathway.

II.2 Manuscript n°2 (in preparation):

Notch pathway restricts the activation of FGF signaling within PP cells to promote their collective migration

L. Wei^{1,2}, A. Al Oustal^{1,2}, P. Blader^{1,2*}, M. Roussigne^{1,2*}

¹ Université de Toulouse, UPS, Center de Biologie du Développement (CBD), Toulouse, France

² CNRS, CBD UMR 5547, F-31062 Toulouse, France

* Authors for correspondence: myriam.roussigne@univ-tlse3.fr, patrick.blader@univ-tlse3.fr

Notch signalling restricts FGF pathway activation in parapineal cells to promote their collective migration.

Lu Wei¹, Amir Al Oustal¹, Patrick Blader¹, Myriam Roussigné¹

¹ Centre de Biologie Intégrative (CBI), Centre de Biologie du Développement (CBD), Université de Toulouse, CNRS (UMR 5547), F-31062 Toulouse, France.

Abstract

Coordinated migration of cell collectives is a fascinating process that underlies embryonic development and tissue homeostasis. To coordinate their behavior within the collective, migrating cells need to integrate various mechanical and chemical cues. Recently, we described that FGF pathway need to be activated in few leading cells to promote migration of the parapineal, a group of neurons arising from the medially located pineal complex and migrating to the left side of the zebrafish brain. Here, we study the role of Notch signalling in modulating FGF activity within parapineal cells. While Notch loss-of-function (LOF) results in up-regulated FGF signalling, ectopic Notch signalling reduces it. This correlates with a defect in parapineal migration observed in both contexts. We also found that Notch pathway is required for the correct specification of parapineal cells, as loss or gain of function Notch triggers respectively an increase or strong reduction in the number of parapineal differentiated cells. Pharmacological inhibition of Notch pathway reveals that both role of Notch in specification and migration of parapineal cells can be uncoupled. Functional epistasis analysis showed that decreasing or increasing FGF signalling can respectively rescue or worsen parapineal migration defect in Notch signalling depleted contexts while not affecting the number of parapineal differentiated cells. This indicates that the role of Notch signalling in controlling parapineal migration depends on its capacity to modulate the level of FGF pathway activation. In contrast, the function of Notch in controlling the number of parapineal differentiated cell does not depend on FGF pathway. As the function and cross-regulation of FGF and Notch pathway might be conserved during the migration of invading tumoral cells, our results could help to better understand these pathway interaction during metastasis.

Introduction

Morphogenesis of tissues and organs depends on group of cell acquiring specific identities and migrating to the correct places at the right times. Coordinated motion of cells collectives is a widespread phenomenon, being seen predominantly during embryonic development but also in adults, during tissue repair for example. Advances in genetic and optical tools have made it possible to study the molecular and cellular mechanisms underlying collective cell migration *in vivo* in different model organisms (Friedl and Gilmour, 2009; Ochoa-Espinosa and Affolter, 2012; Pocha and Montell, 2014; Theveneau and Mayor, 2013). Recent progress in the analysis of mechanical forces and the development of *in vitro* models, together with the use of *in silico* modelling, have improved further our understanding of coordinated cell migration. Such studies have highlighted the variability in mechanisms from one model to another, indicating that collective migration is a highly adaptive and plastic process (Haeger et al., 2015; Theveneau and Linker, 2017).

The mechanistic differences found in different models of collective cell migration might reflect the intrinsic characteristic of the migrating cluster, the physical properties of the surrounding environment and/or the external signalling cues (Haeger et al., 2015). Our understanding of how cell collectives sense and integrate various external cues to coordinate their motion with neighbouring cells and to share tasks within the collective remains limited. This issue has benefited from studies that linked patterns of cell behaviour with *in vivo* dynamics of signalling pathway. For instance, characterising the dynamics of chemokine signalling during the migration of the zebrafish lateral line primordium (LLP), by monitoring the turn-over of Cxcr4b receptor in all LLP cells, has provided important insights into how a polarised migrating cluster of cells can self-shape the gradient of a chemotactic signal (Donà et al., 2013; Venkiteswaran et al., 2013).

Among secreted signals involved in many models of cell migration are the members of the FGF family. For example, FGF signalling is described to promote chemotaxis during the migration of caudal visceral mesoderm cells during gut formation in *Drosophila* (Kadam et al., 2012). The FGF pathway can also promote migration of cell collectives, potentially through the modulation of cell adhesiveness (Ciruna et al., 1997; McMahon et al., 2010) or by increasing random cell motility (Benazeraf et al., 2010). In the LLP, the FGF pathway is required for Notch-dependant formation of neuromast rosettes at the back of the primordium during migration (Durdu et al., 2014; Kozlovskaja-Gumbrienė et al., 2017; Lecaudey et al., 2008; Nechiporuk and Raible, 2008)

and to maintain cluster cohesion (Dalle Nogare et al., 2014), with both of these processes being required for proper LLP migration. Despite the widespread and reiterative role of the FGF pathway in cell migration models, however, it's not clear how the dynamics of FGF signalling correlate with cell behaviours and how they can be modulated by other signals.

To better characterize the dynamics of FGF pathway activation during collective cell migration, we recently analysed the temporal and spatial activation of a previously described FGF reporter transgene, *Tg(dusp6:d2GFP)*, during migration of the parapineal (Molina et al., 2007). The parapineal is a small group of cells that emerges from the anterior part of the pineal complex at the midline of zebrafish epithalamus in the dorsal diencephalon, and migrates almost exclusively to the left side of the brain (Concha et al., 2000; Duboc et al., 2015; Roussigne et al., 2012). Using this *Tg(dusp6:d2GFP)* reporter, we showed that the FGF pathway is activated in an *Fgf8*-dependant manner in only a few parapineal cells located at the migration front (Roussigné et al., 2018). Furthermore, experimentally activating the FGF pathway in a few parapineal cells restores parapineal migration in *fgf8*^{-/-} mutant embryos. Taken together, these findings indicate that the restricted activation of FGF signalling in the parapineal promotes the migration of the parapineal cell collective. While the parapineal can receive *Fgf8* signals from both sides of the midline, focal pathway activation is primarily detected on the left. This asymmetry in FGF pathway activation requires the TGF β /Nodal signalling pathway, which is activated on the left side of the epithalamus prior to parapineal migration (Bisgrove et al., 1999; Concha et al., 2000; Liang et al., 2000). Although the Nodal pathway appears to bias the focal activation of FGF signalling to the left, after a significant delay the restriction of FGF activity still occurs in the absence of the Nodal pathway and the parapineal migrates, although either to the left or the right (Roussigné et al., 2018).

All parapineal cells appear competent to activate the FGF pathway. Thus, it is unclear how the activation of the pathway is restricted to only a few cells in the parapineal. In this study, we address whether the Notch signalling pathway might modulate the activation of FGF pathway in the parapineal. We show that Notch signalling is required to restrict FGF pathway activation; while Notch loss-of-function leads to an expansion of FGF pathway activation in the parapineal, activating the Notch pathway by globally expressing the intracellular domain of Notch causes a strong reduction in the expression of the FGF reporter transgene. These observations correlate with significant defects in parapineal migration in both contexts. Loss or gain of function for

Notch signalling also interferes with the specification of parapineal cell identity. We found that Notch loss-of-function results in a significant increase in the number of *gfi1ab* and *sox1a* expressing parapineal cells, while gain of Notch activity results in the opposite phenotype. In contrast, the number of parapineal cells expressing *tbx2b*, a putative marker for parapineal progenitors cells (Snelson et al., 2008), is not affected in either loss or gain of function for Notch. Pharmacological inhibition of Notch pathway suggests that the roles of Notch in the specification and migration of parapineal cells can be uncoupled. Finally, a global decrease or an increase in the level of FGF signalling can respectively rescue or enhance the parapineal migration defect caused by Notch loss-of-function but does not affect parapineal specification. Our data indicate that the Notch pathway regulates the specification and migration of parapineal cells independently and that the role of Notch signalling in promoting parapineal migration, but not specification, is to restrict FGF activation to a few parapineal cells.

Results

The parapineal of *mindbomb* mutant embryos display expanded FGF pathway activation and an early delay in migration

In models of cell migration during sprouting of tubular epithelia, Notch-Delta mediated cell-cell communication contributes to tip cell selection by restricting the ability of followers cells to activate RTK signalling (Ghabrial and Krasnow, 2006; Ikeya and Hayashi, 1999; Siekmann and Lawson, 2007a). To address whether Notch signalling could similarly restrict FGF pathway activation in the freely moving parapineal, and thus promote its migration, we analysed the expression of an FGF pathway activity reporter transgene, *Tg(dusp6:d2EGFP)* (Molina et al., 2007), in embryos mutant for the *mindbomb* (*mib^{ta52b}*) gene, a well described loss-of-function context for the Notch pathway (Itoh et al., 2003). At 32 hours post-fertilisation (hpf), we observed a larger number of *Tg(dusp6:d2EGFP)* expressing cells in the parapineal of *mib^{-/-}* mutant embryos (7 ± 3 d2EGFP+ cells) compared to siblings (4 ± 2 d2EGFP+ cells; p-value=3.845e-05, Welch t-test) (**Figures 1A-1B', 1E**). The increase in *Tg(dusp6:d2EGFP)* expressing cells was not accompanied by an increase in the number of parapineal cells expressing *sox1a*, an early parapineal marker (Clanton et al., 2013) (**Figures 1C-1D, 1F**), although we observed a slight increase in the total number of parapineal cells as determined using nuclear staining to visualize the parapineal rosette (22 ± 7 in *mib^{-/-}* mutants compared to

19±5 in sibling control embryos; p-value=0.037, Welch t-test) (**Figures 1G**). Interestingly, while in controls the parapineal had usually initiated its migration at 32 hpf, it was still detected at the midline in most stage-matched *mib*^{-/-} mutant embryos (**Figures 1H**). Our results indicate that the FGF signalling pathway is activated in more parapineal cells when Notch signalling is abrogated and that this correlates with an early parapineal migration defect.

Loss of Notch signalling results in defects in parapineal migration and an increase in the number of certain parapineal cell subtypes at later stages.

To address the effect of Notch inhibition on parapineal migration further, we examined *mib*^{-/-} mutant embryos at a later stage, when the parapineal had unambiguously migrated in all controls. Analysing *gfi1ab* expression between 48 and 52 hpf (Dufourcq et al., 2004) revealed that the parapineal failed to migrate in about 35% of *mib*^{-/-} embryos (as defined by parapineal mean position within -15 µm and +15 µm of the midline; n=12 of 35 embryos; **Figures 1J'', 1M**), while it migrated to the left in more than 95% of control embryos (n=39/40, **Figures 1I, 1M**; p-value<0.0001 on Welch t-test on absolute values); the parapineal in *mib*^{-/-} mutant embryos also migrated to the right more often than in controls (17%, n=6/35; **Figures 1J', 1M**).

To confirm that the phenotypes observed in *mib*^{-/-} mutants are caused by Notch pathway loss-of-function, we analysed the position of the parapineal in embryos injected with a morpholino (MO; antisense oligonucleotide) blocking translation of the two zebrafish orthologs of *su(H)/rbpj* (Echeverri and Oates, 2007); Rpbj proteins are transcription factors required for canonical Notch signalling (Fortini and Artavanis-Tsakonas, 1994; Hsieh et al., 1996). In embryos injected with *rbpj a/b* MO (4ng), we found that both parapineal migration *per se* and the orientation of migration were significantly affected. While the parapineal migrated to the left in most uninjected controls (94%, n=31/33), in *rbpj a/b* morphants migration was blocked (13% of the embryos, n=6/46; p-value=0.0001 in Welch t-test on absolute value) or its orientation was partially randomized, with migration being seen to the left (67% of the embryos, n=31/46) or to the right (20% of the embryos, n=9/46; p-value=0.0002 on Wilcoxon test) (**Figures S1A-B', S1D'**). As observed in *mib*^{-/-} mutants, the proportion of *Tg(dusp6:d2EGFP)* expressing cells was also increased in the parapineal of *rbpj a/b* morphants (10±6 d2EGFP+ cells) compared to controls (6±4 d2EGFP+ cells) (p-value=0,0016 Welsh t-test) (**Figures S1F-F''**).

While quantifying parapineal mean position, we also found that the number of *gfi1ab* positive cells at 48 hpf was significantly increased in *mib*^{-/-} mutants (23±5) compared with control embryos (17±4; p-value=3.901e-07, Welch t-test) (**Figures 1I-1J''**, **1N**). Similarly, we observed an overall increase in number of *sox1a* expressing cells in *mib*^{-/-} mutants at this stage despite finding no change at 32 hpf (**Figure 1O**). In contrast, the number of parapineal cells expressing *tbx2b*, a marker for parapineal progenitors (Snelson et al., 2008), was not increased in *mib*^{-/-} mutants (**Figure 1P**). In *rbpj a/b* morphants, we also observed that the number of *gfi1ab* expressing parapineal cells at 48 hpf was significantly increased (19±6) compared to control embryos (14±3; p-value<0.0001) (**Figures S1A-S1B'**, **S1D**); injection of a higher dose of *rbpj a/b* MO (10 ng) resulted in the number of *gfi1ab* positive cells in the parapineal being drastically decreased (4±3) compared to control embryos (15±2; p-value<0.0001) (**Figures S1C-C'**, **S1E**).

Taken together, our data show that loss of Notch signalling results in defects in parapineal migration and, at later stages, an increase in the number of *gfi1ab* and *sox1a* expressing parapineal cells.

The roles of Notch signalling in the specification and migration of parapineal cells can be uncoupled.

Our data show that blocking Notch signalling leads to an expansion of FGF pathway activation in the parapineal, an increase in the number of *gfi1ab* and *sox1a* expressing parapineal cells and defects in parapineal migration. With the aim of unravelling potential causative links between these different phenotypes, we used a pharmacological inhibitor of γ -secretase complex, LY411575, to block Notch signalling pathway during different time windows (Romero-Carvajal et al., 2015; Rothenaigner et al., 2011); γ -secretase activity is required for the release of the intracellular domain of Notch, NICD, during activation of the canonical pathway (Geling et al., 2002).

We first treated wild-type embryos with LY411575 between 22 and 32 hpf, a time window corresponding to when the parapineal segregates from the epiphysis and begins migrating. While no change in *gfi1ab* expression was detected when embryos were treated with 30 μ M LY411575 (**Figures 2C**), a higher concentration of LY411575 (100 μ M) resulted in an increase in the number of *gfi1ab* positive cells in treated embryos (**Figures 2A-2C**); neither treatment resulted in defects in parapineal migration (**Figures 2D**). As this effect of LY411575 treatment

on parapineal size was modest, we next treated embryos heterozygous for *mib* mutation (*mib*^{+/-}) during the same time window thinking that this might provide a sensitized background for the drug. *mib*^{+/-} heterozygous embryos treated with the lower dose of LY411575 show a strong increase in the number of *gfi1ab* expressing parapineal cells (28±5) compared to LY411575 treated wild-type controls (17±3; p-value=1.0e-10) or DMSO treated *mib*^{+/-} heterozygous (20±2; p-value=2.2e-10) (**Figures 2E-2H, 2I**). As before, however, we did not detect a parapineal migration defect in LY411575 treated *mib*^{+/-} embryos (**Figures 2E-2H, 2J**), even when we increased the dose of LY411575 to 200 μM (**Figure S2B**). Therefore, although LY411575 treatment from 22 to 32hpf can synergize with a *mib*^{+/-} heterozygote genetic background to promote an increase in the number of *gfi1ab* positive parapineal cells, it does not affect parapineal migration. These data indicate that the role of Notch in controlling the specification of parapineal cells can be uncoupled from its function in parapineal migration.

Finally, we saw no significant increase in the number of *Tg(dusp6:d2EGFP)* positive cells in *mib*^{+/-} heterozygous embryos treated with LY411575 during the 22 to 32 hpf time window (**Figures 2K**). The wild-type levels of FGF pathway activation and correct migration of the parapineal in LY411575 treated embryos is consistent with our previous results showing that restricted FGF pathway activation being important for correct parapineal migration (Roussigné et al., 2018).

Notch activity is required early for unilateral activation of the Nodal pathway in the epithalamus

To determine whether parapineal migration defects might be an indirect consequence of an earlier role of Notch signalling, we also analysed the epithalamus of embryos treated with LY411575 at an early time window, from 8 to 22 hpf. This early drug treatment did not interfere with the number of *gfi1ab* positive cells (**Figures 2L**), or with migration *per se*, but led to a partial randomization of parapineal migration (**Figure 2M**).

Laterality in the epithalamus is driven by unilateral activation of the Nodal signalling pathway (Concha et al., 2000; Liang et al., 2000; Regan et al., 2009). We hypothesized that the partial randomization of parapineal migration orientation observed in *mib*^{+/-} mutants or in embryos treated with LY411575 from 8 to 22 hpf could be caused by changes in Nodal signalling. To address this possibility, we analysed the expression of *pitx2c*, a Nodal signalling target gene

(Ryan et al., 1998) (Concha et al., 2000; Essner et al., 2000; Liang et al., 2000), in the different contexts where the orientation of parapineal migration was partially randomised. While *pitx2c* expression is detected in the left epithalamus in control embryos between 28 and 32 hpf (n=26/28), we observed that its expression is bilateral in most *mib*^{-/-} mutant embryos (n=26/29) (**Figures S3A-S3B, S3E**), in a majority of *rbpja/b* morphants (n=13/23, **Figures S3F**) and in approximately half of the embryos treated with LY411575 from 8 to 22 hpf, regardless of whether they were heterozygotes for the *mib* mutation (*mib*^{+/-}, n=6/10) or not (n=4/13) (**Figures S3A-S3D, S3H**). As expected, the expression of *pitx2c* was indistinguishable from controls in embryos treated with LY411575 during the later time window (22-32 hpf) (**Figures S3G**).

Our data indicate that the partial randomization of parapineal migration observed in *mib*^{-/-} mutants or *rbpj* morphants is due to an early role of Notch pathway in restricting Nodal signalling to the left epithalamus. As observed for the late time window (22-32 hpf), the early time window of LY411575 treatment (8 to 22 hpf) did not affect parapineal migration *per se* and this correlates with no significant change in the *Tg(dusp6:d2EGFP)* expression pattern (**Figure 2N**).

Notch gain of function inhibits FGF pathway activation in the parapineal, and blocks specification of parapineal neurons and migration

When we abrogated Notch signalling, we observed an increase in the number of *Tg(dusp6:d2EGFP)*⁺ parapineal cells and correlated defects in parapineal migration (**Figures 1E-1H, 1M, Figures S1D', S1E'**).). To address further the role of the Notch pathway in modulating FGF activation, we analysed the phenotypes associated with global activation of Notch pathway. For this, we used previously described transgenic lines, *Tg(hsp70:gal4)* and *Tg(UAS:NICD-myc)* (Scheer and Campos-Ortega, 1999), to induce the expression of the Notch Intracellular Domain (NICD) upon heat shock. In most embryos globally expressing NICD from 26 hpf, we observed a strong decrease in the number of parapineal cells expressing *Tg(dusp6:d2EGFP)* at 36 hpf (3±3 cells) compared with the control embryos (7±4; p-value=0.0004) (**Figures 3A-3B, 3G**); the mean intensity of d2EGFP fluorescence was also significantly decreased in these embryos compared with the controls (p-value=0.0001) (**Figures 3A-3B, 3G'**).

To assess a potential correlation between the inhibition of FGF pathway activation and defects in parapineal migration, we sought to analyse the mean position of *sox1a* or *gfi1ab* expressing

cells at 36 or 48 hpf as we had done for Notch loss-of-function embryos. However, following heat shock at 26 hpf, *sox1a* expression was lost in most 36 hpf embryos (**Figures 3C-D, 3H**) and was strongly decreased at 48 hpf (**Figures 3L-3M, 3Q**). Similarly, although the number of *gfi1ab* positive cells did not vary significantly in *Tg(hsp70:gal4); Tg(UAS:NICD-myc)* embryos heat shocked at 22 and 24 hpf (**Figures S4A-D, S4I-J**), it was strongly decreased in embryos expressing NICD from 26, 28 and 32 hpf (**Figures 3J-K, 3P and Figures S4E-H, S4K-L**); in embryos heat shocked at 26 hpf or 28 hpf, *gfi1ab* staining was often completely lost in the parapineal (n=7/25 or n=8/26 respectively) or detected in less than 4 cells (n=11/25 or n=14/26 respectively) (**Figures 3J-K, 3P, S4E-F, S4K**). On the other hand, nuclear staining indicated that the parapineal rosettes can be detected in most of the embryos expressing NICD (**Figure 3A-3L**, yellow circle), suggesting that the parapineal does form despite global activation of Notch. Similarly, *tbx2b* expression was not affected in NICD expressing embryos either at 36 hpf (**Figure 3E-F, 3I**) or at 48 hpf (**Figure 3N-O, 3R**). Thus, global Notch activation appears to inhibit the specification/differentiation of *gfi1ab*+ or *sox1a*+ cells from *tbx2b* progenitors.

Using nuclear staining we assessed parapineal mean position at 36 hpf and found that it was closer to the midline in embryos expressing NICD from 26 hpf, (-8.7 +- 6.3 μ M; n=16) compared to control embryos (-20.5 +- 8.3 μ M; n=16) (p-value=0.001 in welch t test) (**Figures 3A-F, 3G''**); this migration defect could also be detected by analysing the mean position of *tbx2b* expressing parapineal cells at 36 hpf (p-value=0.0017 in welch t test) (**Figure 3I'**). Defects in parapineal migration were confirmed at 48 hpf using *tbx2b*, *gfi1ab* or *sox1a* markers to assess PP mean position (**Figure 3J-O, 3P'-R''**); for instance, when *gfi1ab* positive cells were detected, their mean position was significantly closer to the midline in embryos expressing NICD from 26 hpf (-10.1 +- 14 μ M; n=18) compared to control embryos (-34.6 +- 7.5 μ M; n=27) (p-value<0.0001 in welch t test) (**Figures 3J-K, 3P'**). Parapineal mean position was also affected in embryos expressing NICD just before parapineal formation (heat shock at 22 and 24 hpf), or after PP formation (heat shock at 28 and 32 hpf), although in the latter cases, the penetrance varies (**Figures S4A-H, S4I'-L'**).

Altogether, our data show that global activation of Notch signalling inhibits the migration of parapineal cells, and that this is correlated with a global decrease in the level of FGF signalling activation. Ectopic Notch signalling also decreases the number of differentiated parapineal cells, a phenotype opposite to that observed in Notch LOF contexts.

Decreasing FGF signalling rescues parapineal migration defects in loss of Notch context while increasing FGF signaling enhances it

Inhibiting or activating the Notch pathway results in reciprocal effects on FGF pathway activation in the parapineal, as seen by an increase or decrease in the number of *Tg(dusp6:d2EGFP)* expressing parapineal cells, respectively. Both contexts are also associated with defects in parapineal migration suggesting that Notch dependant control of FGF activation levels in parapineal cells is important for cluster migration. To investigate the link between Notch and FGF signalling further, we analysed whether the migration phenotype observed in *mib*^{-/-} mutants could be rescued by decreasing FGF signalling, using SU5402, a pharmacological inhibitor of the FGF pathway (Mohammadi et al., 1997). We have previously shown that treating wild-type embryos with 10 μ M SU5402 interferes with parapineal migration (Regan et al., 2009) and with the expression of the *Tg(dusp6:d2EGFP)* FGF reporter (Roussigné et al., 2018). Treating embryos with 5 μ M SU5402, however, does not affect parapineal migration (**Figure 4D**); the parapineal migrates in all SU5402 treated embryos (n=31/31) as well as in all DMSO treated control embryos (n=32/32). Using this suboptimal dose of SU5402, parapineal migration was partially rescued in *mib*^{-/-} embryos (19% of embryos with mean position between -15 and +15 μ m (n=8/41) compared to DMSO treated *mib*^{-/-} embryos (52% of embryos, n=16/31)); p-value=0.0139 on a Chi-square test and p=0.01172 on a Pairwise Wilcoxon test on absolute value (**Figures 4A-4B, 4D**). Suboptimal SU5402 treatment had no effect on parapineal neuron specification, either in *mib*^{-/-} mutant embryos or siblings (**Figures 4C**). As previously observed, we detected an increase in the number of *gfi1ab* expressing parapineal cells in DMSO treated *mib*^{-/-} embryos (18 \pm 5) compared to controls (15 \pm 2; p-value=0.0041). The number of *gfi1ab* positive cells at 48 hpf was also increased in SU5402 treated *mib*^{-/-} embryos (19 \pm 7) compared to SU5402 treated controls (15 \pm 3; p-value=0.0083) and there was no significant difference in the number of *gfi1ab* expressing cells between DMSO treated *mib*^{-/-} embryos and SU5402 treated *mib*^{-/-} embryos (p-value=0.5687). These data show that decreasing the level of FGF signalling activity can partially restore parapineal migration in a context where FGF activation is expanded, thus supporting the hypothesis that Notch acts to restrict FGF pathway activation.

To address the connection between Notch and FGF in an alternative way, we asked whether ectopic activation of the FGF pathway could elicit a more severe phenotype in a loss-of-function context for Notch. To achieve this, we used a transgenic line that expressed a constitutively activated Fgf receptor after heat shock, *Tg(hsp70l:Xla.Fgfr1,cryaa:DsRed)* (Marques et al., 2008), in embryos injected with *rbpja/b* MO (4 to 8 ng *rbpja/b* MO); we chose this Notch context

as parapineal migration defects are more modest than in *mib*^{-/-} mutants. As previously described (Roussigné et al., 2018), widespread expression of constitutively activated receptor (CA-FgfR1) prevented parapineal migration in a small number of embryos (7% of embryos; n=4/55, between -15 and +15 μ m; p-value=0.0011 in Welch's t test on absolute value), while the parapineal consistently migrates in heat shocked control embryos not carrying the transgene (n=54/54 with n=51/54 leftwards and n=3/54 toward the right). In the absence of the CA-FgfR transgene, *rbpja/b* morphant embryos displayed a migration defect at low frequency (7%; n=5/67) (**Figures 4F**). However, in *rbpja/b* morphant embryos expressing the activated receptor, the frequency of embryos in which the parapineal failed to migrate increased significantly (25% of embryos; n=18/73) (p-value=0.0007 Welch's t test on absolute value and p-value=0.0232 in Chi-square test) (**Figures 4F**). The interaction detected between the Notch and FGF pathways in this context appears synergistic as the increase in parapineal migration defects observed in *rbpja/b* morphant embryos expressing the activated Fgf receptor is significantly higher than expected from merely adding the effects of activated receptor transgene and *rbpja/b* MO injections alone (p-value=0.0001 in t test on absolute value and p-value=0.0003 in Chi-square test). The increased frequency of parapineal migration defects occurs in the absence of a significant change in parapineal cell-type specification (**Figures 4E**); the mean number of *gfi1ab* expressing parapineal cells did not vary significantly between heat shocked *rbpja/b* morphant embryos with or without the receptor transgene (14 \pm 6 versus 13 \pm 5; p-value=0.39).

Taken together, our loss-of-function, gain-of-function and epistasis experiments argue that the Notch pathway is required for parapineal migration, and that it acts by restricting FGF activation in parapineal cells.

Discussion

In this study, we address how the activation of FGF pathway is restricted within parapineal cells to promote migration. We show that expression of the *Tg(dusp6:d2EGFP)* reporter transgene is broader in loss-of-function contexts for Notch signalling and is reduced following global activation of the Notch pathway. These changes in FGF activation correlate with defect in parapineal migration. This is further confirmed by epistasis experiments showing that decreasing or increasing FGF signalling can respectively rescue or enhance parapineal

migration defects in Notch loss-of-function contexts. We conclude that the Notch pathway participates to restrict the activation of FGF signalling to cells at the leading edge of the parapineal cluster, thus promoting its migration.

Notch acts upstream of FGF signalling in the parapineal.

In other models describing cross-talk between the Notch and FGF pathways, Notch signalling is more often described to act downstream of FGF pathway. In the zebrafish lateral line primordium (LLP), for instance, ectopic activation of Notch can rescue the formation of neuromast rosettes in absence of FGF pathway activity suggesting that Notch signalling is required downstream of Fgf signals to promote apical constriction and rosette morphogenesis (Kozlovskaja-Gumbriené et al., 2017). Notch signalling is also described to be a downstream effector of FGF pathway for epithelial proliferation in the pancreas in mammalian embryos (Hart et al., 2003). The function of FGF pathway in hematopoietic stem cell emergence or tracheal system development involves its capacity to regulate the expression of Delta ligands (Lee et al., 2014) (Ikeya and Hayashi, 1999), although in the model of tracheal cell migration activated Notch in turn represses FGF activity in follower cells (see below). Our data suggest that the Notch pathway acts upstream of FGF signalling in parapineal cells to restrict FGF pathway activity and promote migration. Therefore, the crosstalk between the FGF and Notch pathway appears highly context specific.

How can Notch restrict the activation of FGF pathway ?

The fact that some *rbpja/b* morphants display parapineal migration defects similar to *mib*^{-/-} mutants strongly supports a role for the canonical Notch pathway rather than a Notch independent role of Mindbomb ubiquitin ligase in parapineal migration. As parapineal migration defects seem more penetrant in *mib*^{-/-} mutants compared to *rbpja/b* morphants (Fig1 versus Fig S1), we cannot exclude that Mindbomb might also regulate migration independently of the Notch pathway, for instance through modulation of Rac1 (Mizoguchi et al., 2017). Altogether, our data indicate that Notch pathway promotes migration by restricting the activation of FGF signalling in parapineal cells. But how could canonical Notch signalling modulate FGF pathway activity? Notch could possibly act by biasing the fate of parapineal cells towards a FGF responsive bias. This is however unlikely as all PP cells seem competent to migrate and to be activated by Fgf8 (Concha et al., 2003; Roussigné et al., 2018). A parsimonious possibility is

that lateral inhibition based cell-cell communication between parapineal cells within the rosette would modulate the capacity of a cell to activate/maintain or to inhibit FGF pathway activity.

Interestingly, Notch signalling has previously been implicated the migration of sheets of epithelial cells (Riahi et al., 2015), trachea cells in *Drosophila* (Ghabrial and Krasnow, 2006; Ikeya and Hayashi, 1999) and in vertebrate blood vessel systems (Siekman and Lawson, 2007b). In this latter two models, Notch-Delta signalling contributes to the selection of the tip cells by restricting the ability of followers cells to activate RTK signalling although the molecular mechanisms are not clear yet (Ghabrial and Krasnow, 2006; Ikeya and Hayashi, 1999; Siekman and Lawson, 2007b). In all these models, migrating cells remains attached to the bulk of the tissue. parapineal migration is thus the first described model of isolated migrating cluster in which Notch signalling plays a role in modulating RTK signalling and in defining leading cells.

How Notch mediated cell-cell communication could inhibit FGF activity in few cells to polarise the migrating cluster is not clear. However, as the ectopic expression of the constitutive activated FGF receptor (CA-FgfR1) does not completely block parapineal migration in wild-type and can rescue migration in *fgf8*^{-/-} mutants (Roussigné et al., 2018), it appears that the restriction mechanism acts downstream of the receptor rather than at the level of receptor gene expression. As described for the *C. elegans* vulva (Berset et al., 2001; Yoo et al., 2004), Notch signalling could directly promote the transcription of Ras/MAPK pathway inhibitors.

Time window of Notch requirement

None of the LY411575 treatment regimes we employed interfered with parapineal migration and, as such, a time window for Notch requirement could not be defined. We cannot exclude, therefore, that an early requirement for Notch would indirectly contribute to modulate the level of mosaicism in FGF activity later in the parapineal. However, the fact that ectopic Notch signalling at later stages can efficiently block migration argues for a role of Notch at the time when the parapineal initiates its migration. If Notch signalling is indeed required before migration, it is unclear why LY411575 treatment does not affect migration while it is able to trigger an increase in the number of *gfi1ab* and *sox1a* positive parapineal cells.

Classically, Notch signalling is thought to act through a lateral inhibition mechanism leading to a Notch-ON, Notch-OFF outcome between neighbouring cells. Recent work, however, suggests that Notch acts in a level-dependent manner rather than in an all-or-nothing mode (Ninov et al.,

2012). In light of this, the differential effect of LY411575 on specification and migration of parapineal cells could reflect a different requirement in Notch signalling threshold, with a lower threshold of Notch signalling being required for migration and a higher one being required to control fate specification of parapineal cells. If LY411575 does not completely block Notch signalling, then residual Notch activity could be sufficient to promote the restriction of FGF activity and parapineal migration while not to limit the specification of *gfi1ab* and *sox1a* positive cells. Consistent with the observation that LY411575 treatment might be partially effective, we observed that the average number of *Tg(dusp6:d2EGFP)+* cells increases slightly in LY411575 treated embryos from 22 to 32 hpf, without reaching statistical significance. Given the high variability observed in the number of *Tg(dusp6:d2EGFP)+* cells in wild-type contexts, we might expect that parapineal migration is robust enough to tolerate a moderate increase in the number of *Tg(dusp6:d2EGFP)+* cells.

Another possibility is that LY411575 might inhibit other factors/peptidases than just γ -Secretases, that would act in synergy with the Notch pathway to promote parapineal cell specification but not migration (Iben et al., 2007). Alternatively, the role of Notch in restricting FGF activity and promoting migration could be rescued by other peptidases that would be less sensitive to LY411575 while the role of Notch in the specification of parapineal cells would not.

Notch effects on cell migration and cell specification can be uncoupled in the parapineal.

Studies addressing the link between cell specification and migration are rare and, as such, our knowledge on whether and how these two processes are coordinated is limited. In the LLP model, proper morphogenesis of the future neuromast at the back of the primordium is required for migration (Lecaudey et al., 2008; Nechiporuk and Raible, 2008). In embryos treated with LY411575 from 22 to 32 hpf, the number of *gfi1ab* and *sox1a* expressing parapineal cells is strongly increased but neither parapineal migration nor *Tg(dusp6:d2EGFP)+* expression are affected. Therefore, our data reveals that cell-type specification and migration can be uncoupled in the parapineal. Our results resemble previous observations describing that specification of cardiac cells and their migration during in heart development (Davidson et al., 2005).

Notch acts downstream of Tbx2b to control the differentiation of parapineal cell fates.

Notch mediated cell-cell communication is well described for its role on cell fate and progenitors maintenance (Cau and Blader, 2009). In neural tissues or in the pancreas, for instance,

inhibition of the Notch signalling pathway causes premature differentiation of the progenitor cells into mature differentiated cells (Li et al., 2015). In loss or gain-of-function for Notch, the number of *gfi1ab* and *sox1a* expressing parapineal cells is affected. However, in both contexts the parapineal rosette is formed and a normal number of *tbx2b* expressing parapineal cells is detected. This suggests that Notch signalling acts downstream of Tbx2b, and probably controls the transition from *tbx2b* expressing putative progenitors to differentiated parapineal cells expressing *sox1a/gfi1ab*. In this were the case, we might expect a reduction in the number of *tbx2b* positive cells in *mib*^{-/-}. However, the number of *tbx2b* positive cells does not decreased concomitantly in embryos with increased *gfi1ab/sox1a* cells in *mib*^{-/-} mutants. This observation might be explained by a compensatory higher level of proliferation of *tbx2b*⁺ cells in *mib*^{-/-} or by the appearance of cells with a mixed identity that would co-express *gfi1ab* and *tbx2b* markers, as shown previously in the pineal gland (Cau et al., 2008).

Synergistic or parallel role of the Nodal and Notch pathways in restricting FGF signaling

The Notch signalling pathway was previously shown to be required for the expression of *Nodal*/TGF- β *signal* around the node and subsequently in the left lateral plate mesoderm (*LPM*) (Krebs et al., 2003; Raya et al., 2003). In zebrafish, expression of a *nodal* related gene (*ndr3/southpaw*) in the left LPM is required for the later expression of a second *nodal* gene (*ndr2/cyclops*) in the left epithalamus, which is required for biasing parapineal migration to the left (Concha et al., 2000; Liang et al., 2000; Regan et al., 2009). In Notch loss-of-function contexts, the Nodal pathway is activated on both sides of the epithalamus. The requirement for Notch signalling for unilateral *ndr2/cyclops* expression in the epithalamus is consistent with an early role of Notch signalling in initial left right asymmetry.

Our previous results indicate that Nodal signaling contributes to restricting FGF pathway activation, as well as biasing it to the left (Roussigné et al., 2018). In this study, we show that the restriction of FGF activity requires Notch activity. As mentioned above, the Nodal pathway is bilateral in the epithalamus of embryos with compromised Notch signaling. However, it is unlikely that the role of the Notch pathway in restricting FGF pathway activation depend on its ability to control Nodal signalling. Indeed, in other contexts of bilateral Nodal signaling, such as in embryos injected with morpholinos against *ntl*, we have shown that FGF pathway activation still becomes restricted to a few parapineal cells (Roussigné et al., 2018); *Tg(dusp6:d2EGFP)* reporter expression in this context is no longer left lateralized and this correlates with the parapineal initiating its migration, either to the left or the right . In absence of Nodal signaling, as

in *spaw* morphants, *Tg(dusp6:d2EGFP)* expression is generally less restricted within the parapineal and this correlates with delayed parapineal migration, indicating that the restriction of FGF activity is influenced by Nodal signaling as well as by Notch pathway. How these two pathways interact to restrict the activation of FGF signaling is not known and future investigations are needed to address whether Nodal and Notch pathway act in a synergic way or in parallel to restrict the FGF pathway.

Materials and Methods

Fish lines

Embryos were raised and staged according to standard protocols (Westerfield, 2000). Embryos homozygous for *midbomb* (*mib*^{ta52b}) (Itoh et al., 2003) and *fgf8* mutations (*fgf8*^{ti282a} / *acerebellar* / *ace*; (Reifers et al., 1998)) were obtained by inter-crossing heterozygous carriers. Carriers of the *fgf8*^{ti282a} allele were identified by PCR as described previously (Roussigné et al., 2018). *mib*^{ta52b+/-} carriers were identified by PCR genotyping using primers 5'-GGTGTGTCTGGATCGTCTGAAGAAC-3' and 5'-GATGGATGTGGTAACTGATGACTC-3' followed by enzymatic digestion with NlaIII. *Tg(hsp70:Gal4)*^{kca4} and *Tg(UAS:myc-Notch1a-intra)*^{kca3} transgenic lines have been described previously (Scheer and Campos-Ortega, 1999). Embryos carrying the *Tg(hsp70:ca-fgfr1; cryaa:DsRed)*^{pd3} transgene (Marques et al., 2008; Neilson and Friesel, 1996) were identified by the presence of DsRed expression in the lens from 48 hpf or, by PCR at earlier stages as described previously (Gonzalez-Quevedo et al., 2010). *Tg(dusp6:d2EGFP)*^{pf6} (Molina et al., 2007) lines were used as reporters for FGF pathway activity. Embryos were fixed overnight at 4°C in 4% paraformaldehyde/1xPBS, after which they were dehydrated through an ethanol series and stored at -20°C until use.

Ethics statement

Fish were handled in a facility certified by the French Ministry of Agriculture (approval number A3155510). The project has received an agreement number APAFIS#3653-2016011512005922. Anaesthesia and euthanasia procedures were performed in Tricaine Methanesulfonate (MS222) solutions as recommended for zebrafish (0,16mg/ml for anaesthesia, 0,30 mg/ml for euthanasia). All efforts were made to minimize the number of animals used and their suffering, in accordance with the guidelines from the European directive on the protection of animals used

for scientific purposes (2010/63/UE) and the guiding principles from the French Decret 2013-118.

LY411575 treatment

Embryos collected from *Tg(dusp6:d2GFP)^{pt6}* carriers outcrossed with wild-type fish or with heterozygous *mib^{ta52b}* were dechorionated and treated from 8 to 22 hpf or 22 to 32 hpf with 30 μ M, 100 μ M or 200 μ M of LY411575 (MedChem; (Rothenaigner et al., 2011)); control embryos were treated with an equal volume of DMSO diluted in E3 medium. *Tg(dusp6:d2GFP)* expressing embryos were incubated in LY411575 at 28°C and fixed at 32 hpf for immunostaining against EGFP; sibling embryos, not carrying the *Tg(dusp6:d2GFP)* transgene, were fixed at indicated time (32 hpf, 36 hpf or 48 hpf) for in situ against different parapineal markers.

SU5402 drug treatment

Embryos collected from in-crosses between *mib^{ta52b}* and *Tg(dusp6:d2EGFP)*; *mib^{ta52b}* mutants were dechorionated and treated with 5 μ M SU5402 (Calbiochem; (Mohammadi et al., 1997)) by diluting a 10 mM DMSO based stock solution in E3 medium; control embryos were treated with an equal volume of DMSO diluted in E3 medium. All embryos were incubated in SU5402 at 28°C from 24 hpf to 32 hpf. *Tg(dusp6:d2EGFP)* embryos were fixed at 32 hpf to analyse the d2GFP expression pattern in both *mib^{ta52b}* mutants and sibling embryos; the remaining half of embryos were fixed at 48 hpf to analyse parapineal migration.

Morpholino injections

Morpholino oligonucleotides targeting both *rbpja /su(H)1* and *rbpjb/su(H)2* (Echeverri and Oates, 2007) were dissolved in water at 3 mM. The resulting stock solution was diluted to working concentrations (0,3 mM, 2.5ng/nl) in water and Phenol Red before injection of 1,5 nl (4ng) or 4nl (10ng) into embryos at the 1 cell stage. Embryos were subsequently fixed and processed for ISH or antibody labelling.

Heat shock procedure

Ectopic expression of the intracellular domain of Notch receptor (NICD) was induced in *Tg(hs70:gal4); Tg(uas:notch1a-intra-myc)* double transgenic embryos by incubating them at 39°C for 45 minutes starting at different time points (22 hpf, 24 hpf, 26 hpf, 28 hpf or 32 hpf). Embryos were then incubated at 28.5 °C and fixed at 36 hpf to analyse *Tg(dusp6:d2EGFP)* expression or at 48 hpf for *in situ* against indicated parapineal markers. Ectopic expression of CA-FgfR1 was induced in *Tg(hsp70:ca-FgfR1; cryaa:DsRed)^{pd3}* heterozygote embryos by performing a first heat shock at 25-26 hpf (39°C, 45 minutes) and a second short heat shock (39°C, 15 min) 3 hours later (28-29 hpf) in order to cover the entire period of parapineal migration.

In situ hybridization and immunostaining

Embryos were fixed overnight at 4°C in BT-FIX (Westerfield, 2000) after which they were dehydrated through ethanol series and stored at -20°C until use. In situ hybridizations were performed using antisense DIG labelled probes for *gfi1ab* (Dufourcq et al., 2004), *sox1a* (Clanton et al., 2013), *pitx2c* (Essner et al., 2000) and *tbx2b* (Snelson et al., 2008); details of the *in situ* hybridization protocol are available upon request. In situ hybridizations were completed using Fast Red (from Roche or Sigma Aldrich) as an alkaline phosphatase substrate. Immunostainings were performed in PBS containing 0,5% triton using anti-GFP (1/1000, Torrey Pines Biolabs) and Alexa 488 or Alexa 555-conjugated goat anti-rabbit IgG (1/1000, Molecular Probes). For nuclear staining, embryos were incubated in ToPro-3 (1/1000, Molecular Probes) for 1h as previously described (Roussigné et al., 2018).

Image acquisition

Confocal images of fixed embryos were acquired on an upright Leica SP8 confocal microscope using the resonant fast mode and either an oil x63 (aperture 1.4) or x20 (aperture 1.4) objective. Confocal stacks were analysed using ImageJ software. Figures were prepared using Adobe Photoshop software.

Quantification of the number and position of *Tg(dusp6:d2EGFP)* positive parapineal cells

The position and number of parapineal cells positive for the *Tg(dusp6:d2GFP)* transgene were analysed using ROI Manager tool on ImageJ software as previously described (Roussigné et al., 2018). The mean intensity of the d2EGFP staining was quantified in an area corresponding to the cell nucleus and the same intensity threshold was used in the different experimental contexts to determine if a cell was *Tg(dusp6:d2EGFP)* positive or not. The total number of parapineal cells was estimated by counting nuclei in the parapineal rosettes using Topro-3 nuclear staining. For each parapineal cell, we calculate its x and y position relative to the center of the parapineal (calculated as the mean of x and y positions of all parapineal cells).

Quantification of the number and position of *gfi1ab*, *sox1a*, *tbx2b* positive parapineal cells

The position and number of *gfi1ab*, *sox1a* or *tbx2b* positive parapineal cells were analysed using the Multipoint tool on ImageJ software and determined as the centre of the cell nucleus detected with the Topro-3 nuclear staining. The position of each parapineal cell was measured relative to the brain midline (reference origin =0) as determined by a line passing along the lumen of the epiphysis. For each embryo, we calculated the number of labelled parapineal cells and their mean position.

Statistical analysis

Statistical comparisons of datasets were performed using R Studio or GraphPad Prism software. For each dataset, we tested the assumption of normality with Shapiro-Wilks tests and variance homogeneity with F tests. Datasets on the number of parapineal cells were usually normal and compared using unpaired t-tests; Welch t-tests were used in the case of unequal variances. Data on parapineal mean position usually did not distribute normally and were compared using the Wilcoxon rank sum non-parametric tests; we also compared parapineal mean position datasets with Welch t-tests using absolute values to discriminate between a defect in left orientation (i.e. left right randomization of parapineal migration) and a defect in migration (i.e. distance from the midline). Data are representative of at least two, but more often three independent experiments and means (\pm SD) are indicated in the text. On dot plots, means (\pm sem) are indicated as horizontal bars with parapineal cells numbers.

Data availability

Data that support the findings described in this study are available from the corresponding author upon request.

References

- Benazeraf, B., Francois, P., Baker, R.E., Denans, N., Little, C.D., and Pourquie, O. (2010). A random cell motility gradient downstream of FGF controls elongation of an amniote embryo. *Nature* *466*, 248–252.
- Bisgrove, B.W., Essner, J.J., and Yost, H.J. (1999). Regulation of midline development by antagonism of lefty and nodal signaling. *Development* *126*, 3253–3262.
- Cau, E., and Blader, P. (2009). Notch activity in the nervous system: to switch or not switch? *Neural Dev* *4*, 36.
- Cau, E., Quillien, A., and Blader, P. (2008). Notch resolves mixed neural identities in the zebrafish epiphysis. *Dev. Camb. Engl.* *135*, 2391–2401.
- Ciruna, B.G., Schwartz, L., Harpal, K., Yamaguchi, T.P., and Rossant, J. (1997). Chimeric analysis of fibroblast growth factor receptor-1 (*Fgfr1*) function: a role for FGFR1 in morphogenetic movement through the primitive streak. *Dev. Camb. Engl.* *124*, 2829–2841.
- Clanton, J.A., Hope, K.D., and Gamse, J.T. (2013). Fgf signaling governs cell fate in the zebrafish pineal complex. *Development* *140*, 323–332.
- Concha, M.L., Burdine, R.D., Russell, C., Schier, A.F., and Wilson, S.W. (2000). A nodal signaling pathway regulates the laterality of neuroanatomical asymmetries in the zebrafish forebrain. *Neuron* *28*, 399–409.
- Concha, M.L., Russell, C., Regan, J.C., Tawk, M., Sidi, S., Gilmour, D.T., Kapsimali, M., Sumoy, L., Goldstone, K., Amaya, E., et al. (2003). Local tissue interactions across the dorsal midline of the forebrain establish CNS laterality. *Neuron* *39*, 423–438.
- Dalle Nogare, D., Somers, K., Rao, S., Matsuda, M., Reichman-Fried, M., Raz, E., and Chitnis, A.B. (2014). Leading and trailing cells cooperate in collective migration of the zebrafish posterior lateral line primordium. *Development* *141*, 3188–3196.
- Davidson, B., Shi, W., and Levine, M. (2005). Uncoupling heart cell specification and migration in the simple chordate *Ciona intestinalis*. *Dev. Camb. Engl.* *132*, 4811–4818.

- Donà, E., Barry, J.D., Valentin, G., Quirin, C., Khmelinskii, A., Kunze, A., Durdu, S., Newton, L.R., Fernandez-Minan, A., Huber, W., et al. (2013). Directional tissue migration through a self-generated chemokine gradient. *Nature* *503*, 285–289.
- Duboc, V., Dufourcq, P., Blader, P., and Roussigné, M. (2015). Asymmetry of the Brain: Development and Implications. *Annu. Rev. Genet.* *49*, 647–672.
- Dufourcq, P., Rastegar, S., Strahle, U., and Blader, P. (2004). Parapineal specific expression of *gfi1* in the zebrafish epithalamus. *Gene Expr Patterns* *4*, 53–57.
- Durdu, S., Iskar, M., Revenu, C., Schieber, N., Kunze, A., Bork, P., Schwab, Y., and Gilmour, D. (2014). Luminal signalling links cell communication to tissue architecture during organogenesis. *Nature* *515*, 120–124.
- Echeverri, K., and Oates, A.C. (2007). Coordination of symmetric cyclic gene expression during somitogenesis by Suppressor of Hairless involves regulation of retinoic acid catabolism. *Dev. Biol.* *301*, 388–403.
- Essner, J.J., Branford, W.W., Zhang, J., and Yost, H.J. (2000). Mesendoderm and left-right brain, heart and gut development are differentially regulated by *pitx2* isoforms. *Development* *127*, 1081–1093.
- Fortini, M.E., and Artavanis-Tsakonas, S. (1994). The suppressor of hairless protein participates in notch receptor signaling. *Cell* *79*, 273–282.
- Friedl, P., and Gilmour, D. (2009). Collective cell migration in morphogenesis, regeneration and cancer. *Nat. Rev. Mol. Cell Biol.* *10*, 445–457.
- Geling, A., Steiner, H., Willem, M., Bally-Cuif, L., and Haass, C. (2002). A gamma-secretase inhibitor blocks Notch signaling in vivo and causes a severe neurogenic phenotype in zebrafish. *EMBO Rep* *3*, 688–694.
- Ghabrial, A.S., and Krasnow, M.A. (2006). Social interactions among epithelial cells during tracheal branching morphogenesis. *Nature* *441*, 746–749.
- Gonzalez-Quevedo, R., Lee, Y., Poss, K.D., and Wilkinson, D.G. (2010). Neuronal Regulation of the Spatial Patterning of Neurogenesis. *Dev. Cell* *18*, 136–147.
- Haeger, A., Wolf, K., Zegers, M.M., and Friedl, P. (2015). Collective cell migration: guidance principles and hierarchies. *Trends Cell Biol.* *25*, 556–566.
- Hart, A., Papadopoulou, S., and Edlund, H. (2003). *Fgf10* maintains notch activation, stimulates proliferation, and blocks differentiation of pancreatic epithelial cells. *Dev. Dyn. Off. Publ. Am. Assoc. Anat.* *228*, 185–193.
- Hsieh, J.J., Henkel, T., Salmon, P., Robey, E., Peterson, M.G., and Hayward, S.D. (1996). Truncated mammalian Notch1 activates CBF1/RBPJk-repressed genes by a mechanism resembling that of Epstein-Barr virus EBNA2. *Mol. Cell. Biol.* *16*, 952–959.

Iben, L.G., Olson, R.E., Balanda, L.A., Jayachandra, S., Robertson, B.J., Hay, V., Corradi, J., Prasad, C.V.C., Zaczek, R., Albright, C.F., et al. (2007). Signal peptide peptidase and gamma-secretase share equivalent inhibitor binding pharmacology. *J. Biol. Chem.* *282*, 36829–36836.

Ikeya, T., and Hayashi, S. (1999). Interplay of Notch and FGF signaling restricts cell fate and MAPK activation in the *Drosophila* trachea. *Development* *126*, 4455–4463.

Itoh, M., Kim, C.H., Palardy, G., Oda, T., Jiang, Y.J., Maust, D., Yeo, S.Y., Lorick, K., Wright, G.J., Ariza-McNaughton, L., et al. (2003). Mind bomb is a ubiquitin ligase that is essential for efficient activation of Notch signaling by Delta. *Dev Cell* *4*, 67–82.

Kadam, S., Ghosh, S., and Stathopoulos, A. (2012). Synchronous and symmetric migration of *Drosophila* caudal visceral mesoderm cells requires dual input by two FGF ligands. *Development* *139*, 699–708.

Kozlovskaja-Gumbriené, A., Yi, R., Alexander, R., Aman, A., Jiskra, R., Nagelberg, D., Knaut, H., McClain, M., and Piotrowski, T. (2017). Proliferation-independent regulation of organ size by Fgf/Notch signaling. *eLife* *6*.

Krebs, L.T., Iwai, N., Nonaka, S., Welsh, I.C., Lan, Y., Jiang, R., Saijoh, Y., O'Brien, T.P., Hamada, H., and Gridley, T. (2003). Notch signaling regulates left-right asymmetry determination by inducing Nodal expression. *Genes Dev.* *17*, 1207–1212.

Lecaudey, V., Cakan-Akdogan, G., Norton, W.H.J., and Gilmour, D. (2008). Dynamic Fgf signaling couples morphogenesis and migration in the zebrafish lateral line primordium. *Development* *135*, 2695–2705.

Lee, Y., Manegold, J.E., Kim, A.D., Pouget, C., Stachura, D.L., Clements, W.K., and Traver, D. (2014). FGF signalling specifies haematopoietic stem cells through its regulation of somitic Notch signalling. *Nat. Commun.* *5*, 5583.

Li, X.-Y., Zhai, W.-J., and Teng, C.-B. (2015). Notch Signaling in Pancreatic Development. *Int. J. Mol. Sci.* *17*.

Liang, J.O., Etheridge, A., Hantsoo, L., Rubinstein, A.L., Nowak, S.J., Izpisua Belmonte, J.C., and Halpern, M.E. (2000). Asymmetric nodal signaling in the zebrafish diencephalon positions the pineal organ. *Development* *127*, 5101–5112.

Marques, S.R., Lee, Y., Poss, K.D., and Yelon, D. (2008). Reiterative roles for FGF signaling in the establishment of size and proportion of the zebrafish heart. *Dev. Biol.* *321*, 397–406.

McMahon, A., Reeves, G.T., Supatto, W., and Stathopoulos, A. (2010). Mesoderm migration in *Drosophila* is a multi-step process requiring FGF signaling and integrin activity. *Development* *137*, 2167–2175.

Mizoguchi, T., Ikeda, S., Watanabe, S., Sugawara, M., and Itoh, M. (2017). Mib1 contributes to persistent directional cell migration by regulating the Ctnnd1-Rac1 pathway. *Proc. Natl. Acad. Sci. U. S. A.* *114*, E9280–E9289.

- Mohammadi, M., McMahon, G., Sun, L., Tang, C., Hirth, P., Yeh, B.K., Hubbard, S.R., and Schlessinger, J. (1997). Structures of the tyrosine kinase domain of fibroblast growth factor receptor in complex with inhibitors. *Science* 276, 955–960.
- Molina, G.A., Watkins, S.C., and Tsang, M. (2007). Generation of FGF reporter transgenic zebrafish and their utility in chemical screens. *BMC Dev Biol* 7, 62.
- Nechiporuk, A., and Raible, D.W. (2008). FGF-dependent mechanosensory organ patterning in zebrafish. *Science* 320, 1774–1777.
- Neilson, K.M., and Friesel, R. (1996). Ligand-independent activation of fibroblast growth factor receptors by point mutations in the extracellular, transmembrane, and kinase domains. *J. Biol. Chem.* 271, 25049–25057.
- Ninov, N., Borius, M., and Stainier, D.Y.R. (2012). Different levels of Notch signaling regulate quiescence, renewal and differentiation in pancreatic endocrine progenitors. *Dev. Camb. Engl.* 139, 1557–1567.
- Ochoa-Espinosa, A., and Affolter, M. (2012). Branching morphogenesis: from cells to organs and back. *Cold Spring Harb. Perspect. Biol.* 4.
- Pocha, S.M., and Montell, D.J. (2014). Cellular and molecular mechanisms of single and collective cell migrations in *Drosophila*: themes and variations. *Annu. Rev. Genet.* 48, 295–318.
- Raya, A., Kawakami, Y., Rodriguez-Esteban, C., Buscher, D., Koth, C.M., Itoh, T., Morita, M., Raya, R.M., Dubova, I., Bessa, J.G., et al. (2003). Notch activity induces Nodal expression and mediates the establishment of left-right asymmetry in vertebrate embryos. *Genes Dev.* 17, 1213–1218.
- Regan, J.C., Concha, M.L., Roussigne, M., Russell, C., and Wilson, S.W. (2009). An Fgf8-Dependent Bistable Cell Migratory Event Establishes CNS Asymmetry. *Neuron* 61, 27–34.
- Reifers, F., Bohli, H., Walsh, E.C., Crossley, P.H., Stainier, D.Y., and Brand, M. (1998). Fgf8 is mutated in zebrafish acerebellar (ace) mutants and is required for maintenance of midbrain-hindbrain boundary development and somitogenesis. *Development* 125, 2381–2395.
- Riahi, R., Sun, J., Wang, S., Long, M., Zhang, D.D., and Wong, P.K. (2015). Notch1-Dll4 signalling and mechanical force regulate leader cell formation during collective cell migration. *Nat. Commun.* 6, 6556.
- Romero-Carvajal, A., Navajas Acedo, J., Jiang, L., Kozlovskaja-Gumbrienè, A., Alexander, R., Li, H., and Piotrowski, T. (2015). Regeneration of Sensory Hair Cells Requires Localized Interactions between the Notch and Wnt Pathways. *Dev. Cell* 34, 267–282.
- Rothenaigler, I., Krecsmarik, M., Hayes, J.A., Bahn, B., Lepier, A., Fortin, G., Götz, M., Jagasia, R., and Bally-Cuif, L. (2011). Clonal analysis by distinct viral vectors identifies bona fide neural stem cells in the adult zebrafish telencephalon and characterizes their division properties and fate. *Dev. Camb. Engl.* 138, 1459–1469.
- Roussigne, M., Blader, P., and Wilson, S.W. (2012). Breaking symmetry: The zebrafish as a model for understanding left-right asymmetry in the developing brain. *Dev. Neurobiol.* 72, 269–281.

Roussigné, M., Wei, L., Tsingos, E., Kuchling, F., Alkobtawi, M., Tsalavouta, M., Wittbrodt, J., Carl, M., Blader, P., and Wilson, S.W. (2018). Left/right asymmetric collective migration of parapineal cells is mediated by focal FGF signaling activity in leading cells. *Proc. Natl. Acad. Sci.* *115*, E9812–E9821.

Ryan, A.K., Blumberg, B., Rodriguez-Esteban, C., Yonei-Tamura, S., Tamura, K., Tsukui, T., Peña, J. de la, Sabbagh, W., Greenwald, J., Choe, S., et al. (1998). Pitx2 determines left–right asymmetry of internal organs in vertebrates. *Nature* *394*, 545–551.

Scheer, N., and Campos-Ortega, J.A. (1999). Use of the Gal4-UAS technique for targeted gene expression in the zebrafish. *Mech. Dev.* *80*, 153–158.

Siekman, A.F., and Lawson, N.D. (2007a). Notch signalling and the regulation of angiogenesis. *Cell Adhes. Migr.* *1*, 104–106.

Siekman, A.F., and Lawson, N.D. (2007b). Notch signalling limits angiogenic cell behaviour in developing zebrafish arteries. *Nature* *445*, 781–784.

Snelson, C.D., Santhakumar, K., Halpern, M.E., and Gamse, J.T. (2008). Tbx2b is required for the development of the parapineal organ. *Development* *135*, 1693–1702.

Theveneau, E., and Linker, C. (2017). Leaders in collective migration: are front cells really endowed with a particular set of skills? *F1000Research* *6*, 1899.

Theveneau, E., and Mayor, R. (2013). Collective cell migration of epithelial and mesenchymal cells. *Cell. Mol. Life Sci. CMLS* *70*, 3481–3492.

Venkiteswaran, G., Lewellis, S.W., Wang, J., Reynolds, E., Nicholson, C., and Knaut, H. (2013). Generation and dynamics of an endogenous, self-generated signaling gradient across a migrating tissue. *Cell* *155*, 674–687.

Westerfield, M. (2000). *The Zebrafish Book. A Guide for The Laboratory Use of Zebrafish (Danio rerio)*, 4th Edition; Eugene, University of Oregon Press.

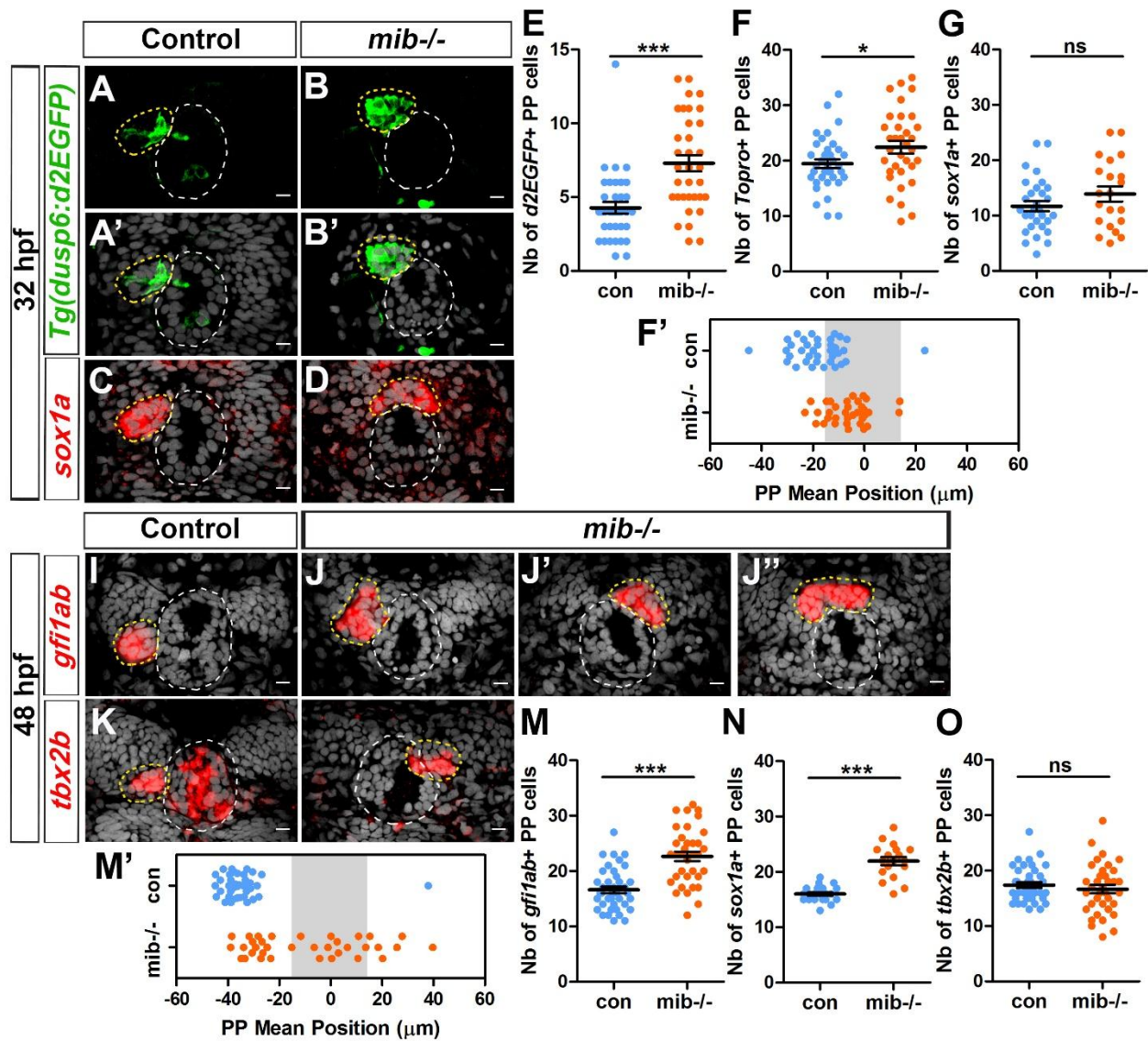


Figure 1. Increased activation of FGF signalling in *midbomb* mutants correlates with parapineal migration defect.

(A-B) Confocal maximum projection (A-B) or sections (A'-D) showing the expression of the *Tg(dusp6:d2EGFP)* transgene (Green, A-B') or *sox1a* (red, C-D) in the epithalamia of 32 hpf in control (A, A', n=36 and C, n=30) and in *mib*^{-/-} mutant embryos (B, B', n=34 and D, n=21); sections are merged with a nuclear staining (grey, A'-D) that makes the epiphysis (white circle) and parapineal (yellow circle) visible.

(E-H) Dot plots showing the number (E-G) and the mean position (H) of *dusp6:d2EGFP* (E, H), *sox1a* (F) and Topro-3 (G) positive parapineal cells in control (blue dots) or *mib*^{-/-} mutant

embryos (orange dots) at 32 hpf stage, with mean \pm SEM. *Tg(dusp6:d2EGFP)* FGF reporter is expressed in more parapineal (PP) cells in *mib*^{-/-} than controls (E) while the expression of *sox1a* is similar in both contexts (F); the average number of parapineal cells counted with a nuclear marker increases slightly (G). Parapineal migration is usually delayed in *mib*^{-/-} mutants at 32 hpf (H).

(I-J'') Confocal sections showing the expression of *gfi1ab* (red) at 48 hpf in control embryos (A; n=40) and in three examples of *mib*^{-/-} mutant embryos (B-B''; n=35) merged with nuclear staining (grey). (K-L) Confocal sections showing the expression of *tbx2b* (red) at 48 hpf in control embryos (K; n=39) and in one right migration example of *mib*^{-/-} mutants embryo (L; n=36).

(M-P) Dot plot showing, the mean parapineal (PP) position for each embryo (in μ m distance to the brain midline (x=0)) (M) and number of parapineal cells (N-P) expressing *gfi1ab* (M, N) *sox1a* (O) and *tbx2b* (P) at 48 hpf stage in control (blue dots) or in *mib*^{-/-} mutant embryos (red dots), with mean \pm SEM. In *mib*^{-/-} mutant embryos, the parapineal either did not migrate (35% of the embryos, n=12/35, have a parapineal mean position between -15 μ m and +15 μ m (shaded zone) relative to brain midline (Reference 0)) or migrates either to the left (49% of the embryos, n=17/35) or to the right (17%, n=6/35) (M). The number of *gfi1ab*⁺ and *sox1a* positive parapineal cells at 48 hpf is increased in *mib*^{-/-} mutant embryos compared with controls (N, O).

Embryo view is dorsal, anterior is up; epiphysis (white circle), parapineal gland (yellow circle); scale bar=10 μ m. Mean \pm SEM are indicated as long and short bars. *** P-value<0.0001; * P-value<0.05 in Welch t-test.

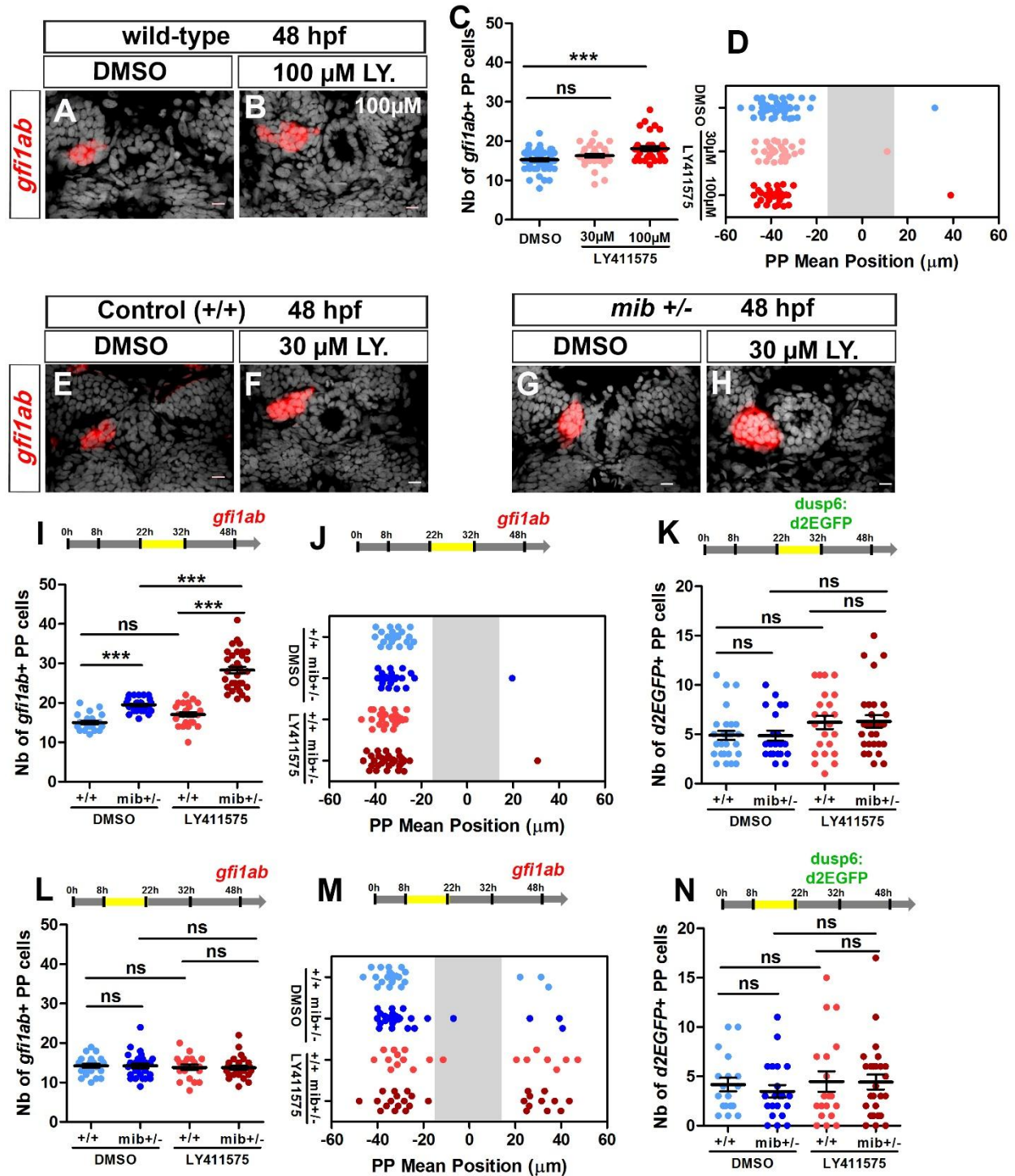


Figure 2. Notch requirement for the specification and migration of parapineal cells, and for extent of FGF pathway activation.

(A-B) Confocal sections showing the expression of *gfi1ab* (red) in embryos treated with DMSO (A; n=24) or 100 μ M LY411575 (B; n=32) from 22 to 32 hpf and fixed at 48 hpf, merged with nuclear staining (grey). Embryo view is dorsal, anterior is up; epiphysis (white circle) and parapineal (yellow circle); scale bar=10 μ m.

(C-D) Dot plots showing the number (C) and the mean position (D) of *gfi1ab* expressing parapineal (PP) cells at 48 hpf in embryos treated with DMSO (controls, blue dots, n=47), with 30 μ M LY411575 (light red dots, n=31) or 100 μ M LY411575 (red dots, n=32) from 22 hpf to 32 hpf, with mean \pm SEM, *** p-value=0.0003, Wilcoxon test.

(E-H) Confocal sections showing the expression of *gfi1ab* (E-H) (red) merged with nuclear staining (grey) at 48 hpf, in wild-type (+/+) (E, F) or *mib*^{+/-} heterozygote embryos (F, H) treated with DMSO (E, n=23 or G, n=26) or with LY411575 (F, n=25 and G, n=34) from 22 to 32 hpf.

(I-N) Upper panels in I, K, L, N show a schematic of the LY411575 treatment timeline. (I-J, L-M) Dot plots showing the number (I, L) and the mean position for each embryo (J, M) of *gfi1ab* expressing cells (48 hpf), in the parapineal (PP) of DMSO treated wild-type (+/+, dark blue dots; I-J, n=23; L-M, n=12), DMSO treated *mib*^{+/-} heterozygote (light blue dots; I-J, n=26; L-M, n=17), LY411575 treated wild-type (dark red dots; I-J, n=25; L-M, n=11) and LY411575 treated *mib*^{+/-} embryos (light red dots, I-J, n=34 or L-M, n=16). (K, N) Dot plots showing the number of *dup6:d2EGFP* expressing cells at 32 hpf for each embryo in DMSO treated wild-type (+/+, dark blue dots; K, n=28; N, n=18), DMSO treated *mib*^{+/-} heterozygote embryos (light blue dots, K, n=21; N, n=21), or at 48 hpf in LY411575 treated wild-type (dark red dots, K, n=23, N, n=19) or LY411575 treated *mib*^{+/-} heterozygote embryos (light red dots, K, n=29, N, n=26); mean \pm SEM is shown. *** P-value<0.0001, in Wilcoxon test.

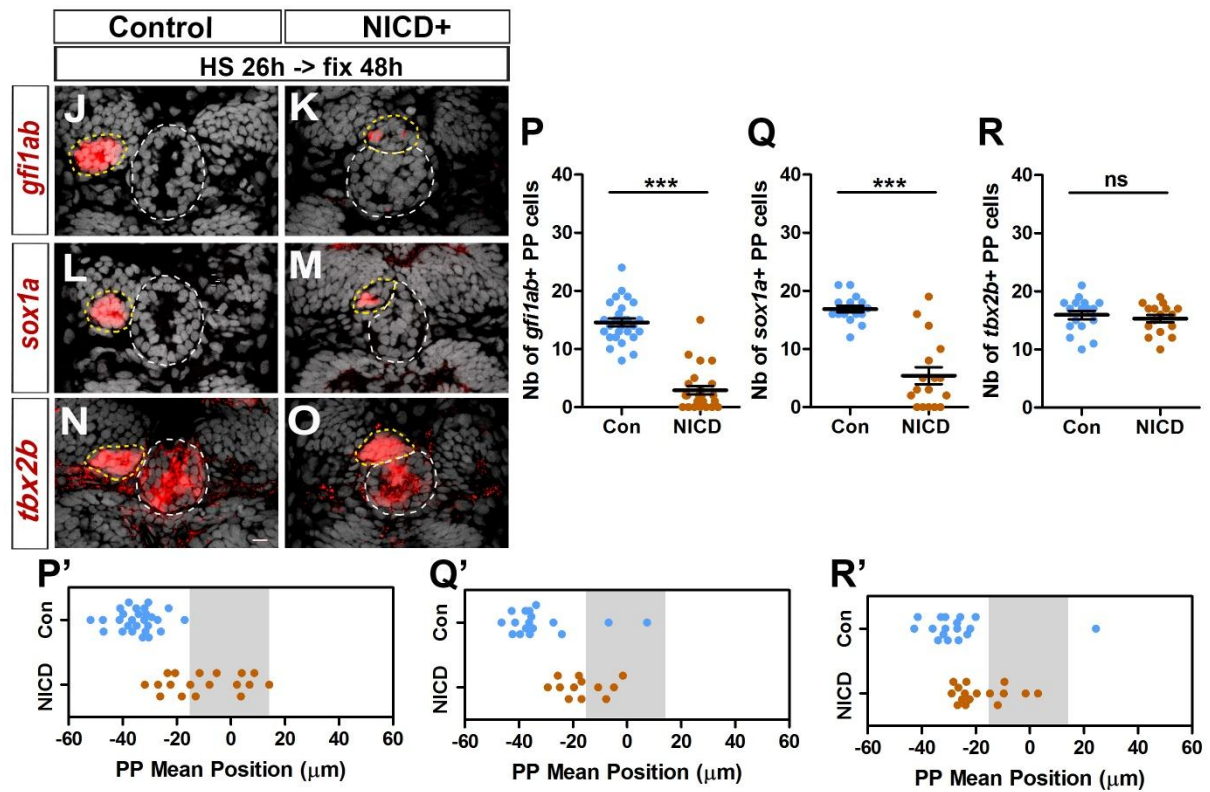
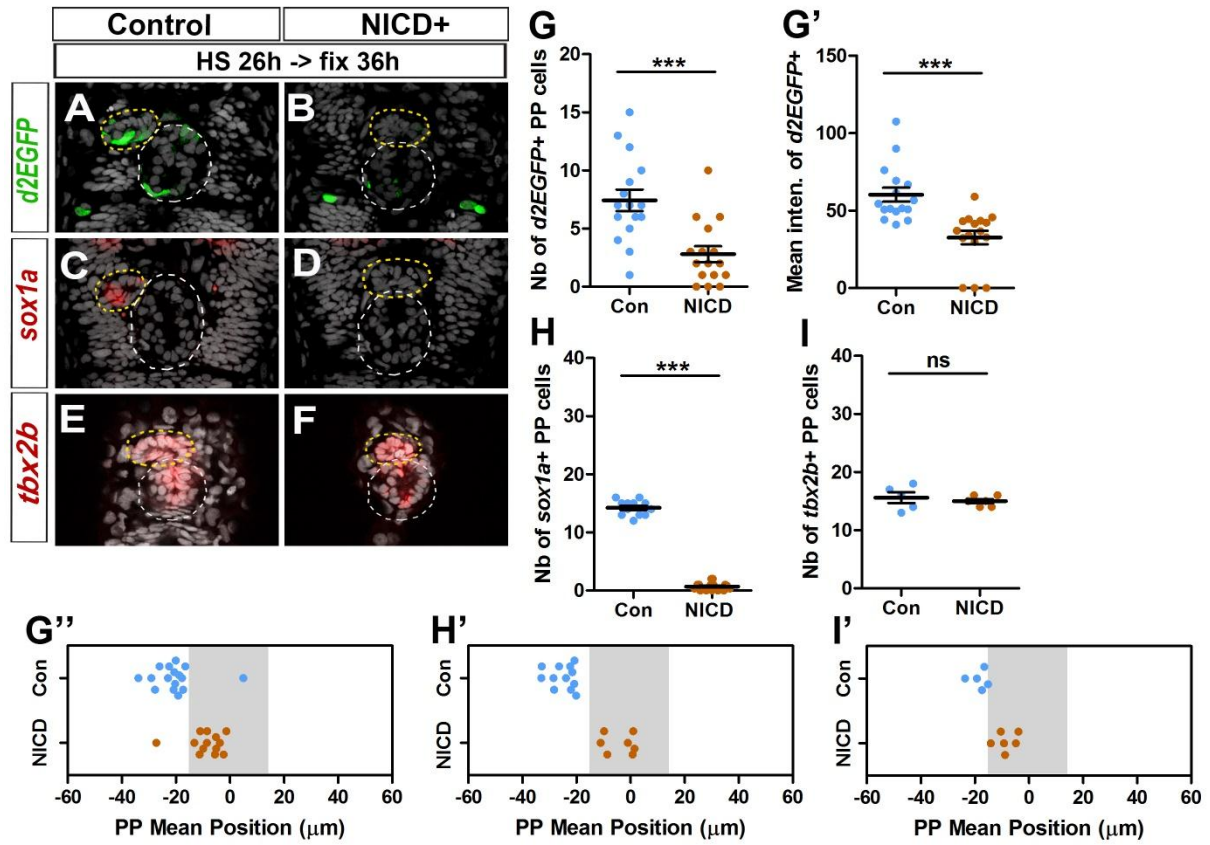


Figure 3. Ectopic Notch signalling triggers a decreased FGF activation and defects in migration and specification of parapineal cells.

(A-B) Confocal sections showing the expression of *Tg(dusp6:d2EGFP)* (green) at 36 hpf in control embryos (A; n=16) or in *Tg(hsp70l:Gal4), Tg(UAS:myc-notch1a-intra)* embryos following a heat-shock (HS) at 26 hpf (B; n=16). Both the number of cells expressing *Tg(dusp6:d2EGFP)* and fluorescence intensity are reduced in the parapineal of NICD expressing embryos.

(G-G'') Dot plots showing the number (G) the mean intensity fluorescence (G') and mean position (G'') of *dusp6:d2EGFP* expressing parapineal (PP) cells in controls (blue dots) or in NICD expressing embryos (red dots) at 36 hpf stage following heat shock at 26 hpf.

(C-F) Confocal sections showing the expression of *sox1a* (C-D) or *tbx2b* at 36 hpf (E-F) (red), merged with nuclei staining (grey), in control embryos (C; n=12; E; n=18) or in *Tg(hsp70l:Gal4); Tg(UAS:myc-notch1a-intra)* transgenic embryos (D; n=17; F; n=18) following heat-shock (HS) at 26 hpf.

(H-I') Dot plots showing the number (H, I) and the mean position (H', I') of *sox1a* expressing parapineal (PP) cells (H, H') or *tbx2b* expressing parapineal cells (I, I') at 36 hpf in controls (blue dots) or in embryos expressing NICD after heat shock at 26 hpf (red dots).

(J-O) Confocal section showing the expression of *gfi1ab* (J-K), *sox1a* (L-M) or *tbx2b* (N-O) (red) merged with nuclei staining (grey), at 48 hpf, in the epithalamia of control (J, n=27; L, n=17; N, n=17) or *Tg(hsp70l:Gal4);Tg(UAS:myc-notch1a-intra)* double transgenic embryos (K, n=25; M, n=17; O, n=16), following heat-shock (HS) at 26 hpf. The expression of *gfi1ab* and *sox1a* is lost while *tbx2b* is still detected in the parapineal of NICD expressing embryos.

(P-R') Dot plots showing the number (P-R) and mean position (P'-R') of *gfi1ab* (P, P'), *sox1a* (Q, Q') and *tbx2b* (R, R') expressing parapineal (PP) cells at 48 hpf in controls (blue dots) or in embryos expressing NICD after heat shock at 26 hpf (dark red dots).

In confocal sections, embryo view is dorsal, anterior is up; epiphysis (white circle) and parapineal gland (yellow circle); scale bar=10 μ m. Mean \pm SEM is indicated on dot plots; *** P-value<0.0001; * P-value<0.05 in Welsh t-test (G, G', H, I, P, Q, R) or Wilcoxon test (G'', H', I', P', Q', R').

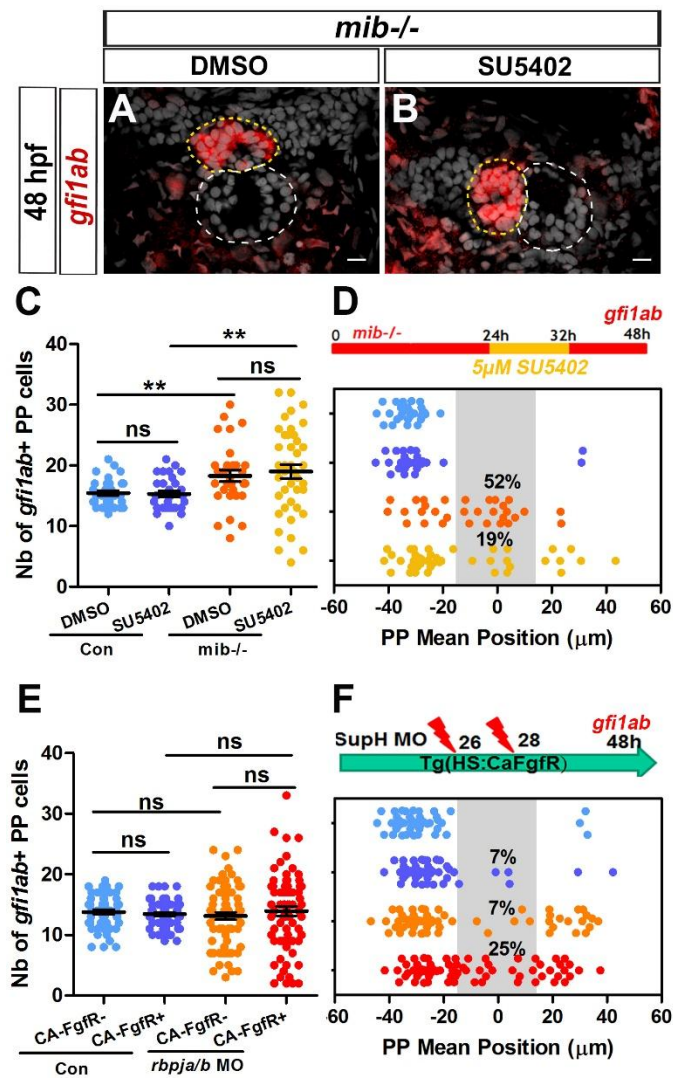


Figure 4. Decreasing or increasing FGF signalling rescues or enhances parapineal migration defect in Notch loss-of-function.

(A-B) Confocal sections showing the expression of *gfi1ab* (red) merged with a nuclei staining (grey) in representative 48 hpf *mib*^{-/-} mutant embryos treated from 24 to 32 hpf with DMSO (A) or 5 μM SU5402 (B); examples show a parapineal that failed to migrate (A) or one that migrated to the left (B). Embryo view is dorsal, anterior is up; epiphysis (white circle) and parapineal (yellow circle); scale bar=10 μm.

(C-D) Upper panel in D show a schematic of the SU5402 (or DMSO) treatment timeline (24-32 hpf) in control and *mib*^{-/-} mutant embryos. Dot plots showing the number (C) and the mean position (D) of *gfi1ab* expressing parapineal (PP) cells in control embryos treated with DMSO

(light blue dots; n=32) or with SU5402 (dark blue dots, n=31), and in *mib*^{-/-} mutant embryos treated with DMSO (orange dots, n=31) or with SU5402 (yellow dots, n=41); mean \pm SEM is shown in C. The number of *gfi1ab* positive cells is increased in *mib*^{-/-} mutants embryos, regardless of whether they were treated with SU5402 or DMSO: DMSO control versus DMSO *mib*^{-/-}, ** P-value=0.0041; SU5402 control versus SU5402 *mib*^{-/-}, ** P-value=0.0083, Welsh t-test . The parapineal fails to migrate in 52% of DMSO treated *mib*^{-/-} mutant embryos (PP mean position between -15 μ m to +15 μ m, shaded area), and this proportion decreases to 19% of SU5402 treated *mib*^{-/-} mutant embryos; * P-value=0.0139, in Chi-square test.

(E-F) Upper panel in F shows a schematic of heat shock timeline in *Tg(hsp70:ca-fgfr1)* embryos injected with *rbpj a/b* morpholinos (MO). Dot plots showing the number (E) and the mean position (F) of *gfi1ab* expressing parapineal (PP) cells in control embryos that carry (purple dots; E-F, n=55) or do not carry the *Tg(hsp70:ca-fgfr1)* transgene (light blue dots; E-F, n=54), and *rbpja/b* MO injected embryos that carry (dark red dots; E-F, n=73) or do not carry the *Tg(hsp70:ca-fgfr1)* transgene (orange dots; E-F, n=67). Mean \pm SEM, * P-value<0.05, ** P-value<0.01, Wilcoxon test.

Supplementary Figures :

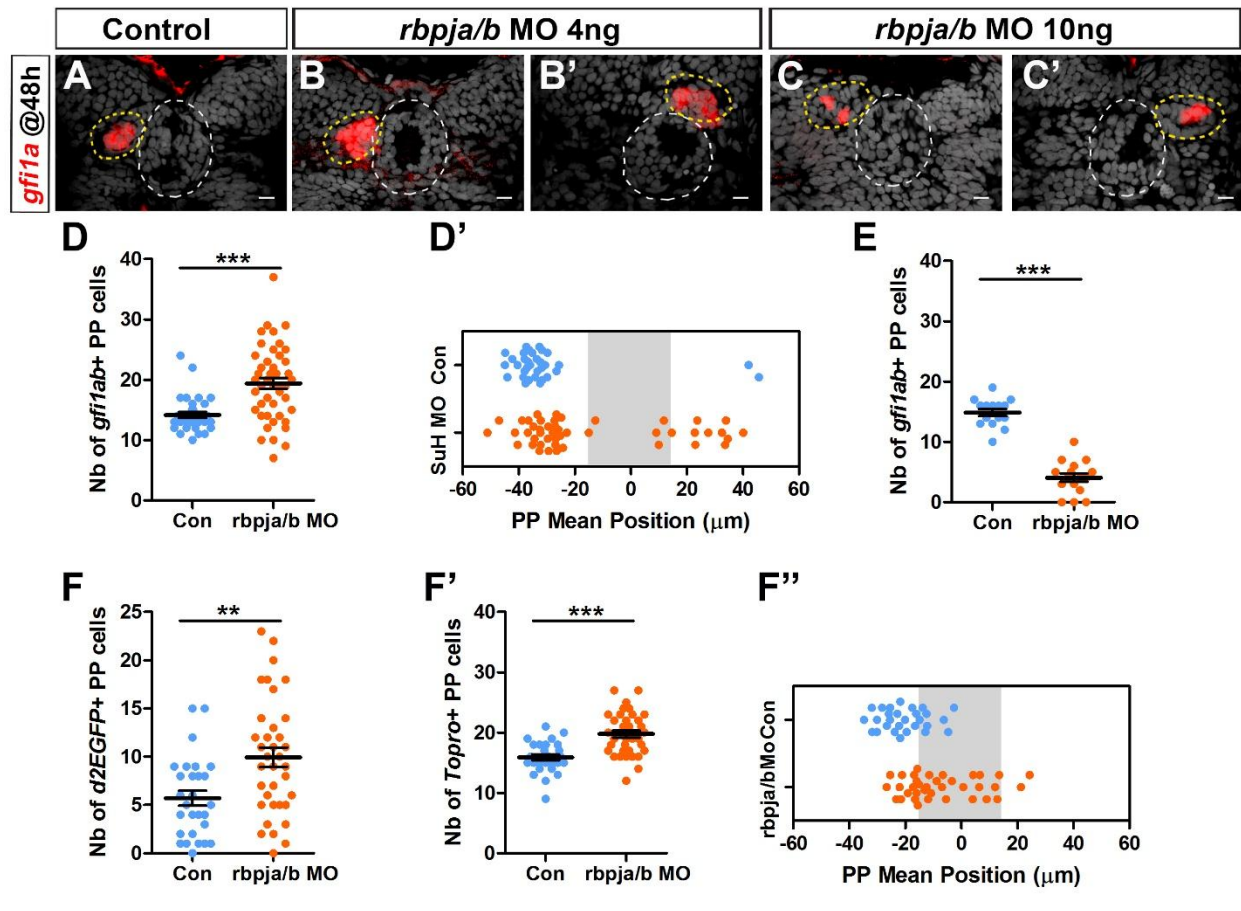


Figure S1. *rbpja/b* morphants phenocopy *mindbomb* mutants.

(A-C') Confocal sections showing the expression of *gfi1ab* (red) at 48 hpf in control embryos (A, n=33) and in 2 representative embryos injected with 4 ng of *rbpja/b* MO (B, B') or with 10 ng *rbpja/b* MO (C, C'); sections are merged with a nuclear staining (grey) to visualize the epiphysis (white circle) and parapineal (yellow circle). Embryo view is dorsal, anterior is up; scale bar=10 μ m.

(D-E) Dot plots showing the number (D, E) and the mean position (D', E') of *gfi1ab* expressing parapineal (PP) cells in non-injected controls (blue dots, D, D', n=33; E, n=15) or in *rbpja/b* MO injected embryos (orange dots, D, D', n=46; E, n=46) at 48 hpf with mean \pm SEM, *** p-value<0.0001; (Welsh t-test).

(F-F'') Dot plots showing the number of *dusp6:d2EGFP* (F) or Topro-3 (F') positive parapineal (PP) cells and the mean position of *dusp6:d2EGFP* (F'') expressing parapineal cells at 32 hpf in embryos injected with 4 ng *rbpja/b* MO (orange dots; n=36) or in controls (blue dots; n=28).

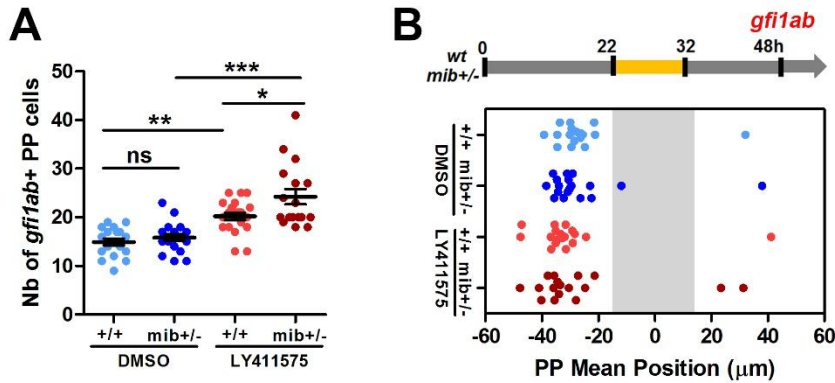


Figure S2. Effect of treatment with high dose of -secretase inhibitor from 22 to 32 hpf on parapineal specification and migration.

(A, B) Upper panel in B shows a schematic of LY411575 treatment timeline: wild-type (wt) or *mib*^{+/-} heterozygote embryos were treated from 22 to 32 hpf with 200 μM of LY411575. Dot plots show, for each embryo, the number (A) and the mean position (B) of *gfi1ab* expressing cells at 48 hpf in the parapineal (PP) of DMSO treated (+/+, dark blue dots; n=18), DMSO treated *mib*^{+/-} heterozygote (light blue dots; n=18), LY411575 treated (dark red dots; n=20) and LY411575 treated *mib*^{+/-} heterozygote embryos (light red dots, n=17). *** P-value<0.0001, ** P-value<0.01, * P-value<0.05, Wilcoxon test.

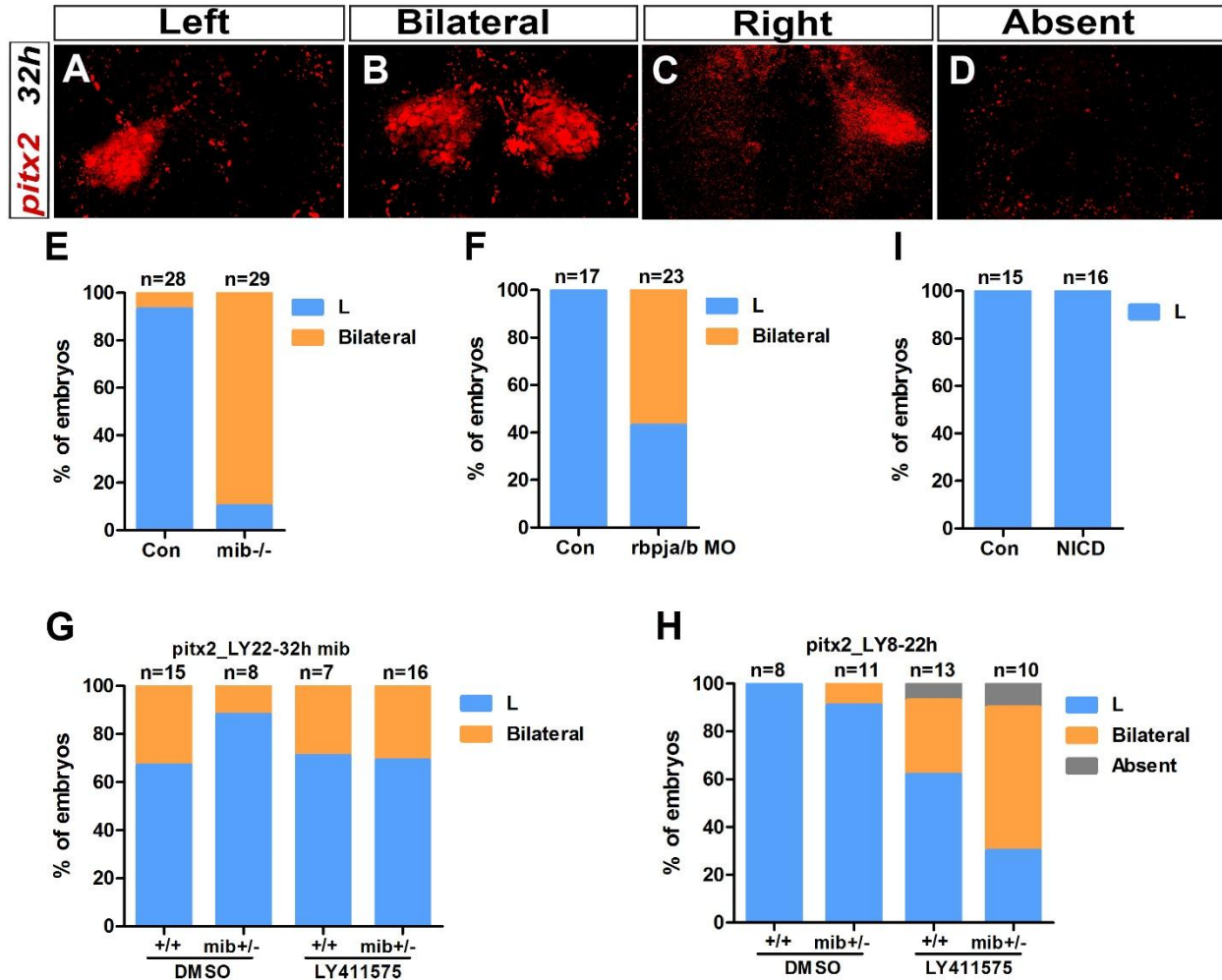


Figure S3. Early loss-of-function for Notch signalling results in bilateral Nodal pathway in the epithalamus.

(A-D) Confocal sections showing Left (A), Bilateral (B), Right (C) or Absent (D) *pitx2c* expression in the epithalamus at 32 hpf (red). Embryo view is dorsal, anterior is up; scale bar=10 μ m.

(E-H) Histogram showing the percentage of embryos with Left (L, blue), Bilateral (orange) and Absent (grey) *pitx2c* expression in *mib*^{-/-} mutant embryos (E), in *rbpja/b* morphant (MO) embryos (F), in embryos treated with 30 μ M of LY411575 from 22 to 32 hpf (G) or from 8 to 22 hpf (H), and in embryos expressing NICD (Notch Intra-cellular Domain) (I). Genetic background, treatment and embryos numbers are indicated below each bar; Con: control sibling embryos.

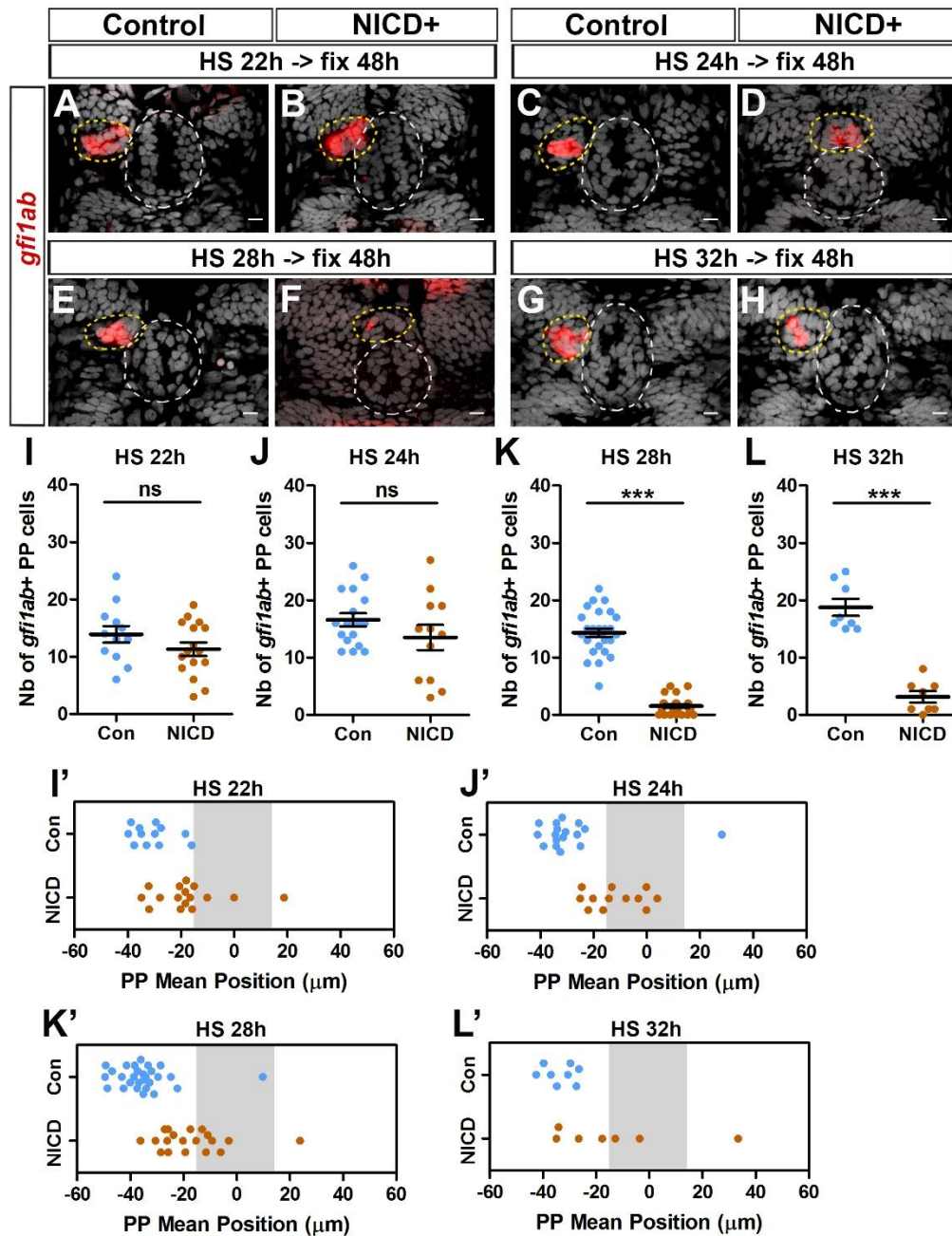


Figure S4. Effect of activation of the Notch pathway at 22, 24, 28 and 32 hpf on parapineal migration and on the expression of parapineal markers.

(A-H) Confocal maximum projections showing the expression of *gfi1ab* (red) at 48 hpf in control embryos (A, n=27; C, n=17; E, n=28; G, n=8) or in *Tg(hsp70l:Gal4);Tg(UAS:myc-Notch1a-intra)* double heterozygote embryos (B, n=16; D, n=12; F, n=26; H, n=8) following heat-shock (HS)

induction at 22 hpf (A, B), 24 hpf (C, D), 28 hpf (E, F), 32 hpf (G, H); images are merged with nuclear staining (grey) to visualize the epiphysis (white circle) and parapineal (yellow circle). Embryo view is dorsal, anterior is up; scale bar=10 μ m.

(I-L') Dot Plots showing the quantification of the number (I, J, K, L) and the mean position (I', J', K', L') of *gfi1ab* expressing parapineal (PP) cells in control (blue dots) or in *NICD+* embryos (dark red dots) at 48 hpf stage following heat-shock (HS) induction at 22 hpf (I, I'), 24 hpf (J, J'), 28 hpf (K, K'), 32 hpf (L, L'). Mean \pm SEM is indicated on dot plots; *** P-value<0.0001, t-test and Wilcoxon test.

II.3 Additional data on the role of Notch signaling in the specification and migration of parapineal cells.

Beside the data presented in Manuscript n°2, I have preliminary results addressing more specifically where the Notch pathway is active and where Notch activity is required (**part II.3. A, B and C**), how the Notch pathway could control the number and fate of parapineal cells (**Part II.3. D, E and F**) and whether the role of the Notch pathway in promoting PP migration and restricting FGF pathway involves its capacity to regulate the Nodal pathway at early stages (**Part II.3. G, H**). I also present preliminary data addressing the pattern of habenular asymmetry in LY411575 treated *mib*^{+/-} embryos (**Part II.3. I**).

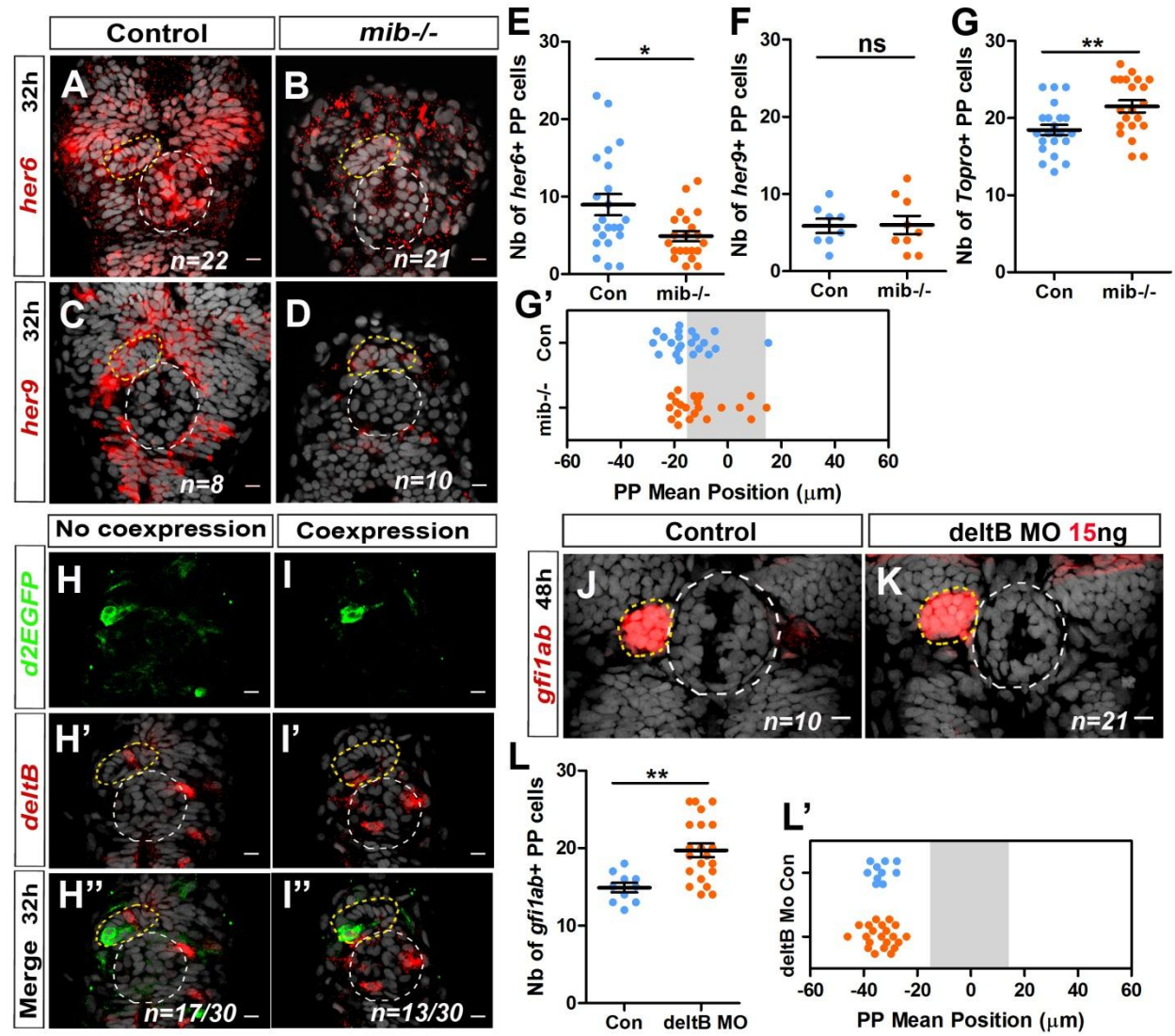


Fig 27. Notch component *her6*, *her9* and *deltaB* are mosaically expressed in the parapineal (PP) cells.

(A-D) Confocal sections showing the expression of *her6* (A, B) and *her9* (C, D) (red) at 32 hpf in control embryos (A, C) and in *mib*^{-/-} mutant embryos (B, D) merged with a cell nuclei staining (grey). (E-G') Dot plots showing the number of *her6* (E), *her9* (F), *topro* (G), and the mean position of *topro* expressing PP cells (G') in control (Blue marks) and *mib*^{-/-} mutant embryos (Orange marks). (H-I'') Confocal sections showing the expression of *Tg(dusp6:d2EGFP)* transgene (green, H-I) or *deltaB* (red, H'-I') and merge (H''-I'') in the epithalamia of 32 hpf embryos. (J-K) Confocal sections showing the expression of *gfi1ab* (red) at 48 hpf in control embryos (A) and in embryos injected with 15 ng of *DeltaB* MO (B). (L-L') Dot plots showing the number (L) and the mean position (L') of *gfi1ab* expressing PP cells in controls (Blue marks) or in *DeltaB* MO injected embryos (Orange marks) at 48 hpf stage. Embryo view is dorsal, anterior is up; epiphysis (white circle), parapineal gland (yellow circle); scale bar=10 μm. Mean±SEM are indicated as long and short bars. ** P-value<0.01; * P-value<0.05 in t test (Wilcoxon test).

II.3.A - Notch target genes, *her6* and *her9*, are expressed in parapineal cells.

To know whether the Notch pathway is active in the parapineal, we have analyzed the expression of known target genes of the pathway. Among various genes of the *her* family that were analysed, including are *her2* (Quillien et al., 2011), *her4* (Chapouton et al., 2011), *her5* (Ninkovic et al., 2005), *her6* (Chapouton et al., 2011), *her9* (Chapouton et al., 2011), *her12* (Nikolaou et al., 2009), *her15* (Webb et al., 2009), we found that two *her* genes, *her6* and *her9*, are mosaically expressed in parapineal cells in addition to other epithalamic regions (**Fig. 27A, 27C**). Although the expression of both *her6* and *her9* seemed to be globally reduced in other brain regions of *mib*^{-/-} mutants (**Fig. 27B, 27D**), the expression of *her6* (**Fig. 27B, 27E**) but not *her9* expression (**Fig. 27D, 27F**) was decreased in the parapineal. As previously described (Manuscript n°2), we also observed a global increase in the total number of PP cells of *mib*^{-/-} mutants embryos (**Fig. 27G**) and a delay in PP migration at 32 hpf (**Fig. 27G'**). These results suggest that *her6* might be a target of Notch pathway in parapineal cells.

II.3.B - Notch ligand, *deltaB*, is mosaically expressed in parapineal cells.

Among the genes encoding Notch ligands, *deltaB* shows the most robust expression in the parapineal at both 28 hpf (n=8/12) and 32 hpf (n=22/30) embryos. *deltaB* was detected in only a few parapineal cells that co-expressed *Tg(dusp6:d2EGFP)* FGF reporter transgene in about half of the cases (n=13/30) (**Fig. 27H-27I''**).

Injecting a morpholino against *deltaB* triggers a significant increase in the number of *gfi1ab*⁺ cells but doesn't affect parapineal migration (**Fig. 27J-27L'**). The fact that *deltaB* MO doesn't affect PP migration, as observed in both *mib*^{-/-} mutants and *Su(H)* morphants, could be due to compensation by *deltaA* gene. Indeed, we found that *deltaA* mRNA was also detected in the PP although more occasionally than *deltaB* mRNA at 32 hpf (n=3/10) (data not shown). However, this data confirms further that the defect in parapineal migration and the increased number of *gfi1ab*⁺ parapineal cells observed in *mib*^{-/-} mutants and *su(H)/rbpj* morphants can be uncoupled.

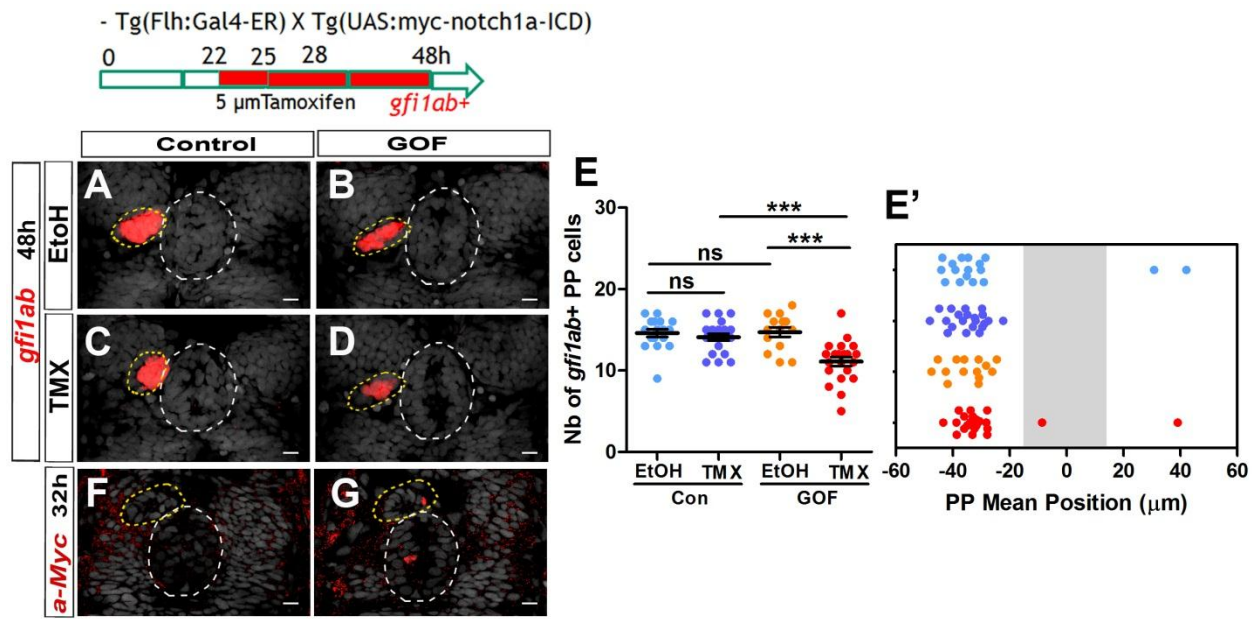


Fig 28. Notch signaling is required in the pineal complex to control the specification of parapineal cells.

(A-D) Schematic showing the timeline of the duration of 5 μM Tamoxifen treatment (22 h-48 h, changed fresh drug at 22 h, 25 h, 28 h) in control and Tg(*flh:gal4-ER*); Tg(*UAS:myc-NICD*) embryos (NICD: Notch Intracellular Domain). Confocal sections showing the expression of *gfi1ab* (red) at 48 hpf in Control embryos that treated with 5 μM Ethanol (A) or Tamoxifen (C), and NICD+ embryos that were treated with 5 μM Ethanol (B) or Tamoxifen (D). Embryos merged with a cell nuclei staining (Topro-3 in grey) that makes the epiphysis (white circle) and parapineal gland (yellow circle) visible. Embryo view is dorsal, Anterior is up. Objective x63, scale bar=10 μm.

(E, E') Dot plots showing the number (E) and the mean position (E') of *gfi1ab* expressing parapineal cells in control embryos treated with Ethanol (light blue marks, n=17) or Tamoxifen (dark blue marks, n=21), and in NICD+ embryos treated Ethanol (orange marks, n=14) or Tamoxifen (dark red marks, n=21) at 48 hpf stage. Mean±SEM, *** P-value<0.0001, non parametric Wilcoxon Test.

(F, G) Confocal sections showing myc-NICD after anti-myc immunostaining (red,) at 32 hpf in Control embryos (F; n=10) or NICD+ embryos (G; n=9).

II.3.C - Is Notch signaling required in parapineal cells?

In *Tg(hsp70:Gal4; UAS:myc-NICD)* double transgenic embryos, the Notch pathway is activated in all cells upon heat shock. To determine whether activation of the Notch pathway is specifically required in PP cells, we used another transgenic line, *Tg(Flh:Gal4-ER)*, in which the expression of a Tamoxifen (TMX) inducible version of Gal4 (Gal4-ER) (Akerberg et al., 2014) is driven in the pineal complex by the promoter of *flh* gene (Concha et al., 2003). In *Tg(flh:gal4-ER; UAS:myc-NICD)* double transgenic embryos, NICD is expressed mosaically in the pineal complex after induction with Tamoxifen (Fig. 28F-G). The number of *gfi1ab* positive PP cells is not affected in control embryos treated with Tamoxifen, or in ethanol treated *Tg(flh:gal4-ER; UAS: myc-NICD)* embryos. In contrast, the expression of *gfi1ab*⁺ PP cells is significantly decreased in Tamoxifen treated double transgenic embryos that express NICD in the pineal complex (11±3) compared to control embryos treated with Tamoxifen (14±2; p-value=0.0001) or *Tg(flh:gal4-ER; UAS:myc-NICD)* embryos treated with ethanol (15±2; p-value=0.0002) (Fig. 28A-28E). This result suggests that Notch is required within the pineal complex for the specification of parapineal cells. The limited penetrance is probably due to the fact that the expression of myc-NICD is very mosaic in the pineal complex (Fig. 28F-28G). Given this mosaicism, we did not expect to observe strong defect in parapineal migration (Fig. 28E'). Nevertheless, we observed PP migration defects in one Tamoxifen treated *Tg(flh:gal4-ER; UAS:myc-NICD)* embryo (n=1 out of 21) (Fig. 28E').

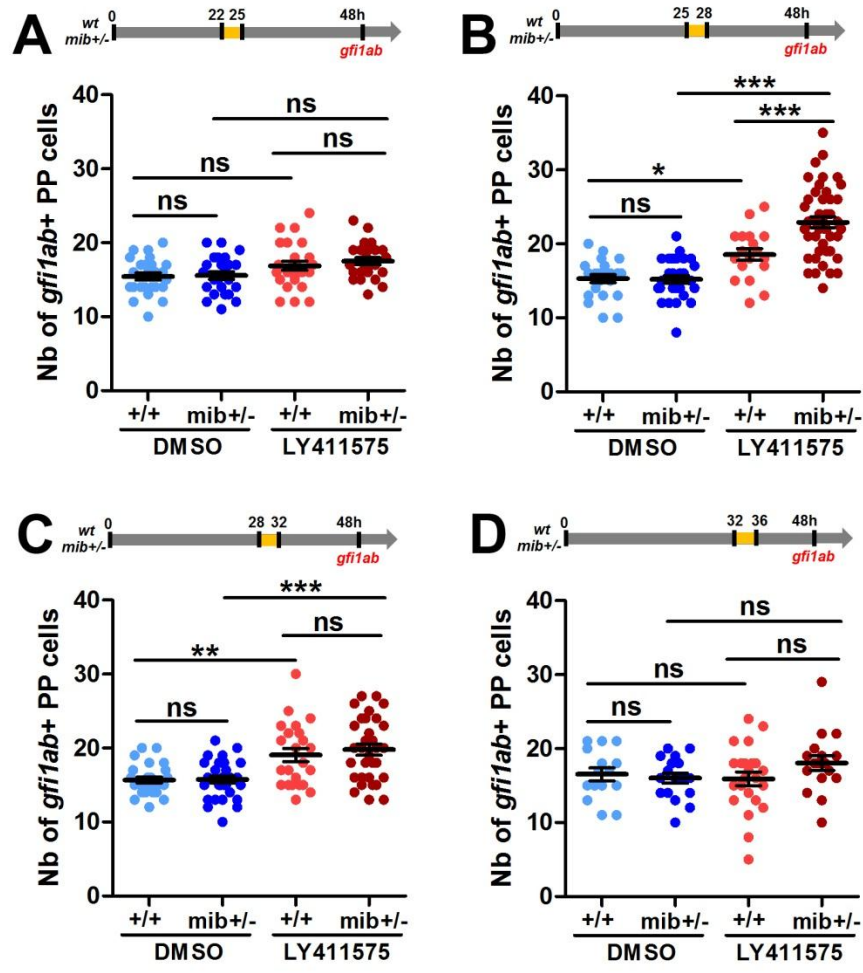


Fig 29. Notch pathway is mainly required between 25 and 32 hpf to control parapineal specific cells.

(A-D) Upper panel in A, B, C, D show a schematic of 30-50 μ M LY411575 treatment timeline (22-25h, 25-28h, 28-32h, 32-36h, respectively). Dot plots showing the number of *gfi1ab*⁺ expressing PP cells at 48 hpf in DMSO treated wt (+/+, light blue marks; A, n=25; B, n=23; C, n=25; D, n=15), DMSO treated *mib*^{+/-} (dark blue marks; A, n=24; B, n=29; C, n=29; D, n=17), LY411575 treated wt (+/+, light red mark; A, n=26; B, n=18; C, n=23; D, n=23) and LY411575 treated *mib*^{+/-} (dark red marks; A, n=24; B, n=44; C, n=32; D, n=17). mean \pm SEM is shown. *** P-value<0.001, ** P-value<0.01, * P-value<0.05, in non parametric Wilcoxon One-way ANOVA Test.

II.3.D - Notch signaling is required between 25 and 32 hpf to control the specification of parapineal cells.

As described before (Manuscript n°2), *mib*^{+/-} heterozygous embryos treated with LY411575 from 22 to 32 hpf show a strong increase in the number of *gfi1ab* expressing parapineal cells (28±5) compared to LY411575 treated wild-type controls (17±3; p-value=1.0e-10) or DMSO treated *mib*^{+/-} heterozygous (20±2; p-value=2.2e-10). To define more precisely the time window during which the Notch pathway is required to control the number of *gfi1ab*⁺ PP cells, we treated *mib*^{+/-} embryos with 30-50 μM LY411575 during 3 shorter time windows: 22- 25 hpf, 25-28 hpf, 28-32 hpf. We also treated embryos between 32 and 36 hpf to know whether the role of Notch could persist after 32 hpf. Our data suggest that the time window of Notch requirement falls around 28 hpf. In fact, we found that the number of *gfi1ab*⁺ PP cells increases in embryos treated with LY411575 in both the 25-28 hpf and 28-32 hpf time windows. In embryos treated with LY411575 between 32 and 36 hpf, we did not observe an increase in the number of *gfi1ab*⁺ PP cells (**Fig. 29A-29D**). This suggests that the Notch pathway is required after 25 hpf and before 32 hpf to control the number of *gfi1ab* PP cells.

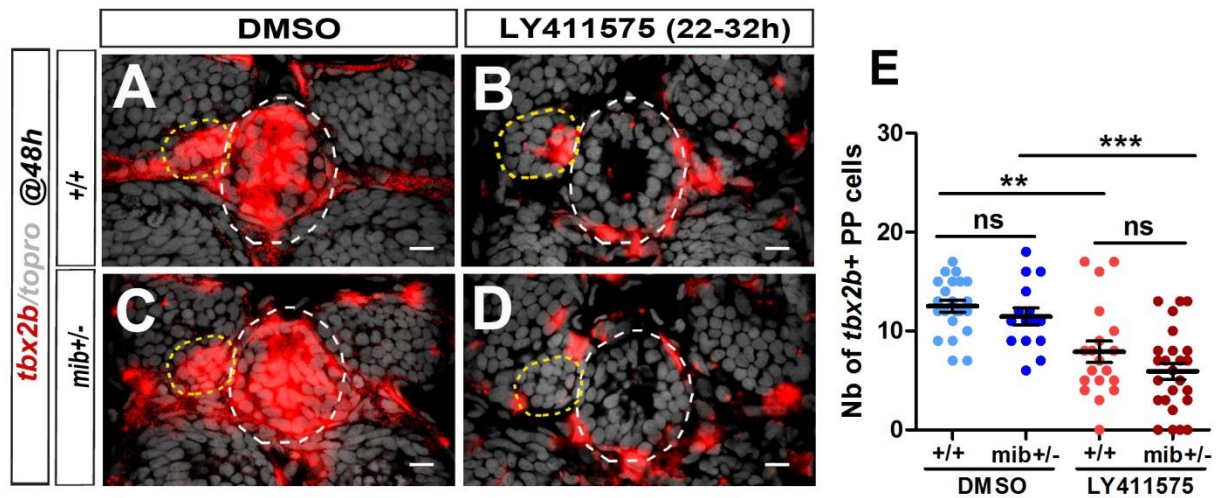


Fig 30. Expression of *tbx2b* PP marker is decreased in LY411575 treated embryos (22-32 hpf).

(A-D) Confocal sections showing the expression of *tbx2b* (red) at 48 hpf in 30 μ M DMSO *mib*^{+/+} (A), DMSO *mib*^{+/-} (C), LY411575 *mib*^{+/+} (B) and LY411575 *mib*^{+/-} (D) treated (22 h-32 h) embryos merged with a cell nuclei staining (Topro-3 in grey) that makes the epiphysis (white circle) and parapineal gland (yellow circle) visible. The expression of *tbx2b* is detected in the parapineal and epiphysis of embryos treated with DMSO, while it is reduced or lost in embryos treated LY411575 (22 h-32 h). Embryo view is dorsal, Anterior is up. Objective x63, scale bar=10 μ m.

(E) Dot plot showing the number of *tbx2b* expressing parapineal cells in DMSO treated wt *+/+* (light blue marks, n=22), DMSO treated *mib*^{+/-} (dark blue marks, n=15) or in LY411575 treated wt *+/+* (light red marks, n=19) and LY411575 treated *mib*^{+/-} (dark red marks, n=25) at 48 hpf. Mean \pm SEM, *** P-value<0.0001, ** P-value<0.01, in non parametric Wilcoxon Test.

II.3.E – Increased numbers of *gfi1ab*⁺/*sox1a*⁺ cells correlate with a decreased number of *tbx2b*⁺ cells in LY411575 treated embryos (22-32 hpf).

In a previous study, Snelson *et al* showed that *tbx2b* is expressed throughout the pineal complex before PP formation, and remains strongly expressed in the migrating PP while its expression decreases in the epiphysis (Snelson *et al.*, 2008b). Moreover, the authors showed that *tbx2b* is required for the correct specification of PP cells, as *tbx2b*^{-/-} mutants only display about 4 *gfi1ab*⁺ PP cells. As *tbx2b* is the earliest marker described for PP cells, we analyzed its expression in Notch LOF or GOF contexts to confirm the defect in the specification of PP cells. We first analyzed its expression in *mib*^{-/-}. In contrast to *gfi1ab* and *sox1a*, we saw no apparent increase in the number of *tbx2b*⁺ PP cells at 48 hpf in *mib*^{-/-} (17±5) compared with the wild-type embryos (17±3) (See Manuscript n°2, Figure 1). To confirm this phenotype, we then analysed *tbx2b* expression in embryos wild-types or heterozygous for *mindbomb* mutation (*mib*^{+/-}) treated with 30-50 µM LY411575 from 22 hpf to 32 hpf, where we also observed an increase in *gfi1ab*⁺ PP cells. The number of *tbx2b* expressing cells was not increased in this context. Rather, contrary to what we observed in *mib*^{-/-} mutants, the number of *tbx2b*⁺ cells were significant decreased in LY411575 treated embryos compared with DMSO treated, regardless of whether they were *mib*^{+/-} or *wild-type* (+/+) (for instance, 6±4 for LY411575 treated *mib*^{+/-} embryos compared to 11±3 for DMSO treated *mib*^{+/-} heterozygous; p-value<0.0001) (Fig. 30A-30E). It is not clear yet why *tbx2b* behaves differently in LY411575 treated embryos (22-32 hpf) and in *mib*^{-/-} mutants but this result correlates with the fact that the number of *gfi1ab*⁺ PP cells is overall more strongly increased in LY411575 treated *mib*^{+/-} (22-32 hpf) than in *mib*^{-/-} mutants. Therefore, the higher number of *gfi1ab*/*sox1a*⁺ PP cells observed in LY411575 treated *mib*^{+/-} (22-32 hpf) could reflect premature differentiation of *tbx2b* expressing PP cells (putative PP progenitor cells) into *gfi1ab*/*sox1a* positive cells (putative differentiated PP cells).

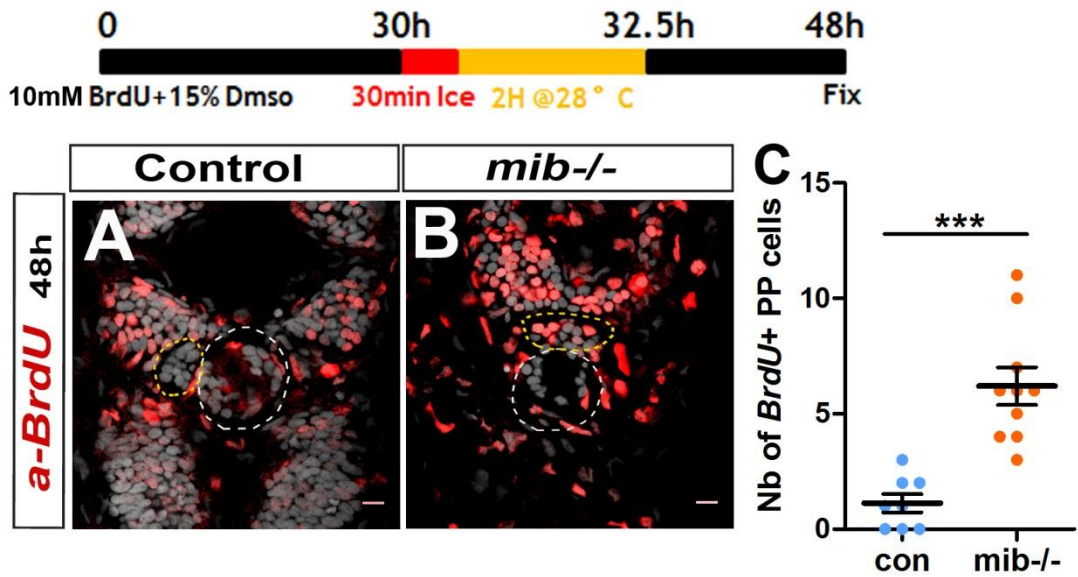


Fig 31. Proliferation of parapineal cells is increased in *mib*^{-/-} mutants.

(A-B) Upper panel showing schematic of the timeline of BrdU treatment. Confocal sections showing the BrdU labeling in control (A) and *mib*^{-/-} mutants (B) embryos at 48 hpf. Embryos merged with a cell nuclei staining (Topro-3 in grey) that makes the epiphysis (white circle) and parapineal gland (yellow circle) visible. Embryo view is dorsal, anterior is up. Objective x63, scale bar=10 μm.

(C) Dot plot showing the number of *BrdU* labeling PP cells in control (blue marks, n=8) and *mib*^{-/-} mutants (orange marks, n=10) embryos at 48 hpf. Mean±SEM, *** P-value<0.0001, non parametric Wilcoxon Test.

II.3.F - Proliferation of PP cells is increased in *mib*^{-/-} mutants.

In *mib*^{-/-} mutants, increased numbers of *gfi1ab/sox1a*⁺ cells do not correlate with a decrease of *tbx2b*⁺ cells. A higher number of *gfi1ab/sox1a*⁺ cells could nevertheless be a consequence of abnormal fate choice (and be associated with a decrease in another PP cell type than *tbx2b*⁺ cells for which we do not have markers) and/or could reflect either an increase in the proliferation of PP cells.

To know whether increased numbers of *gfi1ab/sox1a*⁺ cells are associated to changes in proliferation, I have analyzed and compared the proliferation rate of PP cells in controls embryos and *mib*^{-/-} mutants, using bromodeoxyuridine (BrdU) labeling; embryos were treated at 30 hpf for 30 minutes on ice followed by 2 hours at 28 °C. I found that the number of BrdU⁺ cells is increased in the PP of *mib*^{-/-} mutants (6±2) compared to controls (1±1) (**Fig. 31A-31C**). This result needs to be confirmed using a specific marker of PP cells to identify PP cells without ambiguity. Nonetheless, these preliminary data suggest that increased proliferation of PP cells might contribute to increased number of *gfi1ab/sox1a*⁺ cells in *mib*^{-/-} mutants. This suggests that, in addition to a possible role in PP fate choice, Notch signaling could limit the proliferation of PP cells to control PP size.

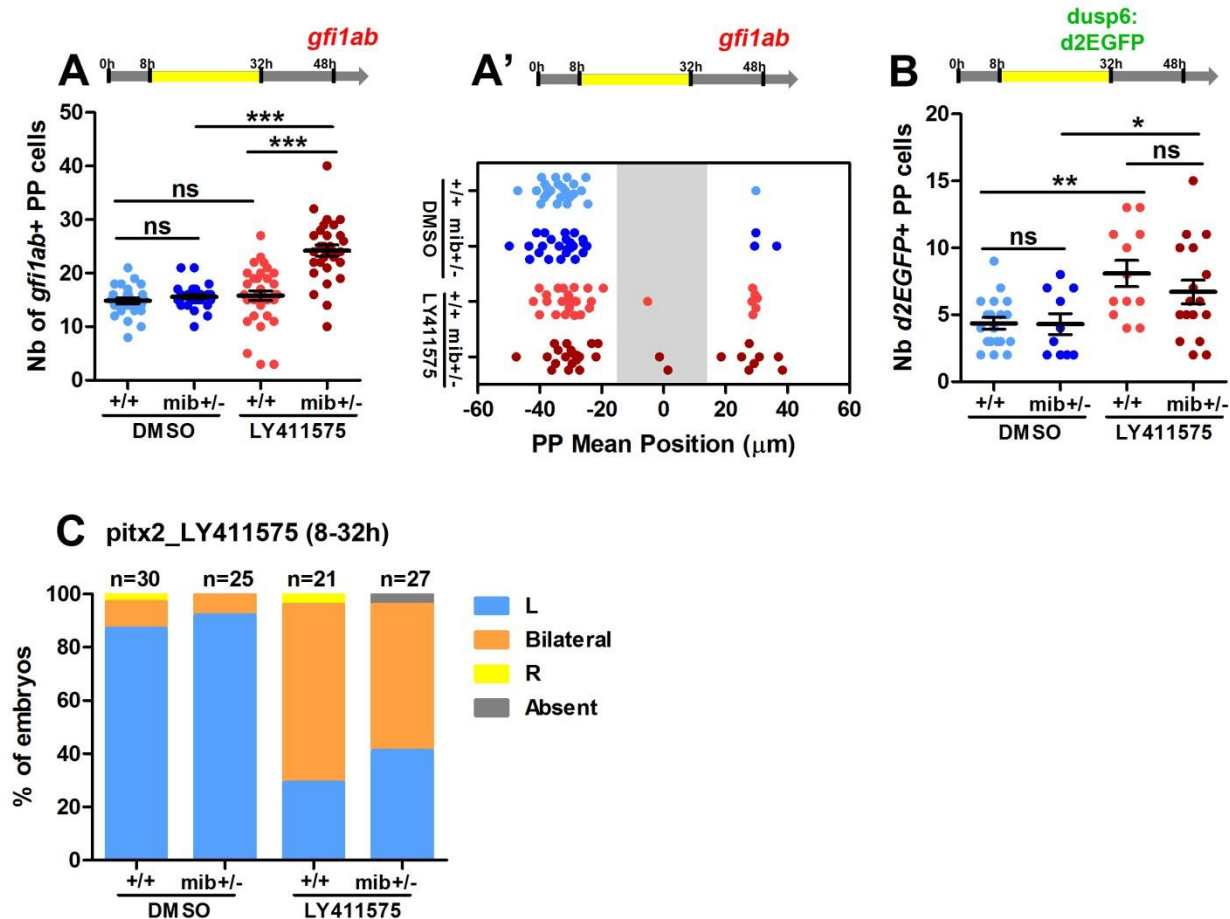


Fig 32. Parapineal migration defect in LY411575 treated embryos (8-32h) correlates with increased FGF signaling.

(A-B) Upper panel in A, A', B show a schematic of 30 μM LY411575 treatment timeline (8-32h). Dot plots showing the number (A) and the mean position (A') of *gfi1ab* expressing PP cells, and the number of *d2EGFP* expressing PP cells (B) in DMSO treated wt +/+ (light blue marks, A, A', n=28, B, n=19), DMSO treated *mib*+/- (dark blue marks, A, A', n=28, B, n=10) or in LY411575 treated wt embryos, +/+ (light red marks, A, A', n=34, B, n=12), or LY411575 treated *mib*+/- (dark red marks, A, A', n=30, B, n=17) at 48 hpf. Mean \pm SEM, *** P-value<0.0001, ** P-value<0.01, * P-value<0.05, non parametric Wilcoxon Test.

(C) Histogram showing the percentage of embryos with left (blue), bilateral (orange), right (yellow) and absent (grey) *pitx2* expression in embryos treated with 30 μM of LY411575 from 8 to 32 hpf. *pitx2* is expressed on the left epithalamus in DMSO treated wt (+/+) (n=26/30), DMSO treated *mib*+/- (n=23/25), LY411575 treated wt (+/+) (n=6/21), LY411575 treated *mib*+/- (n=11/27) embryos. *pitx2* is expressed bilaterally on the epithalamus in DMSO treated wt (n=3/30), DMSO treated *mib*+/- (n=2/25), LY411575 treated wt (n=14/21), LY411575 treated *mib*+/- (n=15/27) embryos. *pitx2* is expressed on the right epithalamus in DMSO treated wt (n=1/30), LY411575 treated wt (n=1/21) embryos. *pitx2* is expressed absent on epithalamus in LY411575 treated *mib*+/- (n=1/27) embryos.

II.3.G – Is the Notch pathway required in both early and late time windows to promote the restriction of FGF signaling and parapineal migration?

We have shown that in both *mib*^{-/-} mutants or in *rbpj/su(H)* morphants, parapineal (PP) migration is affected, PP laterality is partially randomized and the number of *gfi1ab* expressing parapineal cells is increased at 48 hpf. To address whether these 3 phenotypes could reflect different time windows of Notch requirement, we used the LY411575 pharmacological γ -secretase inhibitor to block Notch signaling pathway at different time windows.

In Manuscript n°2, we described that early LY411575 treatment (8-22 hpf) does not interfere with PP migration or with the number of *gfi1ab*⁺ cells but leads to a partial randomization of parapineal migration, as a consequence of the Nodal pathway being activated bilaterally in this context. On the other hand, LY411575 treatment from 22 to 32 hpf can synergize with *mib*^{+/-} heterozygote genetic background to promote a strong increase in the number of parapineal *gfi1ab* positive cell without affecting parapineal migration and laterality. This allows us to conclude that Notch signaling is required early (between 8 and 22 hpf) to promote correct left sided activation of Nodal pathway and PP laterality and later (25-32 hpf) to control the specification of PP cells. However, neither the early nor the late time windows interfered with PP migration *per se*, nor with focal activation of FGF pathway, the mean number of *Tg(dusp6:d2EGFP)* expressing cells being unchanged in these contexts.

We hypothesize that the Notch pathway could be required during both early and late windows to trigger restriction of FGF pathway and promote migration: the early requirement of Notch signaling for establishing left Nodal activity could synergize with a later requirement of Notch pathway within PP cells. To address this possibility, we superimposed early and late time windows of LY411575 treatment by treating controls or *mib*^{+/-} heterozygotes from 8 to 32 hpf. As expected, in *mib*^{+/-} heterozygous embryos treated with 30 μ M LY411575 from 8 to 32 hpf, we observed an increased number of *gfi1ab*⁺ PP cells (24 \pm 6) compared to DMSO treated *mib*^{+/-} (16 \pm 2; p-value<0.0001) or LY411575 treated controls (16 \pm 5; p-value<0.0001) (**Fig. 32A**). Similar to embryos treated with LY411575 from 8 to 22 hpf, we also observed a partial randomization of PP migration (**Fig. 32A'**), which correlates with bilateral *pitx2c* expression in half of the

embryos treated with LY411575 from 8 to 32 hpf (**Fig. 32C**) independently of whether they were heterozygotes for *mib* mutation.

In this context (LY411575 from 8 to 32 hpf), we also observed PP migration defects in both LY411575 treated control embryos (+/+; n=1/34) and LY411575 treated *mib*+/- embryos (n=2/30) (**Fig. 32A'**). Although these 'no migration' phenotypes were rare, they correlate with a significant increase in the number of *d2EGFP*+ cells in both LY411575 treated controls (8±3) or LY411575 treated *mib*+/- embryos (7±4) compared with DMSO treated controls (4±2; p-value=0.0033) or DMSO treated *mib*+/- embryos (4±2; p-value=0.0427) (**Fig. 32B**). This result suggests that Notch pathway could be required at both an early and late time window to promote FGF pathway restriction and PP migration.

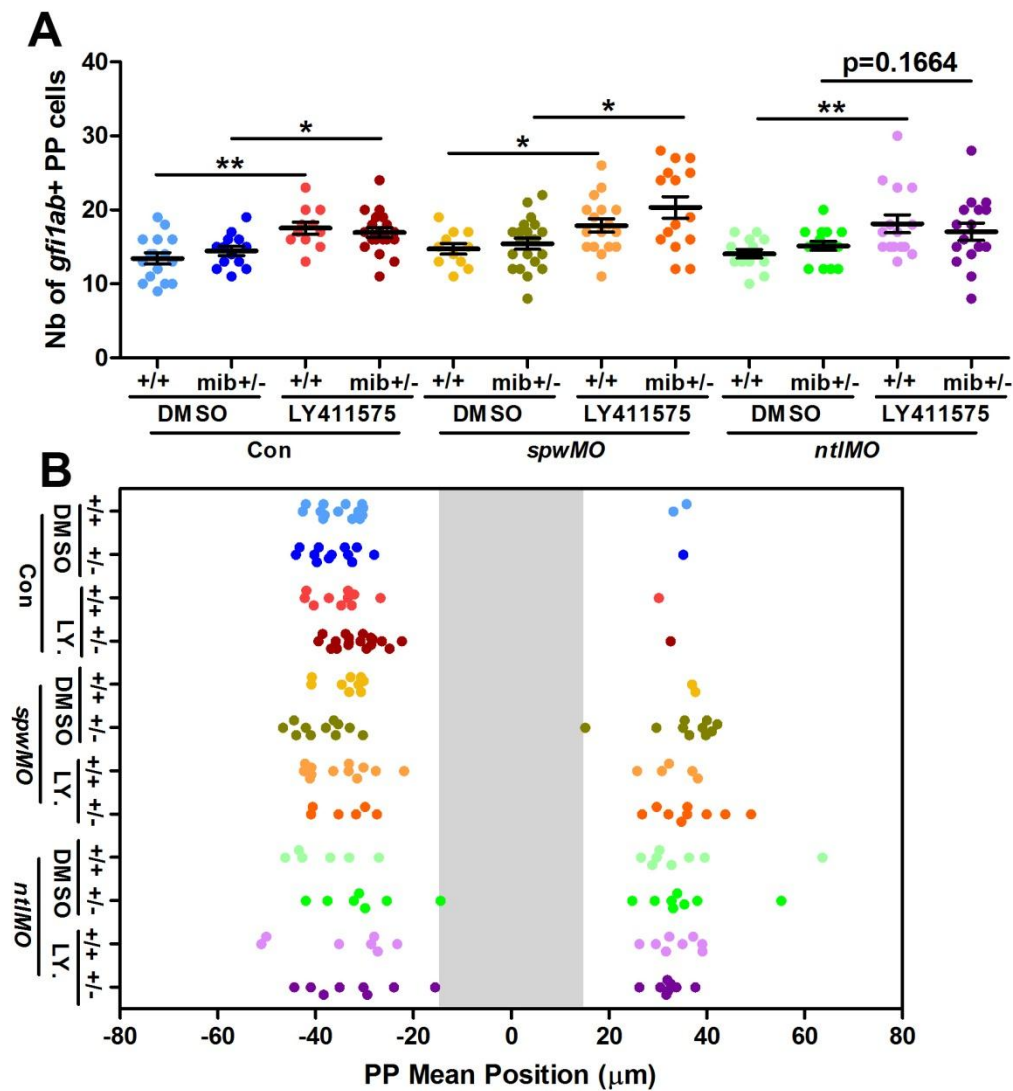


Fig 33. Parapineal migrates well and Parapineal size is increased in Nodal symmetry in loss of function for Notch (22-32h).

(A-B) Dot plot showing the number (A) and the mean position (B) of *gf1tab* expressing parapineal cells in: control embryos treated with DMSO (+/+) (light blue marks, n=16), DMSO treated *mib*+/- (dark blue marks, n=13), LY411575 treated controls (light red marks, n=11), LY411575 treated *mib*+/- (dark red marks, n=19); *spw* MO injected controls treated with DMSO (light orange marks, n=11), DMSO treated *mib*+/- (dark orange marks, n=21), LY411575 treated controls (light pink marks, n=17), LY411575 treated *mib*+/- (dark pink marks, n=15); *ntl* MO injected DMSO treated controls (light green marks, n=14), DMSO treated *mib*+/- (dark green marks, n=15), LY411575 treated controls (light purple marks, n=15), LY411575 treated *mib*+/- (dark purple marks, n=16) at 48 hpf stage. Grey area is in between -15 μ m and 15 μ m. Mean \pm SEM, ** P-value<0.01, *P-value<0.05, in non parametric Wilcoxon Test.

II.3.H – Does Notch synergize with Nodal signaling to restrict FGF pathway activation and promote PP migration?

Above and in Manuscript n°2, we describe that the Notch pathway is required early (8 to 22 hpf) to establish correct left Nodal activity in the epithalamus. On the other hand, we observed that Nodal signaling contributes to restrict FGF activity as the number of *Tg(dusp6:d2EGFP)* expressing cells significantly increased in absence of Nodal signaling (in *spaw* morphants, Manuscript n°1). Therefore, we hypothesize that left Nodal signaling could synergize with Notch to contribute to the restriction of the FGF pathway, and that blocking both pathways could be necessary to interfere with PP migration. This would explain why we need to block the Notch pathway both early (when it affects Nodal pathway) and late (within PP cells) to interfere with PP migration.

To address whether the early requirement of Notch pathway for PP migration could be a consequence of its effect on Nodal signalling, we injected *ntl* MO (Nodal Bilateral) and *spaw* MO (Nodal Absent) in controls (+/+) or *mib*+/- embryos and treated with 30 μ M LY411575 from 22 h to 32 h. No migration defects were detected in these contexts; as expected, PP laterality is randomized in both *ntl* MO and *spaw* MO injected embryos but in LY411575 treated contexts the PP migrates as well as in DMSO treated embryos (**Fig. 33B**). LY411575 treatment was able to increase the number of *gfi1ab*+ PP cells compared to DMSO treated embryos showing that the treatment had worked, although in this single experiment, the number of *gfi1ab* was usually increased in both controls (+/+) and *mib*+/- treated embryos (**Fig. 33A**). Our results might suggest that Nodal cannot synergize with Notch to promote PP migration. However, this experiment is preliminary and needs to be repeated. Moreover, it is possible that LY411575 treatment is not potent enough to interfere with PP migration and thus to assess the synergic contribution of Nodal pathway.

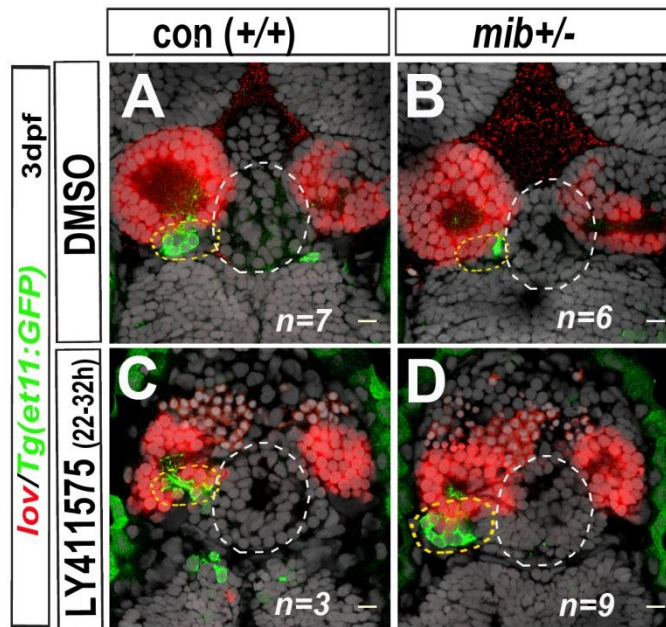


Fig 34. The expression of habenulae specific marker (*lov*) is symmetric in LY411575 treated embryos.

(A-D) Confocal sections showing the expression of *lov* (red) at 3 dpf in *Tg(et11:GFP)* control embryos treated with DMSO (A, *n*=7) or LY411575 (C, *n*=3) and in *mib*^{+/-} embryos treated with DMSO (B, *n*=6) and LY411575 (D, *n*=9); a cell nuclei staining (Topro-3 in grey) makes the epiphysis (white circle) and parapineal gland (yellow circle) visible. Embryo view is dorsal, anterior is up. Objective x63, scale bar=10 μ m.

II.3.1 - Is the role of Notch on habenular asymmetry a consequence of its function on parapineal size?

Habenular nuclei show LR asymmetries in the expression of various markers that are dependent on the PP (Gamse et al., 2003). In the group, it has been shown previously that *pitx2c* loss of function leads to the right habenula adopting aspects of left character; this phenotype was associated with an increase in the number of *gfi1ab+* PP cells in *pitx2c* morphants (Garric et al., 2014; see Introduction part II 2.4.2.2). Garric et al also show that reducing the number of PP cells to wild-type levels by laser ablation could restore habenular asymmetry, indicating that increased PP size (increased number of *gfi1ab+* cells) causes the “double left” habenular phenotype observed in *pitx2c* morphants (Garric et al., 2014).

In Aizawa et al, 2007, the authors show that *mib*^{-/-} mutants display a “double left” habenula phenotype and explain it as a consequence of a role of Notch signaling on the timing of habenular neurogenesis (Aizawa et al., 2007; see Introduction part II 2.4.1). However, in their study, the authors did not address a role for the PP. Given our data on PP defect in *mib*^{-/-} mutants, we hypothesized that the increased number of *gfi1ab+* cells observed in LOF for Notch could also be due to the increase in PP size.

To address this possibility, we analysed the expression of *leftover* (*lov*) marker for habenular asymmetry, at 3 dpf, in embryos treated with LY411575 between 22 and 32 hpf; as described previously (Manuscript n°2), LY411575 treated *mib*^{+/-} display an increase in the number of *gfi1ab+* cells but, in contrast to *mib*^{-/-} mutants, show no defect in PP migration nor any other obvious developmental phenotype. As shown before (Gamse et al., 2003), *lov* gene is expressed at high levels in many cells of the left dorsal habenula, and at reduced levels and in a smaller number of cells in the right habenula in wild type (Fig. 34A, 34B). As described previously in *mib*^{-/-} mutants (Aizawa et al., 2007), we observed that *lov* expression is symmetric and display a ‘double left’ phenotype in habenulae at 72 hpf in LY411575 treated *mib*^{+/-} (Fig. 34D); however, we also observed similar symmetric habenulae in few LY411575 treated control (+/+) embryos (n=3) in which PP size is not supposed to be increased (Fig. 34C). This preliminary data suggests that the defects in habenular asymmetry observed in LY411575 treated *mib*^{+/-} might

be due to a direct role of Notch in the habenulae rather than or in addition to a consequence of PP size. However, this experiment needs to be reproduced and embryo number increased; moreover, the number of PP cells needs to be counted in both LY411575 treated controls and *mib+/-* to definitively conclude if double left habenulae correlate or not with PP size in these contexts.

II.4 Materials and Methods

Most experimental procedures are described in the Materials and Methods sections of the Manuscripts. Below, I described the experimental procedures for additional data presented in Results section, Part II-3.

In situ hybridization

The probes used (References below) are produced using linearized plasmids carrying the corresponding cDNA as templates for *in vitro* transcription performed by Sp6, T7 or T3 polymerase in the presence of digoxigenin labeled rNTP (Promega). *In situ* hybridizations are carried out according to the protocol described in the Supporting Informations for Manuscript n°1.

Probes	References
<i>deltaB</i>	(Haddon et al., 1998)
<i>her6</i>	(Pasini et al., 2004)
<i>her9</i>	(Latimer et al., 2005)

Generation of *Tg(flh:gal4-ER)* transgenic line

To generate *Tg(flh:gal4-ER)* transgenic fish, Myriam Roussigné fused the sequence encoding an optimized version of Gal4 (KalTA4, (Distel et al., 2009)) to the ligand-binding domain of estrogen receptor (ER^{T2}, (Metzger et al., 1995)). This *kalTA4-ER^{T2}* sequence was cloned into the 5'UTR of the 5.5 kb *flh* DNA fragment between the TATA box and the initiation methionine (Concha et al., 2003). I-Sce1 restriction sites were inserted both side of the 5.5 kb *flh* fragment and fertilized eggs were injected with 5.5-*flh:kalTA4-ER^{T2}* plasmid DNA together with I-Sce1 restriction enzyme to facilitate transgene insertion (Thermes et al., 2002). Injected embryos were raised and screened for stable insertion of *Tg(flh:gal4-ER)* transgene by PCR.

Tamoxifen treatment

Embryos collected from *Tg(flh:gal4-ER)* outcrossed with heterozygous *Tg(UAS:myc-notch1a-intra)^{kca3}* fish were dechorionated and treated from 22 hpf to 48 hpf with 5 μ M Tamoxifen (4-OHT, Sigma); embryo medium was changed and fresh 5 μ M Tamoxifen was added at 25 hpf and 28 hpf (Sigma). Control embryos were treated simultaneously with an equal volume of Ethanol diluted in E3 medium. Embryos were incubated at 28°C and fixed at 32 hpf for immune-staining against Myc tag or fixed at 48 hpf for *in situ* against *gfi1ab* parapineal marker.

Immunohistochemical stainings

Immunohistochemical stainings against the Myc tag was performed in PBS containing 0.5% triton using the 9E10 antibody (1/15, Clinisciences) and Alexa 488 goat anti-mouse IgG (1/200, Molecular Probes). For nuclear staining, embryos were incubated in ToPro-3 (1/1000, Molecular Probes) as previously described (Roussigné et al., 2009).

Bromodeoxyuridine (BrdU) staining

mib^{ta52b} mutant embryos collected from incrossed heterozygous *mib^{ta52b}* fish were dechorionated and treated at 30 hpf with 10 mM BrdU diluted in E3 medium with 15% DMSO for 30 minutes on ice, followed by 2 hours at 28 °C. Control embryos were treated simultaneously with an equal volume of DMSO diluted in E3 medium. Embryos were fixed at 48 hpf for anti-BrdU immunostaining as described in (Roussigné et al., 2009).

LY411575 treatment in *ntl* and *spaw* Morpholino injection

Morpholino oligonucleotides (MO) targeting *no tail (ntl)* (Nasevicius and Ekker, 2000) or *southpaw (spw)* (Long et al., 2003) were solubilized at 1 mM in water and diluted to 0.5mM working concentration; about 8 ng for *ntl* MO and 12 ng for *spaw* MO were injected into *Tg(dusp6:d2EGFP)* outcrossed with heterozygous *mib^{ta52b}* eggs at one cell stage. Embryos were dechorionated and treated from 22 to 32 hpf with 30 μ M of LY411575 (MedChem; (Rothenaigner et al., 2011)); control embryos were treated simultaneously with an equal volume of DMSO diluted in E3 medium. Embryos were incubated in LY411575 at 28°C and fixed at 48 hpf for *in situ* against *gfi1ab* parapineal marker.

III. Expression and function of the Matrix Metalloprotease 2 (MMP2) gene in the zebrafish epithalamus

III.1 Context, Aim and Summary of manuscript n°3

From the literature, we hypothesized that the matrix metalloprotease 2 (MMP2) could be candidate involved in restricting the activation of FGF signaling within the PP. Indeed, MMP2 has been described to non-autonomously restrict the activation of FGF pathway in tracheal followers cells during air sac development in *Drosophila* (Wang et al., 2010). Interestingly, Myriam Roussigné had previously observed that MMP2 is mosaically expressed in the PP, in a pattern that partially overlaps with the expression of *Tg(dusp6:d2EGFP)* FGF pathway activity reporter transgene. Therefore, in parallel to my work on the Notch pathway, I analyzed the phenotype of mutants for the *mmp2* gene that had been generated in the Schulte-Merker Lab (Kok et al., 2015).

Using *gfi1ab* marker at 48 hpf, no significant defect in the specification and migration of PP cells was detected in *mmp2*^{-/-} mutant embryos. PP migration was also not affected in *mmp2*^{-/-} mutants upon global activation of FGF signaling. Due to technical issues, we have not yet analysed the expression of *Tg(dusp6:d2EGFP)* in *mmp2*^{-/-} mutant embryos; the presence of the *Tg(fli:GFP)^{y1}* transgene in the *mmp2*^{-/-} carriers we received interferes with the detection of *Tg(dusp6:d2EGFP)* transgene in the PP (Detry et al., 2012). The absence of defect in PP migration suggests that the pattern of FGF activation is not strongly affected in *mmp2*^{-/-} mutants. However, given the high variability of *Tg(dusp6:d2EGFP)* expression in wild-type embryos, we expect that the system is robust and that a moderate increase in the level of FGF activity in the PP could be tolerated. Therefore, it would be important to analyse *Tg(dusp6:d2EGFP)* expression in *mmp2*^{-/-} mutants to definitively conclude if MMP2 contributes to restrict FGF signaling within PP cells.

In *mmp2*^{-/-} mutants, we also found no defect in the expression of asymmetric habenular markers, suggesting that the PP not only migrates but also signals properly to habenular nuclei

in *mmp2*^{-/-} mutants. Therefore, we concluded that MMP2 function in the PP is either subtle or compensated by another protein in the PP (Manuscript n°3, Results Part III).

III.2 Manuscript n°3:

Expression and function of the Matrix Metalloprotease 2 gene in the zebrafish epithalamus

Lu Wei^{1,2,#}, Patrick Blader^{1,2*} and Myriam Roussigné^{1,2,#,*}.

¹ Université de Toulouse III, UPS, Centre de Biologie du Développement (CBD), 118 route de Narbonne, F-31062 Toulouse, France

³ CNRS, CBD UMR 5547, F-31062 Toulouse, France

* Authors for correspondence: myriam.roussigne@univ-tlse3.fr, patrick.blader@univ-tlse3.fr

These authors contributed equally to this work.

(In preparation)

Expression and function of the Matrix Metalloprotease 2 in the zebrafish epithalamus.

Lu Wei^{1,2,#}, Patrick Blader^{1,2*} and Myriam Roussigné^{1,2,#,*} .

¹ Université de Toulouse III, UPS, Centre de Biologie du Développement (CBD), 118 route de Narbonne, F-31062 Toulouse, France

² CNRS, CBD UMR 5547, F-31062 Toulouse, France

These authors contributed equally to this work.

* Authors for correspondence: myriam.roussigne@univ-tlse3.fr, patrick.blader@univ-tlse3.fr

Introduction

The epithalamus is a dorsal segment of the vertebrate brain whose development has been intensively studied in zebrafish embryos as a powerful model to understand how left right (LR) asymmetry is established in the brain (Concha et al., 2012; Roussigne et al., 2012). The epithalamus is composed of a pair of nuclei called the habenulae and of the pineal complex, both structures displaying obvious LR asymmetry. Habenular nuclei display left right asymmetries in the proportion of distinct neuronal subtypes that differ in their molecular signature and connectivity pattern. In between the left and right habenular nuclei is the pineal complex, which consists of the medially located epiphysis, a photoreceptive organ producing melatonin, and the parapineal nucleus (PP) that is found on the left side of the epiphysis in more than 95% of the embryos. Although it resides on left side, the PP derives from a group of cells that delaminates from the anterior part of the epiphysis, on the midline, and migrates collectively leftward to lie next to the left habenula. The function of the mature PP is not clear, but at embryonic stages it is known to have an instructive role on the development of LR differences between the habenulae as laser ablation of PP precursors results in both habenulae developing right character (Gamse et al., 2005). Thus, PP migration leftward is the first asymmetric anatomical event required for the subsequent elaboration of habenular asymmetry.

Previous studies showed that the left bias in PP migration depends on the activity of Cyclops, a secreted signal of the Nodal/TGF β family that is transiently expressed in the left epithalamus prior to PP formation and migration (Bisgrove et al., 2000; Concha et al., 2000; Liang et al., 2000); in embryos lacking Cyclops/Nodal, the PP migrates leftward or rightward with an equal probability. While the Nodal pathway biases the orientation of PP migration, the Fibroblast Growth Factor (FGF) signalling pathway is required for PP cells to migrate away from the midline (Regan et al., 2009); PP cells fail to migrate in homozygote mutants for *fgf8* and an ectopic source of Fgf8 provided locally by implanting an Fgf8 coated bead is able to rescue PP migration in these mutants. To better understand how Fgf8 promotes PP migration, we recently characterized the dynamics of FGF pathway activation in the epithalamus, by analysing the expression of an FGF reporter transgenic line, *Tg(dusp6:d2GFP)* in which a de-stabilised version of the Green Fluorescent Protein (d2GFP) is expressed under the control of the promoter for the *dusp6/mkp3* gene, an early and direct FGF target gene (Molina et al., 2007). We found that Fgf8 induces focal activation of the FGF pathway in leading cells and that this restricted activation is sufficient to promote migration of the whole parapineal structure.

However, as all parapineal cells seem competent to respond to Fgf8 (Roussigne et al, in press), it is still unclear how the activation of the pathway is restricted to few cells.

Recently, we have shown that the Notch pathway is required for PP migration through its capacity to restrict FGF pathway activation to a few PP cells, although the molecular mechanisms downstream Notch signalling are not known yet. Despite PP migration being affected in contexts of loss of function for the Notch pathway (in *midbomb* mutants or *su(H)* morphants), the PP manages to migrate in a majority of embryos and, although increased, FGF activity remains mosaic in the PP of most embryos. These data suggest that other factors or pathways compensate or act in parallel with the Notch pathway to restrict FGF pathway activation and promote PP migration.

During air sac development in *Drosophila*, Matrix Metalloprotease 2 (MMP2) has been proposed to restrict the activation of the FGF pathway in tracheal follower cells non-autonomously (Wang et al., 2010) such that the pathway remains active only in tip cells. MMPs are endopeptidases that contribute to extracellular matrix (ECM) remodelling through degradation of various ECM components such as several types of collagens, proteoglycans, Fibronectin or Laminin proteins (Bauvois, 2012). The function of MMP in ECM remodelling could facilitate tissue growth or cell migration through degradation of potential physical barriers in cell environment. However, MMP2 can also modulate the activity of various signalling pathways through proteolytical processing of other proteins located in the ECM such as pro-angiogenic factors, cell surface receptors and/or membrane-bound diffusible factors. The FGF signaling pathway is one such pathway that can be modulated by MMP proteins but the underlying mechanisms are not fully clear yet. MMP2 gelatinase is one of the MMPs that is over-expressed in a large variety of different cancers and whose expression and activity is associated with poor cancer prognosis (Bauvois, 2012). Both MMP2 protein and components of the Fgf signaling pathway have been implicated in tumour progression and metastasis in various cancer models (Deryugina and Quigley, 2010). Therefore, to gain insight into the function of MMP2 in cancers, it is crucial to better understand its role in modulating FGF signaling in a developmental context.

In the present study, we address whether MMP2 could have a function in Fgf8 dependant collective cell migration of parapineal cells. We first characterised *mmp2* expression in the zebrafish brain at different stages of development and show that *mmp2* gene is expressed in a salt and pepper pattern in both the epiphysis and the PP from 20 hpf to 36 hours

post-fertilisation (hpf). This mosaic expression of *mmp2* partially overlaps with the expression of the *Tg(dusp6:d2GFP)* FGF reporter transgene. The expression of *mmp2* appears to be specific of the pineal complex at this stage as we could not detect any strong *mmp2* expression in other brain regions around the epithalamus. Despite this very specific pattern, no defects in the specification of PP cells or in their migration were detected in embryos mutants for *mmp2* gene. Likewise, parapineal migration was not affected in *mmp2*^{-/-} mutants where the FGF pathway was activated globally with a constitutively active version of FgfR1 (CA-FgfR1). We also found no defect in the expression pattern of different asymmetric habenular markers suggesting that the PP is still able to communicate with developing habenulae and instruct habenular asymmetry in *mmp2*^{-/-} mutants. It remains to be addressed whether MMP2 function in the parapineal is subtle or possibly compensated by other MMP proteins or by other factors.

Materials and Methods:

Fish lines

Embryos were raised and staged according to standard protocols (Westerfield, 2000). We used previously described transgenic lines *Tg(hsp70:ca-FgfR1;cryaa:DsRed)^{pd3}* (Marques et al., 2008) and *Tg(dusp6:d2GFP)^{pt6}* (Molina et al., 2007). Embryos heterozygotes for *Tg(hsp70:ca-FgfR1;cryaa:DsRed)^{pd3}* were identified for the presence of the DsRed transgene expressed in the lens from 48 hpf. A mutant line for *mmp2* gene (*mmp2^{hu10535}*) was described in (Kok et al., 2015). Embryos homozygous for *mmp2^{hu10535}* mutations were obtained by crossing heterozygous carriers with a homozygous mutant female and identified by PCR genotyping using primers CCGCTGCCGCTCCTATTTTC and GTCAGTCTTACGCCGTTCT followed by PvuII enzymatic digestion.

Ethics statement

Fish were handled in a facility certified by the 'Ministère de l'agriculture' (approval number A3155510) in accordance with the guidelines from the European directive on the protection of animals (2010/63/UE). The project has received an agreement number APAFIS#3653-2016011512005922 on the 01/12/2016 and MR has an authorisation to experiment on vertebrates models (N° 311255556) from the 'Direction Départementale de la

Protection des Populations de la Haute-Garonne'. We used Tricaine Methanesulfonate (MS222) solutions for anaesthesia (0,16mg/ml) and performed euthanasia in cold water and MS222 (0,30 mg/ml for). All efforts were made to minimize the number of animals used and their suffering.

Ectopic expression of CA-FgfR1

Ectopic expression of CA-FgfR1 was induced in embryos obtained from outcrossing *mmp2*^{+/-}; *Tg(hsp70:ca-FgfR1)*^{+/-} heterozygote fish with *mmp2*^{-/-} homozygote mutants by performing an heat shock before parapineal migration at 26 hpf (39°C, 45 minutes) and, in one of the two experiments, a second heat shock at 29 hpf (39°C, 15 minutes).

Injection of *mmp2* and *p53* MO

Morpholino oligonucleotides (MO) targeting *mmp2* (Detry et al., 2012) were diluted to 0.5 ng/nl working concentration. About 1 ng of *mmp2* MO or control MO (5'-CCTCTTACCTCAGTTACAATTTATA-3') were injected at the one cell stage, alone or together with a second morpholino targeting p53 pro-apoptotic gene (Robu et al., 2007), and imaged on a bright field microscope (NikonAZ100).

In situ hybridization and immunostaining

Embryos were fixed overnight at 4°C in 4% paraformaldehyde/1xPBS, after which they were dehydrated through an ethanol series and stored at -20°C until use. In situ hybridizations were performed as previously described (Roussigne et al, in press) Antisense DIG labelled probes for *gfi1ab* (Dufourcq et al., 2004), *lov* (Gamse et al., 2003, 2005), and *dex* (Gamse et al., 2003, 2005), were generated using standard procedures. In situ hybridizations were revealed using Fast Red (from Roche or Sigma) as substrate. Immunohistochemical stainings were performed in PBS containing 0,5% triton using anti-GFP (1/1000, Torrey Pines Biolabs) and Alexa 488 conjugated goat anti-rabbit IgG (1/1000, Molecular Probes). For nuclear staining, embryos were incubated in Topro-3 (1/1000, Molecular Probes) as previously described (Kok et al., 2015).

Image Acquisition

Confocal images of fixed embryos were acquired on an upright Leica SP8 microscope using the resonant fast mode and with oil objective x63 (aperture 1.4) or x20 (aperture 1.4). Confocal stacks were analysed using ImageJ software. Images were manipulated using Photoshop (Adobe) software. Scale bars represent 10µm in the objective x63 and 25µm in the 20x.

Statistical analysis

For Figure 3, we used R Studio software to compare the mean position and the number of parapineal cells between four datasets: *mmp2*^{-/-} mutants or *mmp2*^{+/-} heterozygotes in a *Tg(hsp70:ca-fgfr1)* or wildtype background. When datasets were normal and of equal variances (datasets on absolute values for parapineal mean position), we compared them with a pairwise T test. When variances were not homogenous (datasets on the number of parapineal cells), we compared them using the pairwise Wilcoxon rank sum non-parametric test. Unless otherwise mentioned in Figures legends, data are representative of at least two independent experiments. Numbers of parapineal cells are reported as mean (± standard deviation).

Results:

MMP2 is mosaically expressed in the parapineal independently of Fgf8.

Using a *Tg(flh:GFP)* transgene to label the pineal complex (Concha et al., 2000), we found that *mmp2* is robustly expressed in the pineal complex from 20 hpf (**Fig 1A-A'**”; n=14). Expression was always detected in the pineal complex and, in half of the embryos, it was found enriched in the anterior region of the pineal complex, which corresponds to the presumptive parapineal (n=7/14). Weak *mmp2* expression was also detected in the skin and in eye mesenchyme (**Fig 1A**); no expression was detected in other brain regions. *mmp2* expression persists in the pineal complex but becomes restricted to fewer cells from 24 hpf (**Fig 1B-B'**”, n=10). We noticed that *mmp2* expression is mosaic and highly variable between embryos. For instance, at 24 hpf *mmp2* is expressed in between 2 and 12 cells in the pineal complex. At this stage, *mmp2* expression was usually found in the presumptive parapineal (n=7/10). From 28 hpf, *mmp2* is still detected in some epiphyseal cells but become particularly enriched in the parapineal rosette, which is forming anterior to the epiphysis (**Fig 1C-C'**”, n=11).

We have shown previously that a transgenic reporter of FGF pathway activity, *Tg(dusp6:d2GFP)* transgene, is expressed focally in the PP. To know whether *mmp2* expression correlates with the mosaic pattern of FGF pathway activity, we analyzed the expression pattern of *mmp2* in *Tg(dusp6:d2GFP)* embryos at different stage of development. We found that *mmp2* expression in parapineal partially overlaps with *Tg(dusp6:d2GFP)* expressing cells at 28 hpf (**Fig 1D-D''**, n=19). At 32 hpf, *mmp2* is still expressed in the parapineal although usually in fewer cells than at 28 hpf (**Fig 1E-E''**, n=17). Mosaic expression of *mmp2* in the PP is still detected at 36 hpf but no longer at 48 hpf (Data not shown). In contrast to the expression of *Tg(dusp6:d2GFP)* transgene, *mmp2* expression is still detected in the PP of *fgf8*^{-/-} mutants at both 27 hpf and 30 hpf (**Fig S1**). Altogether, our data show that *mmp2* is expressed mosaically in the pineal complex and enriched in the PP when it forms (between 24 and 28 hpf) and initiates migration (from 28 to 32 hpf), and that *mmp2* expression in the PP is not dependant on Fgf8.

***mmp2*^{-/-} morphants display global developmental defects that are partially rescued by p53 MO**

The mosaic expression of *mmp2* in the PP is consistent with a role for this gene in the specification or migration of PP cells, possibly through a modulation of FGF signaling in the PP. To address these possibility, we used morpholinos to characterise the function of MMP2 in the PP relative to the expression of *Tg(dusp6:d2GFP)* transgene at 32 hpf and *gfi1ab* at 48 hpf (Detry et al., 2012); this *mmp2* MO had been previously described to affect lymphatic vessels formation.

In *mmp2* morpholino injected embryos, we noticed a slight increase in the number of *Tg(dusp6:d2GFP)* expressing PP cells at 32 hpf compared to embryos injected with a control MO (**Fig S2 A' vs C'**) and a delay in migration at 32h? . At 48 hpf, PP migration appeared either normal or delayed in *mmp2* morphants (**Fig S2, A'' vs C''**); using *leftover/lov* as a marker, we also observed a severe decrease in the size of habenular nuclei at 72 hpf (**Fig S2, A''' vs C'''**). However, as *mmp2* morphants also display global developmental delay compared to control embryos (**Fig S2 A vs C**) and as all observed phenotypes seemed partially rescued in *mmp2* morphants co-injected with *p53* MO (**Fig S2, D-D''' vs C-C'''**), we did not quantify more precisely the number and position of *Tg(dusp6:d2GFP)*⁺ and *gfi1ab*⁺ parapineal cells in morphant embryos.

Specification and migration of parapineal cells are not significantly affected in *mmp2*^{-/-} mutant.

In light of the global developmental defect observed in *mmp2* morphants, we chose to characterize the phenotype in the epithalamus of embryos carrying a genetic mutation for gene. This *mmp2*^{hu10535} mutant line displays an 8 nucleotides deletion in exon1 that leads to a frame shift and stop codon after amino acid 5, and is predicted to correspond to a complete loss of function for *mmp2* gene (Kok et al., 2015). Given that *mmp2*^{-/-} mutants are viable and fertile as adults, we analysed the phenotype of *mmp2*^{-/-} mutant embryos derived from homozygote *mmp2*^{-/-} mutant females to exclude rescue by maternally provided MMP2.

To address whether MMP2 is involved in the specification and/or migration of the PP, we analysed the expression of the PP markers *sox1a* and *gfi1ab* in *mmp2*^{-/-} embryos. At 32 hpf, using nuclei staining or *sox1a* marker, we could detect the PP rosette that has already initiated its migration to the left in *mmp2*^{-/-} homozygote mutants as in heterozygotes controls (**Fig 2A-B**). Although PP migration appeared delayed in some *mmp2*^{-/-} mutants (mean position of *sox1a* expressing parapineal cells closer to the midline in n=5/28; **Fig 2D**), this difference was not significant. The number of *sox1a*⁺ PP cells was also not affected in *mmp2*^{-/-} mutants at 32 hpf (**Fig 2C**). Using *gfi1ab*, we confirmed that the number and position of PP cells did not differ between heterozygotes and *mmp2*^{-/-} homozygote mutants at 48 hpf (**Fig 2E-F; Fig 2I-J; Table S1 and Table S2**). These data indicate that the specification and migration of parapineal cells are not affected in *mmp2*^{-/-} mutants.

We have shown previously that ectopic expression of a constitutively activated FGF receptor (CA-FgfR1) results in a global increase in the number and intensity of *Tg(dusp6:d2GFP)* positive cells although it does not abrogate its mosaic pattern, which usually remains at the front of the migrating PP. This observation correlates with the fact that ectopic expression of CA-FgfR1 only modestly interferes with PP migration (Roussigne et al, in press). If MMP2 protein contributes to restrict Fgf pathway activation in the PP, we might expect that *mmp2*^{-/-} mutants would display a more obvious phenotype in a context of overactivation of the FGF pathway. To test this possibility, we quantified the position of PP cells in *mmp2*^{-/-} mutants that express CA-FgfR1. As previously described (Roussigne et al, in press), ectopic expression of CA-FgfR1

results in a modest delay of PP migration (**Fig 2E vs 2G; Fig 2I-J; Table S1**). However, even in this context of CA-FgfR1 ectopic expression, we did not observe any obvious defect in PP migration associated with *mmp2*^{-/-} loss of function (**Fig 2F vs 2H; Fig 2I-J; Table S1**). The number of *gfi1ab*⁺ PP cells was also not affected in this context (**Fig 2K; Table S2**). We conclude that the specification and migration of PP cells are not affected in *mmp2*^{-/-} mutants, even in the context of global activation of FGF pathway.

Habenular asymmetry is not affected in *mmp2*^{-/-} mutant.

The PP is required for the correct development of LR differences between the habenular nuclei as laser ablation of PP precursors results in both habenulae adopting right character (Gamse et al., 2003). Although the PP migrates well and expresses *sox1a* and *gfi1ab* in *mmp2*^{-/-} mutants, it is possibly that it might not properly signal to habenulae.

To address whether the PP is functional in *mmp2* mutants, we analysed habenular asymmetry using *leftover/lov* (Gamse et al., 2003). Asymmetric expression of *lov* did not differ between *mmp2*^{-/-} mutants and *mmp2*^{+/-} heterozygotes (**Fig 4A-B**). Likewise, habenular size and asymmetry was also not affected neither in *mmp2*^{-/-} mutants in context of CA-FgfR1 ectopic expression (**Fig 4C-D**).

Discussion:

In the present study, we address the function of MMP2 in an Fgf dependant model of collective migration: the migration of parapineal (PP). We show that *mmp2* is mosaically expressed in PP cells as early as the PP rosette is detected and initiates migration. *mmp2* expression in the parapineal partially overlaps with expression of a *Tg(dusp6:d2GFP)* FGF pathway activity reporter transgene. Given this specific expression pattern and having in mind the previously described role of MMP2 in restricting FGF pathway in a *Drosophila* model of cell migration (Wang et al., 2010), we assessed whether MMP2 could contribute to PP migration by restricting the activation of FGF pathway to few PP cells. The injection of *mmp2* morpholino triggers morphological defects and developmental delay that are consistent with observations made in previous studies (Janssens et al., 2013; Zhang et al., 2003). Moreover, we found that

all developmental defects and epithalamic phenotypes associated with *mmp2* MO are partially rescued by co-injecting p53 MO. Given these global defects, we turned toward analysing the phenotype of *mmp2* genetic mutants. In this context, we did not observe defects in either the specification or the migration of PP cells. PP migration was also not affected in the context of global activation of the FGF pathway. Finally, habenular asymmetry was normal in these mutants suggesting that the parapineal is able to signal normally to habenular nuclei. Our results suggest that MMP2 protein does not have a crucial role in the PP or that its function is compensated by other factors.

MMP are endopeptidases that degrade many types of collagens, as well as other proteins located in the ECM such as pro-angiogenic factors, chemokines or receptors (Bauvois, 2012). MMP proteases have emerged as key proteins involved in angiogenesis, tumor growth and metastasis but their functions are not fully clear (Deryugina and Quigley, 2010; Kessenbrock et al., 2010). Previous studies in both vertebrates and invertebrates described a developmental role for MMP in FGF dependant branching morphogenesis. For instance, in air sac branching in *Drosophila*, MMP2 function triggers the restriction of FGF activation in follower cells in a cell non autonomous way so that FGF pathway is only active in tip cells (Wang et al., 2010). The molecular mechanisms underlying the functions of MMP2 in FGF dependant branching morphogenesis are not clear but data from previous studies have provided some insights. The role of MMP could involve their capacity to degrade and remodel the ECM. For instance MMP2 proteolytic activity has been shown to modulate the FGF signalling pathway by contributing to the release of Fgf2 signals from the cell-ECM interface in the lens capsule (Tholozan et al., 2007). Studies also suggest that MMP function could be independent of their role in ECM degradation. Indeed, MMP2 has been shown to directly cleave the extracellular domain of FGFR1 at the cell surface (Levi et al., 1996); this proteolytic specific cleavage results in the release of a soluble Fgf receptor that can bind Fgf ligands and may thus modulate/inhibit the pathway.

In the epithalamus of *mmp2* morphants, we observed an increased number of *Tg(dusp6:d2GFP)* expressing cells in the PP and, in some cases, a delay in its migration and a decrease in the volume of the habenular nuclei. However, these phenotypes are probably a consequence of global developmental delays due to apoptosis, as they seem partially rescued by p53 MO. Using *mmp2* morpholinos, previous studies have suggested that MMP2 loss of function would result in various developmental defects such as reduced body length (Zhang et

al., 2003), reduced eye size and tectal area (Janssens et al., 2013) and altered lymphangiogenesis (Detry et al., 2012). In view of our results and of work from (Kok et al., 2015), data from all previous studies based on *mmp2* morpholino should be considered with caution. For instance, the function of MMP2 in the branching of lymphatic vessels was not confirmed in genetic mutants (Kok et al., 2015). However, here again, the existence of compensation mechanisms could be a relevant explanation as Detry et al. showed a role of MMP2 in the formation of lymphatic vessels using *in vitro* mouse explant model derived from MMP2 knock out mutant lines.

In *mmp2*^{-/-} mutants, defects in PP specification and migration were not observed. The pattern of *Tg(dusp6:d2GFP)* FGF reporter has still to be addressed in *mmp2*^{-/-} mutants but our data suggest that the pattern of FGF activation will not be strongly affected in this context. Our data could suggest that, despite its specific expression pattern, MMP2 does not have any major role in PP specification and migration. Alternatively, MMP2 could have a role in PP specification or migration that would be compensated in *mmp2*^{-/-} genetic mutants. A recent study has shown that a genetic loss of function can be compensated by the upregulation in the transcription of other genes (Rossi et al., 2015). As this compensation mechanism would not happen in morpholino injected embryos, it could explain the discrepancy between studies in genetic mutants and morpholino studies (Rossi et al., 2015). The function of MMP2 could be compensated by another MMP protein that would have a similar function in the PP or by another mechanism that would act in parallel to MMP proteins.

Acknowledgements

We thank Stephan Schulte-Merker and Andreas van Impel for providing the *mmp2*^{hu10535} mutant line, Qiling Xu for sending the *Tg(hsp70:ca-FgfR1)^{pd3}* line established in Ken Poss' lab, Agnes Noel and Jenny Paupert for sharing the *mmp2* morpholino. We would also like to thank the Toulouse RIO Imaging platform. This work was supported by the Centre National de la Recherche Scientifique (CNRS; PICS 2012-2015); the Institut National de la Santé et de la Recherche Médicale (INSERM); Université de Toulouse III (AO1-2013); Fondation pour la Recherche Médicale (FRM; DEQ20131029166); Fédération pour la Recherche sur le Cerveau (FRC); Association pour la Recherche sur le Cancer (ARC; SFI20101201699 and PJA 20131200173). We thank members of the Blader lab for critical reading of the manuscript.

References :

- Bauvois, B. (2012). New facets of matrix metalloproteinases MMP-2 and MMP-9 as cell surface transducers: Outside-in signaling and relationship to tumor progression. *Biochim. Biophys. Acta BBA - Rev. Cancer* 1825, 29–36.
- Bisgrove, B.W., Essner, J.J., and Yost, H.J. (2000). Multiple pathways in the midline regulate concordant brain, heart and gut left-right asymmetry. *Development* 127, 3567–3579.
- Concha, M.L., Burdine, R.D., Russell, C., Schier, A.F., and Wilson, S.W. (2000). A nodal signaling pathway regulates the laterality of neuroanatomical asymmetries in the zebrafish forebrain. *Neuron* 28, 399–409.
- Concha, M.L., Bianco, I.H., and Wilson, S.W. (2012). Encoding asymmetry within neural circuits. *Nat. Rev. Neurosci.* 13, 832–843.
- Deryugina, E.I., and Quigley, J.P. (2010). Pleiotropic Roles of Matrix Metalloproteinases in Tumor Angiogenesis: Contrasting, Overlapping and Compensatory Functions. *Biochim. Biophys. Acta* 1803, 103–120.
- Detry, B., Erpicum, C., Paupert, J., Blacher, S., Maillard, C., Bruyère, F., Pendeville, H., Remacle, T., Lambert, V., Balsat, C., et al. (2012). Matrix metalloproteinase-2 governs lymphatic vessel formation as an interstitial collagenase. *Blood* 119, 5048–5056.
- Dufourcq, P., Rastegar, S., Strähle, U. and Blader, P. (2004). Parapineal specific expression of *gf1* in the zebrafish epithalamus. *Gene Expr. Patterns* 4, 53-57.
- Egeblad, M., and Werb, Z. (2002). New functions for the matrix metalloproteinases in cancer progression. *Nat. Rev. Cancer* 2, 161–174.
- Gamse, J.T., Thisse, C., Thisse, B., and Halpern, M.E. (2003). The parapineal mediates left-right asymmetry in the zebrafish diencephalon. *Development* 130, 1059–1068.
- Gamse, J.T., Kuan, Y.S., Macurak, M., Brosamle, C., Thisse, B., Thisse, C., and Halpern, M.E. (2005). Directional asymmetry of the zebrafish epithalamus guides dorsoventral innervation of the midbrain target. *Development* 132, 4869–4881.
- Janssens, E., Gaublomme, D., Groef, L.D., Darras, V.M., Arckens, L., Delorme, N., Claes, F., Hove, I.V., and Moons, L. (2013). Matrix Metalloproteinase 14 in the Zebrafish: An Eye on Retinal and Retinotectal Development. *PLOS ONE* 8, e52915.
- Kessenbrock, K., Plaks, V., and Werb, Z. (2010). Matrix Metalloproteinases: Regulators of the Tumor Microenvironment. *Cell* 141, 52–67.
- Kok, F.O., Shin, M., Ni, C.-W., Gupta, A., Grosse, A.S., van Impel, A., Kirchmaier, B.C., Peterson-Maduro, J., Kourkoulis, G., Male, I., et al. (2015). Reverse Genetic Screening Reveals Poor Correlation between Morpholino-Induced and Mutant Phenotypes in Zebrafish. *Dev. Cell* 32, 97–108.

- Levi, E., Fridman, R., Miao, H.Q., Ma, Y.S., Yayon, A., and Vlodavsky, I. (1996). Matrix metalloproteinase 2 releases active soluble ectodomain of fibroblast growth factor receptor 1. *Proc. Natl. Acad. Sci. U. S. A.* *93*, 7069–7074.
- Liang, J.O., Etheridge, A., Hantsoo, L., Rubinstein, A.L., Nowak, S.J., Izpisua Belmonte, J.C., and Halpern, M.E. (2000). Asymmetric nodal signaling in the zebrafish diencephalon positions the pineal organ. *Development* *127*, 5101–5112.
- Marques, S.R., Lee, Y., Poss, K.D., and Yelon, D. (2008). Reiterative roles for FGF signaling in the establishment of size and proportion of the zebrafish heart. *Dev. Biol.* *321*, 397–406.
- Molina, G.A., Watkins, S.C., and Tsang, M. (2007). Generation of FGF reporter transgenic zebrafish and their utility in chemical screens. *BMC Dev Biol* *7*, 62.
- Neilson, K.M., and Friesel, R. (1996). Ligand-independent activation of fibroblast growth factor receptors by point mutations in the extracellular, transmembrane, and kinase domains. *J. Biol. Chem.* *271*, 25049–25057.
- Oxtoby, E., and Jowett, T. (1993). Cloning of the zebrafish *krox-20* gene (*krx-20*) and its expression during hindbrain development. *Nucleic Acids Res.* *21*, 1087–1095.
- Regan, J.C., Concha, M.L., Roussigne, M., Russell, C., and Wilson, S.W. (2009). An Fgf8-Dependent Bistable Cell Migratory Event Establishes CNS Asymmetry. *Neuron* *61*, 27–34.
- Robu, M.E., Larson, J.D., Nasevicius, A., Beiraghi, S., Brenner, C., Farber, S.A., and Ekker, S.C. (2007). p53 Activation by Knockdown Technologies. *PLoS Genet.* *3*.
- Rossi, A., Kontarakis, Z., Gerri, C., Nolte, H., Hölper, S., Krüger, M., and Stainier, D.Y.R. (2015). Genetic compensation induced by deleterious mutations but not gene knockdowns. *Nature* *524*, 230–233.
- Roussigne, M., Blader, P., and Wilson, S.W. (2012). Breaking symmetry: The zebrafish as a model for understanding left-right asymmetry in the developing brain. *Dev. Neurobiol.* *72*, 269–281.
- Tholozan, F.M.D., Gribbon, C., Li, Z., Goldberg, M.W., Prescott, A.R., McKie, N., and Quinlan, R.A. (2007). FGF-2 Release from the Lens Capsule by MMP-2 Maintains Lens Epithelial Cell Viability. *Mol. Biol. Cell* *18*, 4222–4231.
- Wang, Q., Uhlirova, M., and Bohmann, D. (2010). Spatial Restriction of FGF Signaling by a Matrix Metalloprotease Controls Branching Morphogenesis. *Dev. Cell* *18*, 157–164.
- Westerfield, M. (2000). *The Zebrafish Book. A Guide for The Laboratory Use of Zebrafish (Danio rerio)*, 4th Edition; Eugene, University of Oregon Press.
- Zhang, J., Bai, S., Zhang, X., Nagase, H., and Sarras, M.P. (2003). The expression of gelatinase A (MMP-2) is required for normal development of zebrafish embryos. *Dev. Genes Evol.* *213*, 456–463.

Figures and Legends

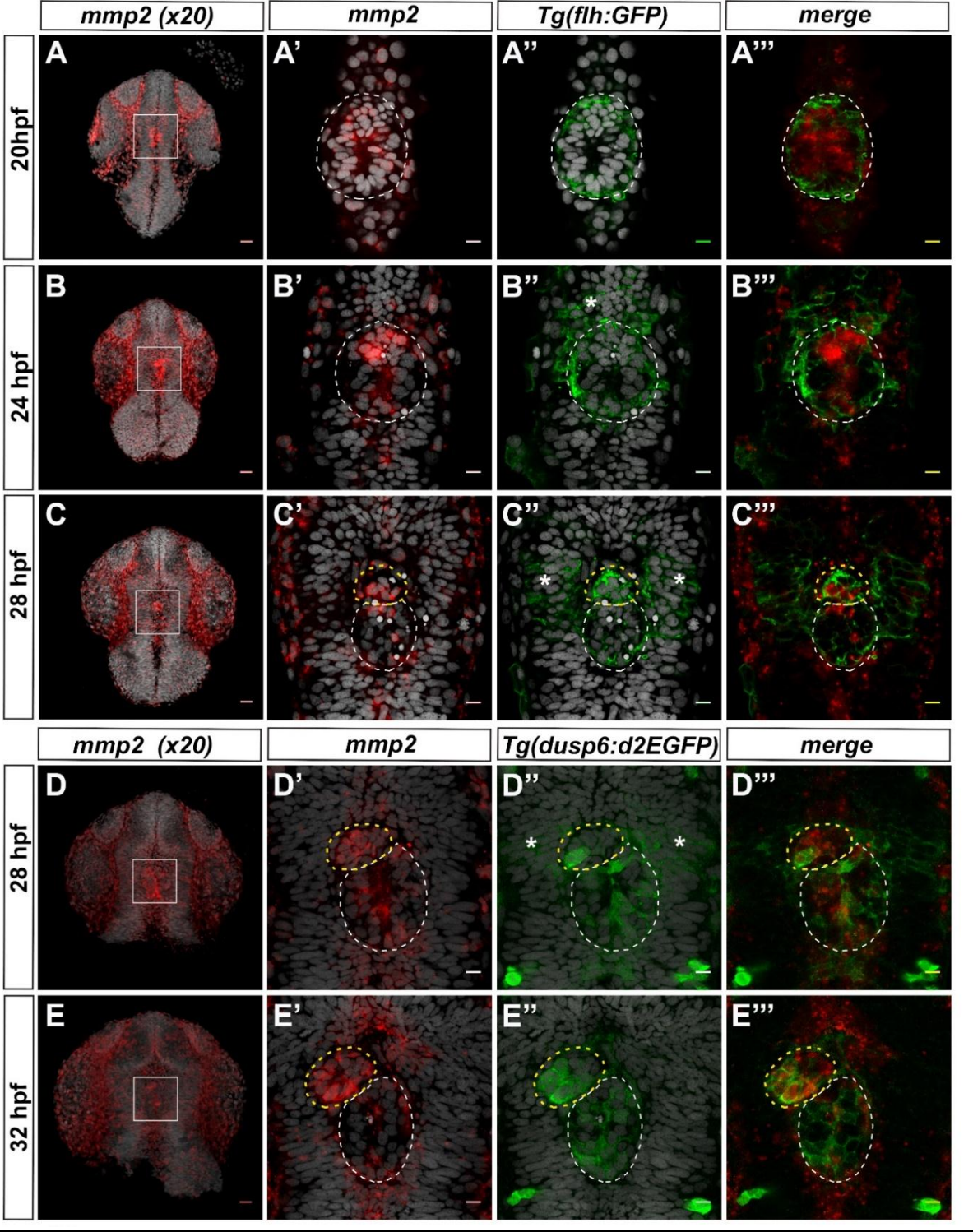


Figure 1: MMP2 is mosaically expressed in the pineal complex and enriched in the parapineal when it initiates its migration.

Confocal 100 μm projections (A,E; 100 μm , stepsize 2 μm ; scale bar: 25 μm) or high magnification confocal sections (A'-E'''; scale bars: 10 μm) showing the expression of *mmp2* (red) detected by *in situ* hybridization and/or the expression of *Tg(flh:GFP)* transgene (green, A-C''') at 20 hpf (n=14), 24 hpf (n=10), and 28 hpf (n=11) or the expression of *Tg(dusp6:d2EGFP)* (green, E-F''') at 28 hpf (n=19) and 32 hpf (n=17) after immunostaining against GFP. Pictures A-E'' are merged with global nuclear staining (Topro-3, grey) that was used to visualise the epiphysis (white outline) and parapineal rosette (yellow outline) at 28 and 32 hpf. *Tg(flh:GFP)* transgene was used to visualize the pineal complex (white circle at 20 hpf and 24 hpf) and labels both the epiphysis and parapineal later at 28 hpf but, due to GFP perdurance, it is also weakly detected in the surrounding cells of the presumptive habenulae (*). *mmp2* is mosaically expressed in the pineal complex at 20 hpf and 24 hpf; its expression is enriched in the parapineal from 28 hpf and partially overlaps with the expression of *Tg(dusp6:d2EGFP)* FGF reporter transgene that is enriched at the front of the migrating parapineal. White boxes in A-E'' are magnified in A'-E''''. Embryo view is dorsal, anterior is up.

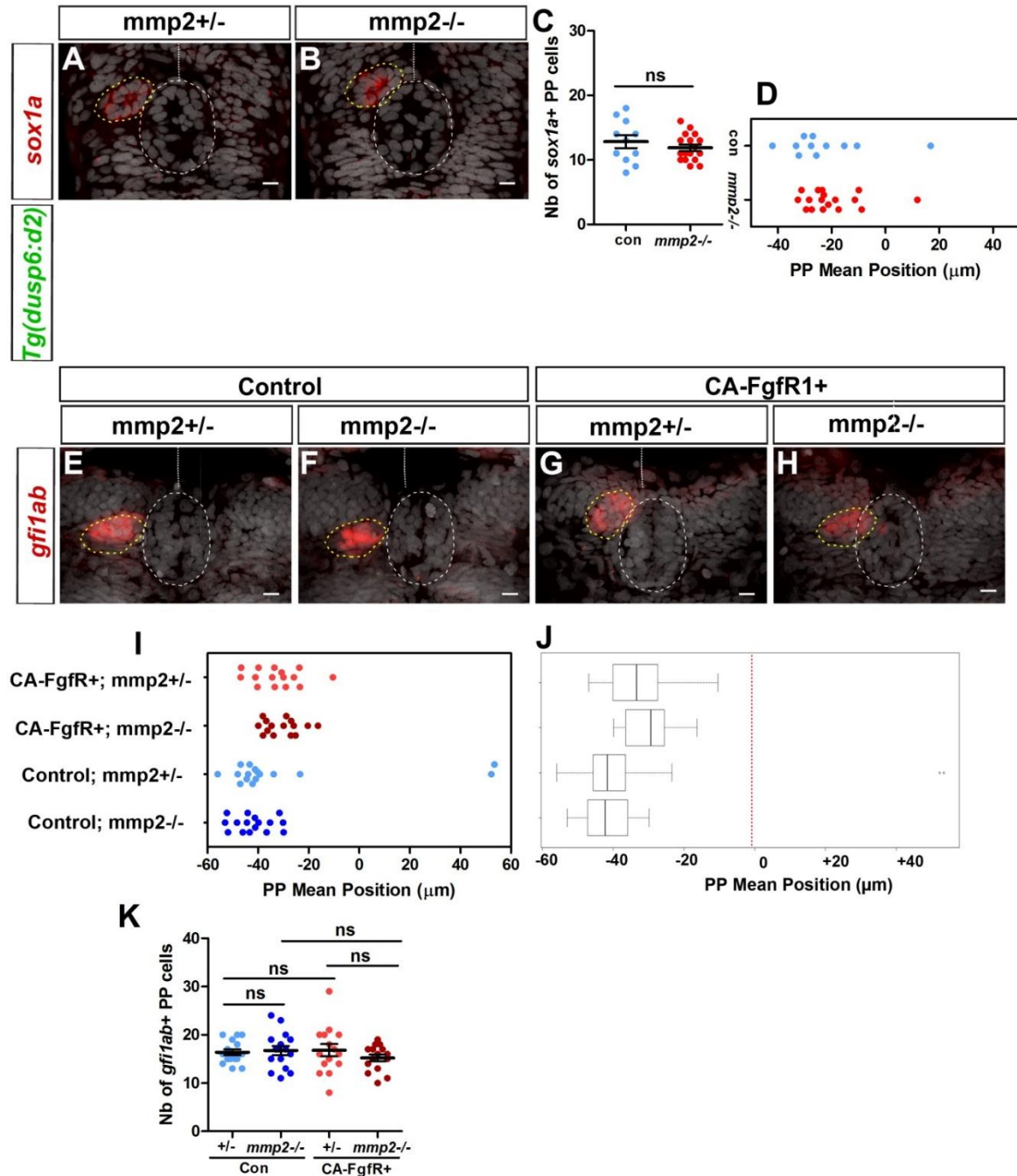


Figure 2: Parapineal specification and migration are not affected in *mmp2*^{-/-} mutants, despite ectopic activation of the Fgf pathway.

(A, B) Confocal sections showing *sox1a* expression (red) and cell nuclei labelling (grey) in representative *mmp2*^{+/-} heterozygote (A) or *mmp2*^{-/-} mutants (B) at 32 hpf; scale bar: 10 μm. Cell nuclei staining helps to visualize the parapineal (yellow outline) and the epiphysis (white outline).

(C, D) Dot plot showing the position of *sox1a*⁺ parapineal cells (C) at 32 hpf with respect to the brain midline (Reference 0) and the average number of *sox1a*⁺ parapineal cells (D) in *mmp2*^{+/-} heterozygote (blue marks; n=11) or *mmp2*^{-/-} mutant (red marks; n=17). The number and position of *sox1a*⁺ cells are not significantly affected in *mmp2*^{-/-} mutants (p=xx, t-test).

(E-H) Confocal maximum projection (8 μm) showing *gfi1ab* expression (red) and cell nuclei (grey) in representative control embryos (CA-FgfR1⁻) (E-F) and embryos expressing CA-FgfR1 (CA-FgfR1⁺) (G-H) that are *mmp2*^{+/-} heterozygotes (E, G) or *mmp2*^{-/-} mutants (F, H); scale bar: 10 μm. Control embryos are siblings of *Tg(hsp70:CA-FgfR1)* transgenic embryos that have been heat-shocked but do not express CA-FgfR1.

(I-K) Dot plot (I) and Boxplot (J) showing for each embryo the mean position of *gfi1ab* expressing PP cells relative to the brain midline (reference 0) or dot plot (H) showing the number of *gfi1ab* expressing cells in control embryos (not expressing CA-FgfR1) that are *mmp2*^{+/-} heterozygotes (light blue marks, n=16) or *mmp2*^{-/-} mutants (dark blue marks, n=16), or embryos expressing CA-FgfR1 that are *mmp2*^{+/-} heterozygotes (light red marks, n=15) or *mmp2*^{-/-} mutants (dark red marks, n=15). PP migration (assessed by mean position of *gfi1ab*⁺ PP cells) is delayed CA-FgfR1⁺ expressing embryos but does not differ between *mmp2*^{+/-} heterozygotes and *mmp2*^{-/-} mutants; see pairwise Wilcoxon rank test in Table S1 and Table S2.

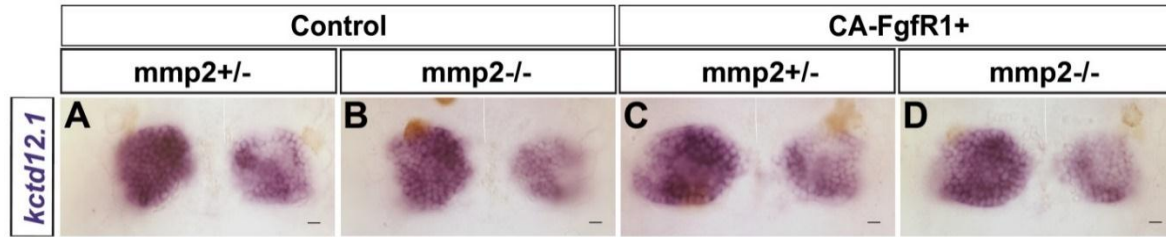


Figure 3: Habenular asymmetries are not affected in *mmp2*^{-/-} mutants even in the context of ectopic activation of the Fgf pathway

(A-D) Bright field pictures (A-D) showing expression of *kctd12.1* in the epithalamus of representative *Tg(hsp70:ca-fgfr1)* transgenic embryos (C-D) or control embryos not carrying *Tg(hsp70:ca-fgfr1)* transgene (A-B) that are *mmp2*^{+/-} heterozygotes (A; n=2, C; n=5) or *mmp2*^{-/-} mutants (B; n=7, D; n=5); scale bar: 10 μm. All embryos were heat-shocked at 26 hpf and fixed at 4 days respectively. One independent experiment.

Supplemental Figures and Legends

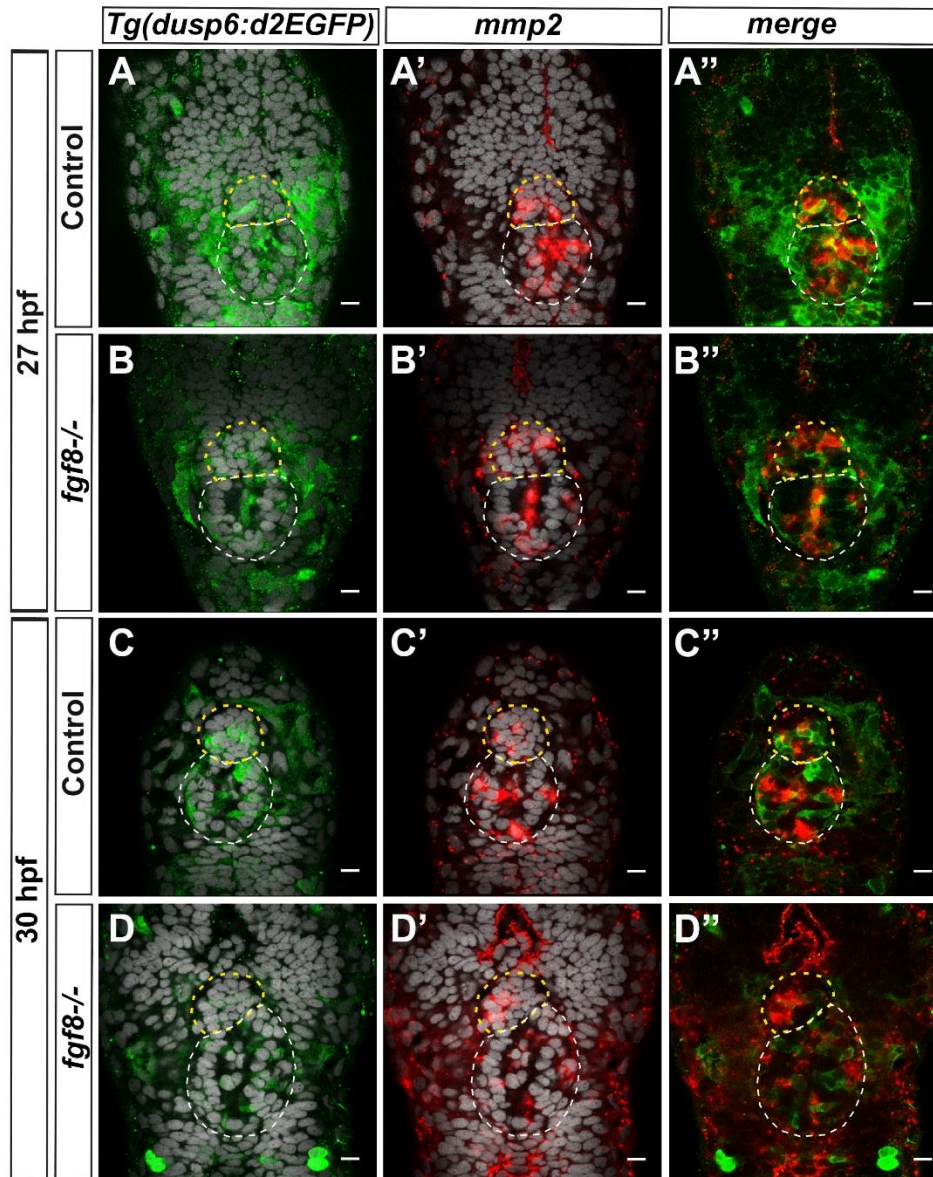


Figure S1

Figure S1: *mmp2* expression in the pineal complex does not dependant on *Fgf8*

Confocal sections showing expression of *Tg(dusp6:d2EGFP)* (green) transgene and *mmp2* (red) at 27 hpf (A-B'') and 30 hpf (C-D'') in control sibling embryos (A-A'', n=9 ; C-C'', n=2) or in *fgf8*^{-/-} mutant embryos (B-B'', n=2; D-D'', n=2). Pictures in A-A'' and B-B'' are merged with a cell nuclei labelling (Topro-3, grey) that helps visualising the epiphysis (white outline) and parapineal (yellow outline); green and red channels are merged in A''-D''. In contrast to *Tg(dusp6:d2EGFP)*

expression that is reduced or absent, *mmp2* expression is not affected in *fgf8*^{-/-} mutants. Embryo view is dorsal, anterior is up; scale bars: 10 μ m. Single experiment to confirm.

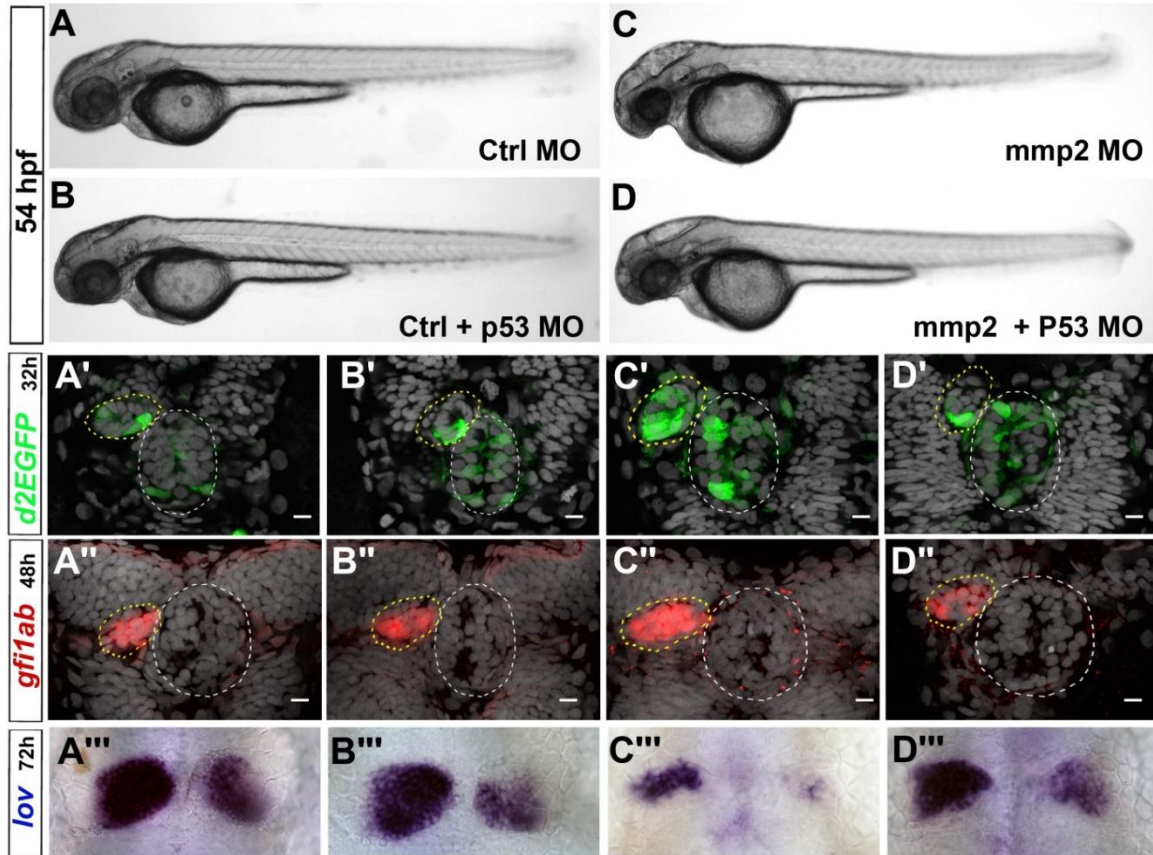


Figure S2: *mmp2* morphants display global developmental defects that are partially rescued by coinjection of p53 MO.

A-D''': Bright field pictures (A-D) showing the morphology of embryos and confocal projection showing *Tg(dusp6:d2EGFP)* expression (green, A'-D') and *gfi1ab* expression (red, A''-D'') merged with cell nuclei staining (grey) in representative embryos injected with a control morpholino (Ctrl MO) alone (A, A'' n=18; A', n=4), a Ctrl MO together with *p53* MO (B, B'' n=16; B', n=4), a MO targeting *mmp2* gene (*mmp2* MO) (C, C'' n=18; C', n=10) and *mmp2* MO together with *p53* MO (D, D'' n=11; D', n=8); Embryo views are lateral with anterior left (A-D) or dorsal with anterior up (A'-D'; A''-D''); scale bar: 10 μ m.

A''-D'': Bright field pictures (A''-D'') showing the expression of *kctd12.1(lov)* in the epithalamus of representative embryos injected with a control morpholino (Ctrl MO) alone (A'', n=14), a Ctrl MO together with *p53* MO (B'', n=13), a MO targeting *mmp2* gene (*mmp2* MO) (C'', n=14) and *mmp2* MO together with *p53* MO (D'', n=14).

Table S1. Pairwise comparisons of parapineal mean position between the four embryo contexts presented Figure 2.

	HSCA-_mmp2-/-	HSCA-_mmp2+/-	HSCA+/-_mmp2-/-
HSCA-_mmp2+/-	<u>1.00000</u>	-	-
HSCA+/-_mmp2-/-	0.00078	8.8e-05	-
HSCA+/-_mmp2+/-	0.04928	0.01031	<u>1.00000</u>

Datasets were compared on R Studio using the function 'pairwise.t.test' with P value adjustment method 'bonferroni'. To avoid any bias due to rare right migration events, we compared absolute values of parapineal position. Parapineal mean position do not differ significantly between *mmp2+/-* heterozygotes and *mmp2-/-* mutants in both contexts of presence or absence of *Tg(hsp70:ca-fgfr1)* transgene. As previously described, mean position of *gfi1ab+* parapineal cells differ in embryos expressing CA-Fgfr1 transgene compared to control embryos.

Table S2. Pairwise comparisons of parapineal cells numbers between the four embryo contexts presented Figure 2.

	HSCA-_mmp2-/-	HSCA-_mmp2+/-	HSCA+/-_mmp2-/-
HSCA-_mmp2+/-	1	-	-
HSCA+/-_mmp2-/-	1	1	-
HSCA+/-_mmp2+/-	1	1	1

The datasets were compared on R Studio using the function 'pairwise.wilcox.test' with the P value adjustment method 'Bonferroni'. Number of parapineal cells do not differ significantly between *mmp2+/-* heterozygotes and *mmp2-/-* mutants in both contexts of presence or absence of *Tg(hsp70:ca-fgfr1)*.

IV. Toward a better characterization of mature parapineal function: preliminary study of the expression of Opsins in parapineal

IV.1 Context and aim

In the zebrafish epithalamus, the pineal complex is composed of the epiphysis (or pineal gland) and of the parapineal (PP). The epiphysis contains two neuronal subtypes, photoreceptors and projection neurons, and is well described for its role in light detection and the regulation of circadian rhythms (Sapède and Cau, 2013). The epiphysis contains different types of photoreceptors defined by the expression of specific Opsins (Cau Elise, 2018). Opsins are a group of light-sensitive proteins that are specific for distinct wavelengths. The PP has also been suggested to be a photoreceptive structure (Concha et al., 2000) but, in contrast to the epiphysis, its function in this regard is unknown. The nature of cells contained in the PP is still unclear. For instance, it is not known whether the PP contains projection neurons and photoreceptors as does the epiphysis. Using a pan-opsin marker, Concha *et al* detected an Opsin expressing cell in about 15% of embryos at 4 days post fertilization (dpf) (Concha et al., 2000). These results suggested that the PP contains photosensitive cells but the fact that Opsins were detected in a subset of embryos is intriguing. This observation suggests that the expression of *opsin* genes might not be yet robust enough to be detected at 4 days or that variability might exist in PP composition. Moreover, it is unknown which specific *opsin* might be expressed by PP cells.

During my thesis, I mostly focused on the molecular mechanisms controlling leftward migration of the PP. However, I was also interested in better characterizing the identity of cell contained in the PP, as a first step to understand the role of the mature PP. The identification of specific *opsin* genes expressed in the PP would also provide useful tools to analyse fate decision in PP cells and better characterize what happens in context where the number of PP cells vary, such as in Notch loss of function context.

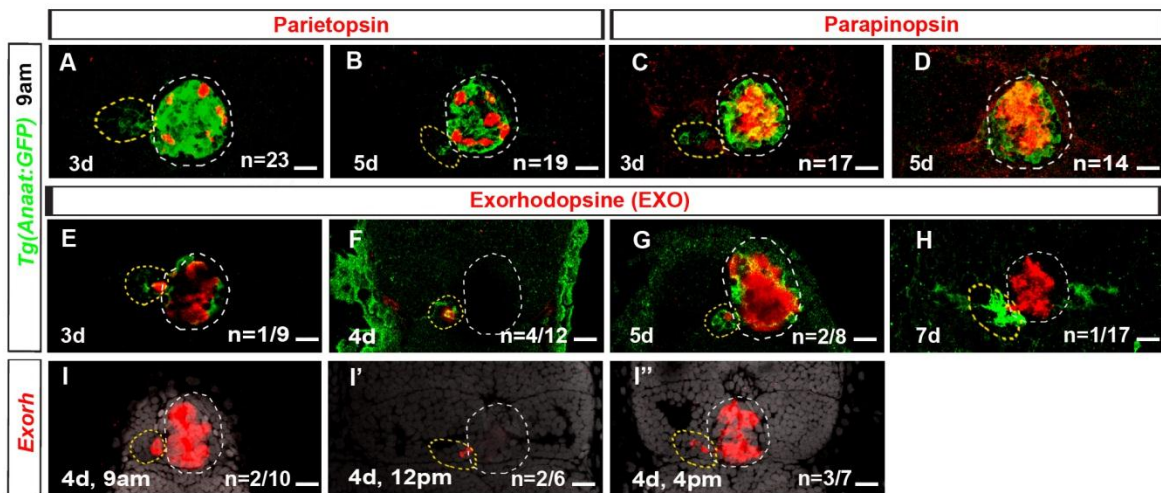


Fig. 35 Opsins (*Parapinopsin/Parietopsin/Exo-rhodopsine*) expression in pineal complex.

(A-H) Confocal sections showing the expression of *parietopsin* (A-B), *parapinopsin-a* (C-D) and *Exo-rhodopsine*(*Exorh*) at 3 days (A, C, E), 4 days (F), 5 days (B, D, G) and 7 days (H) (red) merged with Tg(*AANAT2:GFP*) transgene in embryos fixed at 9 am. Embryos view is dorsal, anterior is up; epiphysis (white circle) and parapineal (PP, yellow circle); scale bar=10 μ m.

(I-I'') Confocal sections showing the expression of *Exo-rhodopsine* (*Exorh*) (red) at 4 days at 9 am (I), 12 pm (I') and 4 pm (I'') merged with a cell nuclei staining (Topro-3 in grey) that makes epithalamus visible.

IV.2 Preliminary results on Opsin expression in parapineal

To better characterize the nature of PP cells, I started to analyze the expression of *aanat2*, a gene usually expressed by pineal photoreceptors and involved in the synthesis of melatonin, using a *Tg(AANAT2:GFP)* transgenic line (Gothilf et al., 2002). We found that PP cells express robustly *Tg(AANAT2:GFP)*, suggesting that PP is mostly composed of photoreceptors.

Then, I analysed the expression of various different *opsin* genes, described to be expressed in either the epiphysis or in the retina; the expression of 12 *opsin* genes: *Exo-rhodopsine(exorh)*, *Parapinopsin*, *Parietopsin*, *opn1lw1 (LWS1)*, *opn1lw2/cxxc1b (LWS2)*, *rhodopsin (Rho)*, *opn1mw1 (RH2-1)*, *opn1mw2 (RH2-2)*, *opn1mw3 (RH2-3)*, *opn1mw4 (RH2-4)*, *opn1sw1 (SWS1)*, and *opn1sw2 (SWS2)* was examined in the PP of *Tg(AANAT2:GFP)* transgenic embryos fixed at 3 days, 4 days and 5 days. We found that *RH2-1*, *RH2-2*, *RH2-3*, *RH2-4*, *SWS1*, *SWS2*, *LWS1*, *LWS2*, *RhO*, *parietopsin* are not detected in the PP although all of them except *RH2-3*, *SWS1* and *SWS2* opsins are expressed in the epiphysis (Fig. 35A-B and data not shown). No expression of *parapinopsin*, an *opsin* gene previously described to be expressed in the parapineal of catfish brain, was detected (Blackshaw and Snyder, 1997) (Fig. 35C-D). We observed that the *exo-rhodopsin (exorh)* gene is expressed in about 10% of embryos (n=1/9) at 3 days old (Fig. 35E) and in 33% of embryos (n=4/12) at 4 days (Fig. 35F). Surprisingly, the number of embryos expressing *exo-rhodopsin* did not increase at 5 days: *exo-rhodopsin* was detected in only 25% (n=2/8) of embryos at 5 days (Fig. 35G). We also checked the expression of *exorh* in 7 days old embryos but found only one expressing embryo (n=1/17) (Fig. 35H); this could be due to technical issues as, at this old stage, probes might not access properly to the tissue. Finally, at all stages analysed, *exo-rhodopsin* was usually detected in only a single cell per PP. Therefore, *exorh* expression appears to vary and does not seem robust in the PP.

All embryos analyzed above were fixed around 9 am in the morning. The lack of robustness in *exorh* expression could be due to its expression being regulated by circadian rhythms (Pierce et al., 2008). To address this possibility, we tested if *exo-rhodopsin* would be expressed more robustly in embryos fixed in the afternoon. In 4 days old embryos fixed at 4 pm, we detected *exorh* expression in the PP of 37% of embryos (n=7/19; data not shown), a proportion of

embryos comparable to the proportion found in embryos fixed at 9 am (n=4/12; **Fig. 35F**). In a second experiment where the same batch of 4 days old embryos was fixed at 3 different time point during the day, we confirmed that *exorh* was expressed similarly in the PP at 9 am (n=2/10), at 4 pm (n=3/7) and at 12 pm (n=2/6) (**Fig. 35I-I''**). Embryo numbers at each time need to be increased to conclude if the level of *exorh* expression is cycling. However, our data show that, at any time of day, *exorh* is expressed in only few embryos and only one or few cells (**Fig. 35I-I''**).

IV.3 Discussion and Prospectives

As a first attempt to characterize better the identity of parapineal (PP) cells, we analysed the expression of 12 opsins by *in situ* hybridization. In zebrafish larval embryos at 3, 4 or 5 days post fertilization (dpf), we found only one opsin gene, *exo-rhodopsine* (*exorh*) that was expressed in the PP. As *exorh* was expressed in only few embryos and only one PP cell (**Fig. 35E**), then we hypothesize that the expression of *exorh* opsin could be cycling during the day. However, this did not appear to be the case as *exorh* opsin was still detected in one PP cell and in few embryos at three days' time (**Fig. 35I-I''**). Although intriguing, our results are consistent with a previous study showing Pan-Op sin positive labeling in the PP of about 15% of embryos only ([Concha et al., 2000](#)).

This lack of robustness in the detection of *exorh* mRNA could be a consequence of a very dynamic expression of *exorh* gene or may also reflect a high variation in PP composition from one embryo to another. Moreover, we expect that other types of Opsins might be expressed in a more robust pattern than *exorh* gene in the PP. For this preliminary study, we used *opsin* probes that Elise had previously collected in the lab. But more genes encoding Opsins have been described and need to be tested ([Lowe et al., 2017](#); [Shichida and Matsuyama, 2009](#); [Terakita, 2005](#)). It would also be important to examine the expression pattern of different paralogs for each *opsin* subfamily in zebrafish larvae; indeed, a study has shown that *opsin* genes have duplicated multiple times across evolution of ray-finned fishes ([Chinen et al., 2003](#)) and, because of this duplication, many *opsin* genes might have lost their gene regulatory elements.

DISCUSSION and PROSPECTIVES

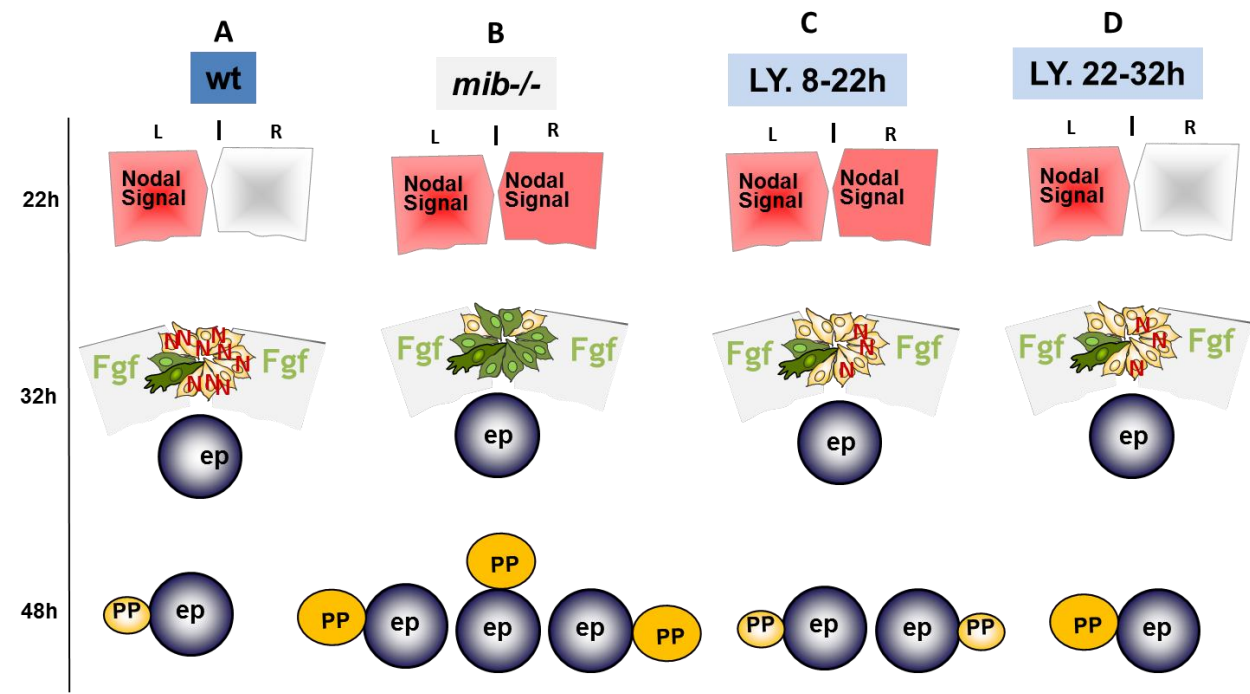


Fig. 36 Summary of the results in wt, *mib*^{-/-} and embryos treated with LY411575 at 8-22 h or 22-32 h.

(A) In wild-type (wt), Nodal signaling is activated in the left epithalamus from 20 hpf; Fgf8 is expressed bilaterally around the pineal complex but the activation of FGF signaling is restricted in few cells on the left posterior side of the parapineal (green cells); this is required for the parapineal (PP) to migrate leftward. We propose that Notch signaling (N) is directly required within PP cells to restrict FGF signaling activity. (B) In *mib*^{-/-}, Notch signaling is lost, Nodal signaling is active bilaterally and the FGF signaling pathway is activated in more PP cells; at 48 hpf, the PP either does not migrate or migrate randomly; it also displays a higher number of *gfi1ab* expressing cells. (C) In LY411575 treated *mib*^{+/-} embryos (8-22 h), Nodal signaling is often bilateral; the PP migrates but with a partially randomized orientation and displays the same size. (D) In LY411575 treated *mib*^{+/-} embryos (22-32h), Nodal signaling is active on the left; at 48 hpf, the PP migrates leftward but displays a higher number of *gfi1ab* expressing cells. In C and D, the number of *Tg(dusp6:d2GFP)*⁺ cells (green PP cells) is not significantly different from controls (although it tends to increase in D); this correlates with normal PP migration.

I. How does the Notch pathway restrict FGF signaling to promote parapineal migration?

I.1 Time windows of Notch requirement

Our results show that collective migration of the parapineal (PP) is achieved by focal activation of FGF pathway in few PP cells at the leading edge of migration (Manuscript n°1). The principal aim of my thesis project was to understand how activation of the FGF pathway is restricted to a few parapineal (PP) cells. Our data indicate that the Notch pathway is required for PP migration by restricting the activation of FGF signaling (Manuscript n°2). In *mib*^{-/-} mutants, we saw a robust increase in the number of *Tg(dusp6:d2EGFP)* expressing PP cells that correlated with defect in PP migration; in *mib*^{-/-}, we also observed a partial randomization of PP laterality and increased number of *gfi1ab*⁺ or *sox1a*⁺ PP cells (**Fig. 36B**). These phenotypes were also observed in embryos injected with morpholinos targeting *rbpj/su(H)*, a gene encoding a transcriptional effector of Notch pathway. However, in both *mib*^{-/-} mutants or in *rbpj/su(H)* morphants, Notch signaling is deficient from the beginning of embryonic development. Therefore, we performed LY411575 drug treatment at different time windows to address when is Notch pathway required for the specification and migration of PP cells and for PP left laterality.

As describe in Manuscript n°2, LY411575 treatment from 8 to 22 hours post-fertilization (hpf) does not interfere with PP migration nor with the number of *gfi1ab*⁺ PP cells but results in randomized PP laterality, probably by triggering bilateral Nodal pathway activation (**Fig. 36C**). On the other hand, late LY411575 treatment (22-32 hpf) results in a strong increase in the number of *gfi1ab*⁺ PP cells without affecting PP migration or laterality (**Fig. 36D**). As neither of these 2 treatment windows significantly affected PP migration or the pattern of FGF activation, we treated embryos with LY411575 treatment through both early and late time windows (8-32 hpf) with the expectation that this would reproduce all *mib*^{-/-} phenotypes. In embryos treated with LY411575 from 8 to 32 hpf, we observed PP migration defects but in few embryos only

that were *mib+/-* (n=2/30) or wild-type (*wt, +/+*) (n=1/34). Although already high, the number of embryos analyzed needs to be increased further if we are to conclude whether LY411575 treatment from 8-32 hpf can indeed trigger significant defects in PP migration. Our data indicate that LY411575 treatment from 8 to 32 hpf does not fully reproduce PP defects observed in *mib-/-* mutants. This could be due to LY411575 efficiency and/or specificity issues as discussed in Manuscript n°2. Although they were rare events, PP migration defects nevertheless correlated with a significant increase in number of *Tg(dusp6:d2EGFP)+* PP cells in LY411575 treated embryos (8-32 hpf) in both *wt (+/+)* and *mib+/-* contexts. We suspect that the increase in number of *Tg(dusp6:d2EGFP)* observed in embryos treated with LY411575 from 8-32 hpf might not be strong enough to affect PP migration.

The fact that we observed an increase in the level of FGF activity together with PP migration defects in few embryos still suggests that Notch could be required during both early (8-22 hpf) and late (22-32 hpf) time windows to promote restriction of FGF activity and PP migration. As early LOF for Notch signaling results in bilateral Nodal signaling, one possibility is that the Notch pathway could be required both early to establish left Nodal signaling and late within PP cells to control the restriction of FGF pathway. However, treating with LY411575 late (22-32 hpf) in symmetric Nodal contexts (*ntl MO* or *spaw MO*) did not affect PP migration (Results Part II.3). One explanation for this might be that an early requirement of Notch in PP migration is not directly a consequence of its ability to render activation of the Nodal pathway symmetric. Indeed, Notch could have others roles early that indirectly contribute to the restriction of FGF pathway later. Alternatively, it is possible that if LY411575 treatment is not efficient enough to allow us to assess the synergic contribution of the Nodal pathway. As discussed in Manuscript n°2, LY411575 treatment might not be potent enough to interfere with the role of Notch in restricting *Fgf* activation and promoting PP migration; this role of Notch could be rescued/compensated by other peptidases that would be less sensitive to LY411575.

Finally, Notch might act only at a late window, once the PP forms and initiates migration. It is possible that treating through both the early and late time window facilitates LY411575 efficiency/penetrance so that it is only truly acting between 22-32 hpf. This idea is supported by

our GOF experiments showing that ectopic Notch signaling can restrict FGF signaling at a late time window: indeed, expression of NICD at 26 hpf and 28 hpf strongly effects PP migration, and this correlates with the decrease in the number and the mean fluorescence intensity of *Tg(dusp6:d2EGFP)* positive PP cells.

Therefore, we propose a model where Notch is directly required within PP cells to restrict FGF signaling activity (**Fig. 36**). We cannot exclude that an early role of Notch also indirectly contributes to restrict FGF activity, through its ability to trigger left Nodal activity for instance. However, as treating with an FgfR inhibitor from 24 hpf can partially restore PP migration in *mib*^{-/-}, we conclude that, regardless of the time windows of Notch requirement (late only or early plus late), PP migration defect observed in absence of Notch is a consequence of an increased FGF activity at the time when PP initially migrates.

I.2 Molecular mechanisms of Notch mediated restriction of FGF pathway

Notch signaling has been implicated in the selection of leading cells during migration by restricting the ability of followers cells to activate receptor tyrosine kinase (RTK) signaling ([Ghabrial and Krasnow, 2006](#); [Ikeya and Hayashi, 1999](#)). How is this achieved? In some case, Notch mediated lateral inhibition is suggested to regulate the expression of the FGF or VEGF receptor ([Thomas et al., 2013](#)). Previous work showed that sprouting tip cells with low Notch activity show high VEGFR2 and low VEGFR1 expression, and increase in VEGF signalling and high levels of Dll4 (Delta-like ligand 4) expression ([Lobov et al., 2007](#)). The only Fgf receptor that we have detected in the parapineal, Fgfr4, is expressed in all PP cells (Fig. 2F in ([Regan et al., 2009](#))). However, there is no decrease in *Tg(dusp6:d2GFP)* expression and no obvious defect in PP migration in Fgfr4 MO injected embryos (data not shown). Thus, it is not clear if Fgfr4 is involved in activating *dusp6* expression downstream of Fgf8 in the PP. However, as the ectopic expression of the constitutive activated receptor (CA-FgfR1) does not completely block PP migration in wild-type and can rescue migration in *fgf8*^{-/-} mutants (Fig. 4 in Manuscript n°1), it

appears more likely that the restriction mechanism in the PP acts downstream of the activated receptor rather than at the level of receptor gene expression.

We propose that Notch could act within PP cells to restrict Fgf signaling via a lateral inhibition mechanism. How could Notch restrict the activation of FGF signaling in the PP? A possibility is that Notch signaling could directly promote the transcription of FGF pathway inhibitors or decrease the transcription of positive effectors of the pathway. Indeed, in the *C. elegans* vulva, Notch signaling directly promotes the transcription of Ras/MAPK pathway inhibitors (Berset et al., 2001). To address this *via* a candidate gene approach, we could test the expression of genes that encode modulators of FGF pathway including positive effectors of the ETS transcription factors family (*erm*, *pea3*, *etv5*) and known inhibitors of FGF pathway (*sef*, *spred*, *sprouty*), in contexts of loss or gain of function for Notch. However, it will be difficult to address whether Notch pathway directly controls the expression of these positive or negative regulators of FGF signaling, as they also are, for the majority, targets genes of FGF pathways. Therefore, if the expression of these FGF genes varies in contexts where Notch signaling is compromised, it will be difficult to conclude whether it would be a direct role of the Notch pathway on modulating their expression or an indirect consequence/ read-out of the fact that Notch modulates FGF signaling. To overcome this problem, we could use local heat shock to express Notch NICD only in few PP cells and then check the dynamic expression of FGF pathway inhibitors and effectors every 30min-1h (+30 min; 1H; +2H) after heat shock.

Previous work showed that Mkp3/Dusp6 can be induced by Fgf8 signal via the PI3K/Akt pathway to inhibit MAPK pathway (Kawakami et al., 2003). This mutual inhibition of PI3K and MAPK pathways could also happen in PP cells. Supporting this, drug inhibition experiments suggested that the PI3 Kinase pathway rather than the MAPK pathway is required downstream of FgfR activation in PP cells for both *Tg(dusp6:d2EGFP)* expression and PP migration (Myriam Roussigné, unpublished data). Thus, Notch signaling could control the expression of factors that would specifically modulate the activation of PI3K pathway to restrict Fgf signaling. It is also possible that the Notch pathway acts at a post-transcriptional level within the PP by regulating the activity of proteins, such as kinases or phosphatases that modulate the activity of

intracellular effectors of FGF pathway. Addressing this, however, would be difficult as we would need a transgenic line, such as a *Tg(sox1a:GFP)*, to sort out PP cells for proteomic analysis.

During my thesis, we explored the possibility that MMP2 might be involved in restricting FGF signaling (Manuscript n°3) as MMP2 would be a candidate to be regulated by Notch pathway. MMP2 is mosaically expressed in the parapineal in a manner that partially over-laps with the expression of the *Tg(dusp6:d2EGFP)* reporter transgene and was previously shown to restrict FGF pathway during air sac development in *Drosophila* (Wang et al., 2010). We found no defect in PP migration in *mmp2*^{-/-} mutants and no specific phenotype in *mmp2* morphants. However, as PP migration seems robust and tolerates significant variation in levels of FGF activity, MMP2 could contribute to restrict FGF signaling despite the absence of PP defects in *mmp2*^{-/-} mutants. Therefore, in the future, we should analyse *Tg(dusp6:d2EGFP)* expression in *mmp2*^{-/-} mutants to conclude if MMP2 does contribute or not to restrict FGF signaling within PP cells. In the case that MMP2 can contribute to restriction of FGF activity, we would analyse if MMP2 could act in parallel or downstream of Notch pathway.

Finally, it is possible that Notch signaling restrict FGF pathway through the transcriptional regulation of one or more unknown factors. Therefore, if our candidate approach does not allow us to find how Notch could modulate FGF pathway, we should perform a non-biased approach. If we are able to sort out all PP cells in the future, we could perform a transcriptomic approach (by high throughput RNA Sequencing) and compare the transcriptome of PP cells isolated from embryos following a loss or a gain of function for Notch pathway.

II. Synergic or parallel role of the Nodal pathway in restricting FGF pathway?

Our results indicate that Nodal signaling contributes to restricting FGF pathway activation as well as left-biasing it (Manuscript n°1, Fig 6). Indeed, in embryos displaying bilateral Nodal signaling, as when injected with *ntl* MO for instance, *Tg(dusp6:d2EGFP)* reporter expression is no longer lateralized to the left. FGF pathway activation is still restricted to a few cells within the parapineal (PP) as in wild-type, and this correlates with the PP initiating its migration either toward the left or the right in most embryos from 29-30 hpf. However, in absence of

Nodal signaling, as in *spaw* morphants, *Tg(dusp6:d2EGFP)* expression is generally less restricted within the parapineal and this correlates with delayed parapineal migration. Therefore, we have shown that not only the left bias in *Tg(dusp6:d2EGFP)* expression but also its restriction is influenced by Nodal signaling (**Fig. 36A**).

As discussed above, we believe that the restriction of FGF activity involves the Notch pathway. Therefore, it would be interesting to test whether the Nodal pathway acts through Notch pathway or in parallel of it. We would predict that if Nodal acts upstream of Notch then blocking both pathways might have little effect on migration over blocking Notch alone. However, if the pathways act in parallel, then blocking both might increase migration defects. This could be tested by injecting *spaw MO* (a context with increased *Tg(dusp6:d2EGFP)* expression) in a context of Notch Loss of function where *Tg(dusp6:d2EGFP)* is also increased (*rbpja/b MO* or *mib-/-*) to see if it creates more PP “No migration” or migration delay phenotype.

If Nodal pathway acts in parallel to the Notch pathway, it could directly influence the expression of inhibitors or positive effectors of the FGF pathway. Therefore, as described previously, we will need first to characterize the expression of modulators of the FGF pathway to better understand how FGF signaling is regulated. As discussed above (Discussion Part I.2), it will difficult to test the role of Nodal signaling on the expression of these factors, as they are not only modulators of specific branch of the FGF pathway but also also targets of the FGF pathway. Therefore, if the expression of these FGF target genes varies in contexts where Nodal signaling is compromised, it will be difficult to conclude whether it would be a direct role of the Nodal pathway on modulating their expression or an indirect consequence/a read-out of the fact that Nodal pathway modulates FGF signaling.

If we believe that Nodal pathway acts through Notch pathway, we could test if Nodal activity could modulate the expression of Notch signaling components. We have data showing the expression of some Notch pathway components in PP cells (**Fig. 27**); Notch ligands *deltaA*, *deltaB* and Notch target genes *her6*, *her9* are expressed mosaically in the PP. Thus, we could

test whether the mosaic expression of Notch ligands and target genes are affected in a context where activation of the Nodal pathway is absent.

III. How does Notch control the specification of parapineal cells?

Our results indicate that the Notch pathway controls migration and specification of the parapineal (PP), that these two processes can be uncoupled, and that only the role of Notch in PP migration is a consequence of defects in the restriction of FGF pathway activation (Manuscript n°2). We found that the number of *gfi1ab+* and *sox1a+* PP cells is robustly increased in Notch LOF (*mib*^{-/-} and LY411575 treatment at 22-32 hpf) contexts at 48 hpf (**Fig. 36D**). When LY411575 treatment was achieved in shorter time windows, we detected the biggest increase in number of *gfi1ab+* expressing PP cells in embryos treated with LY411575 from 25-28 hpf. In addition, we observed that the number of *sox1a+* PP cells did not increase in *mib*^{-/-} and LY411575 treated embryos (22-32 hpf) at 32 hpf although we found the number of *Topro+* PP cell nuclei is slightly increased in these contexts at same stage (32 hpf). We conclude, therefore, that the Notch pathway is required for the specification of a correct number of PP cells and that the increase in number of *gfi1ab+* and *sox1a+* PP cells in Notch LOF mostly occurs from 32h to 48h.

How does Notch control the number of parapineal cells? There is no literature concerning the role of Notch in the formation of PP cells. From what we observe, a hypothesis is that Notch signaling might be involved in proliferation of PP cells that will give rise to *gfi1ab+* cells, after the rosette is specified (**Fig. 37A**). We have preliminary data using bromodeoxyuridine (BrdU) labeling that supports this possibility (**Fig. 31**): there is an increase in *BrdU+* PP cells at 48 hpf in *mib*^{-/-} relative to controls when embryos were incubated with BrdU from 30 hpf. In the future, we plan to confirm our BrdU experiment in *mib*^{-/-} mutants by analyzing the ratio of *BrdU+* to *BrdU-* PP cells in control and Notch LOF contexts, across a broad set of stages, while co-labelling with different markers of PP cells (*gfi1ab*, *sox1a*, *tbx2b*). To know when the PP is getting bigger,

we will also perform time-lapse analysis. For this, we will image live embryos and follow PP cells from 32-48h in *mib*^{-/-} mutant embryos expressing a nuclear fluorescent protein (H2B-RFP) to visualize cell nuclei. From the datasets generated, we will determine the number of mitoses of PP cells in *mib*^{-/-} embryos versus siblings; as an alternative, we will live image embryos treated with LY411575 (25-28h) using expression of *Tg(Foxd3:GFP)* as a marker for PP cells.

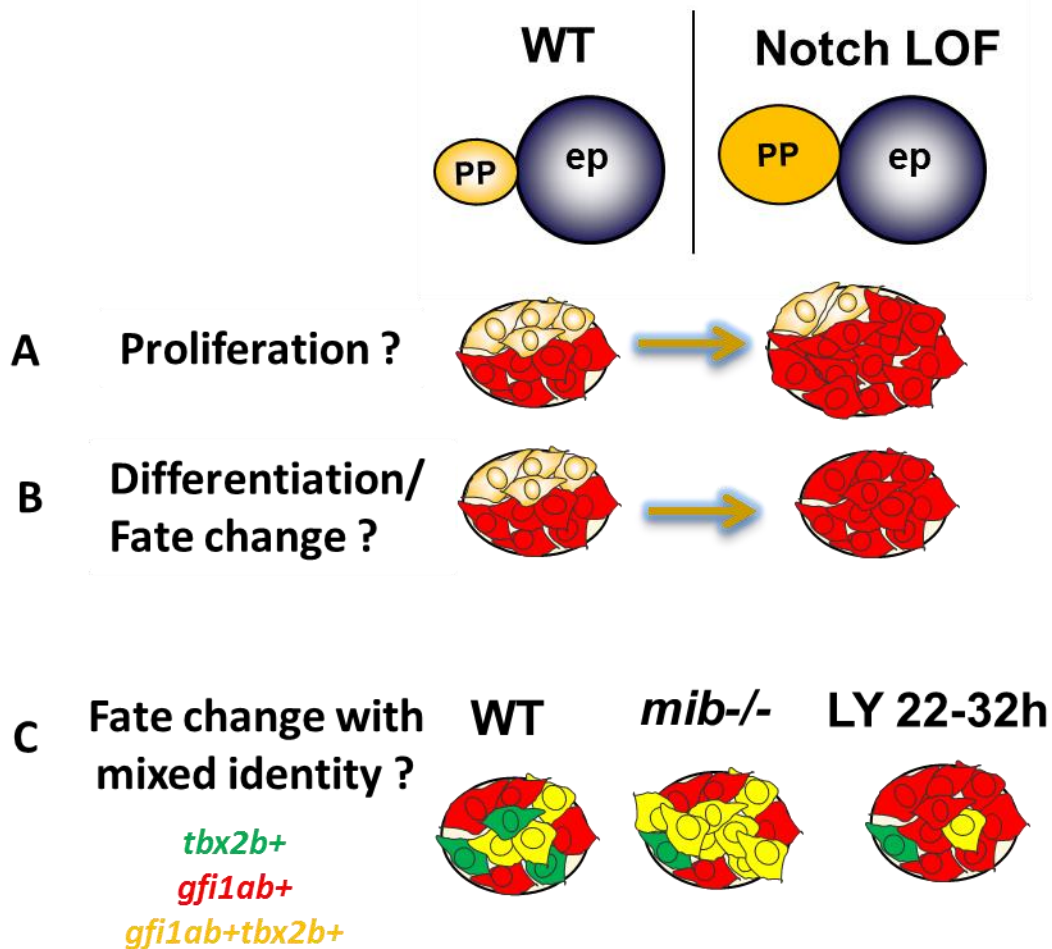


Fig. 37 Schematic showing the putative role of Notch signaling in the specification of parapineal cells.

Notch loss of function (LOF) leads to an increase in the number of parapineal (PP) specific markers (*gfi1ab* or *sox1a*) while *tbx2b* expression is not affected (in *mib*^{-/-}) or slightly decreased (in LY411575 treated embryos from 22 to 32 h). Notch LOF could result in increased proliferation of PP cells giving rise to *gfi1ab/sox1a*⁺ cells (A), increased differentiation or fate change (B) or could lead to an increase in the number of cells with mixed identity (C). In A and B, red cells represent *gfi1ab*⁺ cells and yellow cells correspond to *gfi1ab* negative cells that could be either PP progenitors, PP neurons with a different identity than *gfi1ab*⁺ cells or both.

In addition or instead of controlling PP cells proliferation, Notch pathway could control the balance between different putative sub-types of cells contained in the PP. In the PP of wild-type embryos, we usually observe some cells that are part of the PP rosette but do not express *gfi1ab* or *sox1a*. Therefore, the increase in *gfi1ab*⁺ PP cells in the Notch LOF context could parallel a decrease in this pool of *gfi1ab* negative PP cells (red versus yellow cells in **Fig. 37B**). These *gfi1ab* negative cells could correspond to non-differentiated cells/neuronal progenitors and Notch pathway could be involved in controlling the extend or timing of differentiation from neuronal progenitors to differentiated neurons (**Fig. 37B**). This role of Notch in controlling the timing of neurogenesis is well documented (Cau and Blader, 2009). Alternatively, *gfi1ab* negative PP cells could correspond to differentiated cells with a different specific identity than the one defined by *gfi1ab* marker and Notch could bias the fate choice between these cells subtypes (**Fig. 37B**). To address these possibilities, we need to find new markers that would be expressed in these *gfi1ab* negative cells and would label PP cells with specific identity or PP progenitors.

Tbx2b is thought to be a marker of PP progenitor cells as it is expressed in the pineal complex early (from 14 hpf, *i.e.* long before PP formation) and required for the specification of a correct number of *gfi1ab*⁺ cells (Snelson et al., 2008b). Interestingly, our data show that *tbx2b* expression is not changed in either *mib*^{-/-} mutants (Fig.1 in Manuscript n°2) or Notch GOF context (Fig.3 in Manuscript n°2) in contrast to *gfi1ab* or *sox1a* that are increased or decreased respectively. Therefore, our data suggest that Tbx2b acts upstream of the Notch pathway in the specification of PP cells.

Whether *tbx2b* gene could be a marker for *gfi1ab* negative cells remains to be addressed by double *in situ* hybridization. But if *tbx2b* does label PP progenitors and if Notch pathway promotes premature neuronal differentiation, we would expect that increase in the number of *gfi1ab*⁺ cells would be accompanied by a decrease in the number of *tbx2b*⁺ cells. However, as mentioned above, *tbx2b* expression is not changed in *mib*^{-/-} mutants. Therefore, one possibility is that Notch LOF leads to mixed identity in PP cells and this would be hidden unless we

perform double *in situ* hybridization (*ISH*) for *tbx2b* and *gfi1ab* (**Fig. 37C**). For instance, in wild-type embryos, PP cells could express either *tbx2b*, *gfi1ab* or both markers; in *mib*^{-/-} mutants, the expression of *tbx2b* remains unchanged and *gfi1ab* is increased but this could reflect the appearance of more double *tbx2b*⁺/*gfi1ab*⁺ cells at the expense of those expressing *tbx2b* alone (**Fig. 37C**). The effect of Notch LOF relative to cells of a double identity has already been reported between photoreceptors and projection neurons in the pineal (Cau et al., 2008). To address this possibility of a mixed identity in Notch LOF context, we will perform double *ISH* for *gfi1ab* and *tbx2b* at 48 hpf in *mib*^{-/-} mutants and LY411575 (22-32h) treated *mib*^{+/-} embryos.

The question remains, however, as to why there appears to be a difference between *mib*^{-/-} and LY411575 treated embryos: *tbx2b* expression is overall decreased in LY411575 treated embryos (22-32hpf) while not changed in *mib*^{-/-} mutants. This observation is unclear but perhaps this fate change might be correlated with the level of Notch pathway activity; Notch activity is lost in *mib*^{-/-} mutants while LY411575 treatment might create hypomorphic Notch LOF which might have a more drastic effect for unknown reasons. Alternatively, it is possible that an LY411575 sensitive γ -secretase can modulate *tbx2b* expression and/or the specification of PP cells independently and in addition of *mindbomb* signaling.

Addressing how does Notch control the number and fate of parapineal cells will require to better characterize, in the future, the cell diversity that might exist within the PP and to find new markers. Our preliminary data shows that there are *exorh*⁺ photoreceptors in the PP (**Fig. 35**). It would, therefore, be interesting to address the effects of Notch LOF on the size of this population of PP cells.

Is there a consequence of increased PP size on the establishment of asymmetry in the habenulae? In previous works, the lab has shown that loss of function of the Nodal target gene *pitx2* results in an increased number of PP cells that imposes left habenular isomerism (Garric et al., 2014); indeed, reducing the number of PP cells to wild-type level in *pitx2* LOF by partial ablation of PP progenitors restores habenular asymmetry. Aizawa et al show a “double left”

habenular phenotype in *mib*^{-/-} mutants (Aizawa et al., 2007). I also show that there is an increase in PP size in *mib*^{-/-} mutants raising the question of whether, as for *pitx2* LOF, the habenular phenotype in *mib*^{-/-} mutants would be imposed by the increase in PP size. Our preliminary data showed that LY411575 treatment leads to a “double left” habenular character (Fig. 34). However, we could also observe a “double left” habenula phenotype in LY411575 treated wild-type embryos (that are not *mib*^{+/-} heterozygotes) where we usually don’t observe an increase in PP size. Therefore to further conclude whether the PP is or is not implicated in the changes in habenular asymmetry seen in loss of function for Notch pathway, we need to analyse and correlate, for each LY411575 treated single embryos, the number of *gfi1ab*⁺ cells with the pattern of habenular asymmetry. Moreover, we could ablate PP cells in *mib*^{-/-} mutants or in LY411575 treated embryos (25-32h) to see whether this could restore habenular asymmetry.

REFERENCES

Afzelius, B. (1995). Immotile-cilia syndrome (primary ciliary dyskinesia), including Kartagener syndrome. *The metabolic and molecular bases of inherited disease*, 3943-3954.

Aizawa, H., Bianco, I.H., Hamaoka, T., Miyashita, T., Uemura, O., Concha, M.L., Russell, C., Wilson, S.W., and Okamoto, H. (2005). Laterotopic representation of left-right information onto the dorso-ventral axis of a zebrafish midbrain target nucleus. *Current Biology* *15*, 238-243.

Aizawa, H., Goto, M., Sato, T., and Okamoto, H. (2007). Temporally regulated asymmetric neurogenesis causes left-right difference in the zebrafish habenular structures. *Developmental cell* *12*, 87-98.

Akerberg, A.A., Stewart, S., and Stankunas, K. (2014). Spatial and temporal control of transgene expression in zebrafish. *PLoS one* *9*, e92217.

Aman, A., and Piotrowski, T. (2008). Wnt/ β -catenin and Fgf signaling control collective cell migration by restricting chemokine receptor expression. *Developmental cell* *15*, 749-761.

Aman, A., and Piotrowski, T. (2011). Cell-cell signaling interactions coordinate multiple cell behaviors that drive morphogenesis of the lateral line. *Cell adhesion & migration* *5*, 499-508.

Andrew, R.J. (1991). The nature of behavioural lateralization in the chick. *Neural and behavioural plasticity: The use of the domestic chick as a model*, 536-554.

Ariyomo, T.O., and Watt, P.J. (2013). Aggression and sex differences in lateralization in the zebrafish. *Animal behaviour* *86*, 617-622.

Beatus, P., and Lendahl, U. (1998). Notch and neurogenesis. *Journal of neuroscience research* *54*, 125-136.

Bénazéraf, B., Francois, P., Baker, R.E., Denans, N., Little, C.D., and Pourquié, O. (2010). A random cell motility gradient downstream of FGF controls elongation of an amniote embryo. *Nature* *466*, 248.

Berset, T., Hoier, E.F., Battu, G., Canevascini, S., and Hajnal, A. (2001). Notch inhibition of RAS signaling through MAP kinase phosphatase LIP-1 during *C. elegans* vulval development. *Science* *291*, 1055-1058.

Bianco, A., Poukkula, M., Cliffe, A., Mathieu, J., Luque, C.M., Fulga, T.A., and Rørth, P. (2007). Two distinct modes of guidance signalling during collective migration of border cells. *Nature* *448*, 362.

Bisazza, A., Rogers, L.J., and Vallortigara, G. (1998). The origins of cerebral asymmetry: a review of evidence of behavioural and brain lateralization in fishes, reptiles and amphibians. *Neuroscience & Biobehavioral Reviews* *22*, 411-426.

Bisgrove, B.W., Essner, J.J., and Yost, H.J. (1999). Regulation of midline development by antagonism of lefty and nodal signaling. *Development* *126*, 3253-3262.

Blackshaw, S., and Snyder, S.H. (1997). Parapinopsin, a novel catfish opsin localized to the parapineal organ, defines a new gene family. *Journal of Neuroscience* *17*, 8083-8092.

Böttcher, R.T., and Niehrs, C. (2004). Fibroblast growth factor signaling during early vertebrate development. *Endocrine reviews* *26*, 63-77.

Boutet, A. (2017). The evolution of asymmetric photosensitive structures in metazoans and the Nodal connection. *Mechanisms of development*.

- Bradshaw, J.L., and Rogers, L.J. (1993). The evolution of lateral asymmetries, language, tool use, and intellect (Academic Press).
- Braitenberg, V., and Kemali, M. (1970). Exceptions to bilateral symmetry in the epithalamus of lower vertebrates. *Journal of Comparative Neurology* *138*, 137-146.
- Bravo-Cordero, J.J., Hodgson, L., and Condeelis, J. (2012). Directed cell invasion and migration during metastasis. *Current opinion in cell biology* *24*, 277-283.
- Cai, D., Chen, S.-C., Prasad, M., He, L., Wang, X., Choesmel-Cadamuro, V., Sawyer, J.K., Danuser, G., and Montell, D.J. (2014). Mechanical feedback through E-cadherin promotes direction sensing during collective cell migration. *Cell* *157*, 1146-1159.
- Cameron, R., and Rogers, L. (1999). Hand preference of the common marmoset (*Callithrix jacchus*): Problem solving and responses in a novel setting. *Journal of Comparative Psychology* *113*, 149.
- Campbell, K., and Casanova, J. (2016). A common framework for EMT and collective cell migration. *Development* *143*, 4291-4300.
- Carl, M., Bianco, I.H., Bajoghli, B., Aghaallaei, N., Czerny, T., and Wilson, S.W. (2007). Wnt/Axin1/ β -catenin signaling regulates asymmetric nodal activation, elaboration, and concordance of CNS asymmetries. *Neuron* *55*, 393-405.
- Casey, B., and Hackett, B.P. (2000). Left–right axis malformations in man and mouse. *Current opinion in genetics & development* *10*, 257-261.
- Casey, M.B., and Martino, C.M. (2000). Asymmetrical hatching behaviors influence the development of postnatal laterality in domestic chicks (*Gallus gallus*). *Developmental Psychobiology: The Journal of the International Society for Developmental Psychobiology* *37*, 13-24.
- Cau, E., and Blader, P. (2009). Notch activity in the nervous system: to switch or not switch? *Neural development* *4*, 36.
- Cau, E., Quillien, A., and Blader, P. (2008). Notch resolves mixed neural identities in the zebrafish epiphysis. *Development* *135*, 2391-2401.
- Cau, E., and Wilson, S.W. (2003). Ash1a and Neurogenin1 function downstream of Floating head to regulate epiphysial neurogenesis. *Development* *130*, 2455-2466.
- Cau Elise, R.B., Bessière Laurianne and Blader Patrick (2018). A Notch-mediated heterochrony of response to BMP signalling after division promotes photoreceptor subtype diversification. *PLOS Biology*, In Revision.
- Chang, R. (2013). *Surface enhanced Raman scattering* (Springer Science & Business Media).
- Chapouton, P., Webb, K.J., Stigloher, C., Alunni, A., Adolf, B., Hesel, B., Topp, S., Kremmer, E., and Bally - Cuif, L. (2011). Expression of hairy/enhancer of split genes in neural progenitors and neurogenesis domains of the adult zebrafish brain. *Journal of Comparative Neurology* *519*, 1748-1769.
- Charoy, C., Dinvaut, S., Chaix, Y., Morle, L., Sanyas, I., Bozon, M., Kindbeiter, K., Durand, B., Skidmore, J.M., and De Groef, L. (2017). Genetic specification of left–right asymmetry in the diaphragm muscles and their motor innervation. *eLife* *6*, e18481.

- Chinen, A., Hamaoka, T., Yamada, Y., and Kawamura, S. (2003). Gene duplication and spectral diversification of cone visual pigments of zebrafish. *Genetics* 163, 663-675.
- Chou, M.-Y., Amo, R., Kinoshita, M., Cherng, B.-W., Shimazaki, H., Agetsuma, M., Shiraki, T., Aoki, T., Takahoko, M., and Yamazaki, M. (2016). Social conflict resolution regulated by two dorsal habenular subregions in zebrafish. *Science* 352, 87-90.
- Clanton, J.A., Hope, K.D., and Gamse, J.T. (2013). Fgf signaling governs cell fate in the zebrafish pineal complex. *Development* 140, 323-332.
- Cliffe, A., Doupé, D.P., Sung, H., Lim, I.K.H., Ong, K.H., Cheng, L., and Yu, W. (2017). Quantitative 3D analysis of complex single border cell behaviors in coordinated collective cell migration. *Nature Communications* 8, 14905.
- Concha Miguel L, W.S.W. (2001). Asymmetry in the epithalamus of vertebrates. *The Journal of Anatomy* 199, 63-84.
- Concha, M.L., Bianco, I.H., and Wilson, S.W. (2012). Encoding asymmetry within neural circuits. *Nature Reviews Neuroscience* 13, 832.
- Concha, M.L., Burdine, R.D., Russell, C., Schier, A.F., and Wilson, S.W. (2000). A nodal signaling pathway regulates the laterality of neuroanatomical asymmetries in the zebrafish forebrain. *Neuron* 28, 399-409.
- Concha, M.L., Russell, C., Regan, J.C., Tawk, M., Sidi, S., Gilmour, D.T., Kapsimali, M., Sumoy, L., Goldstone, K., and Amaya, E. (2003). Local tissue interactions across the dorsal midline of the forebrain establish CNS laterality. *Neuron* 39, 423-438.
- Concha, M.L., Signore, I.A., and Colombo, A. (2009). Mechanisms of directional asymmetry in the zebrafish epithalamus. Paper presented at: Seminars in cell & developmental biology (Elsevier).
- Concha, M.L., and Wilson, S.W. (2001). Asymmetry in the epithalamus of vertebrates. *The Journal of Anatomy* 199, 63-84.
- Dalle Nogare, D., Somers, K., Rao, S., Matsuda, M., Reichman-Fried, M., Raz, E., and Chitnis, A.B. (2014). Leading and trailing cells cooperate in collective migration of the zebrafish posterior lateral line primordium. *Development*, dev. 106690.
- Dambly-Chaudière, C., Cubedo, N., and Ghysen, A. (2007). Control of cell migration in the development of the posterior lateral line: antagonistic interactions between the chemokine receptors CXCR4 and CXCR7/RDC1. *BMC developmental biology* 7, 23.
- David, N.B., Sapède, D., Saint-Etienne, L., Thisse, C., Thisse, B., Dambly-Chaudière, C., Rosa, F.M., and Ghysen, A. (2002). Molecular basis of cell migration in the fish lateral line: role of the chemokine receptor CXCR4 and of its ligand, SDF1. *Proceedings of the National Academy of Sciences* 99, 16297-16302.
- Davidson, A.E., Balciunas, D., Mohn, D., Shaffer, J., Hermanson, S., Sivasubbu, S., Cliff, M.P., Hackett, P.B., and Ekker, S.C. (2003). Efficient gene delivery and gene expression in zebrafish using the Sleeping Beauty transposon. *Developmental biology* 263, 191-202.

- Davis, T.A. (1978). Reversible and irreversible lateralities in some animals. *Behavioral and Brain Sciences* 1, 291-293.
- De Renzi, E. (1982). Disorders of space exploration and cognition. JOHN WILEY & SONS, INC, 605 THIRD AVE, NEW YORK, NY 10158 1982.
- Dean, B.J., Erdogan, B., Gamse, J.T., and Wu, S.-Y. (2014). Dbx1b defines the dorsal habenular progenitor domain in the zebrafish epithalamus. *Neural development* 9, 20.
- Degenhardt, K., and Rychik, J. (2016). Fetal situs, isomerism, heterotaxy syndrome: diagnostic evaluation and implication for postnatal management. *Current treatment options in cardiovascular medicine* 18, 77.
- Del Bene, F., and Wyart, C. (2012). Optogenetics: a new enlightenment age for zebrafish neurobiology. *Developmental neurobiology* 72, 404-414.
- Dennis, E.L., and Thompson, P.M. (2013). Mapping connectivity in the developing brain. *International Journal of Developmental Neuroscience* 31, 525-542.
- Detry, B., Erpicum, C., Paupert, J., Blacher, S., Maillard, C., Bruyère, F., Pendeville, H., Remacle, T., Lambert, V., and Balsat, C. (2012). Matrix metalloproteinase-2 governs lymphatic vessel formation as an interstitial collagenase. *Blood*, blood-2011-2012-400267.
- Distel, M., Wullmann, M.F., and Köster, R.W. (2009). Optimized Gal4 genetics for permanent gene expression mapping in zebrafish. *Proceedings of the National Academy of Sciences* 106, 13365-13370.
- Donà, E., Barry, J.D., Valentin, G., Quirin, C., Khmelinskii, A., Kunze, A., Durdu, S., Newton, L.R., Fernandez-Minan, A., and Huber, W. (2013). Directional tissue migration through a self-generated chemokine gradient. *Nature* 503, 285.
- Dragovic, M., and Hammond, G. (2005). Handedness in schizophrenia: a quantitative review of evidence. *Acta Psychiatrica Scandinavica* 111, 410-419.
- Dreosti, E., Llopis, N.V., Carl, M., Yaksi, E., and Wilson, S.W. (2014). Left-right asymmetry is required for the habenulae to respond to both visual and olfactory stimuli. *Current Biology* 24, 440-445.
- Duboc, V., Dufourcq, P., Blader, P., and Roussigné, M. (2015). Asymmetry of the brain: development and implications. *Annual review of genetics* 49, 647-672.
- Durdu, S., Iskar, M., Revenu, C., Schieber, N., Kunze, A., Bork, P., Schwab, Y., and Gilmour, D. (2014). Luminal signalling links cell communication to tissue architecture during organogenesis. *Nature* 515, 120.
- Engbretson, G.A., Reiner, A., and Brecha, N. (1981). Habenular asymmetry and the central connections of the parietal eye of the lizard. *Journal of Comparative Neurology* 198, 155-165.
- Ernst, S., Liu, K., Agarwala, S., Moratscheck, N., Avci, M.E., Dalle Nogare, D., Chitnis, A.B., Ronneberger, O., and Lecaudey, V. (2012). Shroom3 is required downstream of FGF signalling to mediate proneuromast assembly in zebrafish. *Development*, dev. 083253.
- Essner, J.J., Branford, W.W., Zhang, J., and Yost, H.J. (2000). Mesendoderm and left-right brain, heart and gut development are differentially regulated by pitx2 isoforms. *Development* 127, 1081-1093.

- Ferencz, C. (1993). *Epidemiology of congenital heart disease: the Baltimore-Washington Infant Study 1981-1989* (Futura Publishing Company).
- Fradkin, L.G., Garriga, G., Salinas, P.C., Thomas, J.B., Yu, X., and Zou, Y. (2005). Wnt signaling in neural circuit development. *Journal of Neuroscience* *25*, 10376-10378.
- Francescatto, L., Rothschild, S.C., Myers, A.L., and Tombes, R.M. (2010). The activation of membrane targeted CaMK-II in the zebrafish Kupffer's vesicle is required for left-right asymmetry. *Development* *137*, 2753-2762.
- Friedl, P., and Gilmour, D. (2009). Collective cell migration in morphogenesis, regeneration and cancer. *Nature reviews Molecular cell biology* *10*, 445.
- Friedmann, H., and Davis, M. (1938). " Left-handedness" in parrots. *The Auk* *55*, 478-480.
- Fuse, N., Hirose, S., and Hayashi, S. (1994). Diploidy of *Drosophila* imaginal cells is maintained by a transcriptional repressor encoded by *escargot*. *Genes & development* *8*, 2270-2281.
- Gaj, T., Gersbach, C.A., and Barbas III, C.F. (2013). ZFN, TALEN, and CRISPR/Cas-based methods for genome engineering. *Trends in biotechnology* *31*, 397-405.
- Gamse, J.T., Kuan, Y.-S., Macurak, M., Brösamle, C., Thisse, B., Thisse, C., and Halpern, M.E. (2005). Directional asymmetry of the zebrafish epithalamus guides dorsoventral innervation of the midbrain target. *Development* *132*, 4869-4881.
- Gamse, J.T., Shen, Y.-C., Thisse, C., Thisse, B., Raymond, P.A., Halpern, M.E., and Liang, J.O. (2002). *Otx5* regulates genes that show circadian expression in the zebrafish pineal complex. *Nature genetics* *30*, 117.
- Gamse, J.T., Thisse, C., Thisse, B., and Halpern, M.E. (2003). The parapineal mediates left-right asymmetry in the zebrafish diencephalon. *Development* *130*, 1059-1068.
- Garric, L., Ronsin, B., Roussigné, M., Booton, S., Gamse, J.T., Dufourcq, P., and Blader, P. (2014). *Pitx2c* ensures habenular asymmetry by restricting parapineal cell number. *Development* *141*, 1572-1579.
- Gazzaniga, M.S. (2005). Forty-five years of split-brain research and still going strong. *Nature Reviews Neuroscience* *6*, 653.
- Gerhardt, H., Golding, M., Fruttiger, M., Ruhrberg, C., Lundkvist, A., Abramsson, A., Jeltsch, M., Mitchell, C., Alitalo, K., and Shima, D. (2003). VEGF guides angiogenic sprouting utilizing endothelial tip cell filopodia. *The Journal of cell biology* *161*, 1163-1177.
- Geschwind, N., and Levitsky, W. (1968). Human brain: left-right asymmetries in temporal speech region. *Science* *161*, 186-187.
- Ghabrial, A.S., and Krasnow, M.A. (2006). Social interactions among epithelial cells during tracheal branching morphogenesis. *Nature* *441*, 746.
- Ghysen, A., Dambly-Chaudière, C., and Raible, D. (2007). Making sense of zebrafish neural development in the Minervois (BioMed Central).

- Gothilf, Y., Toyama, R., Coon, S.L., Du, S.J., Dawid, I.B., and Klein, D.C. (2002). Pineal - specific expression of green fluorescent protein under the control of the serotonin - N - acetyltransferase gene regulatory regions in transgenic zebrafish. *Developmental Dynamics* 225, 241-249.
- Goto, K., Kurashima, R., Gokan, H., Inoue, N., Ito, I., and Watanabe, S. (2010). Left- right asymmetry defect in the hippocampal circuitry impairs spatial learning and working memory in iv mice. *PLoS One* 5, e15468.
- Graham, A. (2003). The neural crest. *Current Biology* 13, R381-R384.
- Guillemot, F., and Zimmer, C. (2011). From cradle to grave: the multiple roles of fibroblast growth factors in neural development. *Neuron* 71, 574-588.
- Haddon, C., Smithers, L., Schneider-Maunoury, S., Coche, T., Henrique, D., and Lewis, J. (1998). Multiple delta genes and lateral inhibition in zebrafish primary neurogenesis. *Development* 125, 359-370.
- Halluin, C., Madelaine, R., Naye, F., Peers, B., Roussigné, M., and Blader, P. (2016). Habenular neurogenesis in zebrafish is regulated by a hedgehog, Pax6 proneural gene cascade. *PloS one* 11, e0158210.
- Halpern, M.E., Liang, J.O., and Gamse, J.T. (2003). Leaning to the left: laterality in the zebrafish forebrain. *Trends in neurosciences* 26, 308-313.
- Hashimoto, H., Rebagliati, M., Ahmad, N., Muraoka, O., Kurokawa, T., Hibi, M., and Suzuki, T. (2004). The Cerberus/Dan-family protein Charon is a negative regulator of Nodal signaling during left-right patterning in zebrafish. *Development* 131, 1741-1753.
- Heim, S., and Keil, A. (2004). Large-scale neural correlates of developmental dyslexia. *European child & adolescent psychiatry* 13, 125-140.
- Hendricks, M., and Jesuthasan, S. (2007). Asymmetric innervation of the habenula in zebrafish. *Journal of Comparative Neurology* 502, 611-619.
- Herbert, M.R., Ziegler, D.A., Deutsch, C., O'Brien, L.M., Kennedy, D.N., Filipek, P., Bakardjiev, A., Hodgson, J., Takeoka, M., and Makris, N. (2004). Brain asymmetries in autism and developmental language disorder: a nested whole-brain analysis. *Brain* 128, 213-226.
- Hervé, P.-Y., Zago, L., Petit, L., Mazoyer, B., and Tzourio-Mazoyer, N. (2013). Revisiting human hemispheric specialization with neuroimaging. *Trends in cognitive sciences* 17, 69-80.
- Hirokawa, N., Tanaka, Y., Okada, Y., and Takeda, S. (2006). Nodal flow and the generation of left-right asymmetry. *Cell* 125, 33-45.
- Hobert, O. (2014). Development of left/right asymmetry in the *Caenorhabditis elegans* nervous system: from zygote to postmitotic neuron. *Genesis* 52, 528-543.
- Howe, K., Clark, M.D., Torroja, C.F., Torrance, J., Berthelot, C., Muffato, M., Collins, J.E., Humphray, S., McLaren, K., and Matthews, L. (2013). The zebrafish reference genome sequence and its relationship to the human genome. *Nature* 496, 498.

- Hüsken, U., and Carl, M. (2013). The Wnt/beta-catenin signaling pathway establishes neuroanatomical asymmetries and their laterality. *Mechanisms of development* *130*, 330-335.
- Hüsken, U., Stickney, H.L., Gestri, G., Bianco, I.H., Faro, A., Young, R.M., Roussigne, M., Hawkins, T.A., Beretta, C.A., and Brinkmann, I. (2014). Tcf7l2 is required for left-right asymmetric differentiation of habenular neurons. *Current Biology* *24*, 2217-2227.
- Hwang, W.Y., Fu, Y., Reyon, D., Maeder, M.L., Tsai, S.Q., Sander, J.D., Peterson, R.T., Yeh, J.J., and Joung, J.K. (2013). Efficient genome editing in zebrafish using a CRISPR-Cas system. *Nature biotechnology* *31*, 227.
- Idda, M.L., Bertolucci, C., Vallone, D., Gothilf, Y., Sánchez-Vázquez, F.J., and Foulkes, N.S. (2012). Circadian clocks: lessons from fish. In *Progress in brain research* (Elsevier), pp. 41-57.
- Ikeya, T., and Hayashi, S. (1999). Interplay of Notch and FGF signaling restricts cell fate and MAPK activation in the *Drosophila* trachea. *Development* *126*, 4455-4463.
- Ilina, O., and Friedl, P. (2009). Mechanisms of collective cell migration at a glance. *Journal of cell science* *122*, 3203-3208.
- Inestrosa, N.C., and Varela-Nallar, L. (2014). Wnt signaling in the nervous system and in Alzheimer's disease. *Journal of molecular cell biology* *6*, 64-74.
- Jao, L.-E., Wente, S.R., and Chen, W. (2013). Efficient multiplex biallelic zebrafish genome editing using a CRISPR nuclease system. *Proceedings of the National Academy of Sciences* *110*, 13904-13909.
- Job, A., Grateau, P., and Picard, J. (1998). Intrinsic differences in hearing performances between ears revealed by the asymmetrical shooting posture in the army. *Hearing research* *122*, 119-124.
- Juan, T., Géminard, C., Coutelis, J.-B., Cerezo, D., Polès, S., Noselli, S., and Fürthauer, M. (2018). Myosin1D is an evolutionarily conserved regulator of animal left-right asymmetry. *Nature communications* *9*, 1942.
- Jurynec, M.J., Xia, R., Mackrill, J.J., Gunther, D., Crawford, T., Flanigan, K.M., Abramson, J.J., Howard, M.T., and Grunwald, D.J. (2008). Selenoprotein N is required for ryanodine receptor calcium release channel activity in human and zebrafish muscle. *Proceedings of the National Academy of Sciences* *105*, 12485-12490.
- Kato, Y. (2011). The multiple roles of Notch signaling during left-right patterning. *Cellular and Molecular Life Sciences* *68*, 2555-2567.
- Kawakami, Y., Rodríguez-León, J., Koth, C.M., Büscher, D., Itoh, T., Raya, Á., Ng, J.K., Esteban, C.R., Takahashi, S., and Henrique, D. (2003). MKP3 mediates the cellular response to FGF8 signalling in the vertebrate limb. *Nature cell biology* *5*, 513.
- Kimmel, C.B., Ballard, W.W., Kimmel, S.R., Ullmann, B., and Schilling, T.F. (1995). Stages of embryonic development of the zebrafish. *Developmental dynamics* *203*, 253-310.
- Kimmel, C.B., Kane, D.A., Walker, C., Warga, R.M., and Rothman, M.B. (1989). A mutation that changes cell movement and cell fate in the zebrafish embryo. *Nature* *337*, 358.

Klämbt, C., Glazer, L., and Shilo, B. (1992). *breathless*, a *Drosophila* FGF receptor homolog, is essential for migration of tracheal and specific midline glial cells. *Genes & development* *6*, 1668-1678.

Kok, F.O., Shin, M., Ni, C.-W., Gupta, A., Grosse, A.S., van Impel, A., Kirchmaier, B.C., Peterson-Maduro, J., Kourkoulis, G., and Male, I. (2015). Reverse genetic screening reveals poor correlation between morpholino-induced and mutant phenotypes in zebrafish. *Developmental cell* *32*, 97-108.

Korf, H.-W., and Wagner, U. (1981). Nervous connections of the parietal eye in adult *Lacerta s. sicula* Rafinesque as demonstrated by anterograde and retrograde transport of horseradish peroxidase. *Cell and tissue research* *219*, 567-583.

Kozlovskaja-Gumbrienė, A., Yi, R., Alexander, R., Aman, A., Jiskra, R., Nagelberg, D., Knaut, H., McClain, M., and Piotrowski, T. (2017). Proliferation-independent regulation of organ size by Fgf/Notch signaling. *Elife* *6*, e21049.

Krämer, H. (2001). Neuralized: regulating notch by putting away delta. *Developmental cell* *1*, 725-726.

Krebs, L.T., Iwai, N., Nonaka, S., Welsh, I.C., Lan, Y., Jiang, R., Saijoh, Y., O'Brien, T.P., Hamada, H., and Gridley, T. (2003). Notch signaling regulates left-right asymmetry determination by inducing Nodal expression. *Genes & development* *17*, 1207-1212.

Kuan, Y.-S., Roberson, S., Akitake, C.M., Fortuno, L., Gamse, J., Moens, C., and Halpern, M.E. (2015). Distinct requirements for Wntless in habenular development. *Developmental biology* *406*, 117-128.

Kurita, K., Burgess, S.M., and Sakai, N. (2004). Transgenic zebrafish produced by retroviral infection of in vitro-cultured sperm. *Proceedings of the National Academy of Sciences of the United States of America* *101*, 1263-1267.

Ladoux, B., and Mège, R.-M. (2017). Mechanobiology of collective cell behaviours. *Nature Reviews Molecular Cell Biology* *18*, 743.

Lathia, J.D., Mattson, M.P., and Cheng, A. (2008). Notch: from neural development to neurological disorders. *Journal of neurochemistry* *107*, 1471-1481.

Latimer, A.J., Shin, J., and Appel, B. (2005). *her9* promotes floor plate development in zebrafish. *Developmental dynamics* *232*, 1098-1104.

Lawson, R.P., Seymour, B., Loh, E., Lutti, A., Dolan, R.J., Dayan, P., Weiskopf, N., and Roiser, J.P. (2014). The habenula encodes negative motivational value associated with primary punishment in humans. *Proceedings of the National Academy of Sciences* *111*, 11858-11863.

Lecaudey, V., Cakan-Akdogan, G., Norton, W.H., and Gilmour, D. (2008). Dynamic Fgf signaling couples morphogenesis and migration in the zebrafish lateral line primordium. *Development* *135*, 2695-2705.

Lee, T., Hacohen, N., Krasnow, M., and Montell, D.J. (1996). Regulated *Breathless* receptor tyrosine kinase activity required to pattern cell migration and branching in the *Drosophila* tracheal system. *Genes & development* *10*, 2912-2921.

Li, Q., Shirabe, K., and Kuwada, J.Y. (2004). Chemokine signaling regulates sensory cell migration in zebrafish. *Developmental biology* *269*, 123-136.

- Liang, J.O., Etheridge, A., Hantsoo, L., Rubinstein, A.L., Nowak, S.J., Belmonte, J.I., and Halpern, M.E. (2000). Asymmetric nodal signaling in the zebrafish diencephalon positions the pineal organ. *Development* *127*, 5101-5112.
- Lin, A.E., Ticho, B.S., Houde, K., Westgate, M.-N., and Holmes, L.B. (2000). Heterotaxy: associated conditions and hospital-based prevalence in newborns. *Genetics in Medicine* *2*, 157.
- Lobov, I., Renard, R., Papadopoulos, N., Gale, N., Thurston, G., Yancopoulos, G., and Wiegand, S. (2007). Delta-like ligand 4 (Dll4) is induced by VEGF as a negative regulator of angiogenic sprouting. *Proceedings of the National Academy of Sciences* *104*, 3219-3224.
- Long, S., Ahmad, N., and Rebagliati, M. (2003). The zebrafish nodal-related gene southpaw is required for visceral and diencephalic left-right asymmetry. *Development* *130*, 2303-2316.
- Lopes, S.S., Lourenço, R., Pacheco, L., Moreno, N., and Kreiling, J. (2010). Notch signalling regulates left-right asymmetry through ciliary length control. *Development* *137*, 3625-3632.
- Lowe, E.K., Garm, A., Ullrich-Luter, E., and Arnone, M.I. (2017). The crowns have eyes: Multiple opsins found in the eyes of the Crown-of-Thorns Starfish *Acanthaster planci*. *bioRxiv*, 173187.
- Lu, P., and Werb, Z. (2008). Patterning mechanisms of branched organs. *Science* *322*, 1506-1509.
- MacDonald, B.T., Tamai, K., and He, X. (2009). Wnt/ β -catenin signaling: components, mechanisms, and diseases. *Developmental cell* *17*, 9-26.
- Malet-Engra, G., Yu, W., Oldani, A., Rey-Barroso, J., Gov, N.S., Scita, G., and Dupré, L. (2015). Collective cell motility promotes chemotactic prowess and resistance to chemorepulsion. *Current Biology* *25*, 242-250.
- Matsui, T., and Bessho, Y. (2012). Left-right asymmetry in zebrafish. *Cellular and Molecular Life Sciences* *69*, 3069-3077.
- Mayor, R., and Etienne-Manneville, S. (2016). The front and rear of collective cell migration. *Nature reviews Molecular cell biology* *17*, 97.
- Meek, J., and Nieuwenhuys, R. (1998). Holosteans and teleosts. In *The central nervous system of vertebrates* (Springer), pp. 759-937.
- Meng, A., Jessen, J.R., and Lin, S. (1998). Transgenesis. In *Methods in cell biology* (Elsevier), pp. 133-148.
- Metzger, D., Clifford, J., Chiba, H., and Chambon, P. (1995). Conditional site-specific recombination in mammalian cells using a ligand-dependent chimeric Cre recombinase. *Proceedings of the National Academy of Sciences* *92*, 6991-6995.
- Mitchell, R.L., and Crow, T.J. (2005). Right hemisphere language functions and schizophrenia: the forgotten hemisphere? *Brain* *128*, 963-978.
- Miyasaka, N., Morimoto, K., Tsubokawa, T., Higashijima, S.-i., Okamoto, H., and Yoshihara, Y. (2009). From the olfactory bulb to higher brain centers: genetic visualization of secondary olfactory pathways in zebrafish. *Journal of Neuroscience* *29*, 4756-4767.

- Mizoguchi, T., Ikeda, S., Watanabe, S., Sugawara, M., and Itoh, M. (2017). Mib1 contributes to persistent directional cell migration by regulating the Ctnnd1-Rac1 pathway. *Proceedings of the National Academy of Sciences*, 201712560.
- Nachshon, I., Denno, D., and Aurand, S. (1983). Lateral preferences of hand, eye and foot: Relation to cerebral dominance. *International Journal of Neuroscience* 18, 1-9.
- Nasevicius, A., and Ekker, S.C. (2000). Effective targeted gene 'knockdown' in zebrafish. *Nature genetics* 26, 216.
- Nechiporuk, A., and Raible, D.W. (2008). FGF-dependent mechanosensory organ patterning in zebrafish. *Science* 320, 1774-1777.
- Nikolaou, N., Watanabe-Asaka, T., Gerety, S., Distel, M., Köster, R.W., and Wilkinson, D.G. (2009). Lunatic fringe promotes the lateral inhibition of neurogenesis. *Development* 136, 2523-2533.
- Ninkovic, J., Tallafuss, A., Leucht, C., Topczewski, J., Tannhäuser, B., Solnica-Krezel, L., and Bally-Cuif, L. (2005). Inhibition of neurogenesis at the zebrafish midbrain-hindbrain boundary by the combined and dose-dependent activity of a new hairy/E (spl) gene pair. *Development* 132, 75-88.
- Ochoa-Espinosa, A., and Affolter, M. (2012). Branching morphogenesis: from cells to organs and back. *Cold Spring Harbor perspectives in biology*, a008243.
- Palmer, A.R. (2009). Animal asymmetry. *Curr Biol* 19, R473-477.
- Pankov, R., Endo, Y., Even-Ram, S., Araki, M., Clark, K., Cukierman, E., Matsumoto, K., and Yamada, K.M. (2005). A Rac switch regulates random versus directionally persistent cell migration. *J Cell Biol* 170, 793-802.
- Pascual, A., Huang, K.-L., Neveu, J., and Pr at, T. (2004). Neuroanatomy: brain asymmetry and long-term memory. *Nature* 427, 605.
- Pasini, A., Jiang, Y.-J., and Wilkinson, D.G. (2004). Two zebrafish Notch-dependent hairy/Enhancer-of-split-related genes, *her6* and *her4*, are required to maintain the coordination of cyclic gene expression in the presomitic mesoderm. *Development* 131, 1529-1541.
- Peeters, H., and Devriendt, K. (2006). Human laterality disorders. *Eur J Med Genet* 49, 349-362.
- Pierce, L.X., Noche, R.R., Ponomareva, O., Chang, C., and Liang, J.O. (2008). Novel functions for Period 3 and Exo-rhodopsin in rhythmic transcription and melatonin biosynthesis within the zebrafish pineal organ. *Brain research* 1223, 11-24.
- Pocha, S.M., and Montell, D.J. (2014). Cellular and molecular mechanisms of single and collective cell migrations in *Drosophila*: themes and variations. *Annual review of genetics* 48, 295-318.
- Quillien, A., Blanco-Sanchez, B., Halluin, C., Moore, J.C., Lawson, N.D., Blader, P., and Cau, E. (2011). BMP signaling orchestrates photoreceptor specification in the zebrafish pineal gland in collaboration with Notch. *Development* 138, 2293-2302.
- Rajendra, S., and Rogers, L.J. (1993). Asymmetry is present in the thalamofugal visual projections of female chicks. *Experimental brain research* 92, 542-544.

- Raya, A., Kawakami, Y., Rodríguez-Esteban, C., Büscher, D., Koth, C.M., Itoh, T., Morita, M., Raya, R.M., Dubova, I., and Bessa, J.n.G. (2003). Notch activity induces Nodal expression and mediates the establishment of left–right asymmetry in vertebrate embryos. *Genes & development* *17*, 1213-1218.
- Rebagliati, M.R., Toyama, R., Haffter, P., and Dawid, I.B. (1998). Cyclops encodes a nodal-related factor involved in midline signaling. *Proceedings of the National Academy of Sciences* *95*, 9932-9937.
- Regan, J.C., Concha, M.L., Roussigne, M., Russell, C., and Wilson, S.W. (2009). An Fgf8-dependent bistable cell migratory event establishes CNS asymmetry. *Neuron* *61*, 27-34.
- Ridley, A.J. (2015). Rho GTPase signalling in cell migration. *Current opinion in cell biology* *36*, 103-112.
- Roberson, S., and Halpern, M.E. (2017). Convergence of signaling pathways underlying habenular formation and axonal outgrowth in zebrafish. *Development* *144*, 2652-2662.
- Rogers, L.J. (1982). Light experience and asymmetry of brain function in chickens. *Nature* *297*, 223.
- Rogers, L.J. (2002). Advantages and disadvantages of lateralization. *Comparative vertebrate lateralization*, 126-153.
- Rogers, L.J. (2009). Hand and paw preferences in relation to the lateralized brain. *Philosophical Transactions of the Royal Society B: Biological Sciences* *364*, 943-954.
- Rogers, L.J. (2014). Asymmetry of brain and behavior in animals: Its development, function, and human relevance. *Genesis* *52*, 555-571.
- Rogers, L.J., and Vallortigara, G. (2008). From antenna to antenna: lateral shift of olfactory memory recall by honeybees. *PLoS One* *3*, e2340.
- Rothenaigier, I., Krecsmarik, M., Hayes, J.A., Bahn, B., Lepier, A., Fortin, G., Götz, M., Jagasia, R., and Bally-Cuif, L. (2011). Clonal analysis by distinct viral vectors identifies bona fide neural stem cells in the adult zebrafish telencephalon and characterizes their division properties and fate. *Development*, dev. 058156.
- Roussigné, M., Bianco, I.H., Wilson, S.W., and Blader, P. (2009). Nodal signalling imposes left-right asymmetry upon neurogenesis in the habenular nuclei. *Development* *136*, 1549-1557.
- Sackeim, H.A., Gur, R.C., and Saucy, M.C. (1978). Emotions are expressed more intensely on the left side of the face. *Science* *202*, 434-436.
- Sapède, D., and Cau, E. (2013). The pineal gland from development to function. In *Current topics in developmental biology* (Elsevier), pp. 171-215.
- Sarmah, B., Latimer, A.J., Appel, B., and Wenthe, S.R. (2005). Inositol polyphosphates regulate zebrafish left-right asymmetry. *Developmental cell* *9*, 133-145.
- Sato, A., Scholl, A.M., Kuhn, E., Stadt, H.A., Decker, J.R., Pegram, K., Hutson, M.R., and Kirby, M.L. (2011a). FGF8 signaling is chemotactic for cardiac neural crest cells. *Developmental biology* *354*, 18-30.
- Sato, Y., Mori, K., Koizumi, T., Minagawa-Kawai, Y., Tanaka, A., Ozawa, E., Wakaba, Y., and Mazuka, R. (2011b). Functional lateralization of speech processing in adults and children who stutter. *Frontiers in psychology* *2*, 70.

- Shichida, Y., and Matsuyama, T. (2009). Evolution of opsins and phototransduction. *Philosophical Transactions of the Royal Society of London B: Biological Sciences* 364, 2881-2895.
- Shiraishi, I. (2016). Left-Right Asymmetry and Human Heterotaxy Syndrome. In *Etiology and Morphogenesis of Congenital Heart Disease* (Springer), pp. 49-56.
- Signore, I.A., Palma, K., and Concha, M.L. (2016). Nodal signalling and asymmetry of the nervous system. *Phil Trans R Soc B* 371, 20150401.
- Sivak, J.M., Petersen, L.F., and Amaya, E. (2005). FGF signal interpretation is directed by Sprouty and Spred proteins during mesoderm formation. *Developmental cell* 8, 689-701.
- Slack, J., Isaacs, H., Song, J., Durbin, L., and Pownall, M. (1996). The role of fibroblast growth factors in early *Xenopus* development. Paper presented at: Biochemical Society Symposium.
- Snelson, C.D., Burkart, J.T., and Gamse, J.T. (2008a). Formation of the asymmetric pineal complex in zebrafish requires two independently acting transcription factors. *Developmental Dynamics* 237, 3538-3544.
- Snelson, C.D., and Gamse, J.T. (2009). Building an asymmetric brain: development of the zebrafish epithalamus. Paper presented at: Seminars in cell & developmental biology (Elsevier).
- Snelson, C.D., Santhakumar, K., Halpern, M.E., and Gamse, J.T. (2008). *Tbx2b* is required for the development of the parapineal organ. *Development* 135, 1693-1702.
- Snelson, C.D., Santhakumar, K., Halpern, M.E., and Gamse, J.T. (2008b). *Tbx2b* is required for the development of the parapineal organ. *Development* 135, 1693-1702.
- Soukup, V. (2017). Left-right asymmetry specification in amphioxus: review and prospects. *Int J Dev Biol* 61, 611-620.
- Sutherland, D., Samakovlis, C., and Krasnow, M.A. (1996). *branchless* encodes a *Drosophila* FGF homolog that controls tracheal cell migration and the pattern of branching. *Cell* 87, 1091-1101.
- Taylor, R.W., Hsieh, Y.-W., Gamse, J.T., and Chuang, C.-F. (2010). Making a difference together: reciprocal interactions in *C. elegans* and zebrafish asymmetric neural development. *Development* 137, 681-691.
- Terakita, A. (2005). The opsins. *Genome biology* 6, 213.
- Thermes, V., Grabher, C., Ristoratore, F., Bourrat, F., Choulika, A., Wittbrodt, J., and Joly, J.-S. (2002). *I-SceI* meganuclease mediates highly efficient transgenesis in fish. *Mechanisms of development* 118, 91-98.
- Theveneau, E., and Linker, C. (2017). Leaders in collective migration: are front cells really endowed with a particular set of skills? *F1000Research* 6.
- Theveneau, E., and Mayor, R. (2011). Collective cell migration of the cephalic neural crest: the art of integrating information. *genesis* 49, 164-176.

- Theveneau, E., Steventon, B., Scarpa, E., Garcia, S., Trepap, X., Streit, A., and Mayor, R. (2013). Chase-and-run between adjacent cell populations promotes directional collective migration. *Nature cell biology* *15*, 763.
- Thisse, B., and Thisse, C. (2005). Functions and regulations of fibroblast growth factor signaling during embryonic development. *Developmental biology* *287*, 390-402.
- Thisse, C., and Thisse, B. (1999). Antivin, a novel and divergent member of the TGFbeta superfamily, negatively regulates mesoderm induction. *Development* *126*, 229-240.
- Thomas, J.-L., Baker, K., Han, J., Calvo, C., Nurmi, H., Eichmann, A.C., and Alitalo, K. (2013). Interactions between VEGFR and Notch signaling pathways in endothelial and neural cells. *Cellular and Molecular Life Sciences* *70*, 1779-1792.
- Tzourio-Mazoyer, N., Crivello, F., and Mazoyer, B. (2018). Is the planum temporale surface area a marker of hemispheric or regional language lateralization? *Brain Structure and Function* *23*, 1217-1228.
- Ubezio, B., Blanco, R.A., Geudens, I., Stanchi, F., Mathivet, T., Jones, M.L., Ragab, A., Bentley, K., and Gerhardt, H. (2016). Synchronization of endothelial DLL4-Notch dynamics switch blood vessels from branching to expansion. *Elife* *5*, e12167.
- Valentin, G., Haas, P., and Gilmour, D. (2007). The chemokine SDF1a coordinates tissue migration through the spatially restricted activation of Cxcr7 and Cxcr4b. *Current Biology* *17*, 1026-1031.
- van Helvert, S., Storm, C., and Friedl, P. (2018). Mechanoreciprocity in cell migration. *Nature cell biology* *20*, 8.
- Vandenberg, L.N., Morrie, R.D., Seebohm, G., Lemire, J.M., and Levin, M. (2013). Rab GTPases are required for early orientation of the left-right axis in *Xenopus*. *Mechanisms of development* *130*, 254-271.
- Venkiteswaran, G., Lewellis, S.W., Wang, J., Reynolds, E., Nicholson, C., and Knaut, H. (2013). Generation and dynamics of an endogenous, self-generated signaling gradient across a migrating tissue. *Cell* *155*, 674-687.
- Wang, J., Cao, J., Dickson, A.L., and Poss, K.D. (2015). Epicardial regeneration is guided by cardiac outflow tract and Hedgehog signalling. *Nature* *522*, 226.
- Wang, Q., Uhlirova, M., and Bohmann, D. (2010). Spatial restriction of FGF signaling by a matrix metalloprotease controls branching morphogenesis. *Developmental cell* *18*, 157-164.
- Ward, J.P., and Hopkins, W.D. (1993). *Primate laterality: Current behavioral evidence of primate asymmetries* (Springer Science & Business Media).
- Webb, J.R., Schroeder, M.I., Chee, C., Dial, D., Hana, R., Jefee, H., Mays, J., and Molitor, P. (2013). Left-handedness among a community sample of psychiatric outpatients suffering from mood and psychotic disorders. *SAGE Open* *3*, 2158244013503166.
- Webb, K.J., Norton, W.H., Trümbach, D., Meijer, A.H., Ninkovic, J., Topp, S., Heck, D., Marr, C., Wurst, W., and Theis, F.J. (2009). Zebrafish reward mutants reveal novel transcripts mediating the behavioral effects of amphetamine. *Genome biology* *10*, R81.

Weijer, C.J. (2009). Collective cell migration in development. *Journal of cell science* 122, 3215-3223.

Wyart, C., and Del Bene, F. (2011). Let there be light: zebrafish neurobiology and the optogenetic revolution. *Reviews in the neurosciences* 22, 121-130.

Yañez, J., and Anadon, R. (1994). Afferent and efferent connections of the habenula in the larval sea lamprey (*Petromyzon marinus* L.): an experimental study. *Journal of Comparative Neurology* 345, 148-160.

Yang, Y., Jamilpour, N., Yao, B., Dean, Z.S., Riahi, R., and Wong, P.K. (2016). Probing leader cells in endothelial collective migration by plasma lithography geometric confinement. *Scientific reports* 6, 22707.

Zinski, J., Tajer, B., and Mullins, M.C. (2017). TGF- β family signaling in early vertebrate development. *Cold Spring Harbor perspectives in biology*, a033274.

